

© 2019

Zihao Wei

ALL RIGHTS RESERVED

**ASSEMBLY, CHARACTERIZATION AND
APPLICATION OF OVOTRANSFERRIN FIBRILS**

by

ZIHAO WEI

A dissertation submitted to the

School of Graduate Studies

Rutgers, The State University of New Jersey

In partial fulfillment of the requirements

For the degree of

Doctor of Philosophy

Graduate Program in Food Science

Written under the direction of

Dr. Qingrong Huang

And approved by

New Brunswick, New Jersey

May, 2019

ABSTRACT OF THE DISSERTATION

ASSEMBLY, CHARACTERIZATION AND APPLICATION OF OVOTRANSFERRIN FIBRILS

By ZIHAO WEI

Dissertation director:

Qingrong Huang

Ovotransferrin (OVT), which accounts for about 12% of egg white proteins, attracts more and more research interests especially during these years due to multiple biological benefits and excellent solubility. However, since extraction procedures of OVT are very complicated and extraction yield of ovotransferrin is very low, research about OVT has not been widely investigated yet. At present, most of OVT studies focus on extraction and structural characterization, and application of OVT in constructing food polymeric structures and delivery systems has seldom been done.

The overall aim of my PhD thesis was to assemble, characterize and subsequently apply OVT fibrils in emulsion delivery systems, which may help to construct food polymeric structures and delivery systems using OVT as building blocks. Firstly, the optimal environmental condition (pH, temperature, ionic strength,

etc) for OVT fibrillation was explored. Atomic force microscopy (AFM) revealed that OVT fibrils consisted of both long and short fibrils. By decoupling hydrolysis and self-assembly, it was demonstrated that both intact monomers and peptides were the building blocks of OVT fibrils. Circular dichroism results indicated that internal structures of OVT amyloid fibrils could be stacked β -sheet. OVT amyloid fibrils had no *in vitro* cytotoxicity, suggesting great application potential.

Secondly, digestion and stability of OVT fibrils were investigated. Gastrointestinal digestion of OVT nanofibrils was characterized by thioflavin T (ThT) fluorescence and AFM. Most of OVT nanofibrils were disrupted during gastrointestinal digestion, and some OVT nanofibrils showed resistance to proteolytic digestion *in vitro*. OVT fibrils were stable over a wide pH range, and OVT fibrils possessed excellent stability against environmental stresses such as frozen storage–lyophilization–rehydration. The excellent stability indicated that OVT fibrils were stable food polymeric structures and could be applied in design of nutraceutical delivery systems.

Thirdly, impact of many other food ingredients in complex food systems on OVT fibrillation was studied using tools such as ThT fluorescence, SDS-PAGE and AFM. The investigated food ingredients included polyols, saccharides and polyphenols. In terms of effects of polyols on OVT fibrillation, the presence of glycerol or sorbitol could reduce the rate of OVT fibrillation, and slowdown of OVT fibrillation was strongly dependent on concentration of glycerol or sorbitol. Regarding impact of Maillard reaction, glycation could suppress fibrillation of ovotransferrin, and

glucosylation exerted stronger inhibitory impact on fibril formation than lactosylation. Glycation decreased average contour length of ovotransferrin fibrils, When it came to influence of polyphenols, the bound polyphenols (EGCG and GA) could inhibit OVT nanofibrillation, and higher level of complexation of OVT with more polyphenols showed stronger fibril-inhibitory activity. Covalent bound polyphenols exerted stronger inhibitory influence on OVT nanofibrillation than corresponding non-covalent bound polyphenols.

Lastly, OVT fibrils were applied in emulsion delivery systems. OVT fibrils were verified as effective Pickering emulsifiers, and visual appearance confirmed that OVT fibrils could stabilize Pickering emulsions with high emulsified phase volume and stability index at different fibril concentrations and oil fractions. OVT fibrils could be employed to fabricate stable Pickering emulsions at various ionic strengths (0–1000 mM) and pHs (2–7). OVT fibril-stabilized Pickering emulsions could provide curcumin protection, and the distinction in curcumin protection was related to ionic strengths and pHs of emulsions. As demonstrated in TIM-1 and pH-stat digestion models, OVT fibril-stabilized Pickering emulsions could increase curcumin bioaccessibility. To improve freeze-thaw stability of Pickering emulsion systems, organogel-based Pickering emulsions stabilized by OVT fibrils were developed. Organogel-based Pickering emulsions stabilized by OVT fibrils had excellent storage stability, and freeze-thaw stability of organogel-based Pickering emulsions stabilized by OVT fibrils was better than that of conventional Pickering emulsions (without organogel) stabilized by OVT fibrils. In comparison with organogel, organogel-based

Pickering emulsion could improve both extent of lipolysis and hesperidin bioaccessibility. The acquired knowledge in this thesis may facilitate assembly, characterization as well as application of food protein fibrils.

ACKNOWLEDGEMENT

First of all, I would like to express my sincere thanks to my advisor, Dr. Qingrong Huang, for his guidance and support throughout my PhD study in Rutgers University. During the past four years, I have grasped a lot of knowledge in the field of food science due to Dr. Huang's excellence in academics. After systematic research studies, I am equipped with basic skills of conducting independent researches, which helps me prepare for my academic career. Dr. Huang is always supporting my research work with his brilliant research ideas, experiments skills and instrument resources. For me, Dr. Huang is not only a research supervisor, but also a friend who is always caring about my needs. I feel deeply honored to be a member in family of Dr. Huang's lab, and I will always remember the pleasant memory during my stay in Dr. Huang's lab.

Next, I would like to thank Dr. Chi-Tang Ho, Dr. Qingli Wu and Dr. Shiming Li for their willingness to serve as my committee members. It is my great honor to have these excellent professors in my PhD dissertation committee. During my oral qualifying exam, the committee members gave me a lot of advice on my dissertation scheme and experimental details. With their valuable suggestions, my PhD dissertation has been improved significantly.

Many thanks to my labmates and friends. When I encounter difficulty in experiments, they have offered me some solutions. When I feel lonely, we talk with

each other to share sorrow and happiness. When I need to make some decisions, they give me a lot of advice.

I want to express my gratitude to all of my family members for their support and unconditional love. Without their love and encouragement, I would not have completed my PhD study. It's never enough for me to say thank you. This PhD dissertation is dedicated to my dearest parents.

CONTENTS

ABSTRACT OF THE DISSERTATION.....	ii
ACKNOWLEDGEMENT.....	vi
CONTENTS.....	viii
LIST OF TABLES.....	x
LIST OF ILLUSTRATIONS.....	xii
CHAPTER I. INTRODUCTION.....	1
1. Key Concepts Involved in Thesis.....	1
2. Research Rationale and Hypothesis.....	11
3. Specific research objectives.....	14
4. References.....	17
CHAPTER II. ASSEMBLY OF OVOTRANSFERRIN FIBRILS.....	21
1. Introduction.....	21
2. Materials and Methods.....	23
3. Results and Discussion.....	28
4. Conclusion.....	45
5. References.....	46
CHAPTER III. IN VITRO DIGESTION AND STABILITY OF OVOTRANSFERRIN FIBRILS.....	50
1. Introduction.....	50
2. Materials and Methods.....	51
3. Results and Discussion.....	55
4. Conclusion.....	70
5. References.....	70
CHAPTER IV. OVOTRANSFERRIN FIBRIL FORMATION IN THE PRESENCE OF POLYOLS.....	74
1. Introduction.....	74
2. Materials and Methods.....	75
3. Results and Discussion.....	78
4. Conclusion.....	88
5. References.....	88
CHAPTER V. IMPACT OF MAILLARD REACTION ON OVOTRANSFERRIN FIBRILS.....	91
1. Introduction.....	91
2. Materials and Methods.....	92
3. Results and Discussion.....	96
4. Conclusion.....	108
5. References.....	109
CHAPTER VI. IMPACT OF POLYPHENOLS ON OVOTRANSFERRIN FIBRILS.....	111

1. Introduction.....	111
2. Materials and methods.....	112
3. Results and Discussion.....	115
4. Conclusion.....	130
5. References.....	131
CHAPTER VII. FOOD-GRADE PICKERING EMULSIONS STABILIZED BY OVOTRANSFERRIN FIBRILS.....	133
1. Introduction.....	133
2. Materials and Methods.....	133
3. Results and Discussion.....	142
4. Conclusion.....	169
5. References.....	170
CHAPTER VIII. OVOTRANSFERRIN FIBRIL-STABILIZED PICKERING EMULSIONS AS DELIVERY VEHICLES FOR CURCUMIN.....	174
1. Introduction.....	174
2. Materials and Methods.....	174
3. Results and Discussion.....	181
4. Conclusion.....	195
5. References.....	196
CHAPTER IX. DEVELOPMENT OF ORGANOGEL-BASED PICKERING EMULSIONS STABILIZED BY OVOTRANSFERRIN FIBRILS.....	198
1. Introduction.....	198
2. Materials and Methods.....	201
3. Results and Discussion.....	209
4. Conclusion.....	230
5. References.....	230
SUMMARY AND FUTURE WORK.....	235

LIST OF TABLES

Table II-1. Estimation of secondary structure of OVT after heat treatment at pH 2.0.....	41
Table II-2. Surface hydrophobicity (H_0) of OVT after heating at 90 °C and pH 2.0 for 0–24 h.....	44
Table III-1. Relative ThT fluorescence intensity and digestion rate of OVT fibrils after different periods of simulated gastric digestion.....	55
Table III-2. Relative ThT fluorescence intensity and digestion rate of OVT fibrils before and after simulated intestinal digestion.....	58
Table III-3. Relative ThT fluorescence intensity and loss rate of OVT fibrils after treatment of frozen storage–lyophilization–rehydration.....	68
Table III-4. Relative ThT fluorescence intensity and loss rate of OVT fibrils after high-speed shearing.....	70
Table V-1. Emulsified phase volume fraction and stability index of Pickering emulsions stabilized by OVTC fibrils, OGC fibrils and OLC fibrils at different fibril concentrations and oil fractions.....	106
Table V-2. Average emulsion droplet size of Pickering emulsions ($c = 4$ wt%, $\varphi = 0.65$) stabilized by OVTC fibrils, OGC fibrils and OLC fibrils.....	108
Table VI-1. Free amino groups of OVT, OVT–EGCG covalent complexes and OVT–GA covalent complexes.....	116
Table VI-2. Free sulfhydryl groups of OVT, OVT–EGCG covalent complexes and OVT–GA covalent complexes.....	117
Table VI-3. Total phenolic content of OVT–EGCG covalent complexes and OVT–GA covalent complexes.....	117
Table VI-4. Free amino groups of OVT, OVT–EGCG physical complexes and OVT–GA physical complexes.....	119
Table VI-5. Free sulfhydryl groups of OVT, OVT–EGCG physical complexes and OVT–GA physical complexes.....	120
Table VI-6. Surface hydrophobicity of OVT, OVT–polyphenol complexes and fibrils derived from OVT and OVT–polyphenol complexes.....	130
Table VII-1. Emulsified phase volume fraction and stability index of Pickering emulsions stabilized by OVT fibrils at different fibril concentrations and oil fractions.....	149
Table VII-2. Emulsified phase volume fraction and stability index of Pickering emulsions stabilized by OVT fibrils at different ionic strengths.....	157
Table VII-3. Emulsified phase volume fraction and stability index of Pickering emulsions stabilized by OVT fibrils at different pHs.....	164
Table VIII-1. Reaction rate constants (k) of curcumin degradation against UV light exposure in bulk MCT oil and OVT fibril-stabilized Pickering emulsions at different ionic strengths.....	183

Table VIII-2. Reaction rate constants (k) of curcumin degradation against UV light exposure in bulk MCT oil and OVT fibril-stabilized Pickering emulsions at different pHs.....	186
Table IX-1. Gel-sol melting temperature of soybean oil-based organogels structured by different amounts of monostearin or sugar ester.....	211
Table IX-2. Emulsified phase volume fraction and stability index of organogel-based Pickering emulsions stabilized by OVT fibrils at different oil fractions.....	216
Table IX-3. Emulsified phase volume fraction of freshly prepared conventional Pickering emulsions stabilized by OVT fibrils.....	225
Table IX-4. Emulsified phase volume fraction of conventional Pickering emulsions stabilized by OVT fibrils after freezing for 24 h but without thawing.....	226

LIST OF ILLUSTRATIONS

Figure I-1. Structure of hen apo-ovotransferrin (A) and holo-ovotransferrin (B).....	1
Figure I-2. Biological benefits of ovotransferrin.....	2
Figure I-3. TEM micrographs of whey protein isolate fibril solution.....	3
Figure I-4. Microscopic processes underlying amyloid formation and associated rate constants and reaction rates.....	4
Figure I-5. (a) Publication per year analyzed by Web of Science using search item “Pickering emulsion”. (b) Number of citation per year analyzed by Web of Science using search item “Pickering emulsion”.....	5
Figure I-6. Pie chart about the number of articles about food grade Pickering emulsions and non-food Pickering emulsions from year 2014 to 2017.....	6
Figure I-7. Multiple biological activities of turmeric/curcumin.....	7
Figure I-8. Schematic presentation of TIM-1 model.....	8
Figure I-9. Schematic of an in vitro digestion model used to determine the digestion and release of lipids.....	9
Figure I-10. Photographs and optical microscope images of grapeseed oil gels.....	10
Figure II-1. ThT fluorescence intensity of OVT after heating at different pHs and temperatures...28	28
Figure II-2. AFM images of OVT after heating at different pHs and temperatures for 24 h.....	30
Figure II-3. SDS-PAGE profiles (15% separating gel) of OVT after heating at different pHs and temperatures.....	31
Figure II-4. (a) ThT fluorescence intensity for different concentrations of OVT after heating at pH 2 and 90 °C. (b) ThT fluorescence intensity of OVT heated at different ionic strengths. (c) ThT fluorescence intensity of OVT heated at different stirring speeds.....	33
Figure II-5. AFM images of OVT after heating at pH 2 and 90 °C at different protein concentrations for 24 h: (a) 10 mg/mL, (b) 20 mg/mL, (c) 40 mg/mL.....	34
Figure II-6. AFM images of OVT at different ionic strengths after heating at pH 2 and 90 °C for 24 h.....	35
Figure II-7. AFM images of OVT amyloid fibrils prepared at different stirring speeds for 24 h: (a) 0, (b) 100 rpm, (c) 300 rpm.....	37
Figure II-8. ThT fluorescence intensity for OVT solution as function of heating time. OVT solution (40 mg/mL, ionic strength I = 150 mM) was heated at pH 2 and 90 °C under magnetic stirring (300 rpm).....	38
Figure II-9. AFM images of OVT after heating at pH 2 and 90 °C for different periods: (a) 0 h, (b) 1 h, (c) 3 h, (d) 6 h, (e) 9 h, (f) 12 h, (g) 18 h, (h) 24 h. The scan size is 4 μm×4 μm, and the z scale is 20 nm. The scale bar represents 400 nm.....	40
Figure II-10. Far-UV CD spectra of OVT after heat treatment at pH 2.0.....	41
Figure II-11. Section analysis of OVT amyloid fibrils in the purpose of checking periods of OVT	

fibrils.....	43
Figure II-12. <i>In vitro</i> cytotoxicity of OVT amyloid fibrils on cells as measured by MTT assay.....	45
Figure III-1. AFM images of OVT fibrils after different periods of simulated gastric digestion: (a) 0 h, (b) 0.5 h, (c) 1 h, (d) 2 h, (e) 3 h, (f) 4 h.....	57
Figure III-2. AFM image of OVT fibrils after simulated intestinal digestion.....	59
Figure III-3. Zeta potential of OVT fibrils and OVT control as function of pH.....	60
Figure III-4. AFM images of OVT fibrils after 144-h room-temperature storage at different pHs: (a) pH 2, (b) pH 3, (c) pH 4, (d) pH 5, (e) pH 6, (f) pH 7, (g) pH 7.5, (h) pH 8, (i) pH 9, (j) pH 10. The scan size is 4 $\mu\text{m}\times 4\ \mu\text{m}$, and the z scale is 20 nm. The scale bar represents 400 nm.....	62
Figure III-5. AFM images of β -lactoglobulin fibrils after 144-h room-temperature storage at different pHs: (a) pH 2, (b) pH 3, (c) pH 4, (d) pH 5, (e) pH 6, (f) pH 7, (g) pH 8, (h) pH 9, (i) pH 10. The scan size is 10 $\mu\text{m}\times 10\ \mu\text{m}$, and the z scale is 20 nm.....	66
Figure III-6. AFM images of OVT fibrils before and after treatment of frozen storage–lyophilization–rehydration: (a) control, (b) after treatment of frozen storage–lyophilization–rehydration.....	67
Figure III-7. AFM images of OVT fibrils after treatment of high-speed shearing (a) 0 rpm (b) 3500 rpm (c) 5000 rpm (d) 6000 rpm (e) 8000 rpm (f) 12000 rpm. The scan size is 2 $\mu\text{m}\times 2\ \mu\text{m}$, and the z scale is 20 nm. The scale bar represents 200 nm.....	69
Figure IV-1. (a) ThT fluorescence intensity of OVT (ovotransferrin) heated at pH 2 and 90 °C in the presence of different levels (% w/v) of glycerol. (b) ThT fluorescence intensity of OVT heated at pH 2 and 90 °C in the presence of different levels (% w/v) of sorbitol.....	78
Figure IV-2. (a) SDS-PAGE profiles of OVT after heating at 90 °C for 3 h in the presence of different concentrations of glycerol. (b) SDS-PAGE profiles of OVT after heating at 90 °C for 3 h in the presence of different concentrations of sorbitol.....	81
Figure IV-3. (a) SDS-PAGE profiles of OVT after heating at 90 °C for 24 h in the presence of different concentrations of glycerol. (b) SDS-PAGE profiles of OVT after heating at 90 °C for 24 h in the presence of different concentrations of sorbitol.....	83
Figure IV-4. Schematic illustrations about fibrillation pathways of OVT.....	84
Figure IV-5. AFM images of OVT fibrils in the presence of different levels of glycerol: (a) control, (b) 20% glycerol, (c) 40% glycerol, (d) 60% glycerol.....	86
Figure IV-6. AFM images of OVT fibrils in the presence of different levels of sorbitol: (a) sorbitol, (b) 20% sorbitol, (c) 40% sorbitol, (d) 60% sorbitol.....	87
Figure V-1. SDS-PAGE profiles of OVTC, OGC and OLC. Lanes from left to right are protein marker, OVTC, OGC and OLC.....	96
Figure V-2. Free amino groups of OVTC, OGC and OLC.....	97
Figure V-3. Surface hydrophobicity of OVTC fibril, OGC fibril and OLC fibril.....	97
Figure V-4. Zeta potential of OVTC, OGC, OLC, OVTC fibril, OGC fibril and OLC fibril.....	98
Figure V-5. Thioflavin T (ThT) fluorescence of OVTC, OGC and OLC after heating at 90°C and pH 2.....	100
Figure V-6. SDS-PAGE profiles (12% separating gel) of OVTC, OGC and OLC after heating at pH 2 and 90°C for 24 h.....	101
Figure V-7. AFM images of nanofibrils derived from OVTC, OGC and OLC: (a) OVTC fibrils with short or medium length, (b) long OVTC fibrils (c) OGC fibrils, (d) OLC fibrils. The scan size is 4 $\mu\text{m}\times 4\ \mu\text{m}$, and the z scale is 15 nm. The scale bar represents 400 nm.....	103

Figure V-8. Contour length distribution of fibrils analyzed from AFM images: (a) OVTC fibrils, (b) OGC fibrils, (c) OLC fibrils.....	104
Figure V-9. Visual observation of Pickering emulsions stabilized by fibrils (OVTC fibrils, OGC fibrils and OLC fibrils) with different c (2–4 wt%) at various ϕ (0.45–0.65).....	105
Figure V-10. Optical microscopic images of Pickering emulsions stabilized by fibrils (OVTC fibrils, OGC fibrils and OLC fibrils) at the fixed fibril concentration of 4 wt% and oil fraction of 0.65.....	107
Figure VI-1. SDS-PAGE profiles (10% separating gel) of OVT and OVT–polyphenol covalent complexes.....	118
Figure VI-2. Thioflavin T (ThT) fluorescence of OVT and OVT–polyphenol complexes after heating at 90°C and pH 2.0.....	121
Figure VI-3. SDS-PAGE profiles (12% separating gel) of OVT and OVT–polyphenol complexes after heating at pH 2.0 and 90°C for 24 h. For Figure a, lanes from left to right are marker, heated OVT, OEC-L, OEC-M, OEC-H, OEP-L, OEP-M and OEP-H. For Figure b, lanes from left to right are marker, heated OVT, OGC-L, OGC-M, OGC-H, OGP-L, OGP-M and OGP-H.....	123
Figure VI-4. AFM images of nanofibrils derived from OVT and OVT–EGCG complexes after heating at pH 2.0 and 90°C for 24 h: (a) OVT, (b) OEC-L, (c) OEC-M, (d) OEC-H, (e) OEP-L, (f) OEP-M, (g) OEP-H.....	125
Figure VI-5. AFM images of nanofibrils derived from OVT and OVT–GA complexes after heating at pH 2.0 and 90°C for 24 h.	128
Figure VII-1. (a) AFM image of OVT nanofibrils. The scan size is 4 $\mu\text{m}\times 4\ \mu\text{m}$, and the z scale is 10 nm. The scale bar in the upper left corner represents 400 nm. (b) Contour length distribution of OVT fibrils analyzed from AFM images.....	143
Figure VII-2. Raman microscopy image of Pickering emulsion droplet stabilized by OVT fibrils ($c = 3.5\ \text{wt}\%$, $\phi = 0.6$). The scale bar in the lower right corresponds to 10 μm	144
Figure VII-3. CLSM image of Pickering emulsion ($\phi=0.7$) stabilized by OVT fibrils ($c = 3.5\ \text{wt}\%$): (a) excitation at 488 nm, (b) excitation at 355 nm. Oil dyed with Nile red was shown in red, and OVT fibrils stained with thioflavin T (ThT) were shown in blue. The scale bar within the figure is 50 μm in length.....	145
Figure VII-4. Fluorescence microscopy images of Pickering emulsions stabilized by OVT fibrils at the fixed concentration of 3.5 wt% and oil fraction of 0.6. The white scale bar in the lower right is 60 μm in length.....	146
Figure VII-5. Visual observation of Pickering emulsions stabilized by OVT fibrils with different c (0.5–3.5 wt%) at various ϕ (0.5–0.7). The photographs were taken at 3 h and 20 days after preparation of fresh emulsions, and the storage was carried out at 20 °C.....	147
Figure VII-6. Optical microscopic images of emulsions stabilized by OVT fibrils with different c (0.5–3.5 wt%) at the fixed oil fraction of 0.5: (a) $c = 0.5\ \text{wt}\%$, (b) $c = 1.5\ \text{wt}\%$, (c) $c = 2.5\ \text{wt}\%$, (d) $c = 3.5\ \text{wt}\%$. The scale bars within the figures are 100 μm in length.....	151
Figure VII-7. Optical microscopic images of emulsions stabilized by OVT fibrils ($c = 3.5\ \text{wt}\%$) at different oil fractions (ϕ): (a) $\phi = 0.5$, (b) $\phi = 0.6$, (c) $\phi = 0.7$. The scale bars within the figures are 100 μm in length.....	151
Figure VII-8. (a) Average droplet size of freshly prepared Pickering emulsions stabilized by OVT fibrils with different c (0.5–3.5 wt%) at the fixed oil fraction of 0.5. (b) Average droplet size of freshly prepared Pickering emulsions stabilized by OVT fibrils ($c = 3.5\ \text{wt}\%$) at different oil	

fractions. (c) Average droplet size of Pickering emulsions stabilized by OVT fibrils with different c (0.5–3.5 wt%) at the fixed oil fraction of 0.5 after 20-day storage at 20 °C. (d) Average droplet size of Pickering emulsions stabilized by OVT fibrils ($c = 3.5$ wt%) at different oil fractions after 20-day storage at 20 °C.....	152
Figure VII-9. (a) Storage modulus (G') and loss modulus (G'') of Pickering emulsions stabilized by OVT fibrils with different c (0.5–3.5 wt%) at the fixed oil fraction of 0.5. (b) Storage modulus (G') and loss modulus (G'') of Pickering emulsions stabilized by OVT fibrils ($c = 3.5$ wt%) at different oil fractions.....	153
Figure VII-10. (a) Apparent viscosity of Pickering emulsions stabilized by OVT fibrils with different c (0.5–3.5 wt%) at the fixed oil fraction of 0.5. (b) Apparent viscosity of Pickering emulsions stabilized by OVT fibrils ($c = 3.5$ wt%) at different oil fractions.....	154
Figure VII-11. Visual observation of Pickering emulsions stabilized by OVT fibrils ($c = 3.5$ wt%, $\varphi = 0.7$) at different ionic strengths. All photographs were taken at 3 h and 20 days after preparation of fresh emulsions, and the storage was carried out at 20 °C.....	156
Figure VII-12. Influence of ionic strength (0–1000 mM) on electrophoresis mobility of OVT fibril dispersion at pH 2.....	158
Figure VII-13. Optical microscopic images of freshly prepared emulsions stabilized by OVT fibrils ($c = 3.5$ wt%, $\varphi = 0.7$) at different ionic strengths: (a) 0 mM, (b) 100 mM, (c) 300 mM, (d) 500 mM, (e) 1000 mM. The scale bars within the figures are 100 μm in length.....	160
Figure VII-14. (a) Average droplet size of freshly prepared Pickering emulsions stabilized by OVT fibrils ($c = 3.5$ wt%, $\varphi = 0.7$) at different ionic strengths. (b) Average droplet size of Pickering emulsions stabilized by OVT fibrils ($c = 3.5$ wt%, $\varphi = 0.7$) at different ionic strengths after 20-day storage at 20 °C.....	160
Figure VII-15. (a) Storage modulus (G') and loss modulus (G'') of Pickering emulsions stabilized by OVT fibrils ($c = 3.5$ wt%, $\varphi = 0.7$) at different ionic strengths.....	161
Figure VII-16. Zeta potential of OVT fibril dispersion as function of pHs.....	162
Figure VII-17. Visual observation of Pickering emulsions stabilized by OVT fibrils ($c = 3.5$ wt%, $\varphi = 0.7$) at different pHs. All photographs were taken at 3 h and 20 days after preparation of fresh emulsions, and the storage was carried out at 20 °C.....	163
Figure VII-18. Optical microscopic images of emulsions stabilized by OVT fibrils ($c = 3.5$ wt%, $\varphi = 0.7$) at different pHs: (a) pH 2, (b) pH 3, (c) pH 4, (d) pH 5, (e) pH 6, (f) pH 7. The scale bars within the figures are 100 μm in length.....	165
Figure VII-19. (a) Average droplet size of freshly prepared Pickering emulsions stabilized by OVT fibrils ($c = 3.5$ wt%, $\varphi = 0.7$) at different pHs. (b) Average droplet size of Pickering emulsions stabilized by OVT fibrils ($c = 3.5$ wt%, $\varphi = 0.7$) at different pHs after 20-day storage at 20 °C..	166
Figure VII-20. (a) Storage modulus (G') and loss modulus (G'') of Pickering emulsions stabilized by OVT fibrils ($c = 3.5$ wt%, $\varphi = 0.7$) at different pHs. (b) Apparent viscosity of Pickering emulsions stabilized by OVT fibrils ($c = 3.5$ wt%, $\varphi = 0.7$) at different pHs.....	167
Figure VII-21. Visual observation of Pickering emulsions stabilized by OVT fibrils at fibril concentration of 3.5 wt% and oil fraction of 0.7 before and after storage at 50 °C for 10 days...	169
Figure VII-22. Optical microscopic images of emulsions stabilized by OVT fibrils at fibril concentration of 3.5 wt% and oil fraction of 0.7 after storage at 50 °C for 10 days. The scale bar within the figure is 100 μm in length.....	169
Figure VIII-1. (a) Visual appearance of curcumin-loaded Pickering emulsions stabilized by OVT	

fibrils at different ionic strengths. (b) Residual curcumin level in bulk MCT oil and Pickering emulsions stabilized by OVT fibrils at different ionic strengths after UV radiation.....	182
Figure VIII-2. (a) Visual appearance of curcumin-loaded Pickering emulsions stabilized by OVT fibrils at different pHs. The emulsions from left to right are stabilized at pH 2, 4 and 6, respectively. (b) Residual curcumin level in bulk MCT oil and Pickering emulsions stabilized by OVT fibrils at different pHs after UV radiation.....	184
Figure VIII-3. Bioaccessible curcumin (% of input) within a specified period of time after feeding MCT oil and OVT fibril-stabilized Pickering emulsion in TIM-1 model. The samples were analyzed every 30 min during the first 2 h, and they were analyzed every 60 min during the following 4 hours. (a) Bioaccessible curcumin from jejunum section of the TIM-1 system. (b) Bioaccessible curcumin from ileum section of the TIM-1 system. (c) Total bioaccessible curcumin from both jejunum and ileum sections of the TIM-1 system.....	189
Figure VIII-4. Cumulative curcumin bioaccessibility after feeding MCT oil and OVT fibril-stabilized Pickering emulsion in TIM-1 model: (a) from jejunum section of the TIM-1 system; (b) from ileum section of the TIM-1 system. (c) from both jejunum and ileum sections of the TIM-1 system.....	191
Figure VIII-5. (a) Release profile of free fatty acids (FFA) in MCT oil and OVT fibril-stabilized Pickering emulsion in pH-stat digestion model. (b) The extent of lipolysis of MCT oil and OVT fibril-stabilized Pickering emulsion in pH-stat digestion model.....	192
Figure VIII-6. The bioaccessibility of curcumin in MCT oil and OVT fibril-stabilized Pickering emulsion in pH-stat digestion model.....	194
Figure IX-1. Metastable solubility of hesperidin in soybean oil.....	209
Figure IX-2. (a) Photograph of hesperidin-loaded organogel structured by 3% (w/v) monostearin. (b) Photograph of inverted hesperidin-loaded organogel after inverting the vial for 30 min.....	211
Figure IX-3. (a) AFM image of long OVT fibrils. The scan size is 4 $\mu\text{m} \times 4 \mu\text{m}$, and the scale bar in the upper left corner represents 400 nm. (b) AFM image of short OVT fibrils.....	213
Figure IX-4. Visual observation of organogel-based Pickering emulsions stabilized by OVT fibrils at various ϕ (0.50–0.85) before and after storage at room temperature. The oil fraction ϕ is labeled in each vial.....	214
Figure IX-5. (a) Optical microscopic image of freshly prepared organogel-based Pickering emulsion (oil fraction $\phi = 0.7$, ionic strength = 0) stabilized by OVT fibrils. (b) Optical microscopic image of organogel-based Pickering emulsion (oil fraction $\phi = 0.7$, ionic strength = 0) stabilized by OVT fibrils after three freeze-thaw cycles.....	218
Figure IX-6. (a) Fluorescence image of organogel-based Pickering emulsion (stained with Nile red only). (b) Fluorescence image of organogel-based Pickering emulsion (stained with rhodamine B only).....	219
Figure IX-7. (a) Apparent viscosity of organogel and organogel-based Pickering emulsion (oil fraction $\phi = 0.7$, ionic strength = 0) stabilized by OVT fibrils. (b) Storage modulus (G') and loss modulus (G'') of organogel and organogel-based Pickering emulsion (oil fraction $\phi = 0.7$, ionic strength = 0) stabilized by OVT fibrils.....	221
Figure IX-8. Visual observation of initial and freeze-thawed organogel-based Pickering emulsions (oil fraction $\phi = 0.7$) stabilized by OVT fibrils. Organogel-based Pickering emulsions (from left to right) were prepared at an ionic strength of 0, 100, 300 and 500 mM, respectively.....	222
Figure IX-9. (a) Visual observation of organogel-based Pickering emulsions stabilized by OVT fibrils after freezing for 24 h but without thawing (b) Visual observation of organogel-based	

Pickering emulsions stabilized by OVT fibrils after freezing for 24 h and thawing for 0.5 h. Organogel-based Pickering emulsions (from left to right) were prepared at an ionic strength of 0, 100, 300 and 500 mM, respectively.....	223
Figure IX-10. Visual observation of initial and freeze-thawed conventional Pickering emulsions stabilized by OVT fibrils (oil fraction $\phi = 0.7$).....	224
Figure IX-11. (a) Visual observation of conventional Pickering emulsions stabilized by OVT fibrils after freezing for 24 h but without thawing (b) Visual observation of conventional Pickering emulsions stabilized by OVT fibrils after freezing for 24 h and thawing for 0.5 h.....	225
Figure IX-12. (a) Release profile of free fatty acids (FFA) in organogel and organogel-based Pickering emulsion (oil fraction $\phi = 0.7$, ionic strength = 0) stabilized by OVT fibrils. (b) The bioaccessibility of hesperidin in organogel and organogel-based Pickering emulsion (oil fraction $\phi = 0.7$, ionic strength = 0) stabilized by OVT fibrils after <i>in vitro</i> digestion.....	229

CHAPTER I. INTRODUCTION

1. Key Concepts Involved in Thesis

1.1. Ovotransferrin (OVT)

Ovotransferrin (OVT) is an important species of egg white proteins, and OVT accounts for about 12% of egg white proteins. OVT was first called conalbumin, and it was renamed ovotransferrin after it was identified as a transferrin. Like other members of transferrin family such as lactoferrin, ovotransferrin has apo- and holo-form (*1*). As shown in Figure I-1, structures of hen apo-ovotransferrin and holo-ovotransferrin are different. OVT, which contains about 686 amino acids, consists of N-lobe and C-lobe linked by an alpha helix. The iron-binding site is located in each lobe of OVT (*1*). Unlike serum transferrin, OVT may contain a small amount of carbohydrate moieties. When compared with ovalbumin (the major component of egg white proteins), ovotransferrin has better solubility.

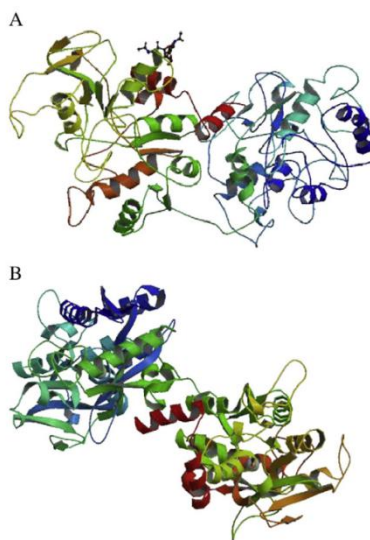


Figure I-1. Structure of hen apo-ovotransferrin (A) and holo-ovotransferrin (B).

(Reprinted from reference 1)

As shown in Figure I-2, OVT may have multiple biological benefits such as anticancer, antiviral, antimicrobial, osteogenic, antioxidant and anti-colitis activities (2–6), and peptides derived from ovotransferrin may have bioactivities such as antihypertensive and anti-inflammatory activity (7, 8). Thus, OVT has potential to be widely utilized in design and engineering of functional foods.

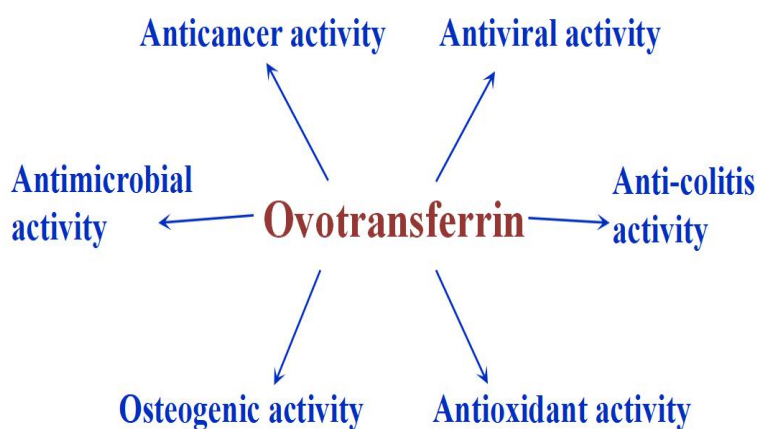


Figure I-2. Biological benefits of ovotransferrin

However, since extraction procedures of ovotransferrin are very complicated and extraction yield of ovotransferrin is very low, research about ovotransferrin has not been widely investigated yet (6, 9). At present, most of ovotransferrin studies focus on extraction and structural characterization (10–13), and application of ovotransferrin in constructing food polymeric structures and delivery systems has seldom been done due to shortage of OVT materials. Conducting related research may deepen understandings of ovotransferrin and facilitate design of food polymeric structures

and nutraceutical delivery systems using ovotransferrin as building blocks.

1.2. Protein fibrillation and application of fibrils

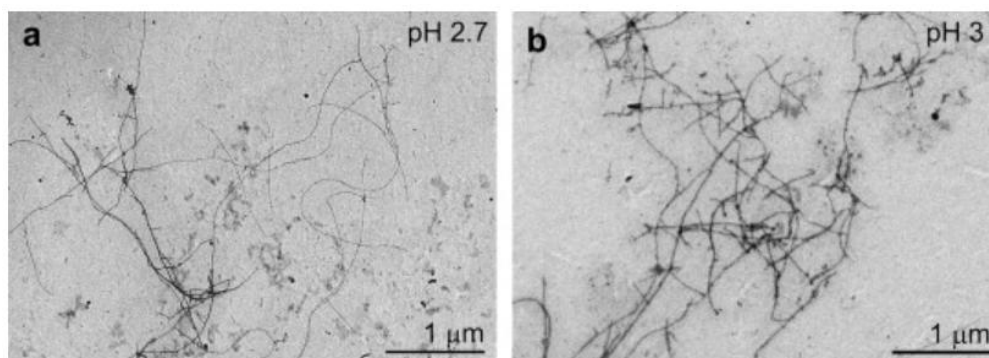


Figure I-3. TEM micrographs of whey protein isolate fibril solution (Reprinted from reference 14)

Proteins may assemble into amyloid (or amyloid-like) fibrils, which have recently attracted increasing attention. As shown in Figure I-3, amyloid protein fibrils generally have linear structures and large length-to-width ratio (14). Since protein fibrils have unique structures and shapes, it is expected that protein fibrils may have unique physicochemical properties and can be utilized in many specific situations (15). In addition, amyloid fibrils are thought to be associated with many diseases such as Alzheimer or Parkinson disease (16). Generally, protein fibrils can be generated at high temperatures. As Figure I-4 shows, there is generally a lag phase during protein fibrillation. During lag phase many microscopic processes including primary nucleation, elongation, secondary nucleation and fragmentation may occur (15). Up to now it proves that some proteins can form protein fibrils (17–19). At the same time, previous studies reveal that some proteins cannot generate protein fibrils. It is

expected that OVT applied in this study may generate protein fibrils, which can be further utilized in constructing food systems.

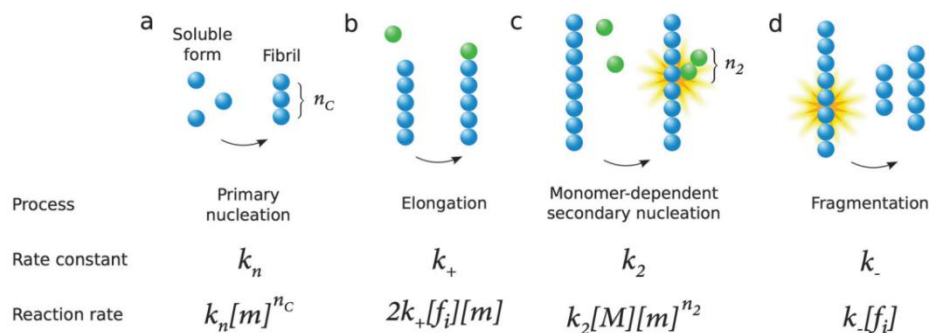
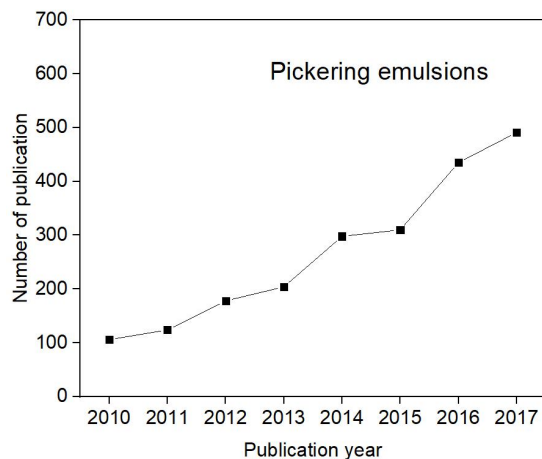


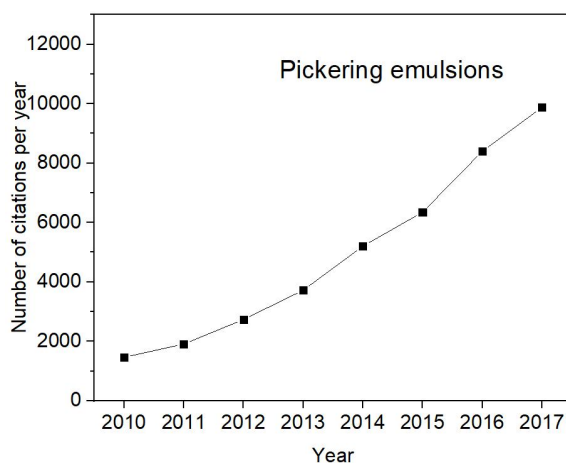
Figure I-4. Microscopic processes underlying amyloid formation and associated rate constants and reaction rates. (Reprinted from reference 15)

Protein fibrils have been applied in many systems due to its excellent properties such as foaming property and so on (20, 21). One previous study shows that amyloid fibril systems may deliver bioavailable iron, suggesting that protein fibrils can be utilized to deliver many nutraceuticals like minerals (22). Another study reveals that inexpensive fibrils can form special composite materials with graphene, and the composite materials have shape-memory and enzyme-sensing properties, indicating that fibrils can be used in biosensor design for detecting enzyme activity (23). Based on these understandings, protein fibrils are prospective biomaterials, which may find great application in many fields.

1.3. Pickering emulsion



(a)



(b)

Figure I-5. (a) Publication per year analyzed by Web of Science using search item “Pickering emulsion”. (b) Number of citation per year analyzed by Web of Science using search item “Pickering emulsion”.

Unlike conventional emulsions stabilized by surfactants or proteins, Pickering emulsions are stabilized by solid particles (24–26). Due to excellent physical stability and limited coalescence of Pickering emulsions, Pickering emulsions have received renewed interest during the past few years (27). As shown in Figure I-5, the increasing attention about Pickering emulsions can be reflected in publication per year and number of citation per year about Pickering emulsions. Successful preparation of

Pickering emulsions requires proper Pickering emulsifiers. Solid particles have to meet some prerequisites to function well as qualified Pickering emulsifiers. Specifically speaking, the particles should not be soluble in either water phase or oil phase. The size of solid particles should be much smaller than the size of emulsion droplets. In addition, the solid particles should have partial wettability (26).

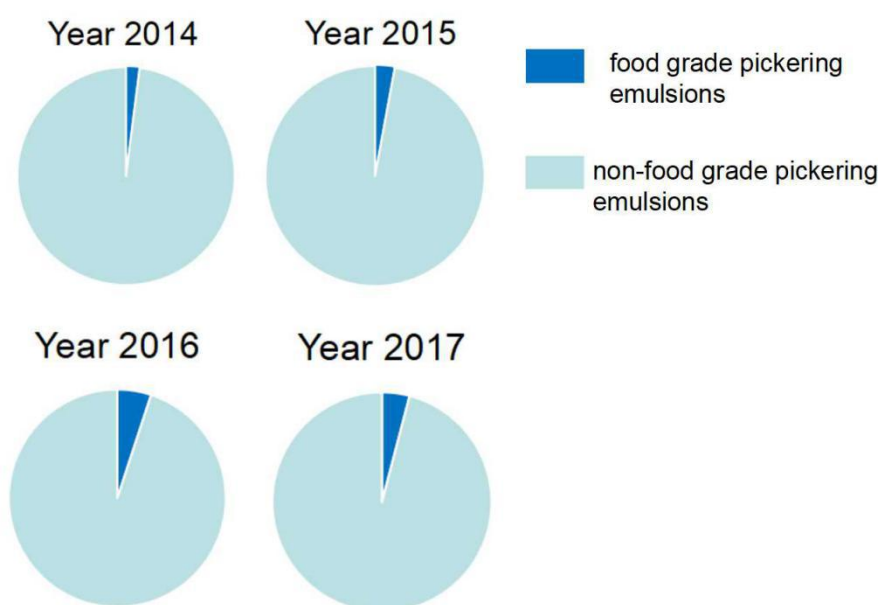


Figure I-6. Pie chart about the number of articles about food grade Pickering emulsions and non-food Pickering emulsions from year 2014 to 2017.

Till now most of investigated Pickering emulsions are stabilized by inorganic particles such as silica, latex and clay (28–30). However, these Pickering emulsions stabilized by inorganic particles cannot be applied in food systems due to low biocompatibility and biodegradability. Therefore, developing food-grade Pickering emulsions is urgent. As Figure I-6 shows, Pickering emulsions can be clarified into food grade Pickering emulsions and non-food Pickering emulsions, and food grade

Pickering emulsions only occupy a small portion of all Pickering emulsions. That is because there are not enough food-grade Pickering emulsifiers. Therefore, we should prepare more food-grade Pickering emulsifiers to enhance application of food-grade Pickering emulsions.

There are generally two methods to fabricate Pickering emulsifiers: bottom-up assembly and breakdown. Breakdown methods include mechanical or chemical breakdown (26). In terms of bottom-up assembly, complexation between proteins and polysaccharides as well as protein fibrillation can be used to fabricate colloidal particles as Pickering emulsifiers (31, 32).

1.4. *In vitro* digestion model of emulsions and bioaccessibility of nutraceuticals

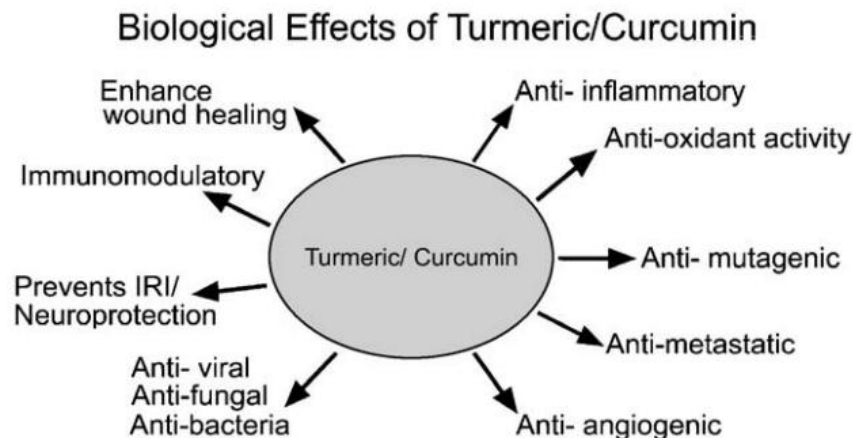


Figure I-7. Multiple biological activities of turmeric/curcumin. (Reprinted from reference 33)

As shown in Figure I-7, a lot of nutraceuticals like curcumin have various biological benefits (33, 34). However, the bioefficacy of these nutraceuticals are often very low due to poor dispersibility and bioaccessibility (35). Thus, these

nutraceuticals are often encapsulated into emulsions to improve dispersibility and bioaccessibility, and it is expected that these nutraceuticals can be absorbed by digestion system and utilized in target parts of our body. Since food emulsions will be digested after oral ingestion and we need to know the fate of encapsulated nutraceuticals, *in vitro* digestion model of emulsions will be applied to understand these aspects.

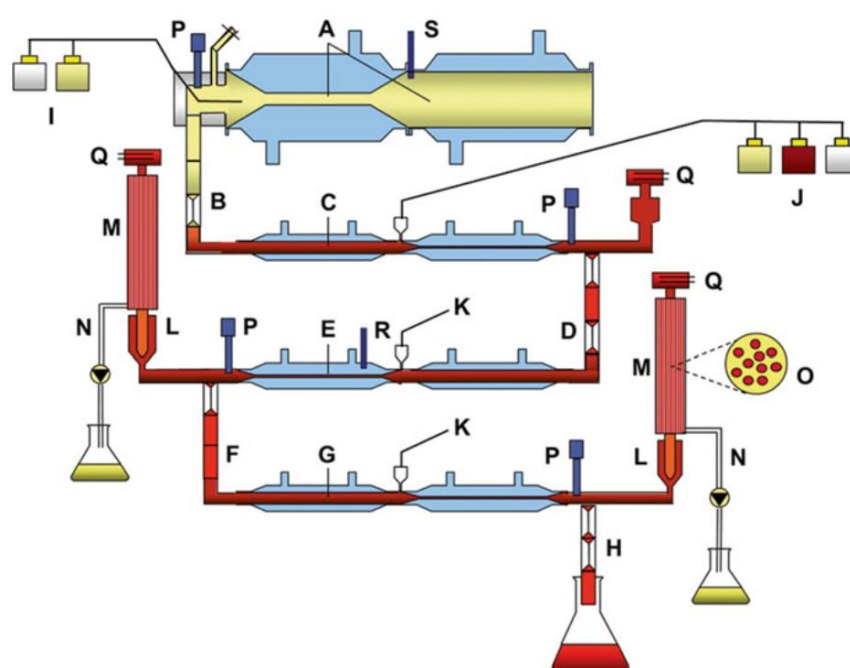


Figure I-8. Schematic presentation of TIM-1 model. (Reprinted from reference 36)

Two digestion models may be applied in our research. As shown in Figure I-8, TIM-1 model (TNO Intestinal Model) is a dynamic digestion model, and TIM-1 model consists of four major compartments: gastric compartment, duodenal compartment, jejunal compartment and ileal compartment (36). There are many advantages of TIM-1 model. Specifically, it considers realistic secretion and removal

of digested compounds. Meanwhile, dynamic conditions in the gastrointestinal tract are taken into account, and TIM-1 model can simulate the peristaltic movements of the small intestine. Overall, TIM-1 model is a good tool to simulate digestion in the upper gastrointestinal tract.

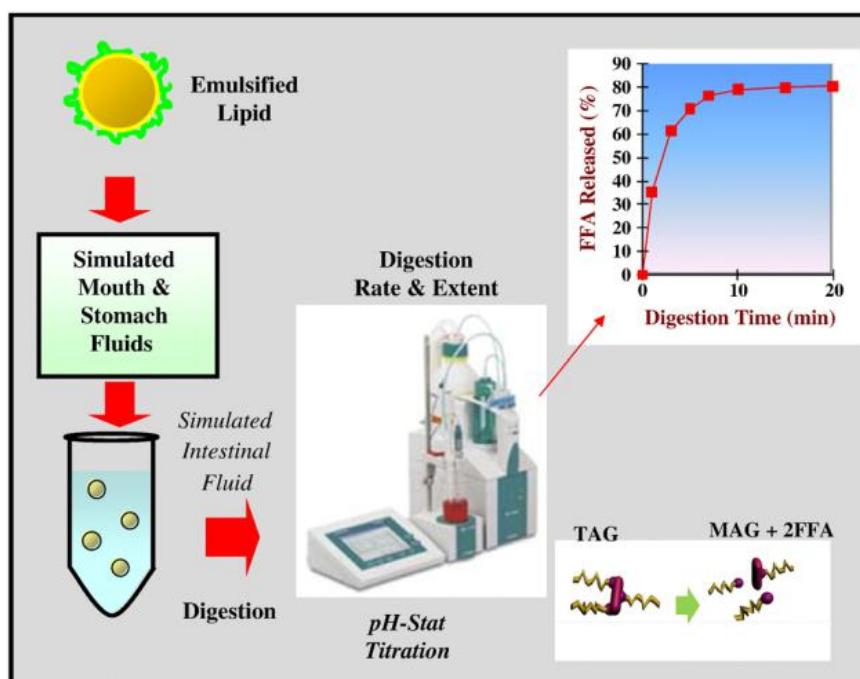


Figure I-9. Schematic of an in vitro digestion model used to determine the digestion and release of lipids. (Reprinted from reference 37)

Another digestion model used in our study is often called pH-stat digestion model. As shown in Figure I-9, pH-stat digestion model is a static digestion model (37). Only several parameters such as pH conditions, enzyme compositions and ionic strength in simulated digestion fluids are considered (38). In pH-stat digestion model, realistic secretion, removal of digested compounds and dynamic conditions in the gastrointestinal tract are all ignored, which may lead to deviations in analysis.

However, we can often obtain lipolysis data of emulsions using pH-stat digestion model. It is interesting to study digestion profile of emulsions and bioaccessibility of nutraceuticals using both TIM-1 model and pH-stat digestion model. The obtained data analyzed by two digestion models may help to predict bioaccessibility of nutraceuticals in realistic conditions precisely.

1.5. Organogel-based delivery systems

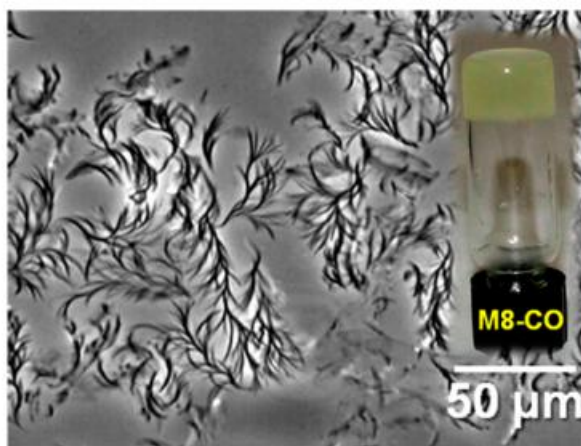


Figure I-10. Photographs and optical microscope images of grapeseed oil gels. (Reprinted from reference 40)

Organogels are a class of gels composed of organic liquids entrapped within three-dimensional cross-linked and thermo-reversible networks, and organogels have found many potential applications in food industry (39). As shown in Figure I-10, organogels can withstand inversion test, suggesting high viscosity of food-grade organogels (40). Organogel-based delivery systems have recently attracted a lot of attention during the past few years, and organogel-based emulsion is one kind of organogel-based delivery systems. Organogel-based emulsions applied in food

science are first developed by our research group (41, 42), and multiple studies have demonstrated that organogel-based emulsions could improve loading of nutraceuticals, increase nutraceutical bioaccessibility and reduce gastric mucosa irritation (42, 43). However, to the best of our knowledge, no organogel-based Pickering emulsions have been developed in field of food science. Considering that food-grade Pickering emulsions have many advantages than food-grade conventional emulsions and organogels are quite different from liquid oil, organogel-based Pickering emulsions may own many other advantages when compared with conventional emulsions. Thus, it is intriguing to investigate organogel-based Pickering emulsions.

2. Research Rationale and Hypothesis

Protein-based materials have found increasing and wide applications in food industry. Food proteins have potential to develop nutraceutical delivery systems with proteins as building blocks, and the delivery matrices may protect and improve bioaccessibility of delivery-sensitive nutraceutical compounds. Since some nutraceutical compounds may degrade rapidly under environmental stresses and have poor bioaccessibility due to factors such as inferior dispersibility, developing nutraceutical delivery systems with desirable properties for some nutraceutical compounds is extremely urgent. Till now, milk proteins and many prolamins have been utilized to develop food-grade nutraceutical delivery systems. Apart from milk proteins and many prolamins, egg white proteins have recently attracted increasing attention due to abundant resources, cost saving, environmental friendliness, biocompatibility and biodegradability. However, ovalbumin occupies more than half

of egg white proteins, and the poor solubility and great tendency to form gel-like structures inhibit application of egg white proteins. One approach to improve utilization degree of egg white proteins is to apply other components of egg white proteins except ovalbumin. Ovotransferrin, which accounts for about 12% of egg white proteins, attracts more and more research interests especially during these years due to excellent solubility. Meanwhile, ovotransferrin has multiple biological benefits such as anticancer, antiviral, antimicrobial, osteogenic, antioxidant and anti-colitis activities. Thus, it is expected ovotransferrin can be widely used in design of food polymeric structures and related nutraceutical delivery systems. However, since extraction procedures of ovotransferrin are very complicated and extraction yield of ovotransferrin is very low, research about ovotransferrin has not been widely investigated yet. At present, most of ovotransferrin studies focus on extraction and structural characterization, and application of ovotransferrin in constructing food polymeric structures and delivery systems has seldom been done. It is of interest and essential to further understand physicochemical properties of ovotransferrin and how ovotransferrin can be utilized as building blocks in different food systems and nutraceutical delivery vehicles.

Protein fibrils derived from food proteins have recently attracted a lot of scholarly attention, and that is because food protein fibrils have excellent properties such as emulsifying property and foaming property. However, physicochemical properties of many food protein fibrils have not been systematically investigated, which hinders application of food protein fibrils. Till now, most of fibril studies focus

on fibrils derived from whey protein isolate, lysozyme and β -lactoglobulin, and the knowledge from these protein fibrils may not apply to ovotransferrin fibrils. Thus, it is interesting and necessary to understand preparation, digestion, stability, building blocks and many other properties of ovotransferrin fibrils.

There are many food ingredients in complex food systems, and these ingredients include sugars, polyphenols, polyols and so on. Interactions between proteins and these food components may be inevitable, which could affect stability and physicochemical properties of protein fibrils. Therefore, it is interesting and necessary to study impact of interactions between food ingredients and proteins on protein fibrils.

Pickering emulsions and organogel-based emulsions are important food systems and nutraceutical delivery vehicles. These food systems may be stabilized by several food polymeric structures and have potential to increase bioaccessibility of nutraceuticals. Considering that protein fibrils generally have good emulsibility, ovotransferrin fibrils can be applied in Pickering emulsions and organogel-based emulsions. A comprehensive study about ovotransferrin fibril-stabilized emulsion systems may facilitate design of emulsion delivery systems with better physicochemical properties.

Based on these understandings, current literature reports and our primary research results, I hypothesize that:

- (1) Fibrillation of ovotransferrin is feasible, and ovotransferrin fibrils can tolerate environmental stresses and maintain stable at various pHs, which ensure that

ovotransferrin fibrils can be applied in design and construction of food delivery systems.

(2) Fibrillation of ovotransferrin can be affected by other food ingredients such as sugars, polyphenols and polyols.

(3) Ovotransferrin fibrils may potentially be applied as Pickering emulsifiers. Stable Pickering emulsions may be stable at different ionic strengths and pHs, and the Pickering emulsion system is a reliable delivery system.

(4) Pickering emulsions stabilized by ovotransferrin fibrils may protect nutraceuticals and increase bioaccessibility of nutraceuticals, and they are suitable nutraceutical delivery platforms.

(5) Organogel-based Pickering emulsions can be stabilized by OVT fibrils, and organogel-based Pickering emulsions may improve nutraceutical bioaccessibility.

We expect that the proposed project may deepen understandings of ovotransferrin fibrils and facilitate design of food polymeric structures and nutraceutical delivery systems using ovotransferrin as building blocks. In addition, the project may enhance utilization of ovotransferrin in practice, which is of great importance for U.S. agriculture and food systems.

3. Specific research objectives

This thesis will present seven specific research objectives to understand assembly, physicochemical properties and application of OVT fibrils.

3.1. Preparation, digestion and stability of OVT fibrils

Optimal formation conditions of OVT fibrils will be explored, and the

optimization parameters include protein concentration, stirring speed and so on. After successful preparation of OVT fibrils, physicochemical properties such as secondary structure and surface hydrophobicity of OVT fibrils will be investigated. *In vitro* digestion of OVT fibrils will be studied. Long-term storage stability of OVT fibrils over a wide range of pH may be examined. Stability of OVT fibrils under freeze-drying treatment will be studied.

3.2. Influence of polyols on OVT fibrils

With the aid of thioflavin T fluorescence, atomic force microscopy and sodium dodecyl sulfate polyacrylamide gel electrophoresis, impact of glycerol and sorbitol on the amount, morphology and building blocks of OVT fibrils will be investigated. By decoupling hydrolysis and self-assembly with glycerol as well as sorbitol, how protein hydrolysis and self-assembly processes modulate OVT fibrillation will be analyzed.

3.3. Influence of Maillard reaction on OVT fibrils

OVT is first glucosylated or lactosylated to obtain OVT–glucose conjugate and OVT–lactose conjugate, respectively. Influence of glucosylation and lactosylation on OVT fibrillation will be investigated. Finally, fibrils derived from OVT–saccharide conjugates are applied as Pickering emulsifiers in oil-in-water emulsions, and influence of glycation on Pickering emulsifier performance of OVT fibrils will be evaluated.

3.4. Influence of polyphenols on OVT fibrils

Epigallocatechin gallate (EGCG) and gallic acid (GA) are chosen as polyphenol models to study influence of polyphenols on OVT fibrils. OVT is first modified with

different amounts of EGCG or GA in non-covalent or covalent ways, and then investigate how the fibrillation and fibril properties can be modulated by polyphenol structures, polyphenol content and distinct OVT–polyphenol interactions.

3.5. Preparation of surfactant-free Pickering emulsions with OVT fibrils

Properties of OVT fibrils will be investigated to see if OVT fibrils meet the requirements of eligible Pickering emulsifiers. Pickering emulsions stabilized by OVT fibrils will be fabricated and characterized to explore visual appearance, microstructures and rheology properties of these Pickering emulsions. Pickering emulsions stabilized by OVT fibrils at different pHs and ionic strengths will be prepared. Visual appearance, microstructures and rheology properties of these Pickering emulsions at different pHs and ionic strengths will be studied.

3.6. Study *in vitro* digestion profiles of Pickering emulsions stabilized by OVT fibrils.

Curcumin will be selected as a model nutraceutical to be encapsulated in Pickering emulsions stabilized by OVT fibrils. Protective effects of these Pickering emulsions on curcumin will be studied. The digestion profiles of Pickering emulsions stabilized by OVT fibrils will be investigated in simulated gastric and intestinal fluid. Bioaccessibility of curcumin will be evaluated using two digestion models (TIM-1 and pH-stat), and the two bioaccessibility results will be compared.

3.7. Study organogel-based Pickering emulsions stabilized by OVT fibrils

Organogel-based Pickering emulsions stabilized by OVT fibrils will be prepared and characterized with tools such as microscopy and rheology. Freeze-thaw stability of organogel-based Pickering emulsions will be investigated and compared with that

of conventional Pickering emulsions (without organogels). Finally, *in vitro* lipolysis and hesperidin bioaccessibility in organogel-based Pickering emulsions will be examined.

4. References

1. Wu, J., & Acero-Lopez, A. (2012). Ovotransferrin: structure, bioactivities, and preparation. *Food Research International*, 46, 480–487.
2. Ibrahim, H. R., & Kiyono, T. (2009). Novel anticancer activity of the autocleaved ovotransferrin against human colon and breast cancer cells. *Journal of Agricultural and Food Chemistry*, 57, 11383–11390.
3. Kobayashi, Y., Rupa, P., Kovacs-Nolan, J., Turner, P. V., Matsui, T., & Mine, Y. (2015). Oral administration of hen egg white ovotransferrin attenuates the development of colitis induced by dextran sodium sulfate in mice. *Journal of Agricultural and Food Chemistry*, 63, 1532–1539.
4. Shang, N., & Wu, J. (2018). Egg white ovotransferrin shows osteogenic activity in osteoblast cells. *Journal of Agricultural and Food Chemistry*, 66, 2275–2282.
5. Son, M., Chan, C. B., & Wu, J. (2018). Egg white ovotransferrin-derived ACE inhibitory peptide ameliorates angiotensin II-stimulated insulin resistance in skeletal muscle cells. *Molecular Nutrition & Food Research*, 62, 1700602.
6. Varon, O., Allen, K. J., Bennett, D. C., Mesak, L. R., & Scaman, C. H. (2013). Purification and characterization of tinamou egg white ovotransferrin as an antimicrobial agent against foodborne pathogenic bacteria. *Food Research International*, 54, 1836–1842.
7. Majumder, K., Chakrabarti, S., Davidge, S. T., & Wu, J. (2013). Structure and activity study of egg protein ovotransferrin derived peptides (IRW and IQW) on endothelial inflammatory response and oxidative stress. *Journal of Agricultural and Food Chemistry*, 61, 2120–2129.
8. Majumder, K., Liang, G., Chen, Y., Guan, S., Davidge, S. T., & Wu, J. (2015). Egg ovotransferrin-derived ACE inhibitory peptide IRW increases ACE2 but decreases proinflammatory genes expression in mesenteric artery of spontaneously hypertensive rats. *Molecular Nutrition & Food Research*, 59, 1735–1744.
9. Brand, J., Dachmann, E., Pichler, M., Lotz, S., & Kulozik, U. (2016). A novel approach for lysozyme and ovotransferrin fractionation from egg white by radial flow membrane adsorption chromatography: Impact of product and process variables. *Separation and Purification Technology*, 161, 44–52.
10. Abeyrathne, E. D. N. S., Lee, H. Y., Ham, J. S., & Ahn, D. U. (2013). Separation

of ovotransferrin from chicken egg white without using organic solvents. *Poultry Science*, 92, 1091–1097.

11. Acero-Lopez, A., Ullah, A., Offengenden, M., Jung, S., & Wu, J. (2012). Effect of high pressure treatment on ovotransferrin. *Food Chemistry*, 135, 2245–2252.

12. Ko, K. Y.; Ahn, D. U. An economic and simple purification procedure for the large-scale production of ovotransferrin from egg white. *Poult. Sci.* **2008**, 87, 1441–1450.

13. Lechevalier, V., Croguennec, T., Pezennec, S., Guérin-Dubiard, C., Pasco, M., & Nau, F. (2003). Ovalbumin, ovotransferrin, lysozyme: Three model proteins for structural modifications at the air–water interface. *Journal of Agricultural and Food Chemistry*, 51, 6354–6361.

14. Akkermans, C., Van der Goot, A. J., Venema, P., Van der Linden, E., & Boom, R. M. (2008). Properties of protein fibrils in whey protein isolate solutions: Microstructure, flow behaviour and gelation. *International Dairy Journal*, 18, 1034–1042.

15. Arosio, P., Knowles, T. P. J., & Linse, S. (2015). On the lag phase in amyloid fibril formation. *Physical Chemistry Chemical Physics*, 17, 7606–7618.

16. Koo, E. H., Lansbury, P. T., & Kelly, J. W. (1999). Amyloid diseases: abnormal protein aggregation in neurodegeneration. *Proceedings of the National Academy of Sciences*, 96, 9989–9990.

17. Loveday, S. M., Anema, S. G., & Singh, H. (2017). β -Lactoglobulin nanofibrils: The long and the short of it. *International Dairy Journal*, 67, 35–45.

18. Munialo, C. D., Martin, A. H., van der Linden, E., & de Jongh, H. H. J. (2014). Fibril formation from pea protein and subsequent gel formation. *Journal of Agricultural and Food Chemistry*. 62, 2418–2427.

19. Tang, C., Zhang, Y., Wen, Q., & Huang, Q. (2010). Formation of amyloid fibrils from kidney bean 7S globulin (Phaseolin) at pH 2.0. *Journal of Agricultural and Food Chemistry*. 58, 8061–8068.

20. Serfert, Y., Lamprecht, C., Tan, C. P., Keppler, J. K., Appel, E., Rossier-Miranda, F. J., et al. (2014). Characterisation and use of β -lactoglobulin fibrils for microencapsulation of lipophilic ingredients and oxidative stability thereof. *Journal of Food Engineering*, 143, 53–61.

21. Wan, Z., Yang, X., & Sagis, L. M. C. (2016). Contribution of long fibrils and peptides to surface and foaming behavior of soy protein fibril system. *Langmuir*, 32, 3679–3690.

22. Shen, Y., Posavec, L., Bolisetty, S., Hilty, F. M., Nyström, G., Kohlbrecher, J., et al. (2017). Amyloid fibril systems reduce, stabilize and deliver bioavailable nanosized iron. *Nature Nanotechnology*, 12, 642–647.

23. Li, C., Adamcik, J., & Mezzenga, R. (2012). Biodegradable nanocomposites of amyloid fibrils and graphene with shape-memory and enzyme-sensing properties. *Nature Nanotechnology*, 7, 421–427.

24. Frelichowska, J., Bolzinger, M., & Chevalier, Y. (2010). Effects of solid particle content on properties of o/w Pickering emulsions. *Journal of Colloid and Interface Science*, 351, 348–356.

25. Tarimala, S., & Dai, L. L. (2004). Structure of microparticles in solid-stabilized emulsions. *Langmuir*, 20, 3492–3494.
26. Xiao, J., Li, Y., & Huang, Q. (2016). Recent advances on food-grade particles stabilized Pickering emulsions: fabrication, characterization and research trends. *Trends in Food Science & Technology*, 55, 48–60.
27. Sharma, T., Kumar, G. S., Chon, B. H., & Sangwai, J. S. (2015). Thermal stability of oil-in-water Pickering emulsion in the presence of nanoparticle, surfactant, and polymer. *Journal of Industrial and Engineering Chemistry*, 22, 324–334.
28. Binks, B. P., & Lumsdon, S. O. (2010). Pickering emulsions stabilized by monodisperse latex particles: Effects of particle size. *Langmuir*, 17, 4540–4547.
29. Frelichowska, J., Bolzinger, M., & Chevalier, Y. (2009). Pickering emulsions with bare silica. *Colloids and Surfaces A: Physicochemical and Engineering Aspects*, 343, 70–74.
30. Nonomura, Y., & Kobayashi, N. (2009). Phase inversion of the Pickering emulsions stabilized by plate-shaped clay particles. *Journal of Colloid and Interface Science*, 330, 463–466.
31. Wei, Z., & Huang, Q. (2019). Assembly of iron-bound ovotransferrin amyloid fibrils. *Food Hydrocolloids*, 89, 579–589.
32. Wei, Z., & Huang, Q. (2019). Edible Pickering emulsions stabilized by ovotransferrin–gum arabic particles. *Food Hydrocolloids*, 89, 590–601.
33. Maheshwari, R. K., Singh, A. K., Gaddipati, J., & Srimal, R. C. (2006). Multiple biological activities of curcumin: A short review. *Life Sciences*, 78, 2081–2087.
34. Esatbeyoglu, T., Huebbe, P., Ernst, I. M. A., Chin, D., Wagner, A. E., & Rimbach, G. (2012). Curcumin—From molecule to biological function. *Angewandte Chemie International Edition*, 51, 5308–5332.
35. Manach, C., Williamson, G., Morand, C., Scalbert, A., & Rémésy, C. (2005). Bioavailability and bioefficacy of polyphenols in humans. I. Review of 97 bioavailability studies. *The American Journal of Clinical Nutrition*, 81, 230S–242S.
36. Minekus, M. The TNO gastro-intestinal model (TIM). In *The Impact of Food Bioactives on Health: in vitro and ex vivo models*, Springer International Publishing: Cham, Switzerland, **2015**, 5, 37–46.
37. McClements, D. J., & Li, Y. (2010). Structured emulsion-based delivery systems: Controlling the digestion and release of lipophilic food components. *Advances in Colloid and Interface Science*, 159, 213–228.
38. Minekus, M., Alminger, M., Alvito, P., Ballance, S., Bohn, T., Bourlieu, C., et al. (2014). A standardised static in vitro digestion method suitable for food—an international consensus. *Food & Function*, 5, 1113–1124.
39. Chaves, K. F., Barrera-Arellano, D., & Ribeiro, A. P. B. (2018). Potential application of lipid organogels for food industry. *Food Research International*, 105, 863–872.
40. Jadhav, S. R., Hwang, H., Huang, Q., & John, G. (2013). Medium-chain sugar amphiphiles: A new family of healthy vegetable oil structuring agents. *Journal of Agricultural and Food Chemistry*, 61(49), 12005–12011.
41. Yu, H., Shi, K., Liu, D., & Huang, Q. (2012). Development of a food-grade

- organogel with high bioaccessibility and loading of curcuminoids. *Food Chemistry*, 131(1), 48–54.
42. Yu, H., & Huang, Q. (2012). Improving the oral bioavailability of curcumin using novel organogel-based nanoemulsions. *Journal of Agricultural and Food Chemistry*, 60(21), 5373–5379.
43. Lu, M., Cao, Y., Ho, C. T., & Huang, Q. (2016). Development of organogel-derived capsaicin nanoemulsion with improved bioaccessibility and reduced gastric mucosa irritation. *Journal of Agricultural and Food Chemistry*, 64(23), 4735–4741.

CHAPTER II. ASSEMBLY OF OVOTRANSFERRIN FIBRILS

The work in this chapter has been published in the title of “Assembly of iron-bound ovotransferrin amyloid fibrils” in Food Hydrocolloids (Volume 89, Pages from 579 to 589) in November 2018.

1. Introduction

Proteins may self-assemble *in vitro* into aggregates with different morphologies, and protein aggregates are amorphous in most cases (1). Formation of aggregates is often regarded as an indication of protein instability and various means have been developed to inhibit aggregation. However, protein aggregation is desirable under certain circumstances (2, 3). Unlike random or spherical irreversible/reversible aggregates, protein fibrils are anisotropic aggregates with linear structures (4). Nanofibrils refer to fibrils with diameters less than 100 nm (5), and most of protein fibrils can be considered as nanofibrils based on the definition (6). Protein nanofibrils generated through self-assembly are also called protein amyloid fibrils (7). The unique rod-like structure and high aspect ratio endow protein amyloid fibrils with particular features such as unique interfacial adsorption behavior, rheological behavior or gelling behavior, thus making protein amyloid fibrils interesting and competitive candidates in application of Pickering emulsions, hydrogels, foam stabilization, nutraceutical delivery and so on (2, 3, 7–10). Like most of potential new ingredients and soft materials in food formulations, formation and structure of protein fibrils should be tailored to satisfy diverse needs in complex food systems (11).

Therefore, a deeper understanding of fibrils is in urgent need to gain precise control over engineering finely structured fibrils.

Ovotransferrin (OVT) is an iron-binding egg white protein containing 686 amino acids (12). OVT is composed of two globular lobes (N and C lobes), and each lobe can bind one Fe^{3+} ion with bicarbonate anions reversibly. The iron-binding ligands in each lobe of OVT contain one aspartic acid, one histidine and two tyrosine residues, and this set facilitates stronger iron binding (12). OVT possesses a variety of bioactivities such as antimicrobial activity, anticancer activity and immune-modulating activity (13–15). Despite multifunctional properties of OVT, there has been little work done about OVT fibrils to our best knowledge. Till now, the published protein fibril studies have covered many globular proteins such as whey protein isolate (WPI), β -lactoglobulin (BLG), lysozyme, soybean proteins, bovine serum albumin and so on (3, 9, 16–21). Proposed fibril theories available now are far from enough and most of them are based on phenomena observed from WPI or BLG fibrils, which do not possibly apply to other fibrils. Till now, there are rare studies about nanofibrils derived from iron-bound proteins. Fibrillation of iron-bound proteins may possibly behave differently from other non-transferrins. Thus, comprehensive research about OVT fibrils can advance understanding of protein fibrils to some extent undoubtedly.

Apart from protein structural factors, protein fibrillation is strongly affected by many environmental parameters such as nuclei, seeding, pH, temperature and so on, and systematic investigation may promote protein fibrillation and give deeper insight

into driving force and molecular origin of fibrillation (22, 23). Some studies demonstrate that protein fibrils may be composed of filaments (24), and it is interesting to decipher structural units of OVT amyloid fibrils. In addition, before exploring potential applications of OVT amyloid fibrils, biocompatibility of OVT amyloid fibrils should be assessed to ensure that OVT amyloid fibrils may be applied safely.

Accordingly, the objectives of the chapter were to first optimize OVT fibrillation by modulating parameters such as pH, temperature, protein concentration, ionic strength and stirring speed systematically. Afterwards, structural characteristics such as internal structure, periodicity and surface hydrophobicity of OVT amyloid fibrils were investigated with the aid of circular dichroism, atomic force microscopy and fluorescent probe. Finally, *in vitro* cytotoxicity of OVT amyloid fibrils was determined by MTT assay. Hopefully, this chapter may give new insights into formation and structure of transferrin amyloid fibrils.

2. Materials and Methods

2.1. Materials

Ovotransferrin (OVT) was obtained from Neova Technologies Inc. (Abbotsford, Canada) with a purity of at least 88%, and OVT had an iron binding activity of 1099 $\mu\text{g Fe/g}$ sample. Coomassie brilliant blue R-250, β -mercaptoethanol and 30% acrylamide/bis solution were purchased from Bio-Rad Laboratories Inc. (Hercules, USA). PageRuler™ Plus prestained protein ladder (10 to 250 kDa) was purchased from Thermo Fisher Scientific, Inc. (Waltham, USA). Other chemicals were

purchased from Sigma-Aldrich (St. Louis, USA) unless otherwise stated. Water used to prepare solutions was purified by a Milli-Q system.

2.2. Fibril formation at different pHs and temperatures

OVT (4%, w/v) was dispersed and dissolved in pH-adjusted Milli-Q water (pH 2, pH 3 or pH 4) and hydrated overnight under mild stirring, and 1M HCl was carefully added to readjust and maintain the corresponding solution pH. Sodium azide (0.02%, w/v) was added in order to retard microbial growth during storage. In order to remove impurities, the OVT solutions were filtered with 0.2 μm pore-sized syringe filters (Thermo Fisher Scientific, Waltham, USA). For fibrillation, OVT solutions were heated in oil bath over a temperature-controlled hot plate stirrer (VWR International, Radnor, USA) at 80 °C or 90 °C without stirring. The heated samples were cooled in an ice-water bath immediately and stored at 4 °C until further analysis. ThT fluorescence and AFM were applied to monitor fibrillation.

2.3. Thioflavin T (ThT) fluorescence spectroscopy

ThT stock solution was freshly prepared by dispersing 8 mg of ThT into 10 mL of phosphate buffer (10 mM, pH 7.0) containing 150 mM NaCl. To remove undissolved ThT, the dispersion was filtered with a 0.2 μm syringe filter. The stock solution was diluted 50 times with the phosphate buffer (10 mM, pH 7.0) to generate working solution, and 40 μL of the tested sample was mixed with 4 mL of the working solution. Excitation was at 440 nm, and emission was measured at 482 nm via a FluoroMax 3 fluorescence spectrophotometer (Horiba Scientific, Kyoto, Japan). The fluorescence intensity was corrected by subtracting the background of the ThT

working solution (25).

2.4. Atomic force microscopy (AFM)

AFM images of OVT amyloid fibrils were collected with NanoScope IIIA Multimode AFM (Veeco Instruments Inc., Santa Barbara, USA) equipped with a silicon-etched RTEP7 cantilever. The scanning was carried out at the tapping mode. Samples (10 μ L) diluted with Milli-Q water at corresponding pH were spread onto surface of freshly cleaved mica. After 2 min of adsorption, samples were dried under a nitrogen stream prior to imaging. AFM data were analyzed by NanoScope Analysis Software and FiberApp (26).

2.5. Sodium dodecyl sulfate polyacrylamide gel electrophoresis (SDS-PAGE)

SDS-PAGE was performed as previously reported on a vertical gel electrophoresis unit (Bio-Rad Laboratories, Hercules, USA). Aliquots (10 μ L) of diluted samples were loaded, and the electrophoresis was operated at a constant voltage of 80 V (27).

2.6. Effects of protein concentration, ionic strength and stirring on fibril formation

Influence of protein concentration, ionic strength and stirring on OVT fibril formation was further examined at 90 °C and pH 2. To investigate effects of protein concentration, different concentrations of OVT solutions (10 mg/mL, 20 mg/mL and 40 mg/mL) were heated at rest. For impact of ionic strength, ionic strength of OVT solutions was adjusted by adding NaCl. The OVT solutions (40 mg/mL) were heated at ionic strength $I = 0, 50, 100$ or 150 mM without stirring. For influence of stirring, OVT solutions (40 mg/mL, $I = 150$ mM) were heated at a constant stirring speed of 0,

100 or 300 rpm. Fibrillation process was analyzed by ThT fluorescence and AFM. OVT nanofibrils in the rest of this study was prepared by heating OVT solutions (pH 2, 40 mg/mL, $I = 150$ mM) at 90 °C and a constant stirring speed of 300 rpm for 24 h unless otherwise stated.

2.7. Far-UV circular dichroism (CD)

Far-UV CD spectra of OVT heated at pH 2 and 90 °C were recorded using an Aviv 420SF circular dichroism spectrometer (Aviv Biomedical, Lakewood, USA) at 25 °C. Samples were diluted with Milli-Q water (pH 2) to a protein concentration of 0.2 mg/mL, and all spectra were corrected by subtracting background. The spectra were averaged over three scans and smoothed with OriginPro 2018. The compositions of secondary structures were determined with Contin method using DichroWeb (28,29).

2.8. Surface hydrophobicity (H_0)

Surface hydrophobicity (H_0) of OVT before and after heating at 90 °C and pH 2.0 was determined using 1-anilino-8-naphthalensulfonate (ANS) method as described previously (30, 31). The index of protein surface hydrophobicity was calculated as the initial slope (S_0) of the fluorescence intensity versus soluble protein concentration (30).

2.9. Cytotoxicity study

Cytotoxicity of OVT amyloid fibrils was evaluated by MTT assay on colon carcinoma cell line Caco-2. Caco-2 colon cancer cells were cultured in Dulbecco's modified Eagle's medium (DMEM) supplemented with fetal bovine serum, penicillin,

streptomycin and non-essential amino acids (32). Caco-2 cells were incubated in the CO₂ incubator (5% CO₂) at 37 °C. The cells were harvested with trypsin-EDTA upon reaching confluency, and the cell suspension was centrifuged and suspended in the growth medium for further analysis (32). OVT amyloid fibril dispersions (10–1000 µg/mL) were prepared by dilution and adjusted to pH 7.4 carefully just before use. Caco-2 cells were seeded into a 96 well plate at a density of 50000 cells/well (33). The cells were incubated with OVT fibril dispersions for 12 h, and the control group consisted of cells in media without exposure to OVT amyloid fibril dispersions. Subsequently, the cells were incubated with MTT (3-(4,5-dimethylthiazol-2-yl)-2,5-diphenyltetrazolium bromide) solution for 4 h, followed by incubation with solubilization buffer for 1 h. Afterwards, the optical density was recorded at 570 nm employing BioTek Synergy HT multimode microplate reader (BioTek Instruments, Winooski, USA) (33). The cell viability was determined as follows:

$$Cell\ viability = (OD_t - OD_m) / (OD_c - OD_m) \times 100\% \quad (1)$$

OD_t was optical density of the cells treated with OVT amyloid fibrils, OD_c was optical density of the untreated cells, and OD_m was optical density of the medium. Experiments were carried out in triplicate, and six replicate wells were performed for every sample during each experiment.

2.10. Statistical analysis

All experiments were performed at least in triplicate. OriginPro 2018 software was used to perform statistical analysis. One-way analysis of variance (ANOVA)

procedure with Fisher LSD test was used to determine statistical differences, and differences were considered to be significant with $p < 0.05$.

3. Results and Discussion

3.1. Impact of pH and temperature on nanofibril formation

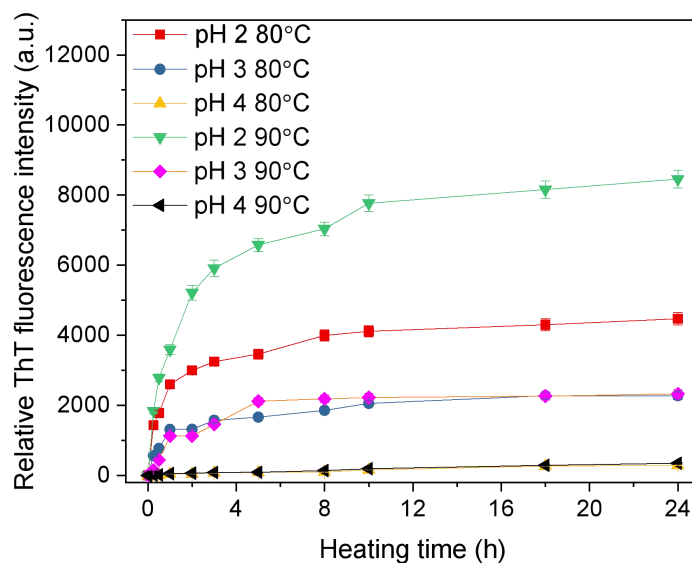


Figure II-1. ThT fluorescence intensity of OVT after heating at different pHs and temperatures.

ThT fluorescence has proved to be a sensitive method to detect presence of fibrillar aggregates (25). Figure II-1 shows ThT fluorescence intensity at 482 nm for OVT (4% w/v) heated at different pHs and temperatures. As depicted in Figure II-1, ThT intensities for OVT followed the order: at pH 2 and 90 °C > at pH 2 and 80 °C > at pH 3 and 90 °C > at pH 3 and 80 °C > at pH 4 and 90 °C \approx at pH 4 and 80 °C, indicating that pH 2 and 90 °C was the most conducive to OVT fibrillation. It also seems safe to conclude that 90 °C is more appropriate for fibrillation than 80 °C, which may be attributed to increasing hydrophobic interactions and collision frequencies of molecules at higher temperatures (1). It was noteworthy that very few

fibrillar structures were generated at pH 4, corresponding to approximately flat lines in Figure II-1.

For the cases of pH 2 and pH 3, the ThT fluorescence intensity of OVT increased sharply upon heating, then intensity increase slowed down gradually and reached a plateau eventually. Previous research shows that fibrillation of many proteins may consist of three stages: a lag phase, a growth phase and a final plateau (2, 16, 34). It is proposed that the lag phase is not simply a waiting time, but a combination of microscopic processes such as primary nucleation, elongation, secondary nucleation and fragmentation are active during the lag time (34). It is worth pointing out that OVT fibrillation doesn't undergo a lag phase, and two explanations can account for this. One interpretation is that growth and proliferation of nuclei when heated are fast enough to produce large amounts of OVT amyloid fibrils in short time. The other explanation is that OVT fibrils are generated via nucleation-independent pathways, and massive nucleation is not an essential mechanism to induce rapid OVT fibrillation.

AFM was used to confirm morphology of OVT fibrils. As depicted in Figure II-2, amyloid fibrils with contour length of around 37–264 nm formed at pH 2, and the maximum contour length of amyloid fibrils generated at pH 3 was 136 nm. Plenty of random aggregates appeared at pH 4, and few fibrillar structures were detected. Since isoelectric point of OVT studied here was around 6.2 (35), it can be postulated that OVT fibrillar structures cannot form at pHs relatively closer to the isoelectric pH than the cases at pH 3 and 2.

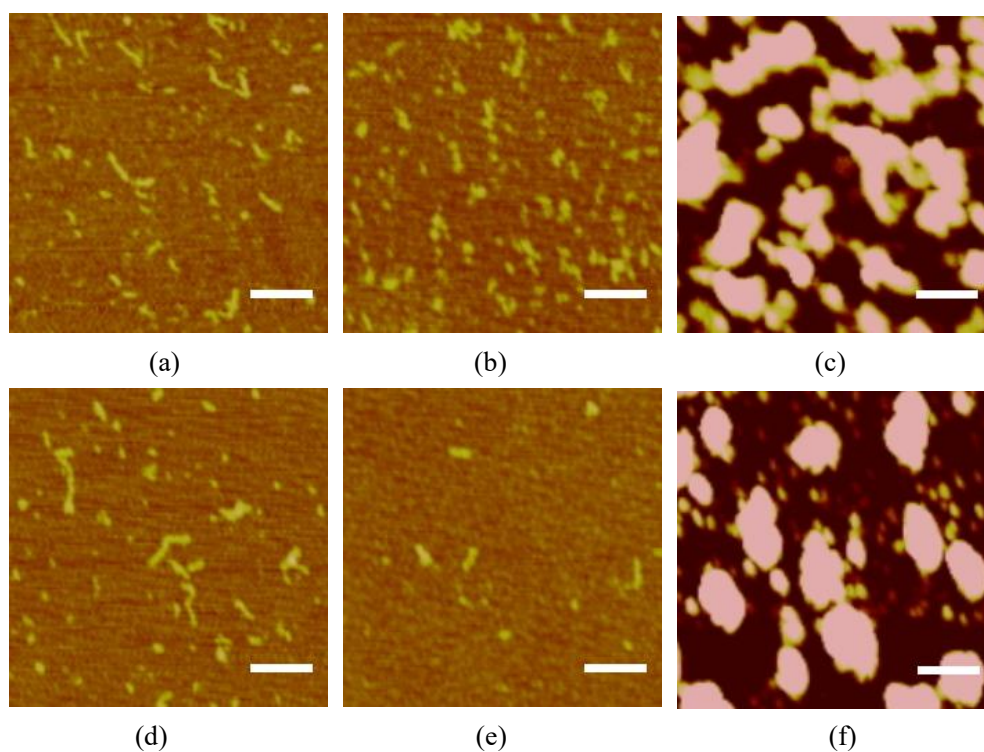


Figure II-2. AFM images of OVT after heating at different pHs and temperatures for 24 h: (a) at pH 2 and 80 °C, (b) at pH 3 and 80 °C, (c) at pH 4 and 80 °C, (d) at pH 2 and 90 °C, (e) at pH 3 and 90 °C, (f) at pH 4 and 90 °C. The scan size is 1 μm \times 1 μm , and the z scale is 20 nm. The scale bar represents 200 nm.

SDS-PAGE was utilized to assess protein hydrolysis during OVT fibrillation. As depicted in Figure II-3, almost all of OVT samples were hydrolyzed into peptides after 24 h in all cases except at pH 4 and 80 °C. Analysis of the intensities of intact OVT bands revealed that hydrolysis rate at the same temperature followed the order: at pH 2 > at pH 3 > at pH 4. No peptide fragments with molecular weight over 35 kDa were detected at pH 2, and the three obvious peptide bands ranged from 10 to 35 kDa. The majority of peptides generated at pH 3 had molecular masses between 25 and 55 kDa. Considering the fact that ThT fluorescence and AFM results revealed that more and longer OVT amyloid fibrils formed at pH 2 than at pH 3, it may be assumed that peptide fragments with smaller molecular weights are more beneficial to OVT

fibrillation. From the aforementioned discussion, 90 °C and pH 2 was optimal for OVT nanofibrillation among all pH and temperature combinations.

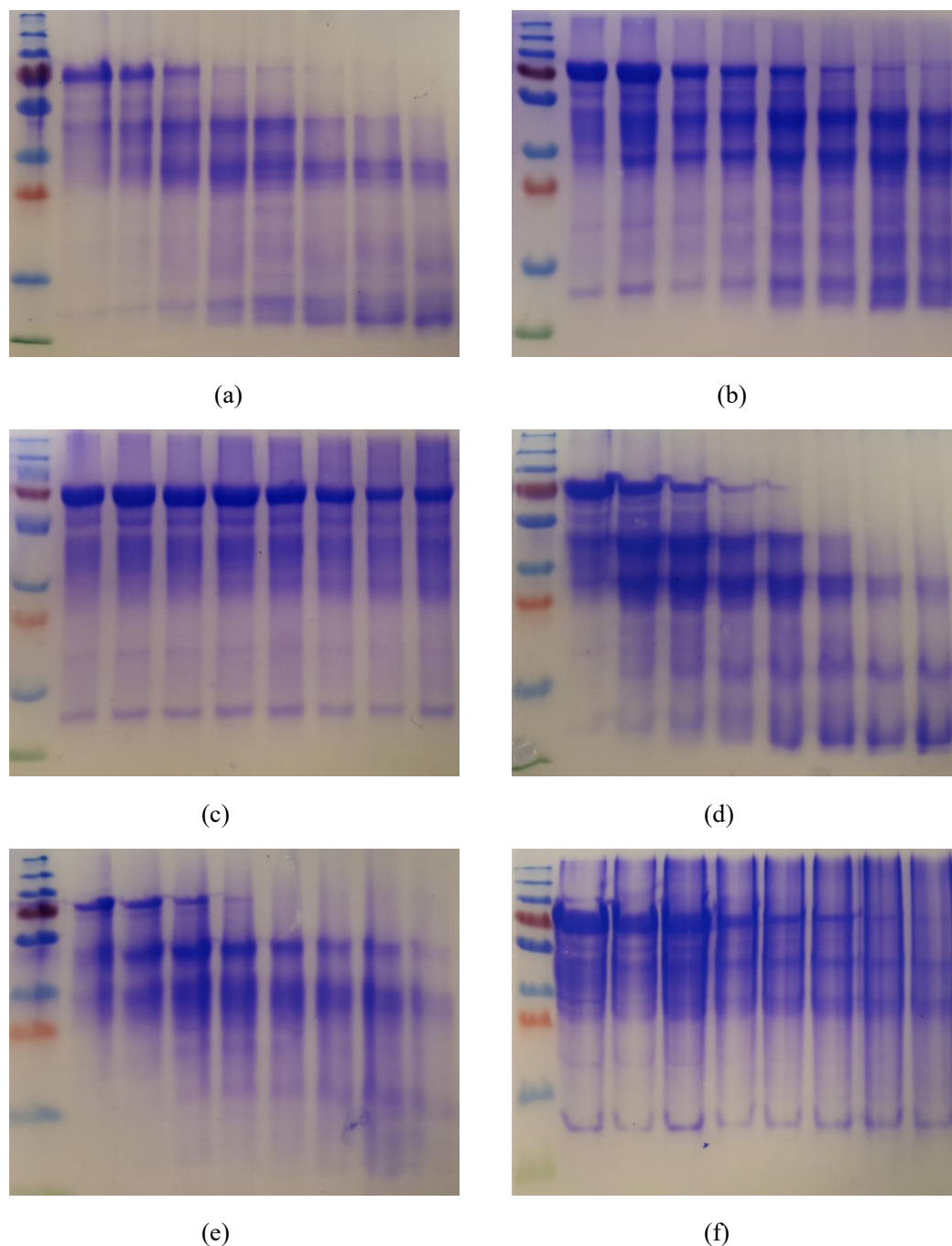


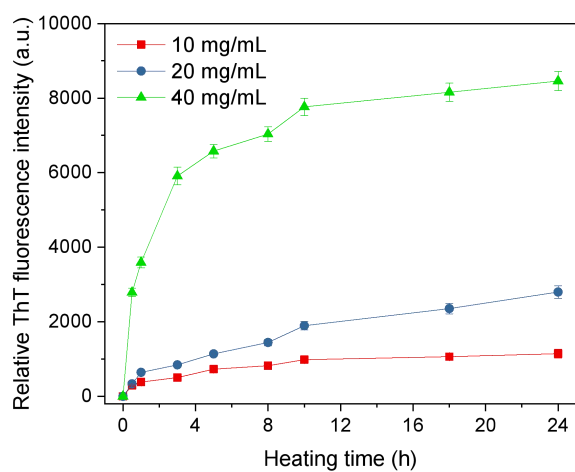
Figure II-3. SDS-PAGE profiles (15% separating gel) of OVT after heating at different pHs and temperatures: (a) at pH 2 and 80 °C, (b) at pH 3 and 80 °C, (c) at pH 4 and 80 °C, (d) at pH 2 and 90 °C, (e) at pH 3 and 90 °C, (f) at pH 4 and 90 °C. Lanes from left to right are: protein marker, OVT heated for 0, 0.25, 0.5, 1, 3, 5, 10

and 24h, respectively. The marker bands from down to up correspond to 10, 15, 25, 35, 55, 70, 100, 130 and 250 kDa.

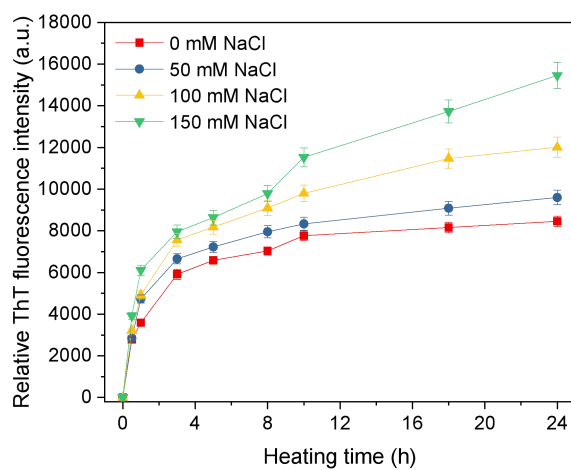
3.2. Impact of protein concentration, ionic strength, and stirring on fibril formation

Figure II-4a shows that ThT fluorescence intensity of OVT decreased remarkably as protein concentrations declined, implying that sufficient building blocks are necessary for fibril construction. Figure II-5 illustrates AFM images of OVT at different protein concentrations. It is noteworthy that plenty of small spherical-like aggregates were observed at OVT concentration of 10 and 20 mg/mL, which may be accounted for by the fact that lack of enough building blocks around the active growth ends limit elongation of aggregates.

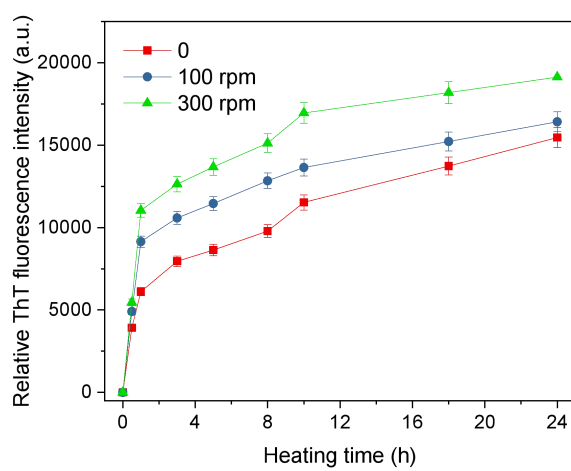
Figure II-4b shows that ThT fluorescence intensity of OVT rose with increasing ionic strengths during heat treatment, and the ThT intensity at an ionic strength of 150 mM was almost twice as much as the case at $I = 0$, implying that higher ionic strength could accelerate OVT fibrillation markedly. A previous study also shows that electrostatic screening in the presence of NaCl can improve amyloid fibril assembly of soy β -conglycinin (20). Since the added cations and anions own strong electrostatic screening capacity and can significantly weaken electrostatic interactions among polymers, improved OVT fibrillation may be attributed to diminished electrostatic short-range interactions. It implies that electrostatic short-range interactions are not dominant driving forces for OVT nanofibrillation, and OVT nanofibrillation could possibly be a balance of hydrophobic short-range attraction, electrostatic long-range repulsion and cooperative hydrogen bonds (36–38).



(a)



(b)



(c)

Figure II-4. (a) ThT fluorescence intensity for different concentrations of OVT after heating at pH 2 and 90 °C. (b) ThT fluorescence intensity of OVT heated at different

ionic strengths. (c) ThT fluorescence intensity of OVT heated at different stirring speeds.

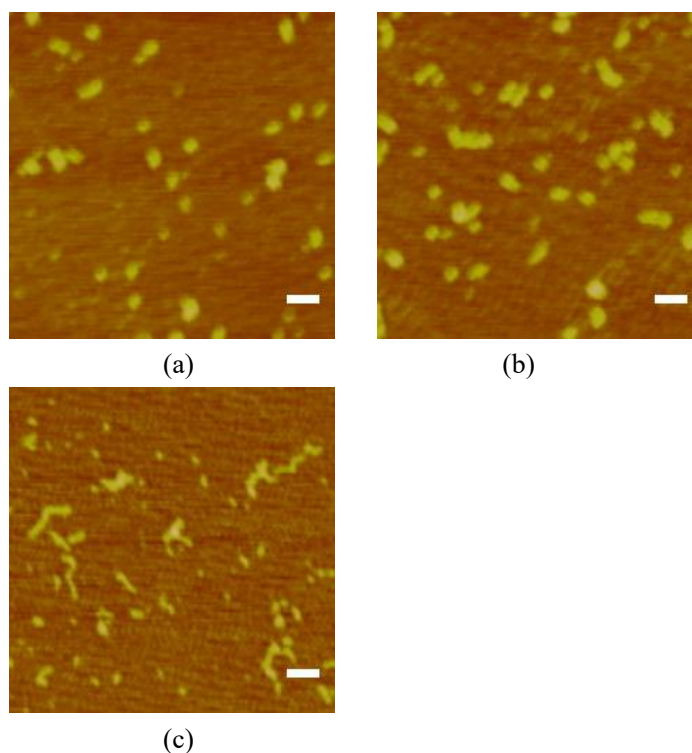


Figure II-5. AFM images of OVT after heating at pH 2 and 90 °C at different protein concentrations for 24 h: (a) 10 mg/mL, (b) 20 mg/mL, (c) 40 mg/mL. The scan size is 1 μm \times 1 μm , and the z scale is 20 nm. The scale bar represents 100 nm.

As illustrated in Figure II-6, OVT fibrils generated at different ionic strengths exhibited similar contour length, indicating that morphology of OVT fibrils is possibly independent of the ionic strengths. Nevertheless, fibrillar aggregation of BLG depends strongly on the ionic strength, and BLG fibrils can become shorter and more flexible at higher ionic strength (39). Besides, Figure II-6 depicts that more amyloid fibrils were detected with elevated ionic strengths, implying that the AFM result was consistent with the ThT fluorescence result.

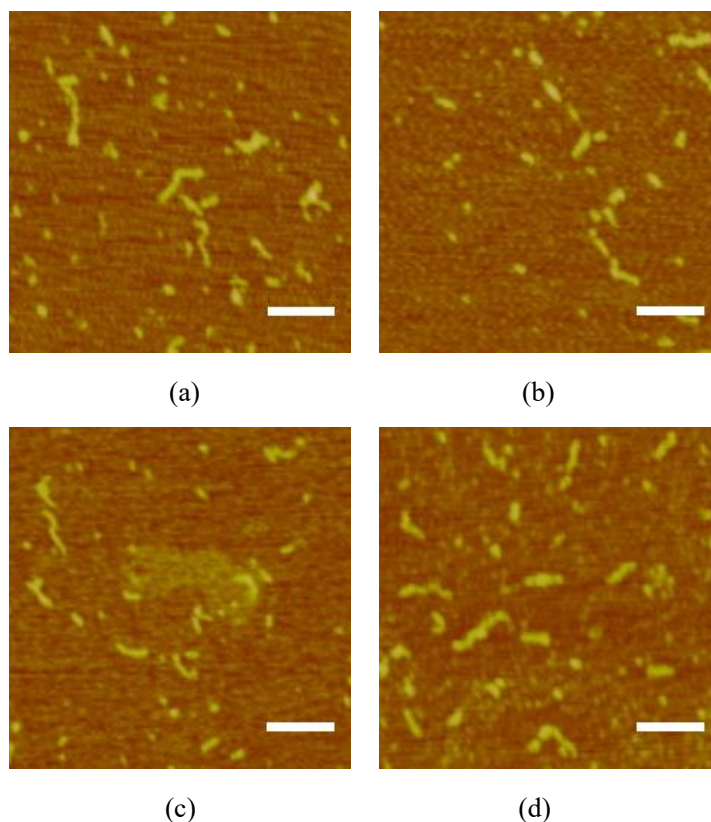


Figure II-6. AFM images of OVT at different ionic strengths after heating at pH 2 and 90 °C for 24 h: (a) 0, (b) 50 mM, (c) 100 mM, (d) 150 mM. The scan size is 1 $\mu\text{m} \times 1 \mu\text{m}$, and the z scale is 20 nm. The scale bar represents 200 nm.

Effect of stirring on formation of amyloid fibrils in OVT solutions was also studied. As depicted in Figure II-4c, OVT that was continuously stirred during heating had higher ThT fluorescence intensity than sample heated at rest, indicating a much higher conversion into OVT amyloid fibrils. Figure II-7 illustrate that the fibrillation of OVT was enhanced with increasing stirring speeds. Specifically speaking, the majority of amyloid fibrils heated at rest had contour length below 170 nm. When the stirring speed was increased to 100 rpm, contour length of OVT fibrils ranged from

63 to 554 nm, and the average contour length was 226.8 nm. Long and rigid fibrils with contour length over 800 nm were observed at a stirring speed of 300 rpm, and flexible and semiflexible fibrils with contour length ranging from 85 to 620 nm coexisted. Three theories may account for these phenomena. First, since monomers (a single protein or peptide chain) in immature fibrils are reversibly bound and susceptible to breakup in the presence of environmental perturbation, stirring may break up immature fibrils into larger amounts of shorter active fibrils with more active growth ends. The active non-assembled monomers may be assembled and incorporated into immature fibrils. As heating goes on, the immature fibrils turn mature due to formation of irreversible linkage bonds, and the mature fibrils don't disassemble against gentle stirring (40). As a result, more amyloid fibrils were generated. Second, growth or elongation of fibrils may slow down or terminate due to exhaustion of active monomers surrounding the active fibril ends. Stirring may deliver the active monomers in the distance to the vicinity of the fibril ends, thus eliminating the limitation of supply of building blocks. Thereafter, lengths of fibrils were extended. Last but not least, heterogeneity exists under unstirred conditions, which does not facilitate extensive fibrillation. Some fibrillar structures in local region may entangle into gel structures both theoretically and practically (41), and protein concentrations in certain regions are likely not enough to ensure assembly of OVT into amyloid fibrils. Stirring may help to maintain solution homogeneity and distribute OVT amyloid fibrils evenly.

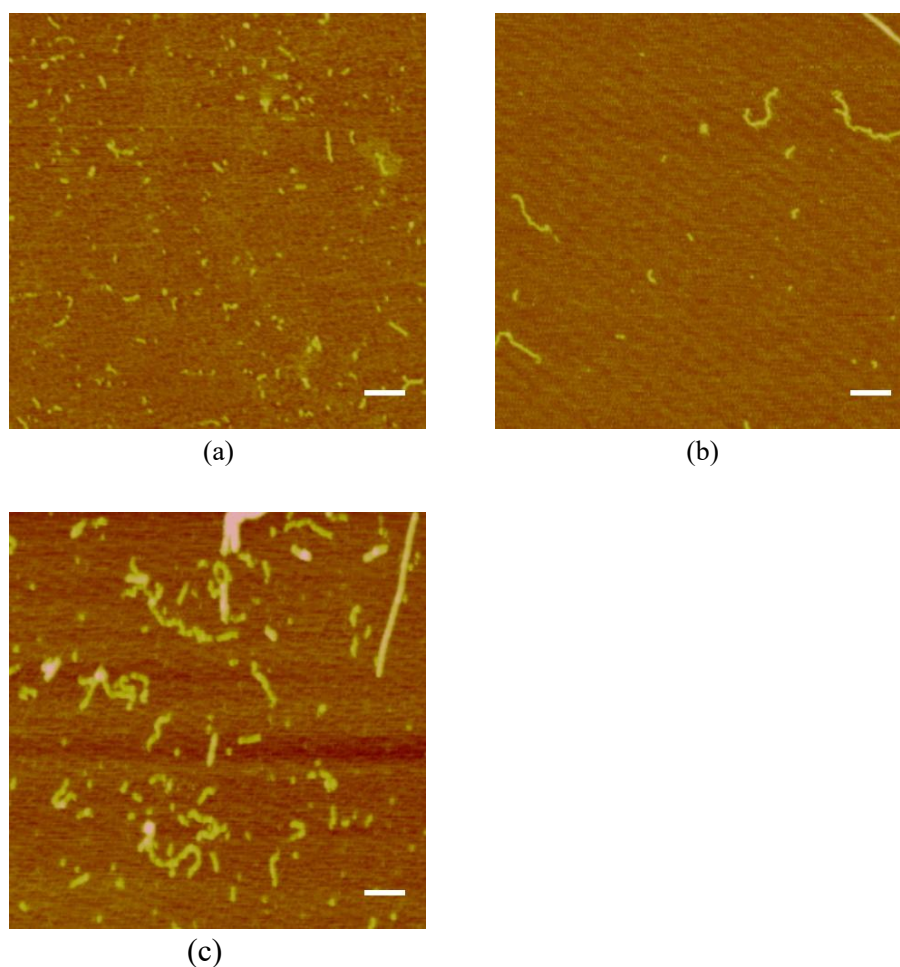


Figure II-7. AFM images of OVT amyloid fibrils prepared at different stirring speeds for 24 h: (a) 0, (b) 100 rpm, (c) 300 rpm. The scan size is $2\ \mu\text{m}\times 2\ \mu\text{m}$, and the z scale is 20 nm. The scale bar represents 200 nm.

It is worthwhile to study OVT fibrillation under magnetic stirring (300 rpm) over a longer period. As Figure II-8 depicts, ThT fluorescence intensity of OVT did not change obviously within the heating period of 24–32 h and it was apparent that the ThT fluorescence intensity of OVT decreased as heating time was extended from 32 h to 48 h. One possibility for the minor decrease in ThT fluorescence is that excessive heating might disrupt OVT fibrillar structures, and two speculations may explain this. First, since a significant amount of building blocks (a single protein or peptide) have been assembled into fibrillar structures, suitable building blocks of

amyloid fibrils are almost used up, leading to termination of fibril construction. Second, during prolonged heating the assembled building blocks may be hydrolyzed into very small peptides which are not suitable for fibrillation, resulting in dissociation of a small quantity of amyloid fibrils. Another possibility for the slight decrease in measured ThT fluorescence is that OVT fibrils could further assemble into nanotubes during prolonged heating (42). Since this research focuses on fibrils instead of nanotubes, nanotube formation is not desirable. From the aforementioned discussions, heat treatment of a maximum of 24 h was chosen for following experiments while taking into account energy conservation and fibril conversions.

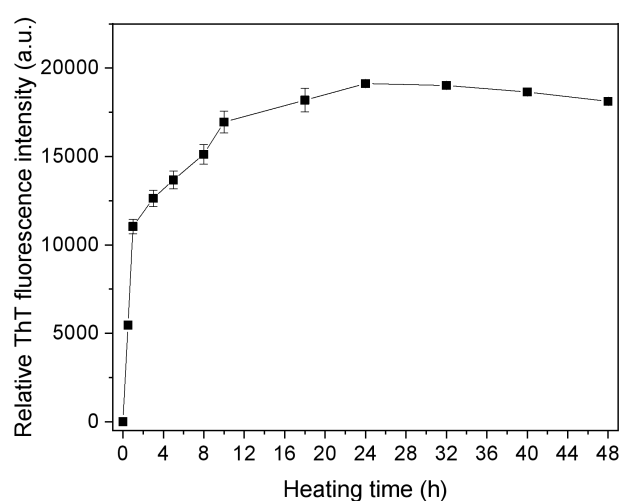
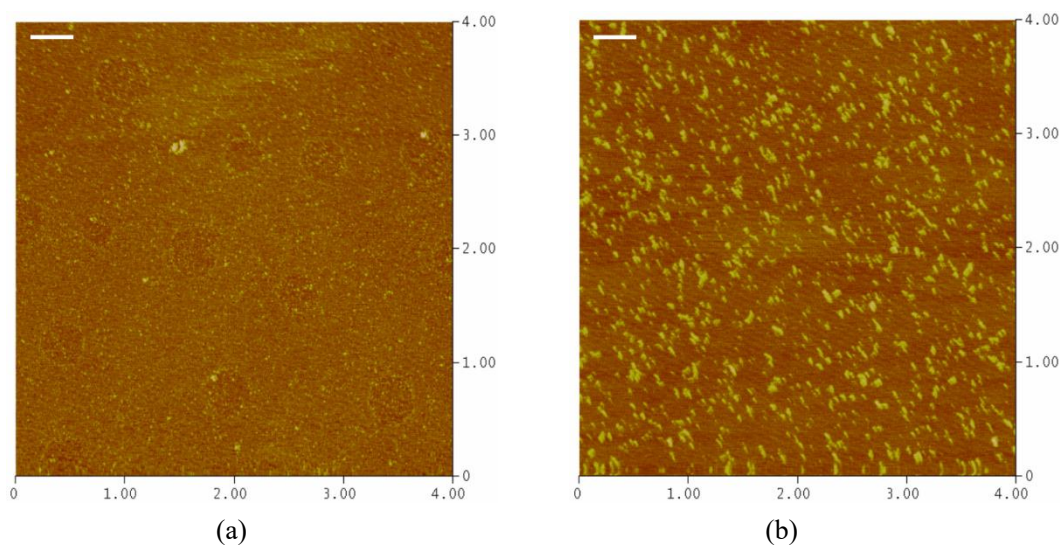


Figure II-8. ThT fluorescence intensity for OVT solution as function of heating time. OVT solution (40 mg/mL, ionic strength $I = 150$ mM) was heated at pH 2 and 90 °C under magnetic stirring (300 rpm).

3.3. Impact of heating time on fibril morphology

Since ThT fluorescence cannot provide information about shapes and sizes, AFM was applied to study fibril morphology as function of time. As shown in Figure II-9,

OVT appeared like dots with an average diameter below 10 nm prior to heating. Short fibrillar aggregates with contour length below 50 nm were detected upon heating for 1 h. Longer fibrils with a maximum contour length of 276 nm were observed when heating lasted 3 h. It was noteworthy that the long and straight OVT fibrils with contour length over 800 nm were first detected after heating for 6 h. After thermal treatment of 12 h, more long fibrils were detected with coexistence of short fibrils, and the estimated average contour length of OVT fibrils was 264.4 nm. When heating period reached 24 h, the length of long OVT fibrils did not further increase to over 2 μm , and the average contour length of OVT fibrils increased to about 298.4 nm. Previous studies reveal that BLG fibrils and lysozyme fibrils may have a contour length above 5 μm (17, 43, 44), implying that OVT fibrils are shorter than BLG fibrils and lysozyme fibrils.



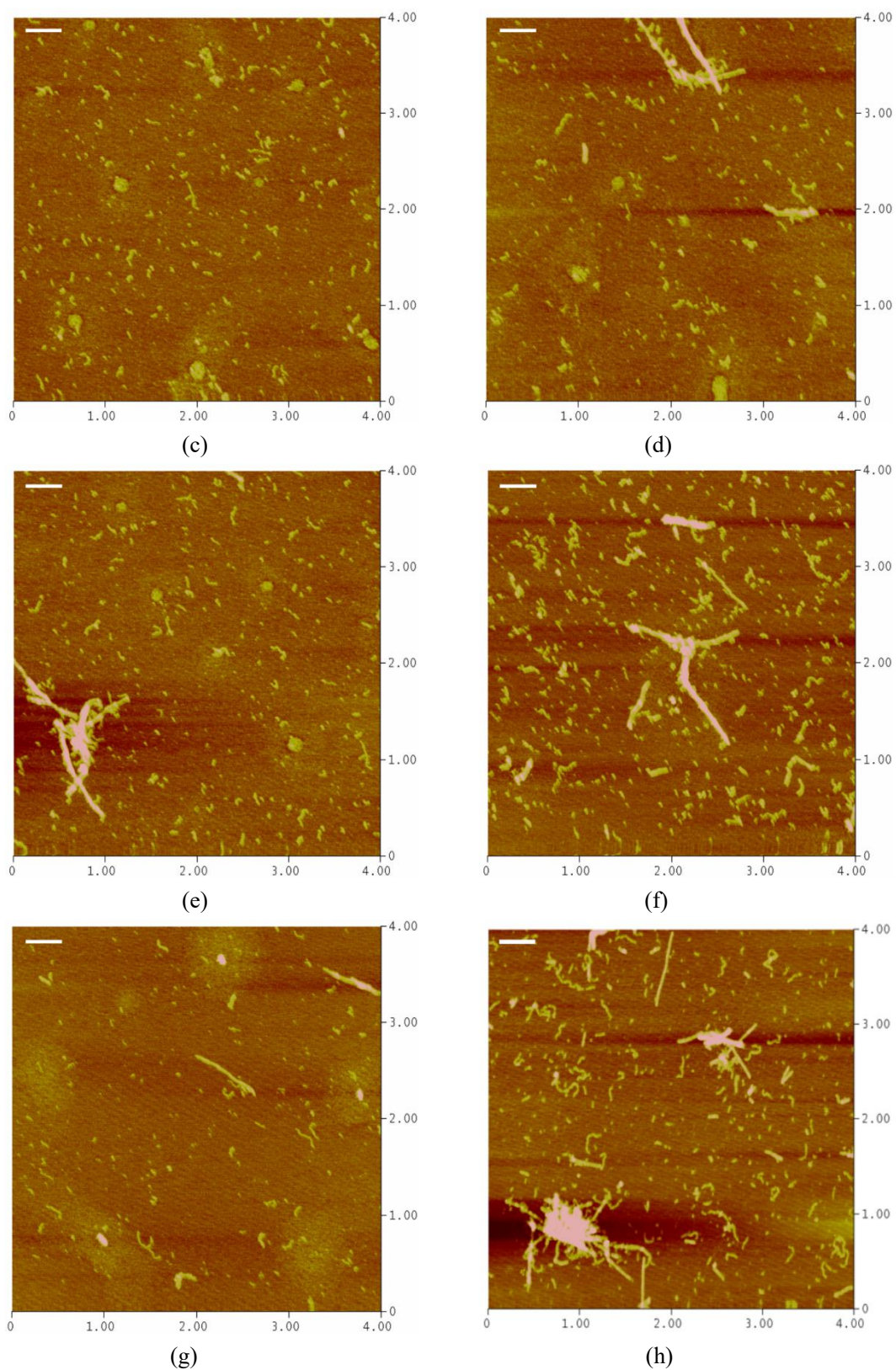


Figure II-9. AFM images of OVT after heating at pH 2 and 90 °C for different periods: (a) 0 h, (b) 1 h, (c) 3 h, (d) 6 h, (e) 9 h, (f) 12 h, (g) 18 h, (h) 24 h. The scan size is 4 μm \times 4 μm , and the z scale is 20 nm. The scale bar represents 400 nm.

3.4. Secondary structure analysis

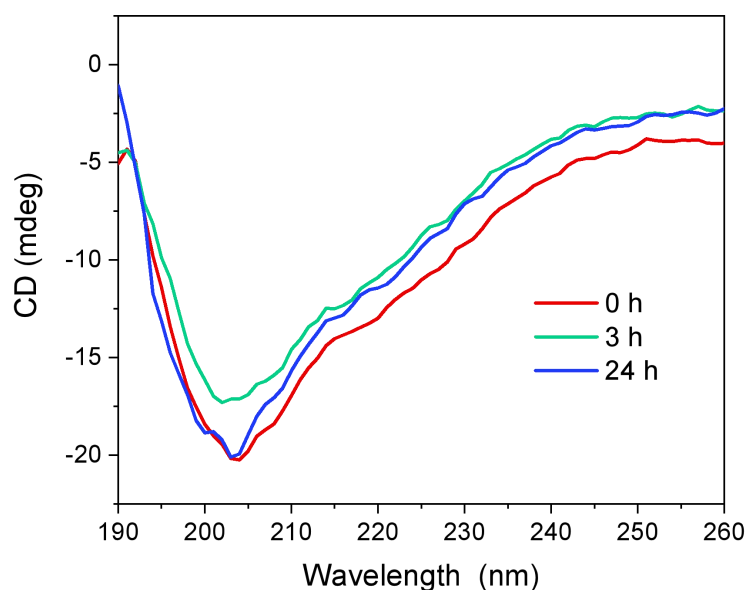


Figure II-10. Far-UV CD spectra of OVT after heat treatment at pH 2.0.

Table II-1. Estimation of secondary structure of OVT after heat treatment at pH 2.0

Heating time (h)	α -Helix (%)	β -Sheet (%)	β -Turn (%)	Unordered (%)
0	13.5	15.2	27.8	43.5
3	12.8	21.4	26.1	39.7
24	14.4	25.3	25.4	34.9

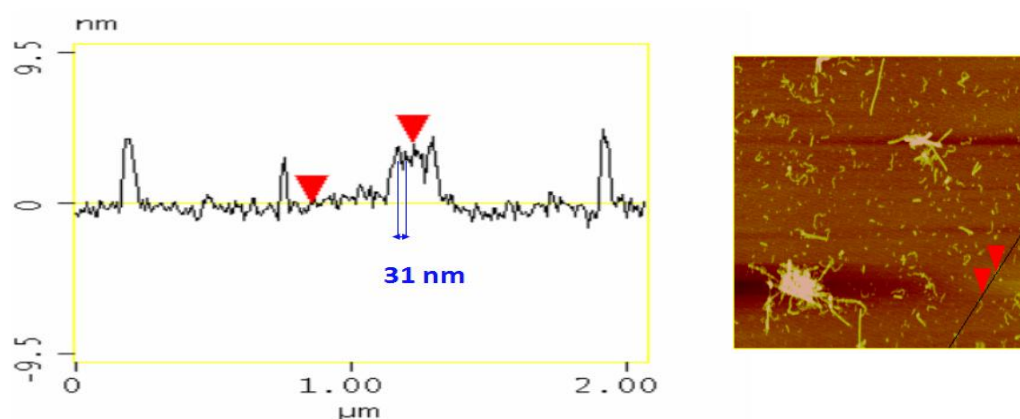
Figure II-10 shows far-UV CD spectra of OVT after heating for 0–24 h, and secondary structure proportions of the samples are summarized in Table II-1. Upon heat incubation, there was a corresponding loss of unordered structures, indicating formation of more ordered structures. After treatment of 24 h, fractions of β -sheet structures increased from 15.2% to 25.3%, implying that internal structures of OVT

amyloid fibrils could be stacked β -sheet. Increase of β -sheets in circular dichroism spectra for amyloid fibrillation is not always the case, and there is a considerable loss of β -sheet structures during fibrillation of pea protein at pH 2 (41).

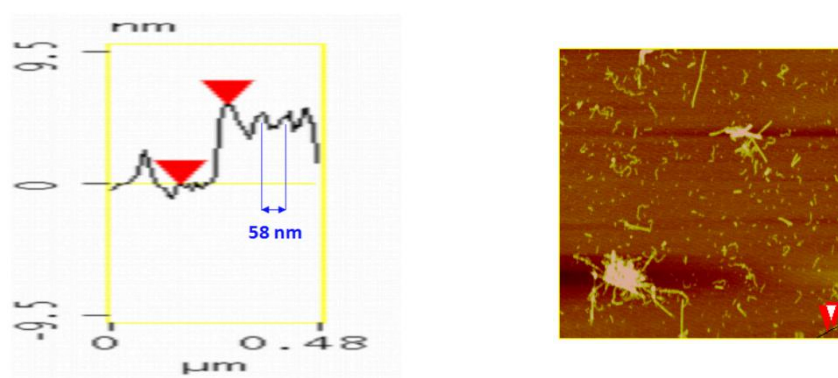
3.5. Periodicity of OVT amyloid fibrils

OVT amyloid fibrils may include shorter subunits, and cross section along contour length of OVT amyloid fibrils allows us to characterize the structural details. Period of amyloid fibrils is defined as distance from one maximum height to the adjacent one along contour length of fibrils (43), and AFM images of OVT amyloid fibrils were chosen to analyze fibril periodicity. As shown in Figure II-11, OVT fibrils had two different periods (31 and 58 nm), corresponding to fibril heights of 3.776 and 5.779 nm. The periodicity of OVT amyloid fibrils increased as height of the fibrils rose. Meanwhile, cross-section analysis of plenty of AFM images (data not shown) showed that most OVT fibrils had periodicity of 30 ± 3 or 60 ± 3 nm, and the maximum height of most OVT fibrils were centered at 3.0 ± 0.8 or 6.0 ± 0.8 nm. It was noteworthy that periods of OVT amyloid fibrils were approximately multiples of ~ 30 nm, and maximum heights of OVT amyloid fibrils were about multiples of ~ 3.0 nm. This finding was similar to a previous study focusing on helical periodicity of fibrils (36), which revealed that the periods of BLG amyloid fibrils were approximately multiples of ~ 36 nm. Since it is postulated that the periodicity of fibrils is a result of multi-stranded filaments (36), it may be assumed that OVT amyloid fibrils have a multi-stranded helical shape. On the basis that BLG fibrils with periods of 35 nm consist of two filaments (36), it is supposed that OVT fibrils with periodicity of 30 ± 3

nm may be 2-filament fibrils. Considering the fact that two 2-filament fibrillar structures can interact to yield a 4-filament ribbon (24), OVT fibrils with periodicity of 60 ± 3 nm should be 4-filament fibrils. To sum up, OVT fibrils possibly have 2-filament or 4-filament multi-stranded structures.



(a)



(b)

Figure II-11. Section analysis of OVT amyloid fibrils in the purpose of checking periods of OVT fibrils. (a) The period of fibrils was 31 nm. The marked height was 3.776 nm. (b) The period of fibrils was 58 nm. The marked height was 5.779 nm

3.6. Surface hydrophobicity of OVT amyloid fibrils

Surface structure of OVT amyloid fibrils was investigated via measuring surface

hydrophobicity. Table II-2 shows that surface hydrophobicity increased slightly during the initial three hours, which was explained by that unfolding and hydrolysis of OVT led to more hydrophobic patches available on the surface. After heating for 3 h, surface hydrophobicity gradually decreased, which might be accounted for by the fact that hydrophobic patches on β -sheets could align to ordered structures during self-assembly into OVT amyloid fibrils (45).

Table II-2. Surface hydrophobicity (H_0) of OVT after heating at 90 °C and pH 2.0 for 0–24 h.

Heating time (h)	H_0
0	1519.6±31.7 ^d
3	1638.0±22.4 ^e
6	1546.2±22.0 ^d
12	1293.3±19.9 ^c
18	1182.7±20.3 ^b
24	1021.4±19.2 ^a

Values are means \pm SD (n=3). Different superscript letters in the same column indicate significant differences ($p < 0.05$).

3.7. Cytotoxicity of OVT amyloid fibrils

Since some protein fibrils are associated with cellular cytotoxicity, there are safety concerns related to application of protein fibrils (46). The MTT assay is a rapid and quantitative cell viability assay, which helps to evaluate *in vitro* cytotoxicity of biomaterials (33, 47). Therefore, cytotoxicity of OVT amyloid fibrils was estimated using the MTT assay. Figure II-12 shows cytotoxicity of OVT amyloid fibrils as function of concentration. It was observed that OVT amyloid fibrils exhibited no

cytotoxicity in the concentration range of 10–1000 $\mu\text{g/mL}$, indicating the biocompatibility of OVT amyloid fibrils. Similar results are found in previous studies, which show that amyloid fibrils from crystallin, whey protein isolate, insulin, ovalbumin, lysozyme and soy protein isolate have no cell cytotoxicity (7, 48–50). It is noteworthy that not all proteins do not exhibit cytotoxicity, and it proves that amyloid fibrils from some proteins such as mammalian prion protein are highly toxic to cultured cells (50). The excellent biosafety of OVT amyloid fibrils indicated that OVT fibrils could be potentially applied in many fields such as cosmetic, food and pharmaceutical industries.

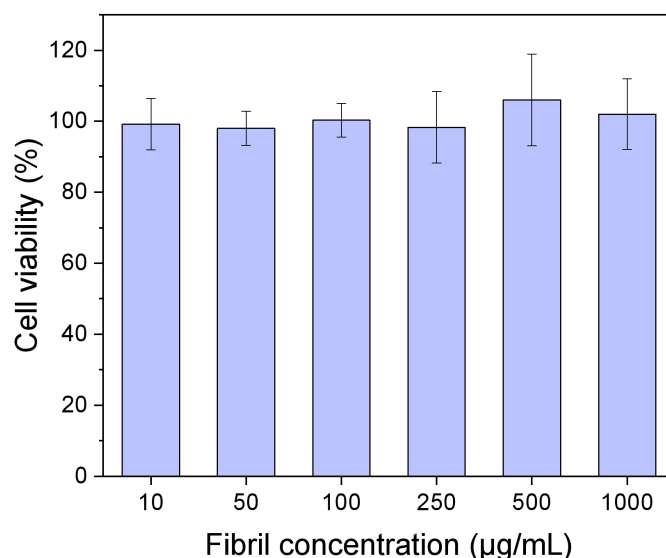


Figure II-12. *In vitro* cytotoxicity of OVT amyloid fibrils on cells as measured by MTT assay.

4. Conclusion

In summary, apart from rigid and long amyloid fibrils, flexible and short amyloid fibrils were also detected during self-assembly of OVT into fibrillar structures. Short

OVT amyloid fibrils (with contour length below 800 nm) were generated upon heating for 1 h, and long OVT amyloid fibrils (with contour length above 800 nm) appeared after 6 h heating. The optimal environmental condition for OVT nanofibrillation was pH 2, 90 °C, an ionic strength of 150 mM and a stirring speed of 300 rpm. Internal structures of OVT amyloid fibrils could be stacked β -sheet, and OVT amyloid fibrils might consist of 2 or 4 multi-stranded filaments. Surface hydrophobicity of OVT amyloid fibrils was lower than that of untreated OVT. OVT amyloid fibrils had no *in vitro* cytotoxicity, suggesting great application potential. The knowledge obtained from this chapter may facilitate better understanding of amyloid fibrils derived from iron-bound proteins.

5. References

1. Wang, W. (2005). Protein aggregation and its inhibition in biopharmaceutics. *International Journal of Pharmaceutics*, 289(1–3), 1–30.
2. Gao, Z., Zhao, J., Huang, Y., Yao, X., Zhang, K., Fang, Y., et al. (2017). Edible Pickering emulsion stabilized by protein fibrils. Part 1: Effects of pH and fibrils concentration. *LWT-Food Science and Technology*, 76, 1–8.
3. Peng, J., Simon, J. R., Venema, P., & van der Linden, E. (2016). Protein fibrils induce emulsion stabilization. *Langmuir*, 32(9), 2164–2174.
4. Jones, O. G., & Mezzenga, R. (2012). Inhibiting, promoting, and preserving stability of functional protein fibrils. *Soft Matter*, 8, 876–895.
5. Chinga-Carrasco, G. (2011). Cellulose fibres, nanofibrils and microfibrils: the morphological sequence of MFC components from a plant physiology and fibre technology point of view. *Nanoscale Research Letters*, 6(1), 417.
6. Mohammadian, M., & Madadlou, A. (2018). Technological functionality and biological properties of food protein nanofibrils formed by heating at acidic condition. *Trends in Food Science & Technology*, 75, 115–128.

7. Hu, B., Shen, Y., Adamcik, J., Fischer, P., Schneider, M., Loessner, M. J., et al. (2018). Polyphenol-binding amyloid fibrils self-assemble into reversible hydrogels with antibacterial activity. *ACS Nano*, 12(4), 3385–3396.
8. Li, C., Adamcik, J., & Mezzenga, R. (2012). Biodegradable nanocomposites of amyloid fibrils and graphene with shape-memory and enzyme-sensing properties. *Nature Nanotechnology*, 7(7), 421–427.
9. Shen, Y., Posavec, L., Bolisetty, S., Hilty, F. M., Nyström, G., Kohlbrecher, J., et al. (2017). Amyloid fibril systems reduce, stabilize and deliver bioavailable nanosized iron. *Nature Nanotechnology*, 287(2), 252–260.
10. Wan, Z., Yang, X., & Sagis, L. M. C. (2016). Nonlinear surface dilatational rheology and foaming behavior of protein and protein fibrillar aggregates in the presence of natural surfactant. *Langmuir*, 32(15), 3679–3690.
11. Mezzenga, R., Schurtenberger, P., Burbidge, A., & Michel, M. (2005). Understanding foods as soft materials. *Nature Materials*, 4, 729–740.
12. Wu, J., & Acero-Lopez, A. (2012). Ovotransferrin: Structure, bioactivities, and preparation. *Food Research International*, 46(2), 480–487.
13. Ibrahim, H. R., & Kiyono, T. (2009). Novel anticancer activity of the autocleaved ovotransferrin against human colon and breast cancer cells. *Journal of Agricultural and Food Chemistry*, 57(23), 11383–11390.
14. Kobayashi, Y., Rupa, P., Kovacs-Nolan, J., Turner, P. V., Matsui, T., & Mine, Y. (2015). Oral administration of hen egg white ovotransferrin attenuates the development of colitis induced by dextran sodium sulfate in mice. *Journal of Agricultural and Food Chemistry*, 63(5), 1532–1539.
15. Varon, O., Allen, K. J., Bennett, D. C., Mesak, L. R., & Scaman, C. H. (2013). Purification and characterization of tinamou egg white ovotransferrin as an antimicrobial agent against foodborne pathogenic bacteria. *Food Research International*, 54(2), 1836–1842.
16. Dave, A. C., Loveday, S. M., Anema, S. G., Loo, T. S., Norris, G. E., Jameson, G. B., et al. (2013). β -Lactoglobulin self-assembly: Structural changes in early stages and disulfide bonding in fibrils. *Journal of Agricultural and Food Chemistry*, 61(32), 7817–7828.
17. Humblet-Hua, N. P., Sagis, L. M. C., & van der Linden, E. (2008). Effects of flow on hen egg white lysozyme (HEWL) fibril formation: Length distribution, flexibility, and kinetics. *Journal of Agricultural and Food Chemistry*, 56(24), 11875–11882.
18. Loveday, S. M., & Gunning, A. P. (2018). Nanomechanics of pectin-linked β -lactoglobulin nanofibril bundles. *Biomacromolecules*, 19(7), 2834–2840.
19. Mantovani, R. A., de Figueiredo Furtado, G., Netto, F. M., & Cunha, R. L. (2018). Assessing the potential of whey protein fibril as emulsifier. *Journal of Food Engineering*, 223, 99–108.
20. Tang, C. H., Wang, S. S., & Huang, Q. (2012). Improvement of heat-induced fibril assembly of soy β -conglycinin (7S Globulins) at pH 2.0 through electrostatic screening. *Food Research International*, 46(1), 229–236.

21. Usov, I., Adamcik, J., & Mezzenga, R. (2013). Polymorphism in bovine serum albumin fibrils: morphology and statistical analysis. *Faraday Discussions*, 166, 151–162.
22. Bolder, S. G., Sagis, L. M. C., Venema, P., & van der Linden, E. (2007). Effect of stirring and seeding on whey protein fibril formation. *Journal of Agricultural and Food Chemistry*, 55(14), 5661–5669.
23. Tan, J. Y., Xu, H. H., Xie, M. M., Wang, X., Dong, S. R., Li, T. J., et al. (2018). Comparative experiments of fibril formation from whey protein concentrate with homogeneous and secondary nuclei. *Food Research International*, 111, 556–564.
24. Lashuel, H. A., LaBrenz, S. R., Woo, L., Serpell, L. C., & Kelly, J. W. (2000). Protofilaments, filaments, ribbons, and fibrils from peptidomimetic self-assembly: Implications for amyloid fibril formation and materials science. *Journal of the American Chemical Society*, 122(22), 5262–5277.
25. Nilsson, M. R. (2004). Techniques to study amyloid fibril formation in vitro. *Methods*, 34(1), 151–160.
26. Usov, I., & Mezzenga, R. (2015). FiberApp: an open-source software for tracking and analyzing polymers, filaments, biomacromolecules, and fibrous objects. *Macromolecules*, 48(5), 1269–1280.
27. Laemmli, U. K. (1970). Cleavage of structural proteins during the assembly of the head of bacteriophage T4. *Nature*, 227(5259), 680–685.
28. Sreerama, N. & Woody, R.W. (2000). Estimation of protein secondary structure from circular dichroism spectra: comparison of CONTIN, SELCON, and CDSSTR methods with an expanded reference set. *Analytical Biochemistry*, 287(2), 252–260.
29. Whitmore, L. & Wallace, B.A. (2008). Protein secondary structure analyses from circular dichroism spectroscopy: Methods and reference databases. *Biopolymers*, 89(5), 392–400.
30. Alizadeh-Pasdar, N., & Li-Chan, E. C. (2000). Comparison of protein surface hydrophobicity measured at various pH values using three different fluorescent probes. *Journal of Agricultural and Food Chemistry*, 48(2), 328–334.
31. Wei, Z., Yang, W., Fan, R., Yuan, F., & Gao, Y. (2015). Evaluation of structural and functional properties of protein–EGCG complexes and their ability of stabilizing a model β -carotene emulsion. *Food Hydrocolloids*, 45, 337–350.
32. Xiao, J., Nian, S., & Huang, Q. (2015). Assembly of kafirin/carboxymethyl chitosan nanoparticles to enhance the cellular uptake of curcumin. *Food Hydrocolloids*, 51, 166–175.
33. Hu, B., Ting, Y., Zeng, X., & Huang, Q. (2012). Cellular uptake and cytotoxicity of chitosan–caseinophosphopeptides nanocomplexes loaded with epigallocatechin gallate. *Carbohydrate Polymers*, 89(2), 362–370.
34. Arosio, P., Knowles, T. P. J., & Linse, S. (2015). On the lag phase in amyloid fibril formation. *Physical Chemistry Chemical Physics*, 17(12), 7606–7618.
35. Wei, Z., Zhu, P., & Huang, Q. (2019). Investigation of ovotransferrin conformation and its complexation with sugar beet pectin. *Food Hydrocolloids*, 87, 448–458.

36. Adamcik, J., Jung, J. M., Flakowski, J., De Los Rios, P., Dietler, G., & Mezzenga, R. (2010). Understanding amyloid aggregation by statistical analysis of atomic force microscopy images. *Nature Nanotechnology*, 5(6), 423–428.
37. Knowles, T. P., Fitzpatrick, A. W., Meehan, S., Mott, H. R., Vendruscolo, M., Dobson, C. M., et al. (2007) Role of intermolecular forces in defining material properties of protein nanofibrils. *Science*, 318(5858), 1900–1903.
38. Zhao, Y. L., & Wu, Y. D. (2002). A theoretical study of β -sheet models: is the formation of hydrogen-bond networks cooperative? *Journal of the American Chemical Society*, 124(8), 1570–1571.
39. Arnaudov, L. N., & de Vries, R. (2006). Strong impact of ionic strength on the kinetics of fibrillar aggregation of bovine β -lactoglobulin. *Biomacromolecules*, 7(12), 3490–3498.
40. van der Linden, E. (2012). From peptides and proteins to micro-structure mechanics and rheological properties of fibril systems. *Food Hydrocolloids*, 26(2), 421–426.
41. Munialo, C. D., Martin, A. H., van der Linden, E., & de Jongh, H. H. J. (2014). Fibril formation from pea protein and subsequent gel formation. *Journal of Agricultural and Food Chemistry*, 62(11), 2418–2427.
42. Lu, K., Jacob, J., Thiyagarajan, P., Conticello, V. P., & Lynn, D. G. (2003). Exploiting amyloid fibril lamination for nanotube self-assembly. *Journal of the American Chemical Society*, 125(21), 6391–6393.
43. Arnaudov, L. N., & de Vries, R. (2005). Thermally induced fibrillar aggregation of hen egg white lysozyme. *Biophysical Journal*, 88(1), 515–526.
44. Loveday, S. M., Anema, S. G., & Singh, H. (2017). β -Lactoglobulin nanofibrils: The long and the short of it. *International Dairy Journal*, 67, 35–45.
45. Liu, G., & Zhong, Q. (2013). Dispersible and thermal stable nanofibrils derived from glycated whey protein. *Biomacromolecules*, 14(7), 2146–2153.
46. Xue, W. F., Hellewell, A. L., Gosal, W. S., Homans, S. W., Hewitt, E. W., & Radford, S. E. (2009). Fibril fragmentation enhances amyloid cytotoxicity. *Journal of Biological Chemistry*, 284(49), 34272–34282.
47. van Meerloo, J., Kaspers, G. J. L., & Cloos, J. (2011). *Cancer cell culture: Methods and protocols*. (2nd ed.). New York: Humana Press, (Chapter 20).
48. Kaur, M., Healy, J., Vasudevamurthy, M., Lassé, M., Puskar, L., Tobin, M. J., et al. (2014). Stability and cytotoxicity of crystallin amyloid nanofibrils. *Nanoscale*, 6(21), 13169–13178.
49. Lassé, M., Ulluwishewa, D., Healy, J., Thompson, D., Miller, A., Roy, N., et al. (2016). Evaluation of protease resistance and toxicity of amyloid-like food fibrils from whey, soy, kidney bean, and egg white. *Food Chemistry*, 192, 491–498.
50. Novitskaya, V., Bocharova, O. V., Bronstein, I., & Baskakov, I. V. (2006). Amyloid fibrils of mammalian prion protein are highly toxic to cultured cells and primary neurons. *Journal of Biological Chemistry*, 281(19), 13828–13836.

CHAPTER III. IN VITRO DIGESTION AND STABILITY OF OVOTRANSFERRIN FIBRILS

1. Introduction

Fibrils derived from food proteins are regarded as attractive food ingredients, and it is essential to study digestion of protein fibrils in gastrointestinal system before practical application. Adequate understanding of fibril digestibility helps to understand performance of delivery systems constructed by fibrils (1). However, few studies about fibril digestibility have been carried out to date, and the limited digestion studies focus on β -lactoglobulin (2, 3).

Stability of protein fibrils is vital during handling and application of fibrils (4). Apart from structural characteristics such as N-terminal region and phosphorylation of fibrils themselves (5, 6), fibril stability is also affected and controlled by various environmental factors. It is worthwhile to understand stability of protein fibrils against different types of environmental stresses. Since protein aggregation is sometimes controlled by pH and protein conformation is dependent on pH (7, 8), fibrils may be unstable at some specific pHs. To our best knowledge, long-term storage stability of food protein fibrils over a wide range of pH has seldom been done before. Relevant research may give practical guidance for storage of fibrils and help to reveal influence of surface charge on fibril stability. Moreover, environmental stresses such as frozen storage, freeze-drying and high-speed shearing are likely to disrupt structures of fibrils, and excellent stability of food protein fibrils against these environmental

stresses is desirable for food processing.

Thus, the objectives of this chapter were to study *in vitro* digestion and stability against environmental stresses of OVT fibrils. Digestibility of OVT fibrils in an *in vitro* gastrointestinal digestion model was evaluated using thioflavin T fluorescence and atomic force microscopy. Subsequently, long-term storage stability of OVT fibrils over a wide range of pH was examined. Finally, stability of OVT fibrils against environmental stresses such as frozen storage, freeze-drying and high-speed shearing was evaluated.

2. Materials and Methods

2.1. Materials

Ovotransferrin (OVT) (purity > 88%) was purchased from Neova Technologies Inc. (Abbotsford, Canada), and OVT had an iron binding activity > 1000 $\mu\text{g Fe/g}$ sample. Thioflavin T (ThT) was purchased from Acros Organics (Geel, Belgium). Pepsin (1:3000) was purchased from Amresco (Solon, USA), and pancreatin was obtained from Thermo Fisher Scientific, Inc. (Waltham, USA). β -Lactoglobulin (BLG) (>93.4%, purity) was obtained from Davisco Foods International Inc. (Le Sueur, USA).

2.2. Preparation of OVT fibrils

The optimal environmental condition for OVT fibrillation was obtained in our previous study (9). OVT stock solutions (4%, w/v) were prepared by dispersing and dissolving OVT in pH-adjusted NaCl solution (pH 2, 150 mM NaCl), followed by full hydration overnight. The pH was readjusted and maintained at pH 2 by titrating HCl

carefully. Sodium azide (0.02%, w/v) was added so as to inhibit microbial growth. The OVT stock solutions were filtered with 0.2 μm pore-sized syringe filters (Thermo Fisher Scientific, Waltham, USA) to remove impurities. Subsequently, OVT solutions were heated in oil bath over a temperature-controlled hot plate stirrer (VWR International, Radnor, USA) at 90 °C and a constant stirring speed of 300 rpm. After 24 h, the acquired OVT fibril dispersions were cooled in an ice-water bath immediately. OVT fibril dispersions were kept in the refrigerator (4 °C) until further analysis. To characterize OVT fibrils more clearly, OVT protein without any treatment was set as OVT control.

2.3. *In vitro* digestion of OVT fibrils

Fibril digestion in simulated gastric fluid (SGF) was studied based on a previously published method (2). OVT fibrils were first diluted with SGF (34 mM NaCl, pH 1.5, no enzyme) to obtain a final protein concentration of 3 mg/mL. Pepsin solution (pH 2, 10 mg/mL) was freshly prepared and added to diluted fibril dispersions to make a final pepsin concentration of 2 mg/mL. The samples were shaken at 37°C at a speed of 50 rpm in VWR 1585 shaking incubator (VWR International, Radnor, USA). As gastric emptying of a meal was often completed between 3 and 4 h (10), the gastric digestion duration was set as 4 h. Aliquots (160 μL) were drawn for ThT fluorescence analysis after different incubation periods (0–240 min), and 0.2 M Na_2CO_3 was added to inactivate pepsin and cease simulated gastric digestion. The loss rate of OVT fibrils was calculated as $(I_0 - I_1)/I_0$, where I_0 was the initial ThT fluorescence before digestion, and I_1 was the ThT fluorescence at any time

during digestion. Morphology of OVT fibrils during simulated gastric digestion was studied employing AFM.

For the stage of simulated intestinal digestion, the pH of the mixture dispersions was first adjusted to pH 7.0 with 0.1 M NaHCO₃. A mixture solution containing pancreatin (10 mg/mL), CaCl₂ (25 mM) and bile salt (25 mg/mL) was added to initiate simulated intestinal digestion, and final pancreatin concentration was 2 mg/mL. The samples were shaken at 37°C at a speed of 50 rpm for 120 min, and ThT fluorescence as well as AFM were applied to analyze digestibility of OVT fibrils immediately.

2.4. Thioflavin T (ThT) fluorescence spectroscopy

Based on method described in a previous study (11). ThT fluorescence intensity was measured as described in Chapter II.

2.5. Atomic force microscopy (AFM)

Based on method described in a previous study (12), morphology of OVT fibrils was measured as described in Chapter II.

2.6. Zeta potential measurements

The zeta potential of OVT control and OVT fibrils was measured using a Zetasizer Nano-ZS90 instrument (Malvern Instruments, Worcestershire, UK).

2.7. Long-term storage stability of OVT fibrils at different pHs

OVT fibrils were diluted to a protein concentration of 0.1 mg/mL with pH-adjusted Milli-Q water (pH 2–10), and the solutions were readjusted to corresponding pH with 0.1M HCl or NaOH carefully. Sodium azide was added to inhibit microbial growth. Afterwards, OVT fibril dispersions were stored at room

temperature for 144 h, and AFM was applied to analyze storage stability of OVT fibrils immediately.

In order to make comparisons and better understand long-term storage stability of protein fibrils at different pHs, long-term storage stability of β -lactoglobulin (BLG) fibrils was also studied. Preparation of BLG fibrils was similar to that of OVT fibrils as described in 2.2. Briefly speaking, BLG stock solutions (4%, w/v) were prepared by dispersing and dissolving BLG in pH-adjusted NaCl solution (pH 2, 50 mM NaCl), and sodium azide (0.02%, w/v) was added to retard microbial growth. Afterwards, BLG solutions (pH 2) were heated in oil bath over a temperature-controlled hot plate stirrer (VWR International, Radnor, USA) at 80 °C and a constant stirring speed of 300 rpm. The acquired BLG fibril dispersions were diluted to a protein concentration of 0.1 mg/mL with pH-adjusted Milli-Q water (pH 2–10), and the solutions were readjusted to corresponding pH with 0.1M HCl or NaOH carefully. Subsequently, BLG fibril dispersions were stored at room temperature for 144 h (with sodium azide as preservative), and AFM imaging was employed to evaluate storage stability of BLG fibrils.

2.8. Impact of frozen storage–lyophilization–rehydration on OVT fibrils

For this part, OVT fibrils were frozen at -20°C for two weeks. Afterwards, OVT fibrils were lyophilized (FreeZone Freeze Dry System, Labconco Corporation, Kansas, USA) and rehydrated with Milli-Q water (pH 2) to obtain dispersions at protein concentrations of 40 mg/mL. Aliquots (40 μL) were drawn for ThT fluorescence analysis, and AFM imaging was also used to monitor stability of OVT fibrils. The loss

rate of OVT fibrils was calculated as $(I_0 - I_1)/I_0$, where I_0 was the initial ThT fluorescence without treatment, and I_1 was the ThT fluorescence after treatment of frozen storage–lyophilization–rehydration.

2.9. Impact of high-speed shearing on OVT fibrils

OVT fibril dispersions were sheared using an Ultra-Turrax (IKA-Werke GmbH & Co., Germany) at a speed of 3,500–12,000 rpm for 6 min. ThT fluorescence and AFM were used to monitor fibril stability. The loss rate of OVT fibrils was calculated as $(I_0 - I_1)/I_0$, where I_0 was the initial ThT fluorescence without treatment, and I_1 was the ThT fluorescence after treatment of high-speed shearing.

3. Results and Discussion

3.1. *In vitro* digestion of OVT fibrils

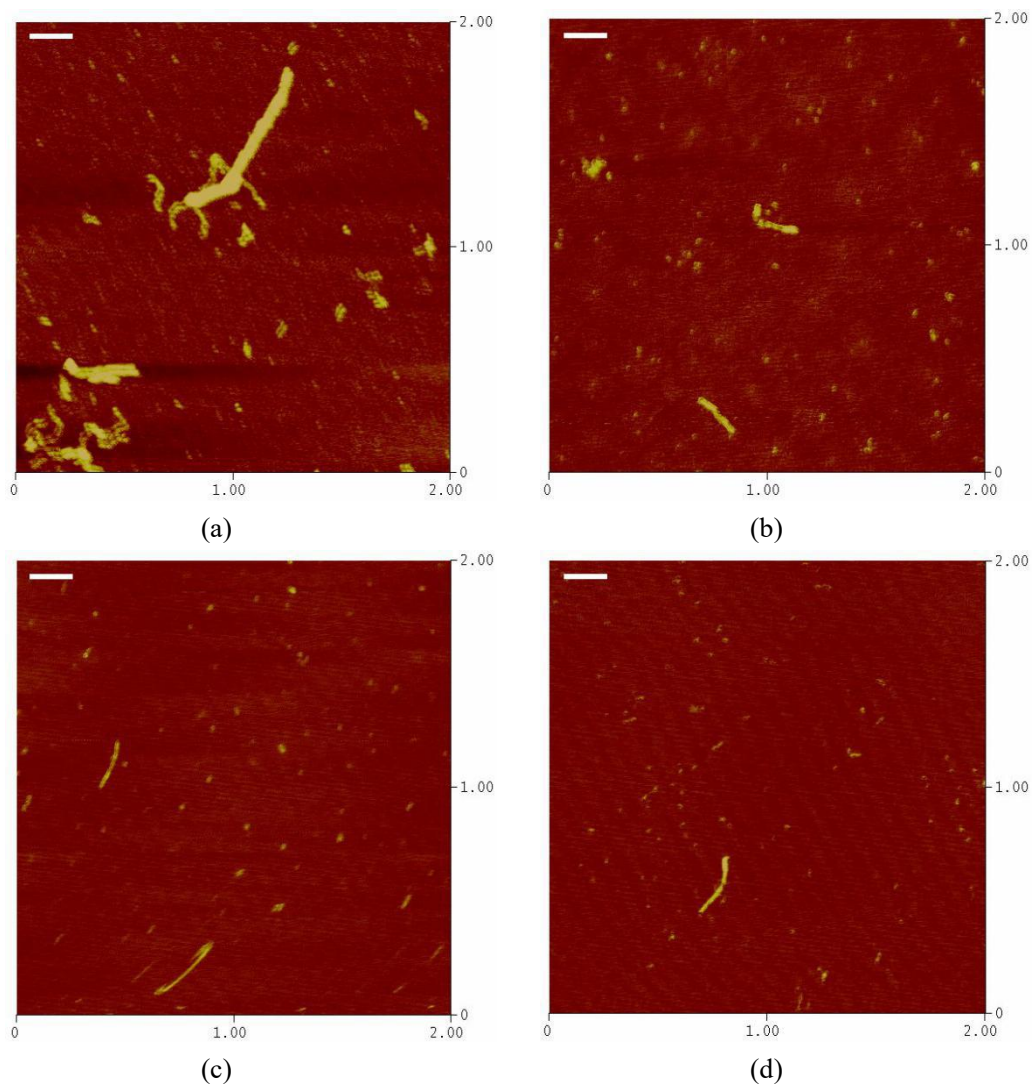
Table III-1. Relative ThT fluorescence intensity and digestion rate of OVT fibrils after different periods of simulated gastric digestion

Digestion time (min)	Relative ThT intensity (a.u.)	Loss rate (%)
0	5737.3±97.4 ^g	0 ^a
5	4582.9±114.7 ^f	20.1±3.7 ^b
10	4101.9±100.9 ^e	28.5±3.5 ^c
15	3820.6±76.8 ^d	33.4±3.0 ^{cd}
30	3632.4±89.3 ^c	36.7±3.3 ^{de}
60	3367.7±74.2 ^b	41.3±3.0 ^{ef}
120	3223.5±68.2 ^b	43.8±2.9 ^f
180	2873.2±55.0 ^a	49.9±2.6 ^g
240	2851.4±63.9 ^a	50.3±2.8 ^g

Different superscript letters in the same column indicate significant differences ($p < 0.05$).

To the best of our knowledge, β -lactoglobulin (BLG) fibrils have been applied in

design of some nutraceutical delivery vehicles (1, 13, 14), but there are no studies about application of OVT fibrils in food systems so far. Since OVT fibrils exhibited no detrimental effects on cell viability in an *in vitro* Caco-2 cell model and the non-toxic character made OVT fibrils potential food materials (9), *in vitro* digestion of OVT fibrils was further investigated.



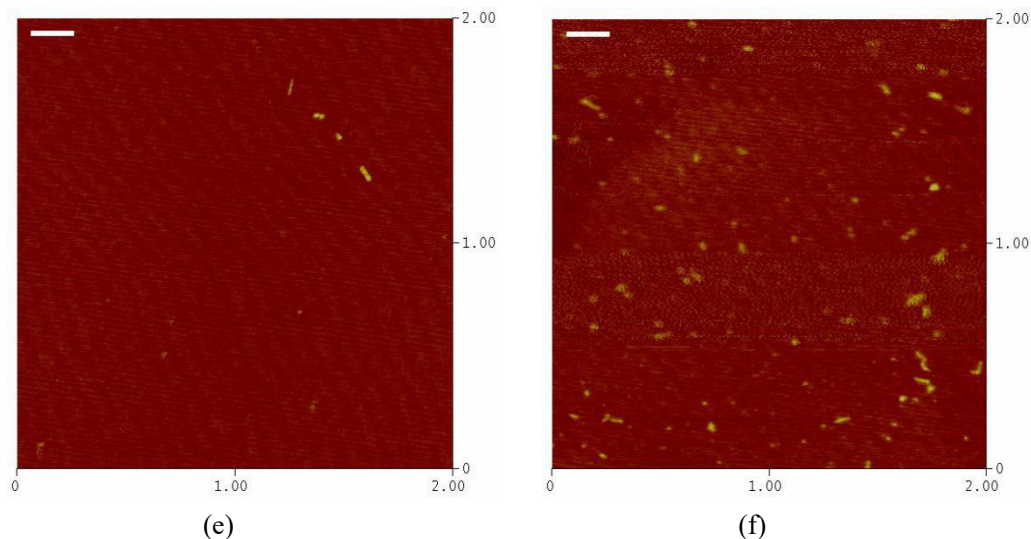


Figure III-1. AFM images of OVT fibrils after different periods of simulated gastric digestion: (a) 0 h, (b) 0.5 h, (c) 1 h, (d) 2 h, (e) 3 h, (f) 4 h. The scan size is $2\ \mu\text{m}\times 2\ \mu\text{m}$, and the z scale is 10 nm. The scale bar represents 200 nm.

Since thioflavin T (ThT) fluorescence is a sensitive method to detect fibrillar structures (15), ThT fluorescence was employed to study digestion of OVT fibrils. Table III-1 shows that ThT fluorescence decreased as the digestion time was increased, suggesting that plenty of fibrillar structures were disrupted during *in vitro* gastric digestion. The fastest reduction in the amount of OVT fibrils occurred within the first 5 min, and 50.3 percent of initial fibrillar structures disappeared at a digestion time of 4 h. Two explanations may account for reduction of OVT fibrils. First, since some fibrillar structures may consist of intact OVT monomers (4, 16, 17), the pepsin proteolysis may cleave the intact protein molecules into several fragments, which results in collapse of fibrillar structures. Second, apart from intact OVT monomers, it may be speculated that certain peptides derived from OVT can also form OVT fibrils (4, 18). During *in vitro* gastric digestion, pepsin can break up OVT peptides into peptides with smaller molecular mass via cleavage of peptide bonds and the smaller

peptides may not be suitable to stabilize fibrillar structures, leading to disintegration of OVT fibrils. It should also be noted that reformation of OVT fibrils may occur during gastric digestion. A previous study demonstrates that some new peptides can be produced via pepsin hydrolysis, which are suitable for further fibrillation (3). Meanwhile, it can be inferred from ThT fluorescence data in Table III-1 that reformation of OVT fibrils is much slower than disintegration if reformation of OVT fibrils exists.

Atomic force microscopy is an accurate technique to probe shape and size of protein fibrils visually (19), so influence of *in vitro* gastric digestion on morphology of OVT fibrils was also investigated using AFM. Figure III-1 depicts that long and straight fibrils with contour length over 500 nm vanished after digestion of 0.5 h. Medium-length fibrils with contour length above 250 nm still existed at a digestion time of 0.5–2 h, and only short fibrils with contour length below 200 nm were observed as the digestion time was increased to 3–4 h.

Table III-2. Relative ThT fluorescence intensity and digestion rate of OVT fibrils before and after simulated intestinal digestion

Digestion time (min)	Relative ThT intensity (a.u.)	Loss rate (%)
240 ^a	2851.4±63.9	50.3±2.8
360 ^b	969.1±41.5	83.1±1.0

Notes: The superscript letter “a” indicates that OVT fibrils underwent 4 h of simulated gastric digestion before initiating simulated intestinal digestion. The superscript letter “b” indicates that OVT fibrils underwent 4 h of simulated gastric digestion and 2 h of simulated intestinal digestion.

After simulated gastric digestion, OVT fibrils underwent subsequent simulated intestinal digestion. Table III-2 shows that further reduction in the amount of OVT fibrils occurred upon digestion in simulated intestinal fluid. This phenomenon implies that action of pancreatin may disrupt OVT fibrillar structures via hydrolysis of peptide bonds. Besides, impact of bile salts and calcium in simulated intestinal fluid on fibrillar structures of OVT fibrils should not be ignored. Micelles of surfactants (bile salts, etc) may disrupt structures of protein fibrils (20), and calcium can induce interfibril and intrafibril entanglements (21), which contributes to decrease of fibrils. As depicted in Figure III-2, although OVT fibrils could still be detected, the fibrillar structures turned a bit vague. The survival of some fibrillar structures during digestion indicated that OVT fibrils showed resistance to proteolytic digestion *in vitro* to a certain degree. Similar result was found in a previous study, which demonstrated that some of SPI (soy protein isolate) fibrils exhibited protease resistance (22).

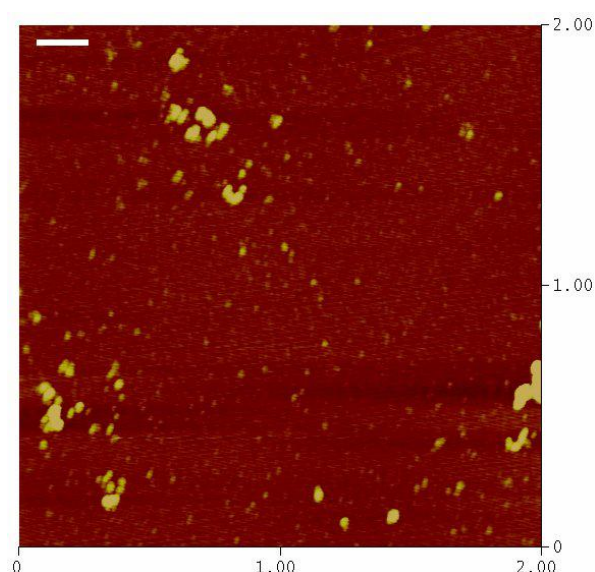


Figure III-2. AFM image of OVT fibrils after simulated intestinal digestion. The scan size is 2 μm×2 μm, and the z scale is 10 nm. The scale bar represents 200 nm.

3.2. Zeta potential of OVT fibrils

Since zeta potential is related to surface charge of particles and crucial to colloidal stability in various systems (23, 24), zeta potential of OVT fibrils was studied here. Figure III-3 depicts zeta potential of OVT fibril dispersion and OVT control. The isoelectric point of OVT control was around pH 6.2, and upon fibrillation the isoelectric point of OVT fibrils shifted to about pH 7.0. OVT fibrils carried slightly fewer positive charges than OVT control in the pH range of 2 to 5, and zeta potential of OVT fibrils was evidently larger than that of OVT control over the pH range of 7–10. The alterations in zeta potential reflected that charge patches on the surface reached a new equilibrium after OVT fibrillation. During protein fibrillation, processes such as denaturation, hydrolysis and assembly of structural units may occur (4, 25), which may contribute to variations in surface charge patches and subsequent change in zeta potential.

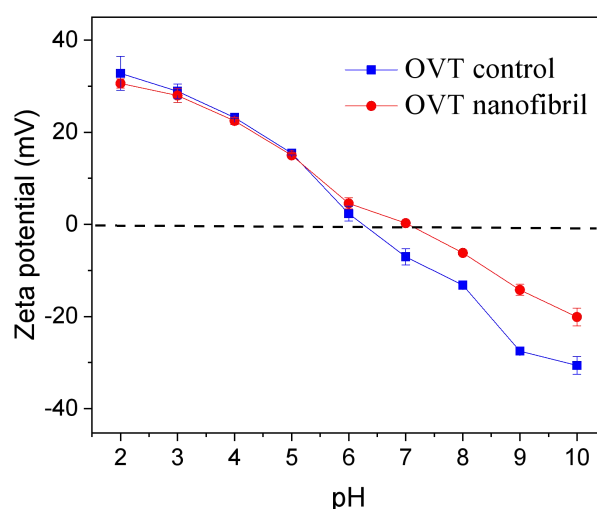
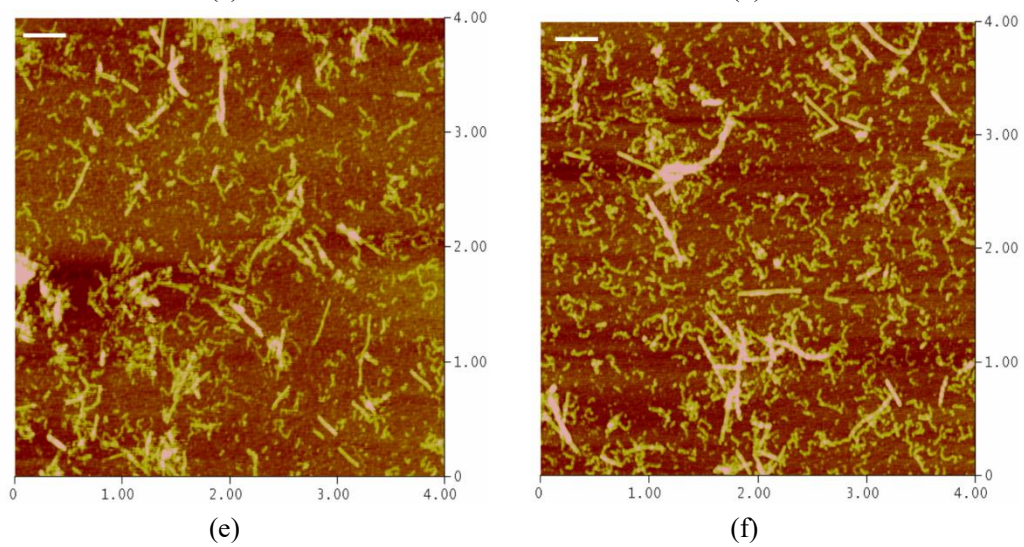
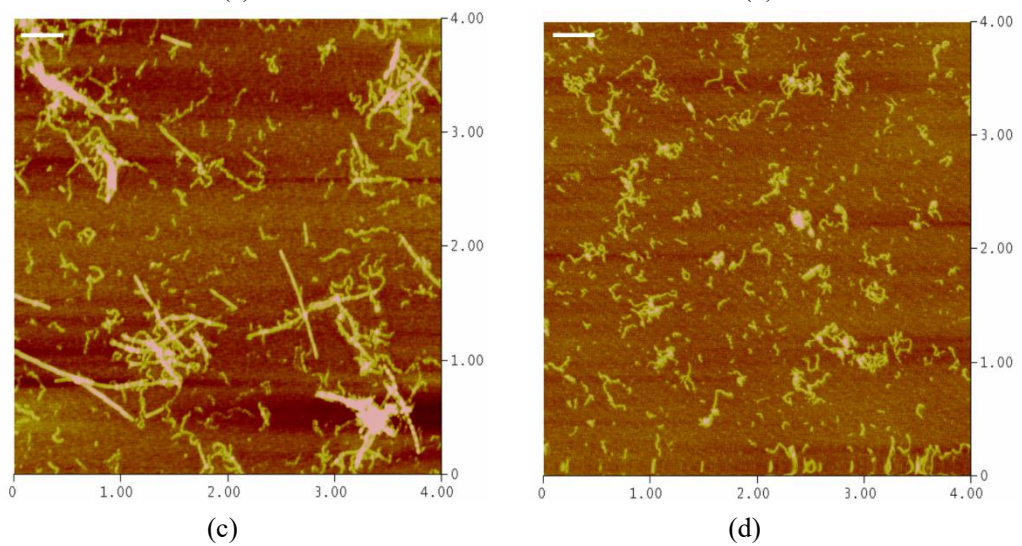
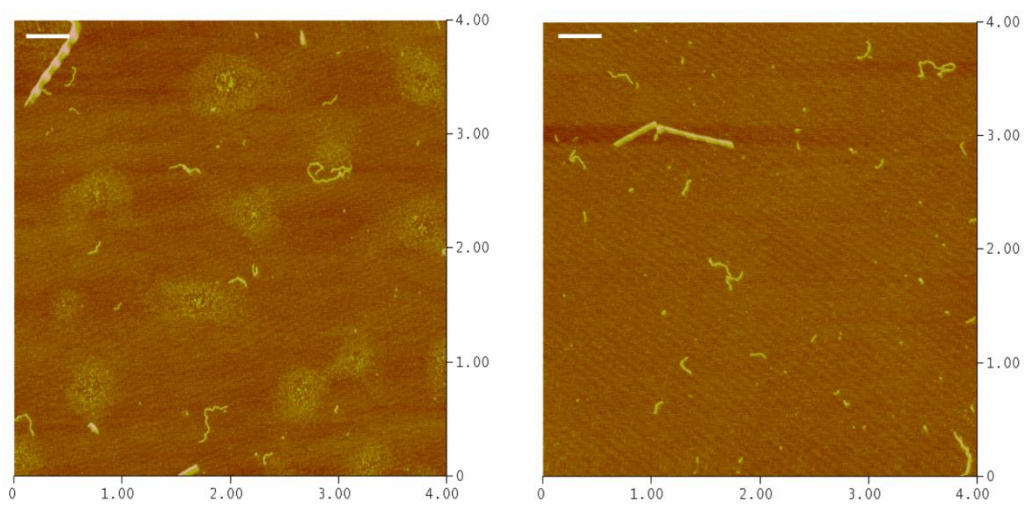


Figure III-3. Zeta potential of OVT fibrils and OVT control as function of pH.

3.3. Long-term storage stability of OVT fibrils over a wide pH range



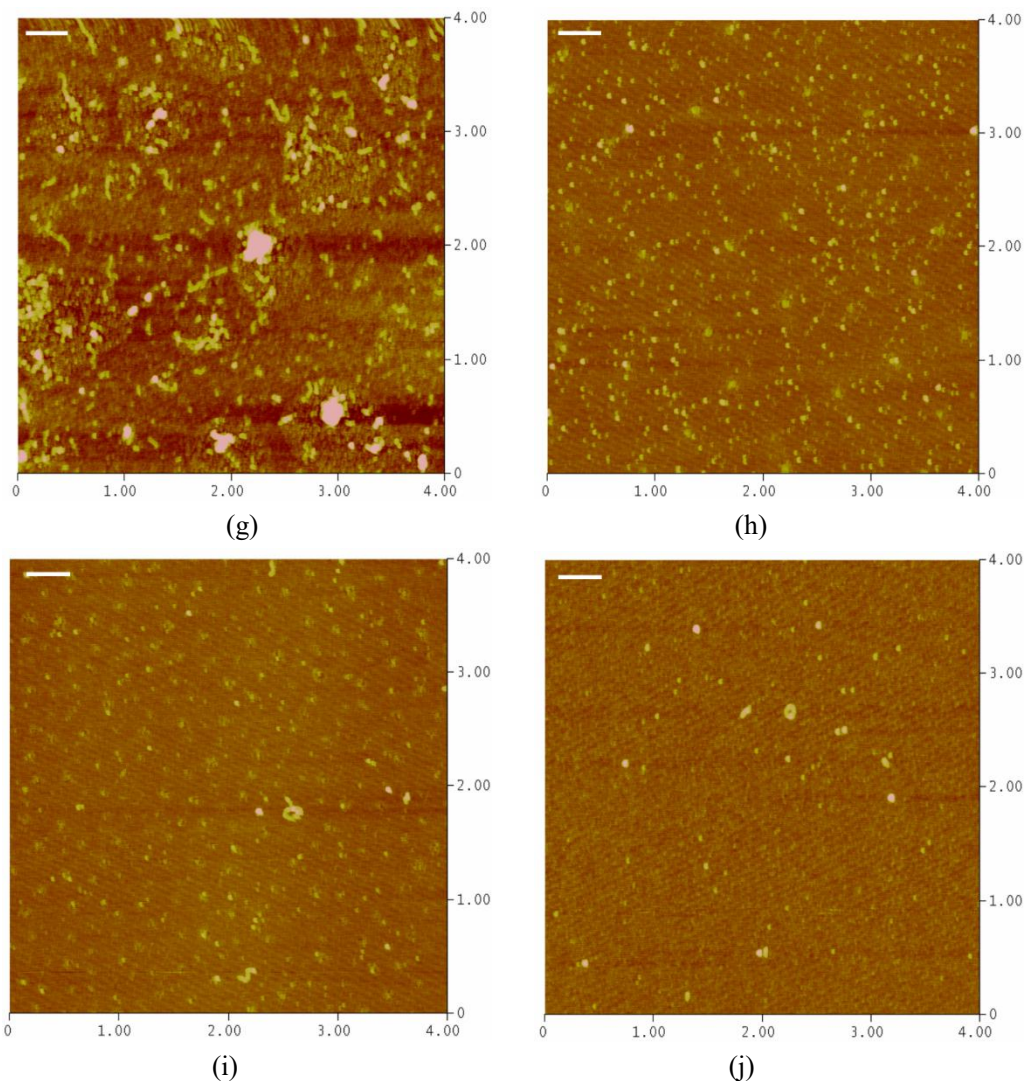


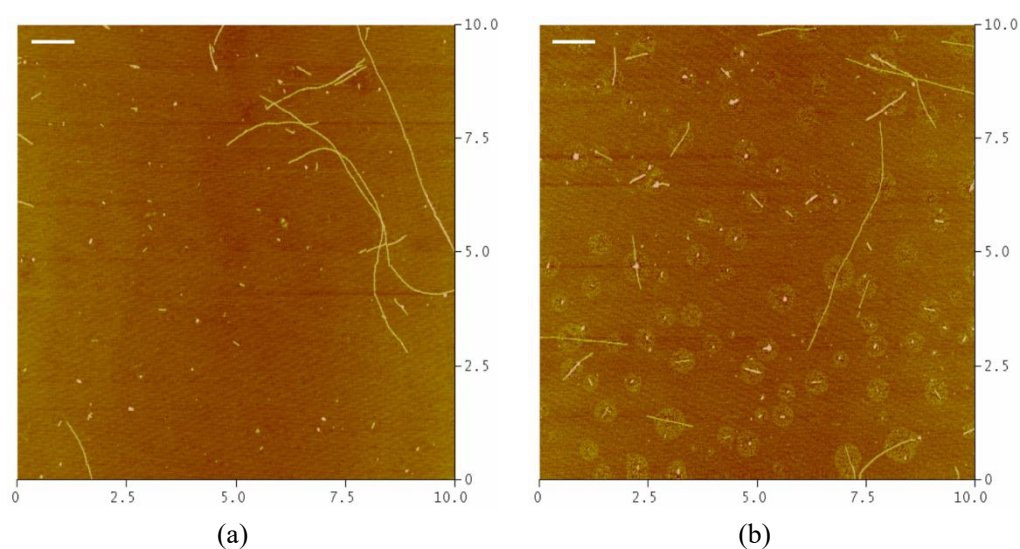
Figure III-4. AFM images of OVT fibrils after 144-h room-temperature storage at different pHs: (a) pH 2, (b) pH 3, (c) pH 4, (d) pH 5, (e) pH 6, (f) pH 7, (g) pH 7.5, (h) pH 8, (i) pH 9, (j) pH 10. The scan size is $4\ \mu\text{m}\times 4\ \mu\text{m}$, and the z scale is 20 nm. The scale bar represents 400 nm.

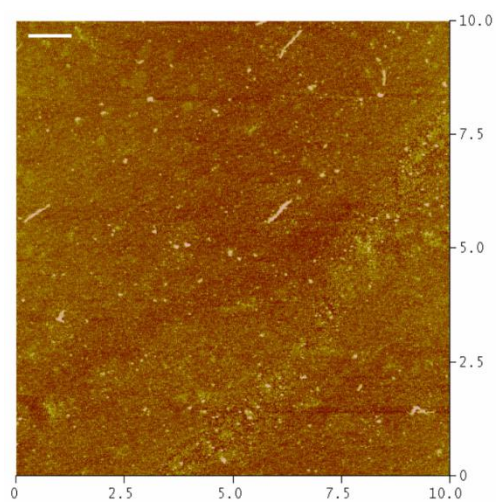
Although stability of protein fibrils at various pHs has already been investigated, most of relevant measurements are conducted shortly after placing fibrils in pH-adjusted environments (26). As far as we know, comparatively little is known about long-term storage stability of protein fibrils at various pHs, although long-term storage study of fibrils actually has more practical significance. Figure III-4 shows AFM pictures of OVT fibrils after long-term storage at various pHs. It was apparent

that fibrillar structures existed in the range of pH 2 to 7. At pH 7.5, it was observed that plenty of OVT fibrils were fractured into a large amount of small spherical aggregates. Only spherical aggregates were detected after long-term storage at pH 8. Although very few fibrillar structures with either closed or open contours could still be observed after storage at pH 9 or 10, almost all of fibrils disappeared and smaller spherical aggregates were dispersed uniformly. In other words, OVT fibrils were not stable during storage above pH 7, and it was worthwhile to note that pH 7 was close to isoelectric point of OVT fibril dispersion.

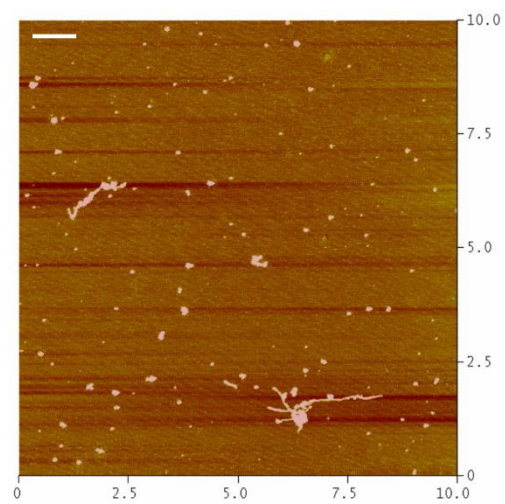
Meanwhile, long-term storage stability of BLG (β -lactoglobulin) fibrils at different pHs was also studied, and the systematic research could help to find general rules about storage stability of protein fibrils. Preparation of BLG fibrils was based on results shown in previous studies (27, 28). Figure III-5 illustrates that obvious fibrillar structures with contour length above 800 nm existed after long-term storage over the pH range 2 to 5. After 144-h storage above pH 5, BLG fibrils were fractured into small globular aggregates and almost all of fibrillar structures vanished, suggesting that BLG fibrils were unstable at pHs above 5. It was worth noting that pH 5 approached isoelectric point of BLG fibril dispersion (26). In summary, for both OVT fibrils and BLG fibrils, the critical pH point associated with destabilization of fibrils during long-term storage was close to their respective isoelectric point. The storage stability of protein fibrils at different pHs may be accounted for by following explanations. The factors that affect formation and stability of protein fibrils consist of hydrogen bondings, electrostatic, hydrophobic as well as aromatic interactions (29,

30). Thus, altering electrostatic interactions may be detrimental to fibril stability (31). It may be speculated that some peptides which participate in the self-assembly of food protein fibrils may have a lot of free carboxyl groups and few free amino groups, and the overall electrical charge of these peptides may be almost zero at pHs below isoelectric points. When pH increases above isoelectric points, these peptides may carry a lot of negative charges, which generates strong electrostatic repulsion among the structural units of fibrils. The strong electrostatic repulsion can be sufficient to disrupt stabilization forces of fibrillar structures and lead to dissociation of fibrils. The underlying mechanisms will be further explored and confirmed using tools such as liquid chromatography–mass spectrometry and molecular dynamics simulations in our future studies (32).

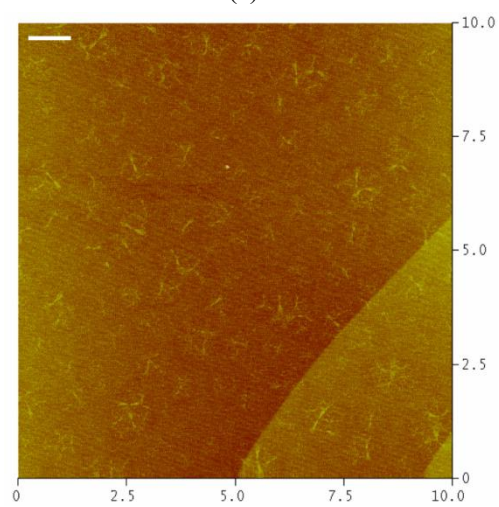




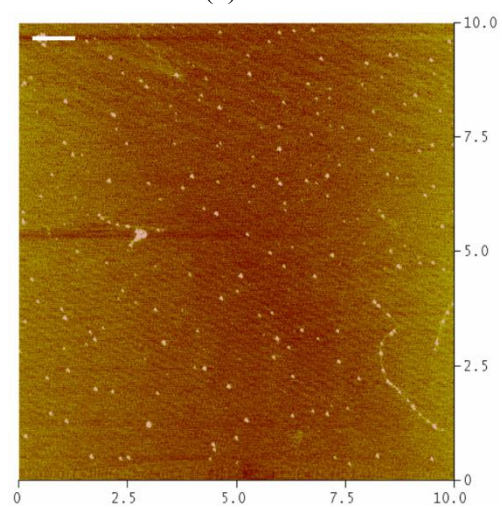
(c)



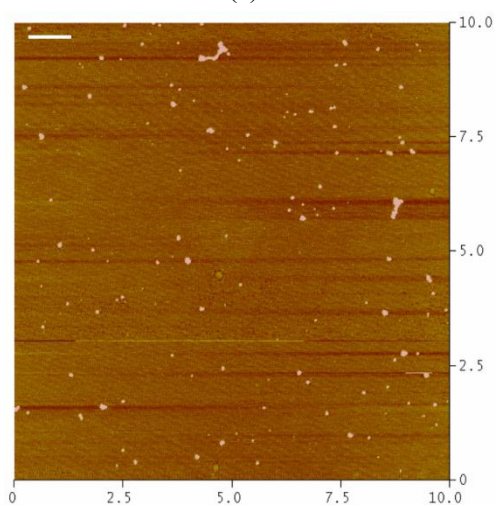
(d)



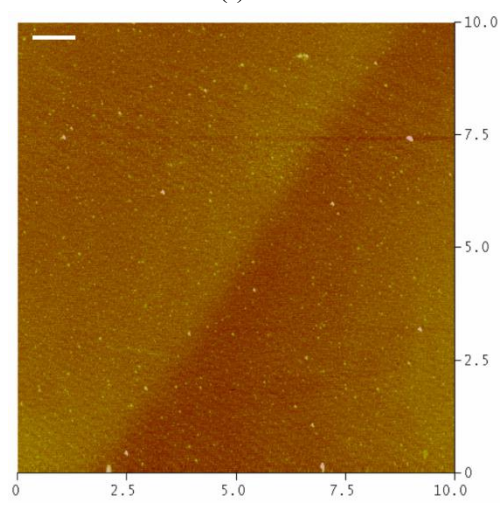
(e)



(f)



(g)



(h)

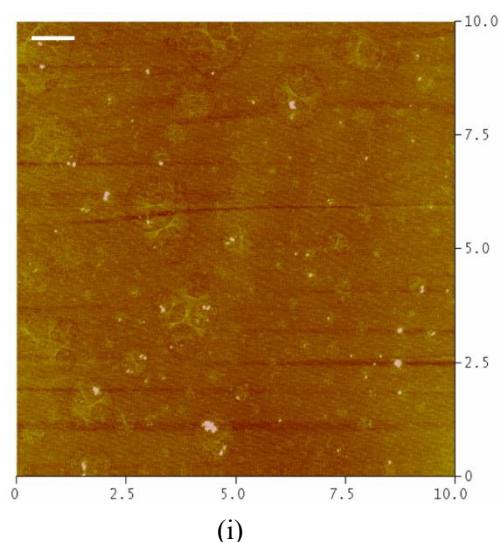


Figure III-5. AFM images of β -lactoglobulin fibrils after 144-h room-temperature storage at different pHs: (a) pH 2, (b) pH 3, (c) pH 4, (d) pH 5, (e) pH 6, (f) pH 7, (g) pH 8, (h) pH 9, (i) pH 10. The scan size is $10\ \mu\text{m}\times 10\ \mu\text{m}$, and the z scale is 20 nm.

3.4. Fibril stability against frozen storage–lyophilization–rehydration

Freeze-dried powders provide advantages at the shipping, storage and distribution stages while allowing for factors such as shelf-life, microbial contamination, convenience and transportation costs (33, 34). Therefore, lyophilization of fibrils is essential in practical applications. Influence of frozen storage, lyophilization and rehydration on OVT fibrils was investigated, which helped to reveal commercial potential of OVT fibrils. As shown in Figure III-6, no obvious changes in morphology of OVT fibrils were found after a series of processes including frozen storage, lyophilization and rehydration, suggesting that OVT fibrils sustained little damage. When compared with frozen storage and rehydration, lyophilization is a relatively gentle process (33, 34). The mechanical stresses mainly come from initial freezing and rehydration (33), and the invulnerable characteristic implies that OVT fibrils are stable against these mechanical stresses. Specifically

speaking, very small fine ice crystals are formed at relatively fast cooling rate (34), and the induced mechanical stresses may not be strong enough to disrupt fibrillar structures of OVT fibrils. In terms of rehydration, the mechanical impact of rapid imbibing of water by OVT fibril powders may also be negligible. In the case of WPI (whey protein isolate) fibrils, after treatment of frozen storage–lyophilization–rehydration, curly WPI fibrils suffered little damage, but straight WPI fibrils were fractured into shorter fibrils (35). Overall, OVT fibrils possessed better stability against frozen storage–lyophilization–rehydration than WPI fibrils. Table III-3 shows that the loss rate of fibrillar structures was less than 1%, which was consistent with AFM data in Figure III-6.

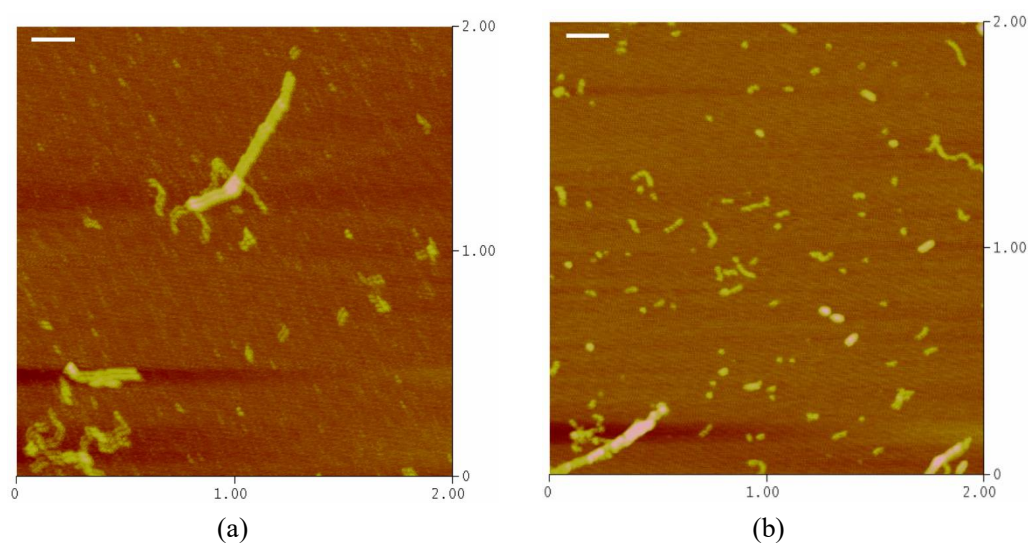


Figure III-6. AFM images of OVT fibrils before and after treatment of frozen storage–lyophilization–rehydration: (a) control, (b) after treatment of frozen storage–lyophilization–rehydration. The scan size is $2\ \mu\text{m}\times 2\ \mu\text{m}$, and the z scale is 20 nm. The scale bar represents 200 nm.

Table III-3. Relative ThT fluorescence intensity and loss rate of OVT fibrils after treatment of frozen storage–lyophilization–rehydration

Sample	Relative ThT intensity (a.u.)	Loss rate (%)
Control OVT fibril	19124.4±10.6	0
Treated OVT fibril	19010.2±15.3	0.59±0.13

3.5. Fibril stability against high-speed shearing

Given that fibrillar structures with various lengths may behave differently and shear flow is likely to alter shape as well as size of protein aggregates (13, 36, 37), influence of high-speed shearing on OVT fibrils was studied. As shown in Figure III-7, average contour length of OVT fibrils decreased with increasing shearing speed, and average contour length of OVT fibrils after shear treatment of 12,000 rpm was about 72 nm. Upon shear treatment, it was apparent that the amount of straight and semiflexible fibrils decreased, and more curly and flexible fibrils appeared. Since stiff (semiflexible) protein fibrils have higher mechanical strength than flexible ones (38), OVT fibrils after high-speed shear treatment may be applied to create softer nutraceutical delivery vehicles. Table III-4 reveals that OVT fibrils suffered limited loss of fibrillar structures, suggesting that shear treatment could lead to generation of shorter fibrils without destroying fibrillar structures. Considering the fact that many physicochemical and biological properties of protein fibrils depend largely on contour length and flexibility of protein fibrils, high-speed shearing may provide a reliable means to tailor OVT fibrils to the specific needs.

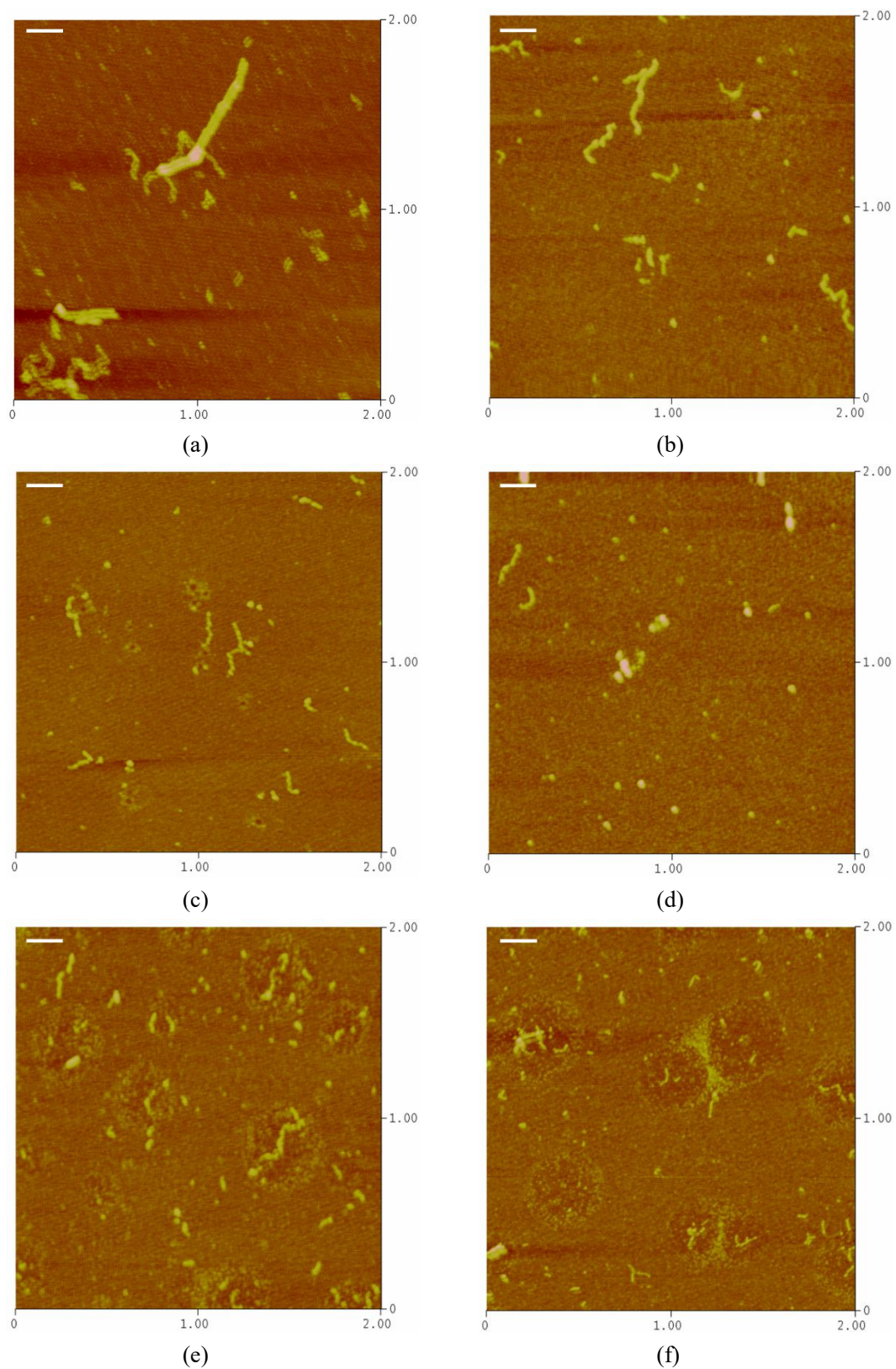


Figure III-7. AFM images of OVT fibrils after treatment of high-speed shearing (a) 0 rpm (b) 3500 rpm (c) 5000 rpm (d) 6000 rpm (e) 8000 rpm (f) 12000 rpm. The scan size is $2\ \mu\text{m} \times 2\ \mu\text{m}$, and the z scale is 20 nm. The scale bar represents 200 nm.

Table III-4. Relative ThT fluorescence intensity and loss rate of OVT fibrils after high-speed shearing.

Shearing speed (rpm)	Relative ThT intensity (a.u.)	Loss rate (%)
0	19124.4±10.6 ^a	0 ^a
3500	19021.0±12.1 ^b	0.54±0.12 ^b
5000	18765.3±11.8 ^c	1.88±0.12 ^c
6000	18664.4±18.6 ^d	2.41±0.15 ^d
8000	18657.1±15.1 ^d	2.44±0.13 ^d
12000	18588.2±23.8 ^e	2.80±0.18 ^e

Different superscript letters in the same column indicate significant differences ($p < 0.05$).

4. Conclusion

In conclusion, most of OVT fibrils were disrupted during *in vitro* gastrointestinal digestion, and some OVT fibrils showed resistance to proteolytic digestion *in vitro*. During long-term room-temperature storage, OVT fibrils were stable at pHs below isoelectric point, but they were unstable at pHs above isoelectric point. OVT fibrils possessed excellent stability against frozen storage–lyophilization–rehydration. OVT fibrils were fractured into short and curly fibrils without destroying fibrillar structures after high-speed shearing.

5. References

1. Mantovani, R. A., Pinheiro, A. C., Vicente, A. A., & Cunha, R. L. (2017). *In vitro* digestion of oil-in-water emulsions stabilized by whey protein nanofibrils. *Food Research International*, 99, 790–798.
2. Bateman, L., Ye, A., & Singh, H. (2010). In vitro digestion of β -lactoglobulin fibrils formed by heat treatment at low pH. *Journal of Agricultural and Food Chemistry*, 58(17), 9800–9808.
3. Bateman, L., Ye, A., & Singh, H. (2011). Re-formation of fibrils from hydrolysates of β -lactoglobulin fibrils during *in vitro* gastric digestion. *Journal of Agricultural and*

Food Chemistry, 59(17), 9605–9611.

4. Jones, O. G., & Mezzenga, R. (2012). Inhibiting, promoting, and preserving stability of functional protein fibrils. *Soft Matter*, 8(4), 876–895.
5. Brännström, K., Öhman, A., Nilsson, L., Pihl, M., Sandblad, L., & Olofsson, A. (2014). The N-terminal region of amyloid β controls the aggregation rate and fibril stability at low pH through a gain of function mechanism. *Journal of the American Chemical Society*, 136(31), 10956–10964.
6. Rezaei-Ghaleh, N., Amininasab, M., Kumar, S., Walter, J., & Zweckstetter, M. (2016). Phosphorylation modifies the molecular stability of β -amyloid deposits. *Nature Communications*, 7, 11359.
7. Ju, Z. Y., & Kilara, A. (1998). Gelation of pH-aggregated whey protein isolate solution induced by heat, protease, calcium salt, and acidulant. *Journal of Agricultural and Food Chemistry*, 46(5), 1830–1835.
8. Wei, Z., Zhu, P., & Huang, Q. (2019a). Investigation of ovotransferrin conformation and its complexation with sugar beet pectin. *Food Hydrocolloids*, 87, 448–458.
9. Wei, Z., & Huang, Q. (2019b). Assembly of iron-bound ovotransferrin amyloid fibrils. *Food Hydrocolloids*, 89, 579–589.
10. Minekus, M., Alminger, M., Alvito, P., Ballance, S., Bohn, T., Bourlieu, C., et al. (2014). A standardised static *in vitro* digestion method suitable for food—an international consensus. *Food & Function*, 5(6), 1113–1124.
11. Nilsson, M. R. (2004). Techniques to study amyloid fibril formation *in vitro*. *Methods*, 34(1), 151–160.
12. Usov, I., & Mezzenga, R. (2015). FiberApp: An open-source software for tracking and analyzing polymers, filaments, biomacromolecules, and fibrous objects. *Macromolecules*, 48(5), 1269–1280.
13. Serfert, Y., Lamprecht, C., Tan, C. P., Keppler, J. K., Appel, E., Rossier-Miranda, M. J., et al. (2014). Characterisation and use of β -lactoglobulin fibrils for microencapsulation of lipophilic ingredients and oxidative stability thereof. *Journal of food Engineering*, 143, 53–61.
14. Shen, Y., Posavec, L., Bolisetty, S., Hilty, F. M., Nyström, G., Kohlbrecher, J., et al. (2017). Amyloid fibril systems reduce, stabilize and deliver bioavailable nanosized iron. *Nature Nanotechnology*, 12(7), 642–647.
15. Biancalana, M., & Koide, S. (2010). Molecular mechanism of Thioflavin-T binding to amyloid fibrils. *Biochimica et Biophysica Acta (BBA)–Proteins and Proteomics*, 1804(7), 1405–1412.
16. Bolder, S. G., Sagis, L. M. C., Venema, P., & van der Linden, E. (2007). Effect of stirring and seeding on whey protein fibril formation. *Journal of Agricultural and Food Chemistry*, 55(14), 5661–5669.
17. Hamada, D., Tanaka, T., Tartaglia, G. G., Pawar, A., Vendruscolo, M., Kawamura, M., et al. (2009). Competition between folding, native-state dimerisation and amyloid aggregation in β -lactoglobulin. *Journal of Molecular Biology*, 386(3), 878–890.
18. Dave, A. C., Loveday, S. M., Anema, S. G., Jameson, G. B., & Singh, H. (2014). Modulating β -lactoglobulin nanofibril self-assembly at pH 2 using glycerol and

- sorbitol. *Biomacromolecules*, 15(1), 95–103.
19. Adamcik, J., & Mezzenga, R. (2012). Study of amyloid fibrils via atomic force microscopy. *Current Opinion in Colloid & Interface Science*, 17(6), 369–376.
 20. Pandey, N. K., Ghosh, S., & Dasgupta, S. (2013). Effect of surfactants on preformed fibrils of human serum albumin. *International Journal of Biological Macromolecules*, 59, 39–45.
 21. Loveday, S. M., Su, J., Rao, M. A., Anema, S. G., & Singh, H. (2011). Effect of calcium on the morphology and functionality of whey protein nanofibrils. *Biomacromolecules*, 12(10), 3780–3788.
 22. Lassé, M., Ulluwishewa, D., Healy, J., Thompson, D., Miller, A., Roy, N., et al. (2016). Evaluation of protease resistance and toxicity of amyloid-like food fibrils from whey, soy, kidney bean, and egg white. *Food Chemistry*, 192, 491–498.
 23. Hunter, R. J. (1981). *Zeta potential in colloid science: principles and applications*. San Diego: Academic Press, (Chapter 1).
 24. Velegol, D., Feick, J. D., & Collins, L. R. (2000). Electrophoresis of spherical particles with a random distribution of zeta potential or surface charge. *Journal of Colloid and Interface Science*, 230(1), 114–121.
 25. Straub, J. E., & Thirumalai, D. (2011). Toward a molecular theory of early and late events in monomer to amyloid fibril formation. *Annual review of physical chemistry*, 62, 437–463.
 26. Mantovani, R. A., Fattori, J., Michelon, M., & Cunha, R. L. (2016). Formation and pH-stability of whey protein fibrils in the presence of lecithin. *Food Hydrocolloids*, 60, 288–298.
 27. Arnaudov, L. N., & de Vries, R. (2006). Strong impact of ionic strength on the kinetics of fibrillar aggregation of bovine β -lactoglobulin. *Biomacromolecules*, 7(12), 3490–3498.
 28. Kroes-Nijboer, A., Venema, P., Bouman, J., & van der Linden, E. (2009). The critical aggregation concentration of β -lactoglobulin-based fibril formation. *Food Biophysics*, 4(2), 59–63.
 29. Marshall, K. E., Morris, K. L., Charlton, D., O'Reilly, N., Lewis, L., Walden, H., et al. (2011). Hydrophobic, aromatic, and electrostatic interactions play a central role in amyloid fibril formation and stability. *Biochemistry*, 50(12), 2061–2071.
 30. Tsemekhman, K., Goldschmidt, L., Eisenberg, D., & Baker, D. (2007). Cooperative hydrogen bonding in amyloid formation. *Protein Science*, 16(4), 761–764.
 31. Shammas, S. L., Knowles, T. P. J., Baldwin, A. J., MacPhee, C. E., Welland, M. E., Dobson, C. M., et al. (2011). Perturbation of the stability of amyloid fibrils through alteration of electrostatic interactions. *Biophysical Journal*, 100(11), 2783–2791.
 32. Nguyen, H. D., & Hall, C. K. (2004). Molecular dynamics simulations of spontaneous fibril formation by random-coil peptides. *Proceedings of the National Academy of Sciences*, 101(46), 16180–16185.
 33. Abdelwahed, W., Degobert, G., Stainmesse, S., & Fessi, H. (2006). Freeze-drying of nanoparticles: Formulation, process and storage considerations. *Advanced Drug*

Delivery Reviews, 58(15), 1688–1713.

34. Roy, I., & Gupta, M. N. (2004). Freeze-drying of proteins: some emerging concerns. *Biotechnology and Applied Biochemistry*, 39(2), 165–177.

35. Loveday, S. M., Su, J., Rao, M. A., Anema, S. G., & Singh, H. (2012). Whey protein nanofibrils: The environment–morphology–functionality relationship in lyophilization, rehydration, and seeding. *Journal of Agricultural and Food Chemistry*, 60(20), 5229–5236.

36. Bekard, I. B., Asimakis, P., Bertolini, J., & Dunstan, D. E. (2011). The effects of shear flow on protein structure and function. *Biopolymers*, 95(11), 733–745.

37. Xue, W. F., Hellewell, A. L., Gosal, W. S., Homans, S. W., Hewitt, E. W., & Radford, S. E. (2009). Fibril fragmentation enhances amyloid cytotoxicity. *Journal of Biological Chemistry*, 284(49), 34272–34282.

38. Humblet-Hua, N. P. K., van der Linden, E., & Sagis, L. M. C. (2012). Microcapsules with protein fibril reinforced shells: Effect of fibril properties on mechanical strength of the shell. *Journal of Agricultural and Food Chemistry*, 60(37), 9502–9511.

CHAPTER IV. OVOTRANSFERRIN FIBRIL FORMATION IN THE PRESENCE OF POLYOLS

1. Introduction

Polyols, organic compounds containing several alcoholic hydroxyl groups, are usually applied in food science and polymer chemistry (1, 2). Common polyols used in food industry consist of glycerol, sorbitol, xylitol, maltitol, erythritol and so on. Since various kinds of polyols exist in foods, interactions between polyols and other food ingredients cannot be ignored. Glycerol and sorbitol have attracted considerable scientific attention among all polyols, and impact of glycerol and sorbitol on some food systems such as edible films and protein gels has been extensively investigated during the past few years (3–5). Nevertheless, influence of glycerol and sorbitol on protein fibrils remains largely unknown, and relevant research may promote understanding about protein fibrillation and facilitate application of protein fibrils in food systems.

Over the last few years there has been a fierce debate about whether peptides or unhydrolyzed proteins are building blocks of fibrils. One viewpoint is that intact proteins do not exist in fibrils, and fibrils are entirely composed of peptide fragments (6). Another prevalent standpoint is that active intact proteins instead of hydrolyzed ones are able to assemble into fibrils, and hydrolysis of non-assembled proteins may contribute to termination of fibril growth (7). Sorbitol may stabilize proteins against unfolding and hydrolysis, which provides one technique to explore the building

blocks of fibrils (2, 8). Furthermore, glycerol, another kind of polyols, may preferentially prevent protein aggregation (self-assembly) (9). Glycerol may help to clarify how self-assembly contributes to protein fibrillation. Thus, by decoupling hydrolysis and self-assembly, glycerol and sorbitol are two powerful tools to explore the building blocks of OVT fibrils and comprehend contribution of self-assembly in OVT fibrillation.

Accordingly, this chapter aimed to investigate influence of two polyols (glycerol and sorbitol) on OVT fibrillation. With the aid of thioflavin T fluorescence, atomic force microscopy and sodium dodecyl sulfate polyacrylamide gel electrophoresis, impact of glycerol and sorbitol on the amount, morphology and building blocks of OVT fibrils were elucidated. By decoupling hydrolysis and self-assembly with glycerol as well as sorbitol, how protein hydrolysis and self-assembly processes modulate OVT fibrillation were analyzed and discussed in this chapter.

2. Materials and Methods

2.1. Materials

OVT (ovotransferrin) with an iron binding activity $> 1000 \mu\text{g Fe/g}$ sample was purchased from Neova Technologies Inc. (Abbotsford, Canada), and purity of OVT was above 88%, as indicated by the analysis report from the manufacturer. Glycerol ($>99\%$, purity) was purchased from Sigma-Aldrich (St. Louis, USA). D-sorbitol (97%, purity) and thioflavin T (ThT) were purchased from Acros Organics (Geel, Belgium). PageRuler™ Plus prestained protein ladder (10 to 250 kDa) was obtained from Thermo Fisher Scientific, Inc. (Waltham, USA). β -Mercaptoethanol, 30% acrylamide/bis

solution and Coomassie brilliant blue R-250 were bought from Bio-Rad Laboratories Inc. (Hercules, USA).

2.2. Fibril formation

Optimal condition for heat-induced OVT fibrillation was acquired in our previous study (10). OVT (0.32 g) was dispersed and dissolved in 8 mL of pH-adjusted NaCl solution (pH 2, 150 mM NaCl), and titrating HCl was applied to maintain pH at 2. To inhibit microbial growth, sodium azide (0.02%, w/v) was added. After hydration overnight at 4 °C, the OVT solution was filtered with 0.2 µm pore-sized syringe filter (Thermo Fisher Scientific, Waltham, USA) to eliminate impurities. Afterwards, the OVT solution was heated at 90 °C and a constant stirring speed of 300 rpm in oil bath over a temperature-controlled hot plate stirrer (VWR International, Radnor, USA). After heating treatment for 24 h, the acquired OVT fibril dispersions were immediately cooled in an ice-water bath and subsequently stored in the refrigerator (4 °C) prior to further analysis.

2.3. Influence of glycerol and sorbitol on fibril formation

The OVT stock solution (pH 2) was mixed with glycerol or sorbitol solution to obtain the desired glycerol or sorbitol concentration (20–60% w/v). The final volume, OVT concentration and ionic strength of all samples was 8 mL, 40 mg/mL and 150 mM, respectively. The samples were readjusted to pH 2 with 1M HCl and stirred at room temperature for 4 h. Sodium azide (0.02%, w/v) was added as preservative. For OVT fibrillation, all samples were heated at 90 °C and a constant stirring speed of 300 rpm as described in 2.2. To analyze impact of glycerol and sorbitol on OVT

fibrillation, samples intended for ThT fluorescence assay, SDS-PAGE and AFM were drawn after different incubation periods. The acquired OVT fibrils in the presence of glycerol or sorbitol were stored in the refrigerator (4 °C) and analyzed within 12 h.

2.4. Thioflavin T (ThT) fluorescence spectroscopy

Based on a method in previous study (11), ThT fluorescence was determined as described in Chapter II.

2.5. Atomic Force Microscopy (AFM)

Atomic force microscopy (AFM) was performed as described in Chapter II. The acquired AFM data were analyzed employing NanoScope Analysis Software and FiberApp (13).

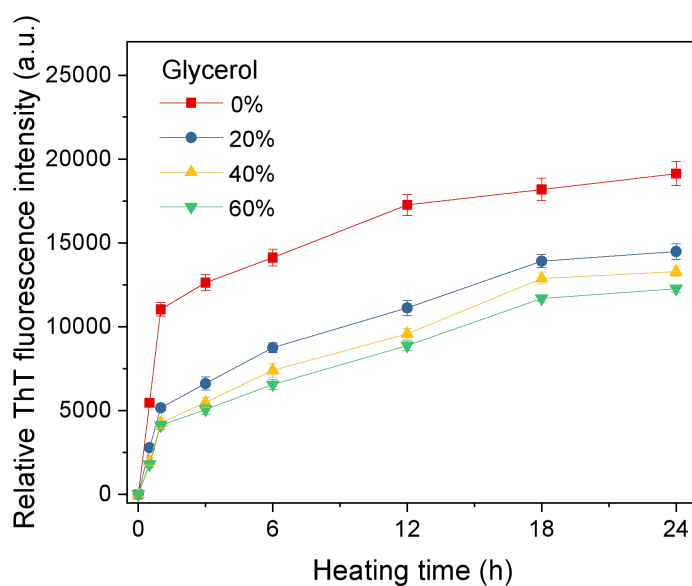
2.6. Sodium Dodecyl Sulfate Polyacrylamide Gel Electrophoresis (SDS-PAGE)

Sodium dodecyl sulfate polyacrylamide gel electrophoresis (SDS-PAGE) under reducing conditions was performed as previously reported on a vertical gel electrophoresis unit (Bio-Rad Laboratories, Hercules, USA) (14). First, the samples were diluted with Milli-Q water, and the diluted samples were mixed with electrophoresis sample buffer (277.8 mM Tris-HCl, pH 6.8, 44.4% (v/v) glycerol, 4.4% SDS, 0.02% bromophenol blue) at 1:1 ratio. Subsequently, β -mercaptoethanol was added to generate reducing condition. The mixtures were heated at 95 °C for 5 min, and aliquots (10 μ L) were loaded onto the polyacrylamide gel. The electrophoresis was operated at a constant voltage of 80 V using 10% separating gel and 4% stacking gel. After the SDS-PAGE run, the gel was stained overnight using 0.25% (w/v) Coomassie brilliant blue. Afterwards, the gel was destained with a

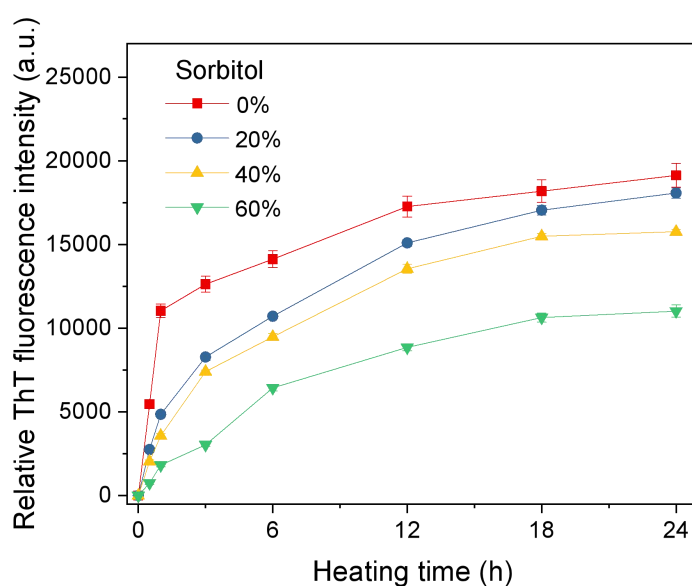
mixture composed of acetic acid/ethanol/water (1:4:5) for 24 h with 4 changes of destaining solution.

3. Results and Discussion

3.1. ThT fluorescence in the presence of glycerol or sorbitol



(a)



(b)

Figure IV-1. (a) ThT fluorescence intensity of OVT (ovotransferrin) heated at pH 2

and 90 °C in the presence of different levels (% w/v) of glycerol. (b) ThT fluorescence intensity of OVT heated at pH 2 and 90 °C in the presence of different levels (% w/v) of sorbitol.

In our previous work, it proved that stirring might accelerate the kinetics of OVT fibrillation and promote formation of more active OVT fibrils, and presence of salts could facilitate OVT fibril assembly through electrostatic screening (10). Thus, OVT fibrillation was conducted under stirring and moderate ionic strength conditions in this work. Since ThT fluorescence is a sensitive and accurate method to detect amount of protein fibrils (11, 15), ThT fluorescence was applied to analyze impact of glycerol or sorbitol on self-assembly of iron-bound OVT into fibrils. As shown in Figure IV-1, ThT fluorescence of OVT control (without presence of glycerol or sorbitol) increased sharply during the first hour of thermal treatment, and growth rate of ThT fluorescence slowed down gradually until ThT fluorescence reached a near-equilibrium state eventually. This indicated that OVT fibrils were already generated at the very start of thermal treatment, and there was no lag phase for OVT fibrillation. It is noteworthy that macroscopic aggregation curve for protein fibril formation typically consists of three stages: a lag phase, a growth phase and a final plateau (16). For many proteins such as β -lactoglobulin, fluorescence intensity increases extremely slowly during the lag phase (17, 18), suggesting formation of negligible fibrils during the beginning of incubation. Because during the lag phase a significant amount of primary nuclei that is essential for protein aggregation may form (16), it can be inferred that primary nucleation is essential for formation of many protein fibrils but not necessary for fibrillation of iron-bound OVT. Considering that

molecular mechanism of OVT fibrillation may be distinct from fibrillation process of many other proteins and the currently known knowledge about other fibrils may not apply to OVT fibrils, although one paper has currently been available about impact of polyols on β -lactoglobulin fibrils (17), it is essential to investigate impact of polyols on formation and structural characteristics of OVT fibrils.

Figure IV-1 shows ThT fluorescence intensity of OVT in the presence of different amounts of glycerol and sorbitol. As depicted in Figure IV-1a, addition of glycerol decreased yield of OVT fibrils, and slowdown of OVT fibrillation was strongly dependent on glycerol concentration. The more glycerol there was, the slower OVT fibrillation proceeded. As far as we are aware, polyols may stabilize proteins via distinct mechanisms in view of their differences in size, structure and amphiphilic character (2, 17). Specifically, glycerol may stabilize proteins and inhibit protein aggregation (self-assembly) without suppressing hydrolysis of proteins (9, 17). It could be inferred from the fluorescence decline in the presence of glycerol that alignment and self-assembly of fibril building blocks were a necessary step during fibrillation of iron-bound OVT. As indicated in Figure IV-1b, upon addition of sorbitol, OVT fibrillation was strongly restrained in the first 3 h, and higher concentration of sorbitol led to fewer OVT fibrils. Since sorbitol can suppress protein fibrillation by stabilizing proteins against unfolding and hydrolysis (17), a smaller amount of OVT fibrils in the presence of sorbitol may be attributed to the fact that limited hydrolysis can lead to fewer fibril-forming peptides, which results in slower OVT fibrillation. Figure IV-1b shows that the inhibitory effects of sorbitol on OVT

fibrillation weakened 3 h later, which could be ascribed to enhanced hydrolysis of OVT during prolonged thermal treatment. Inhibitory influence of sorbitol on OVT proteolysis is likely to reduce after treatment for 3 h. Hydrolysis of OVT accelerates and all OVT samples may be totally hydrolyzed, and OVT fibrillation is no longer a hydrolysis-limited process. The ample peptides ensure rapid generation of OVT fibrillar structures. These explanations are supported by SDS-PAGE data shown in Figure IV-2 and Figure IV-3. Overall, hydrolysis-limited OVT fibrillation reflects that peptides are building blocks of OVT fibrils.

3.2. SDS-PAGE in the presence of glycerol or sorbitol

SDS-PAGE was a powerful tool to analyze how glycerol and sorbitol affected hydrolysis of OVT, and SDS-PAGE could also help to find out building blocks of OVT fibrils. Therefore, SDS-PAGE profiles of OVT heated in the presence of glycerol or sorbitol were systematically studied.

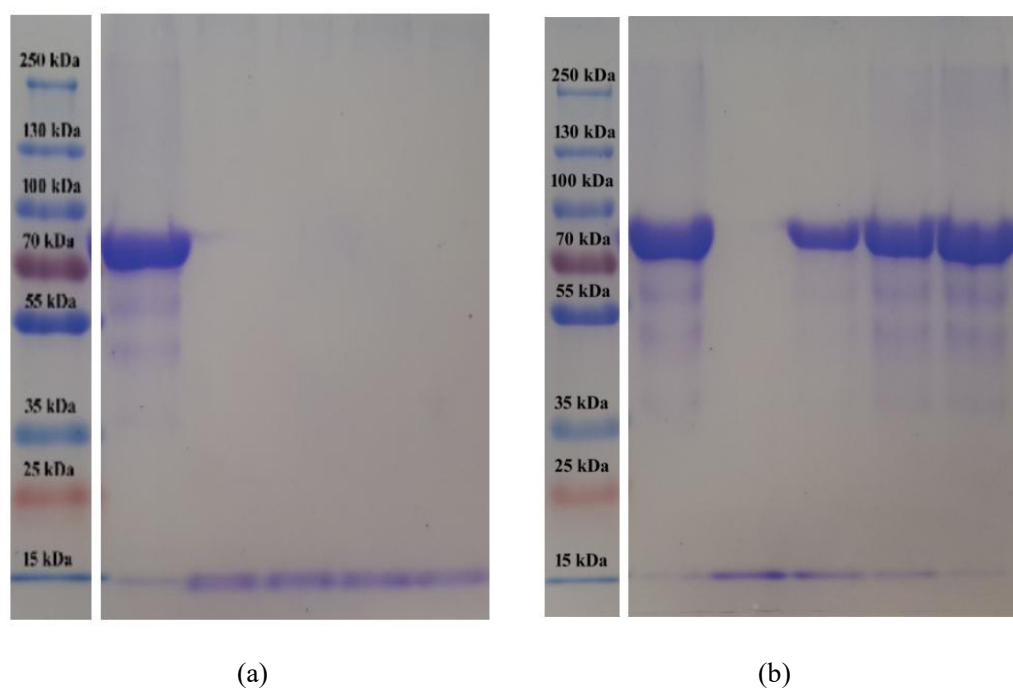


Figure IV-2. (a) SDS-PAGE profiles of OVT after heating at 90 °C for 3 h in the

presence of different concentrations of glycerol. Lanes from left to right are marker, unheated OVT, heated OVT in the presence of 0, 20%, 40% and 60% glycerol, respectively. The marker bands from top to down correspond to 250, 130, 100, 70, 55, 35, 25 and 15 kDa. (b) SDS-PAGE profiles of OVT after heating at 90 °C for 3 h in the presence of different concentrations of sorbitol. Lanes from left to right are marker, unheated OVT, heated OVT in the presence of 0, 20%, 40% and 60% sorbitol, respectively.

Figure IV-2 shows SDS-PAGE profiles of OVT after heating for 3 h. It was observed OVT used in this work had a molecular weight around 80 kDa, which was in good agreement with the statement that OVT had a molecular weight of 76 kDa with 686 amino acids (19). As depicted in Figure IV-2a, glycerol exerted little influence on hydrolysis of OVT, and OVT in the presence of different amounts of glycerol were hydrolyzed completely to peptides after 3-h thermal treatment. As indicated in Figure IV-2b, sorbitol effectively inhibited hydrolysis of OVT during the first 3 h, and higher concentration of sorbitol could exert a stronger inhibitory effect on fibrillation of iron-bound OVT. Densitometry analysis of SDS-PAGE bands in Figure IV-2b using Image J software revealed that hydrolysis of OVT was entirely inhibited in the presence of 60% sorbitol, suggesting that no peptides existed in heated OVT solutions. As illustrated in Figure IV-1b, for OVT in the presence of 60% sorbitol, fibrillar structures were obtained during the first 3 h, and occurrence of OVT fibrils was also confirmed by AFM analysis (data not shown). This clearly demonstrated that OVT fibrillation indeed occurred without peptides as building blocks, and it was suggested that intact OVT monomers should act as building blocks of OVT fibrils in the presence of 60% sorbitol during the first 3 h. Therefore, it is clear that intact OVT monomers can be building blocks of OVT fibrils.

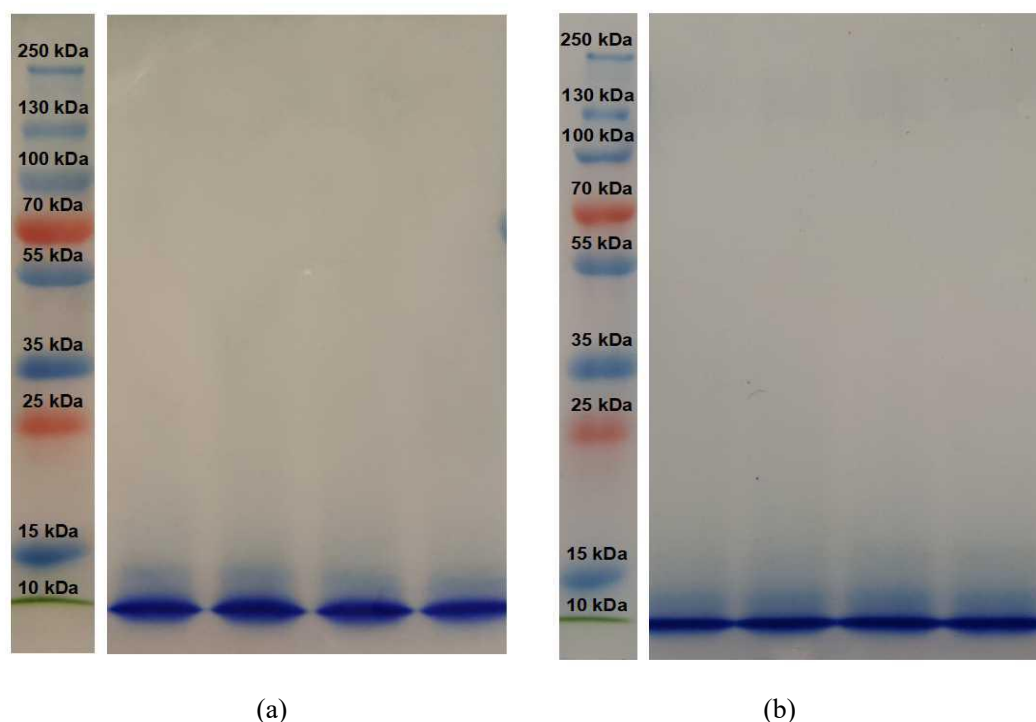


Figure IV-3. (a) SDS-PAGE profiles of OVT after heating at 90 °C for 24 h in the presence of different concentrations of glycerol. Lanes from left to right are marker, heated OVT in the presence of 0, 20%, 40% and 60% glycerol, respectively. The marker bands from top to down correspond to 250, 130, 100, 70, 55, 35, 25, 15 and 10 kDa. (b) SDS-PAGE profiles of OVT after heating at 90 °C for 24 h in the presence of different concentrations of sorbitol. Lanes from left to right are marker, heated OVT in the presence of 0, 20%, 40% and 60% sorbitol, respectively.

Figure IV-3 shows SDS-PAGE profiles of iron-bound OVT in the presence of glycerol or sorbitol after thermal treatment for 24 h. SDS-PAGE bands with a molecular weight around 10 kDa were detected in Figure IV-3a, indicating that peptides derived from OVT in the absence or presence of glycerol had an average molecular weight around 10 kDa after heating for 24 h. Figure IV-2a demonstrates that peptides derived from OVT in the absence or presence of glycerol had an average molecular weight around 15 kDa after heating for 3 h, suggesting that hydrolysis of OVT continued after 3-h thermal treatment. In addition, as depicted in Figure IV-3b,

no SDS-PAGE bands in the presence of sorbitol were located around 76 kDa after 24 h of thermal treatment, indicating that all of OVT samples in the presence of different amounts of sorbitol were hydrolyzed into peptides. This implied that capacity of sorbitol against hydrolysis of OVT diminished over time, and inhibitory influence of sorbitol on OVT proteolysis could vanish in the end. It was noteworthy that inhibitory influence of sorbitol on β -lactoglobulin proteolysis did not diminish after prolonged thermal treatment (17), suggesting that stabilizing impact of sorbitol on proteins against unfolding and hydrolysis could vary with the type of proteins.

3.3. Both intact monomers and peptides are building blocks of OVT fibrils

Based on aforementioned analysis and discussion, it can be concluded that both intact OVT monomers and peptides derived from OVT are building blocks of OVT fibrils. The proposed schematic illustrations about fibrillation pathways of iron-bound OVT are shown in Figure IV-4.

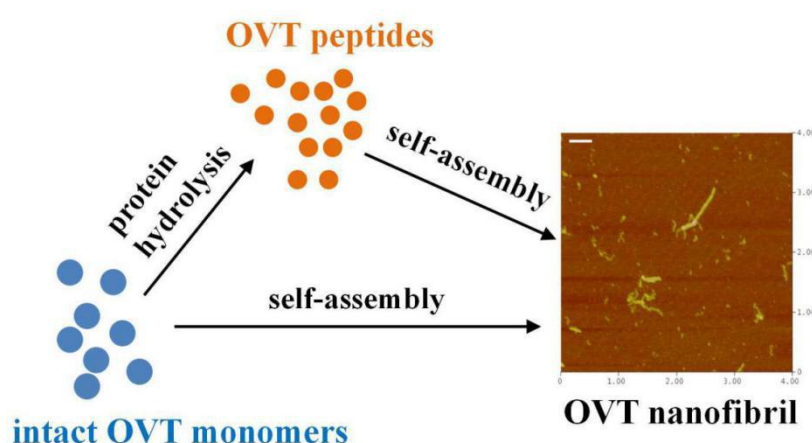
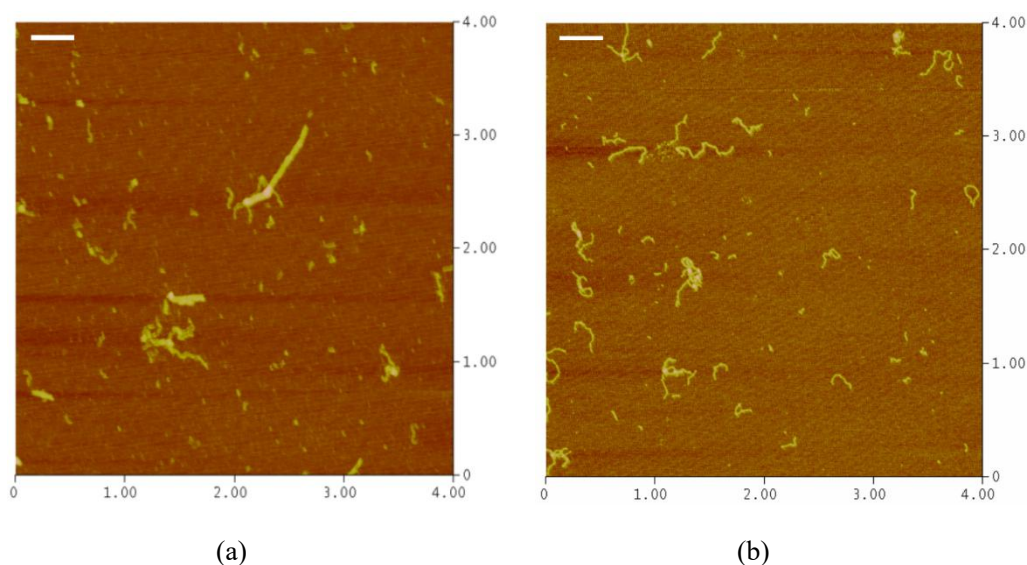


Figure IV-4. Schematic illustrations about fibrillation pathways of OVT.

Generally, there are two pathways of OVT fibrillation. One pathway is direct self-assembly of intact OVT monomers into OVT fibrils. In terms of the other pathway, OVT peptides are acquired after heat-induced hydrolysis of OVT, followed by self-assembly of these peptides into fibrillar structures. A previous study demonstrates that short peptides (as short as tetrapeptides) already contain all the essential molecular information for generation of protein fibrils (20), and it is not surprising that both intact OVT monomers and OVT-derived peptides can be utilized to construct OVT fibrils. As already mentioned in our introduction part, there are two different opinions regarding building blocks of protein fibrils, and there is still no agreement about whether protein fibrils are entirely composed of intact protein monomers or protein-derived peptides (6, 7). In this work, although it proves that OVT fibrils are composed of both intact OVT monomers and OVT-derived peptides, we cannot reach a final conclusion that all protein fibrils are composed of both intact protein monomers and peptides.

3.4. Morphology of OVT fibrils in the presence of glycerol or sorbitol



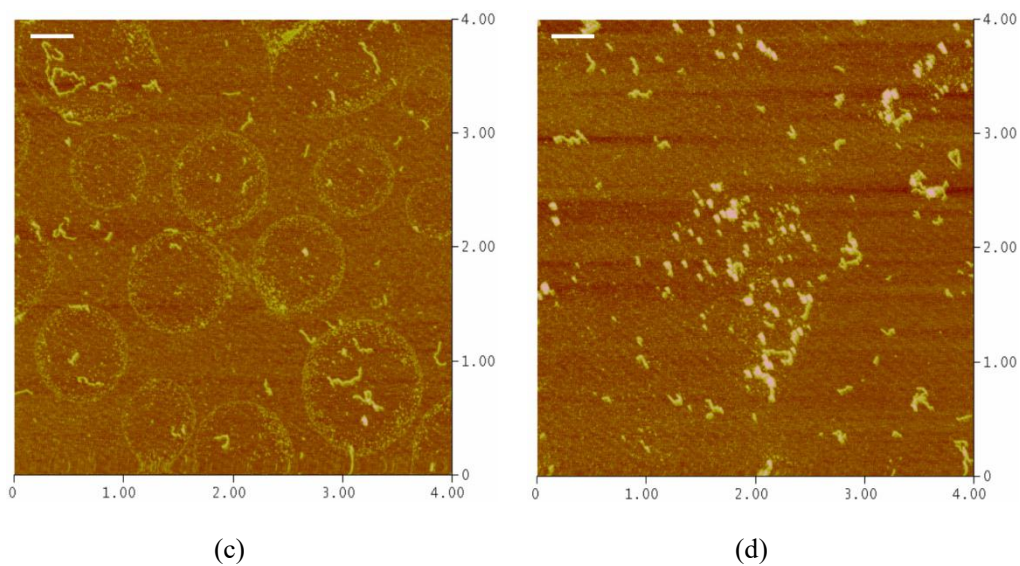
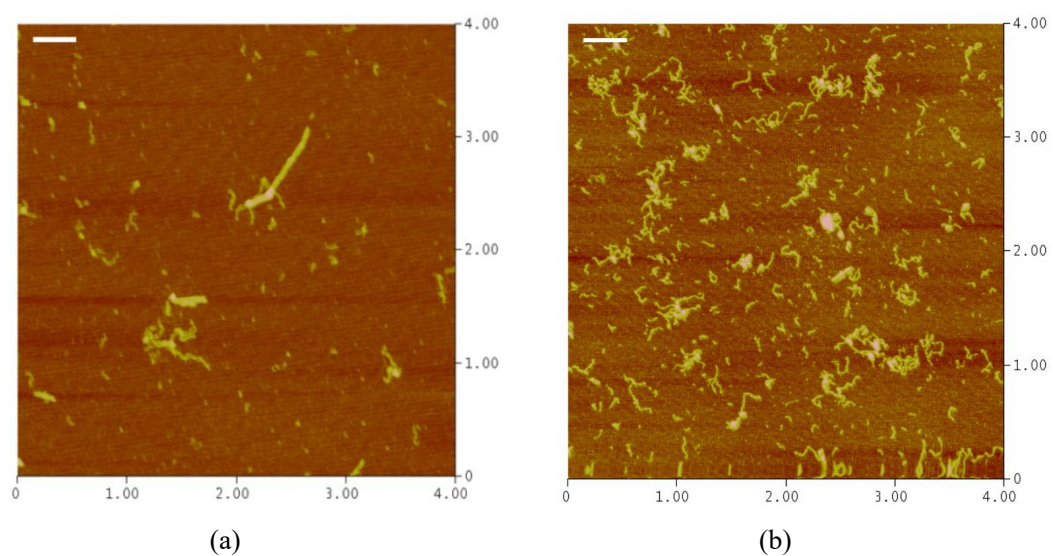


Figure IV-5. AFM images of OVT fibrils in the presence of different levels of glycerol: (a) control, (b) 20% glycerol, (c) 40% glycerol, (d) 60% glycerol. The scan size is $4\ \mu\text{m}\times 4\ \mu\text{m}$, and the z scale is 20 nm. The scale bar represents 400 nm.

Given that AFM is a powerful tool to investigate the structural characteristics of protein fibrils (12), polyol-induced morphology changes of OVT fibrils were studied using AFM.



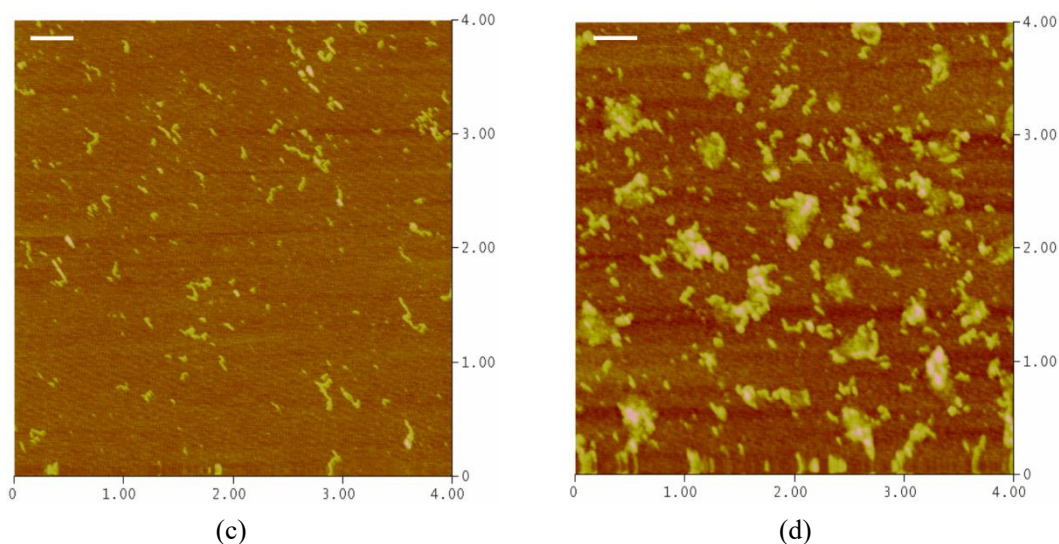


Figure IV-6. AFM images of OVT fibrils in the presence of different levels of sorbitol: (a) sorbitol, (b) 20% sorbitol, (c) 40% sorbitol, (d) 60% sorbitol. The scan size is $4\ \mu\text{m} \times 4\ \mu\text{m}$, and the z scale is 20 nm. The scale bar represents 400 nm.

As shown in Figure IV-5, upon addition of glycerol, long and rigid OVT fibrils with contour length over 800 nm disappeared. It was apparently found that contour length of OVT fibrils decreased with increasing glycerol concentration. Specifically, the average contour length of OVT fibrils in the presence of 20% glycerol was 256 nm, and the average contour length of OVT fibrils decreased to 209 nm when there was 40% glycerol. As glycerol concentration was further elevated to 60%, more fibrils with contour length below 100 nm were observed and average contour length of OVT fibrils was 149 nm. Since glycerol may perturb self-assembly of fibril building blocks (9), linear aggregation can be disturbed in the presence of glycerol and OVT fibrils are eventually shortened. Figure IV-6 illustrates that most of OVT fibrils were flexible and curly in the presence of sorbitol, and addition of sorbitol shortened OVT fibrils. Reduction of fibril length may be due to limited peptides as fibril building blocks around the active growth ends. To sum up, addition of glycerol and sorbitol altered

morphology of OVT fibrils observably. Previous study reports that glycerol and sorbitol have no obvious effects on morphology of β -lactoglobulin fibrils (17), suggesting that OVT fibrils are more susceptible to interference of glycerol and sorbitol than β -lactoglobulin fibrils.

4. Conclusion

In summary, the presence of glycerol or sorbitol could reduce the rate of OVT fibrillation, and slowdown of OVT fibrillation was strongly dependent on concentration of glycerol or sorbitol. The more glycerol or sorbitol there was, the slower OVT fibrillation proceeded. Glycerol exerted little influence on heat-induced hydrolysis of OVT, and sorbitol could significantly retard hydrolysis of OVT. Inhibitory influence of sorbitol on OVT proteolysis diminished over time, and the inhibiting effect vanished eventually. Both intact OVT monomers and OVT-derived peptides were building blocks of OVT fibrils. The presence of glycerol or sorbitol shortened OVT fibrils, and most of OVT fibrils were flexible and curly in the presence of glycerol or sorbitol.

5. References

1. Liang, J., Xia, Q., Wang, S., Li, J., Huang, Q., & Ludescher, R. D. (2015). Influence of glycerol on the molecular mobility, oxygen permeability and microstructure of amorphous zein films. *Food Hydrocolloids*, 44, 94–100.
2. Liu, F. F., Ji, L., Zhang, L., Dong, X. Y., & Sun, Y. (2010). Molecular basis for polyol-induced protein stability revealed by molecular dynamics simulations. *The Journal of Chemical Physics*, 132(22), 225103.

3. Chanasattru, W., Decker, E. A., & McClements, D. J. (2007). Modulation of thermal stability and heat-induced gelation of β -lactoglobulin by high glycerol and sorbitol levels. *Food Chemistry*, 103(2), 512–520.
4. Farhan, A., & Hani, N. M. (2017). Characterization of edible packaging films based on semi-refined kappa-carrageenan plasticized with glycerol and sorbitol. *Food Hydrocolloids*, 64, 48–58.
5. Thomazine, M., Carvalho, R. A., & Sobral, P. J. A. (2005). Physical properties of gelatin films plasticized by blends of glycerol and sorbitol. *Journal of Food Science*, 70(3), E172–E176.
6. Akkermans, C., Venema, P., van der Goot, A. J., Gruppen, H., Bakx, E. J., Boom, R. M., et al. (2008). Peptides are building blocks of heat-induced fibrillar protein aggregates of β -lactoglobulin formed at pH 2. *Biomacromolecules*, 9(5), 1474–1479.
7. Bolder, S. G., Sagis, L. M. C., Venema, P., & van der Linden, E. (2007). Effect of stirring and seeding on whey protein fibril formation. *Journal of Agricultural and Food Chemistry*, 55(14), 5661–5669.
8. Wimmer, R., Olsson, M., Neves Petersen, M. T., Hatti-Kaul, R., Petersen, S. B., & Müller, N. (1997). Towards a molecular level understanding of protein stabilization: the interaction between lysozyme and sorbitol. *Journal of Biotechnology*, 55(2), 85–100.
9. Vagenende, V., Yap, M. G. S., & Trout, B. L. (2009). Mechanisms of protein stabilization and prevention of protein aggregation by glycerol. *Biochemistry*, 48(46), 11084–11096.
10. Wei, Z., & Huang, Q. (2019). Assembly of iron-bound ovotransferrin amyloid fibrils. *Food Hydrocolloids*, 89, 579–589.
11. Nilsson, M. R. (2004). Techniques to study amyloid fibril formation in vitro. *Methods*, 34(1), 151–160.
12. Adamcik, J., & Mezzenga, R. (2012). Study of amyloid fibrils via atomic force microscopy. *Current Opinion in Colloid & Interface Science*, 17(6), 369–376.
13. Usov, I., & Mezzenga, R. (2015). FiberApp: An open-source software for tracking and analyzing polymers, filaments, biomacromolecules, and fibrous objects. *Macromolecules*, 48(5), 1269–1280.
14. Laemmli, U. K. (1970). Cleavage of structural proteins during the assembly of the head of bacteriophage T4. *Nature*, 227(5259), 680–685.
15. Khurana, R., Coleman, C., Ionescu-Zanetti, C., Carter, S. A., Krishna, V., Grover, R. K., et al. (2005). Mechanism of thioflavin T binding to amyloid fibrils. *Journal of Structural Biology*, 151(3), 229–238.
16. Arosio, P., Knowles, T. P. J., & Linse, S. (2015). On the lag phase in amyloid fibril formation. *Physical Chemistry Chemical Physics*, 17(12), 7606–7618.
17. Dave, A. C., Loveday, S. M., Anema, S. G., Jameson, G. B., & Singh, H. (2014). Modulating β -lactoglobulin nanofibril self-assembly at pH 2 using glycerol and sorbitol. *Biomacromolecules*, 15(1), 95–103.
18. Gao, Z., Zhao, J., Huang, Y., Yao, X., Zhang, K., Fang, Y., et al. (2017). Edible Pickering emulsion stabilized by protein fibrils. Part 1: Effects of pH and fibrils concentration. *LWT—Food Science and Technology*, 76, 1–8.

19. Abeyrathne, E., Lee, H. Y., & Ahn, D. U. (2013). Egg white proteins and their potential use in food processing or as nutraceutical and pharmaceutical agents—a review. *Poultry Science*, 92(12), 3292–3299.
20. Gazit, E. (2005). Mechanisms of amyloid fibril self-assembly and inhibition: Model short peptides as a key research tool. *The FEBS Journal*, 272(23), 5971–5978.

CHAPTER V. IMPACT OF MAILLARD REACTION ON OVOTRANSFERRIN FIBRILS

1. Introduction

Maillard reaction, a nonenzymatic interaction between reducing sugars and proteins, is an appealing strategy to improve functional properties of food proteins (1–3). Maillard reaction can possibly be a tool to modulate physicochemical properties of ovotransferrin. It is postulated that modification of ovotransferrin by Maillard reaction may exert influence over fibrillation. Meanwhile, glucose and lactose are monosaccharide and disaccharide, respectively. These saccharides may affect fibrillation of ovotransferrin at different levels, and related research may advance understandings about how the saccharide type affected fibril self-assembly.

To the best of our knowledge, Pickering emulsions stabilized by fibrils derived from glycated proteins have not been reported. It remains unknown about how covalent bound saccharides alter Pickering emulsifier performance of fibrils at emulsion interfaces. Therefore, it is essential to explore how glycation manipulated Pickering emulsifier performance of nanofibrils at oil–water interfaces, and the systematic research may provide new insight about emulsibility of fibrils.

In this chapter, ovotransferrin was first glucosylated or lactosylated to obtain ovotransferrin–glucose conjugate and ovotransferrin–lactose conjugate, respectively. Influence of glucosylation and lactosylation on ovotransferrin fibrillation was investigated. Finally, fibrils derived from ovotransferrin–saccharide conjugates were

applied as Pickering emulsifiers in oil-in-water emulsions, and influence of glycation on Pickering emulsifier performance of ovotransferrin fibrils was evaluated.

2. Materials and Methods

2.1. Materials

Ovotransferrin with purity above 88% was purchased from Neova Technologies Inc. (Abbotsford, Canada). According to analysis report, iron binding capacity of the ovotransferrin was 1099 $\mu\text{g Fe/g}$. Glucose and lactose were purchased from Sigma-Aldrich (St. Louis, USA). Medium chain triglyceride (Neobee 1053, Lot number: 7746036) was generously provided by Stepan Company (Northfield, USA). PageRuler™ Plus prestained protein ladder (#26619) was obtained from Thermo Fisher Scientific, Inc. (Waltham, USA).

2.2. Preparation of Maillard reaction products

Ovotransferrin and saccharides (glucose or lactose) at a mass ratio of 4:1 were dissolved in Milli-Q water. The mixture was adjusted to pH 7 and stirred overnight at room temperature, followed by freeze-drying. The lyophilized powders were incubated at 60°C and 79% relative humidity in a desiccator (with saturated KCl solution) for 12 h. The powders after glycation were dispersed and stirred in Milli-Q water, and the resultant solutions were dialyzed (molecular weight cutoff 3500 Da) against Milli-Q water to remove free saccharides. The dialyzed samples were subsequently freeze-dried to obtain glycosylated ovotransferrin. In order to make this paper concise, ovotransferrin–glucose conjugate and ovotransferrin–lactose conjugate were denoted as OGC and OLC, respectively. The protein content of OGC and OLC

was determined by Bradford method. Ovotransferrin control (OVTC) was prepared according to the aforementioned procedures but without the addition of saccharides.

2.3. Characterization of Maillard reaction products

2.3.1. Sodium dodecyl sulfate polyacrylamide gel electrophoresis (SDS-PAGE)

SDS-PAGE was performed using 10% acrylamide separating gel in a vertical gel electrophoresis cell (4). The electrophoresis was run at a constant voltage of 80 V.

2.3.2. Free amino groups

Free amino groups of OVTC, OGC and OLC were determined via a modified OPA method (5, 6).

2.3.3. Surface hydrophobicity

The surface hydrophobicity of OVTC, OGC and OLC was measured using ANS (1-anilino-8-naphthalensulfonate) as fluorescence probe (7).

2.3.4. Zeta potential

The samples were dissolved into Milli-Q water to make a protein concentration of 1 mg/mL, and the solutions were adjusted to specific pHs (2–9) with HCl or NaOH. Measurements were performed employing a Zetasizer Nano-ZS90 instrument (Malvern Instruments, Worcestershire, UK).

2.4. Preparation and characterization of nanofibrils

2.4.1. Preparation of nanofibrils

The fibrillation condition was optimized in our previous study (8). OVTC, OGC and OLC were dispersed in pH-preset Milli-Q water (pH 2, 150 mM NaCl) at a protein concentration of 40 mg/mL, respectively. The samples were stirred to ensure

complete dissolution and HCl was added to maintain pH when necessary. Sodium azide (0.02%, w/v) was added to inhibit microbial growth. The samples were filtered with 0.2 μm pore-sized syringe filters and then placed into screw-capped vials. The hermetic vials were heated in oil bath over a temperature-controlled hot plate stirrer (VWR International, Radnor, USA) at 90°C and a stirring speed of 300 rpm. The heated samples were cooled immediately and stored at 4°C until further analysis. The fibrillation process was analyzed using ThT fluorescence, AFM and SDS-PAGE, and samples intended for ThT fluorescence assay were drawn after different incubation periods.

2.4.2. Thioflavin T (ThT) fluorescence assay

ThT fluorescence was measured as described in Chapter II.

2.4.3. SDS-PAGE

SDS-PAGE was carried out using 12% acrylamide separating gel, and the electrophoresis was operated at 80 V.

2.4.4. Atomic force microscopy (AFM)

AFM was measured as described in Chapter II.

2.4.5. Surface hydrophobicity

Surface hydrophobicity of fibril dispersions was measured as 2.3.3.

2.4.6. Zeta potential

Zeta potential of fibril dispersions was determined as 2.3.4.

2.5. Influence of glycation on Pickering emulsifier performance of nanofibrils

2.5.1. Preparation of Pickering emulsions stabilized by nanofibrils

Fibril dispersions (OVTC fibrils, OGC fibrils or OLC fibrils) with lower particle concentration (2 wt%) were obtained by diluting fibril dispersions (4 wt%) with pH-preset Milli-Q water (pH 2, 150 mM NaCl). The fibril dispersions (2–4 wt%) were mixed with MCT oil (medium chain triglyceride) to obtain mixtures (total volume= 8 mL) with different oil fractions ϕ (0.45–0.65). The mixtures were homogenized employing an Ultra-Turrax (IKA-Werke GMBH & CO., Germany) at 8000 rpm for 2 min. The Pickering emulsions were named as A–B (A: particle concentration c ; B: oil fraction ϕ) and stored at room temperature (9). The emulsion type was examined by testing the dispersibility of emulsions in water or pure MCT oil. Oil-in-water (water-in-oil) emulsions could disperse readily in water (oil), but remained immiscible in oil (water).

2.5.2. Measurement of emulsified phase volume fraction and stability index

After preparation of fresh Pickering emulsions, the heights of emulsified phase (H_e) and heights of total formulation (H_t) after specific storage (3 h and 15 days) were recorded. The emulsified phase volume fraction was defined as $(H_e/H_t) \times 100$, and the stability index was calculated as $(\text{emulsified phase volume fraction after 15-day storage}) / (\text{emulsified phase volume fraction after 3-h storage}) \times 100$ (9, 10).

2.5.3. Microstructure visualization

Microstructures of Pickering emulsions stabilized by fibrils were observed using 20 \times objective microscope (Nikon Eclipse TE 2000-U, Nikon Corporation, Tokyo, Japan), and Image J was employed to estimate the average diameter of Pickering emulsion droplets (9, 11).

3. Results and Discussion

3.1. Synthesis and characterization of glycated ovotransferrin

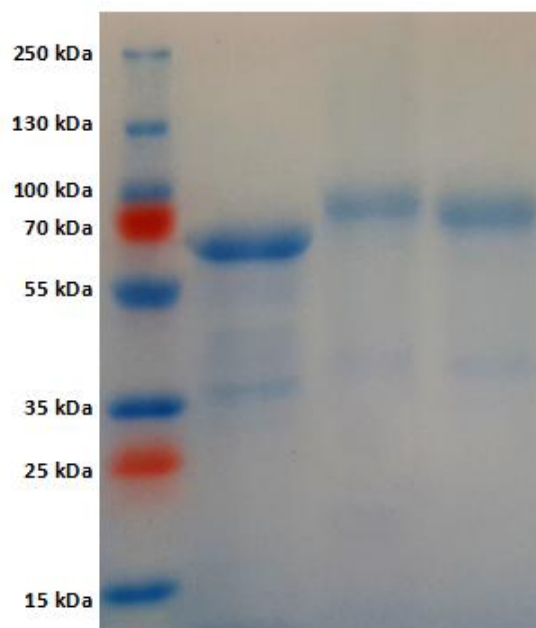


Figure V-1. SDS-PAGE profiles of OVTC, OGC and OLC. Lanes from left to right are protein marker, OVTC, OGC and OLC.

Because SDS could destroy non-covalent protein interactions, SDS-PAGE was utilized to confirm Maillard conjugates. As Figure V-1 shows, the bands of OGC and OLC migrated up in comparison with that of OVTC, implying that ovotransferrin and saccharides were linked through covalent bonds. It was found that OGC had larger molecular weight than OLC, indicating that glucose had stronger reactivity toward Maillard reaction with ovotransferrin than lactose. As Maillard conjugates were synthesized between amino groups of proteins and carbonyl groups of reducing saccharides (12), the amount of free amino groups was measured to verify reactivity order of the saccharides. As depicted in Figure V-2, glucosylation induced a larger decrease in free amino groups of ovotransferrin when compared with lactosylation,

which could also serve as proof that glucose showed higher protein cross-linking ability than lactose.

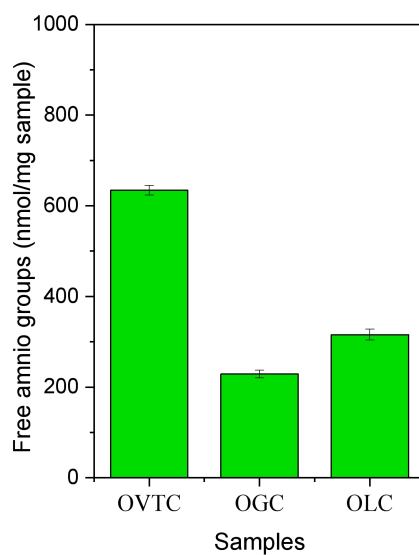


Figure V-2. Free amino groups of OVTC, OGC and OLC.

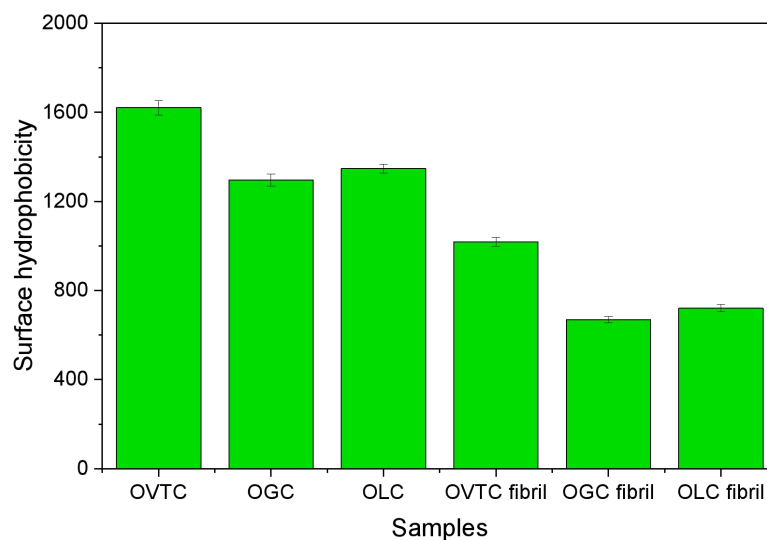


Figure V-3. Surface hydrophobicity of OVTC, OGC, OLC, OVTC fibril, OGC fibril and OLC fibril.

Conjugation of saccharides onto ovotransferrin could induce structural changes of protein surfaces. As illustrated in Figure V-3, glycation lowered surface

hydrophobicity of ovotransferrin due to introduction of the hydrophilic saccharides onto surfaces, and OLC exhibited higher surface hydrophobicity than OGC. Figure V-4 indicates that glycation shifted isoelectric point of ovotransferrin from pH 6.2 to around pH 4.8. The blocking of positively charged nucleophilic groups like amino groups of lysines might explain why isoelectric point of ovotransferrin shifted downwards.

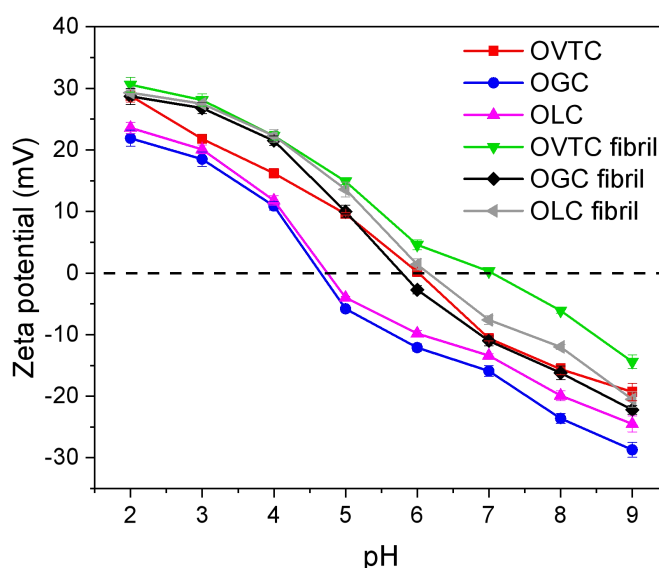


Figure V-4. Zeta potential of OVTC, OGC, OLC, OVTC fibril, OGC fibril and OLC fibril.

3.2. Impact of covalent bound saccharides on fibrillation

Formation kinetics of fibrils can be detected using ThT, a fluorescence dye (13). Figure V-5 shows that ThT intensities followed the order: OVTC > OLC > OGC. It was apparent that glycation could suppress fibrillation of ovotransferrin, and glucosylation could exert stronger inhibitory influence on fibril formation than lactosylation. The following explanations can interpret these phenomena. First, as

discussed later in SDS-PAGE section, major building blocks of these fibrils are peptides. The attached saccharides on peptides may bring steric hindrance to prevent the amyloid aggregation of these building peptides, resulting in fewer OGC fibrils and OLC fibrils. Since glucose had stronger reactivity toward glycation than lactose as discussed earlier, more saccharides are attached to OGC-derived peptides when compared with OLC-derived peptides and stronger steric hindrance is caused, which helps to explain why glucosylation could exert stronger suppression on fibril formation than lactosylation. Second, hydrophobic interactions are generally believed to be one of major driving forces of fibrillation (14). As shown in Figure V-3, glycation induced a decrease in surface hydrophobicity of intact protein monomers and hydrolyzed peptides, thus it was obvious that building blocks of OGC fibrils and OLC fibrils exhibited lower surface hydrophobicity than those of OVTC fibrils. The decreased surface hydrophobicity may lead to reduced hydrophobic interactions (15), which account for weakened fibrillation of ovotransferrin. Since building blocks of OLC fibrils have higher surface hydrophobicity than OGC fibrils, the stronger hydrophobic interactions contribute to more synthesized fibrils. Third, as fibrillation of OVTC and glycated ovotransferrin was conducted in the presence of high ionic strength (150 mM NaCl), the electrostatic interactions were greatly inhibited. Electrostatic interactions should be a negligible factor while explaining differences in formation kinetics of fibrils. There is a possibility that hydrolysis of OGC and OLC may lead to some non-fibril-forming peptides, which cannot form intermolecular β -sheets with other peptides in proximity. The reduced amount of fibril-forming

peptides may bring about fewer fibrils.

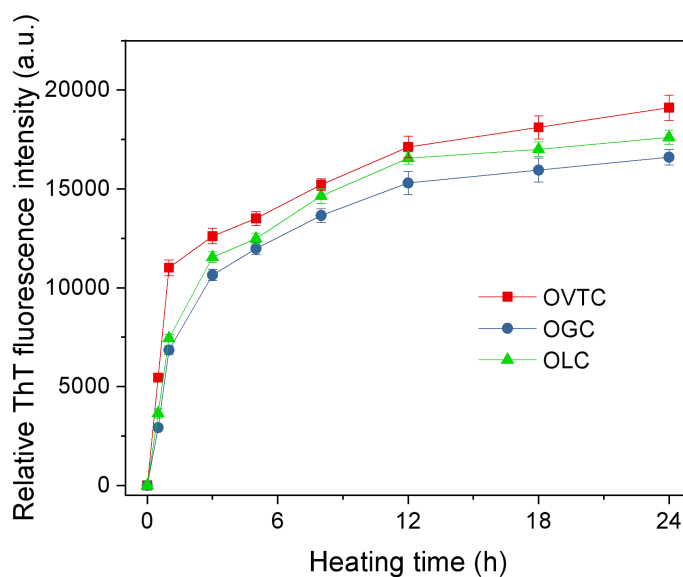


Figure V-5. Thioflavin T (ThT) fluorescence of OVTC, OGC and OLC after heating at 90°C and pH 2.

As depicted in Figure V-6, the major building blocks of OVTC fibrils, OGC fibrils and OLC fibrils were peptides hydrolyzed from corresponding proteins. In terms of heated OVTC, SDS-PAGE bands with molecular weight around 10 kDa were found, indicating that major building blocks of OVTC fibrils were peptides with molecular weight about 10 kDa. Figure V-6 shows that SDS-PAGE bands of heated OGC and OLC migrated up in comparison with heated OVTC, suggesting that building blocks of OGC fibrils and OLC fibrils were slightly larger than those of OVTC fibrils. Specifically, the building peptides of these fibrils may have different composition, sequence and number of amino acids.

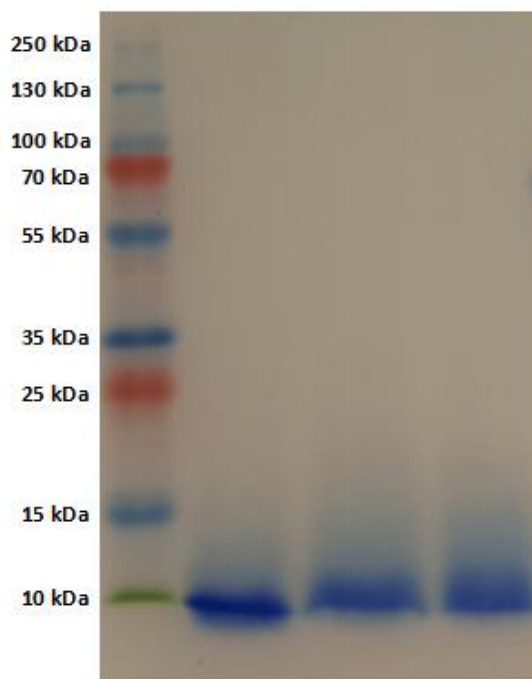
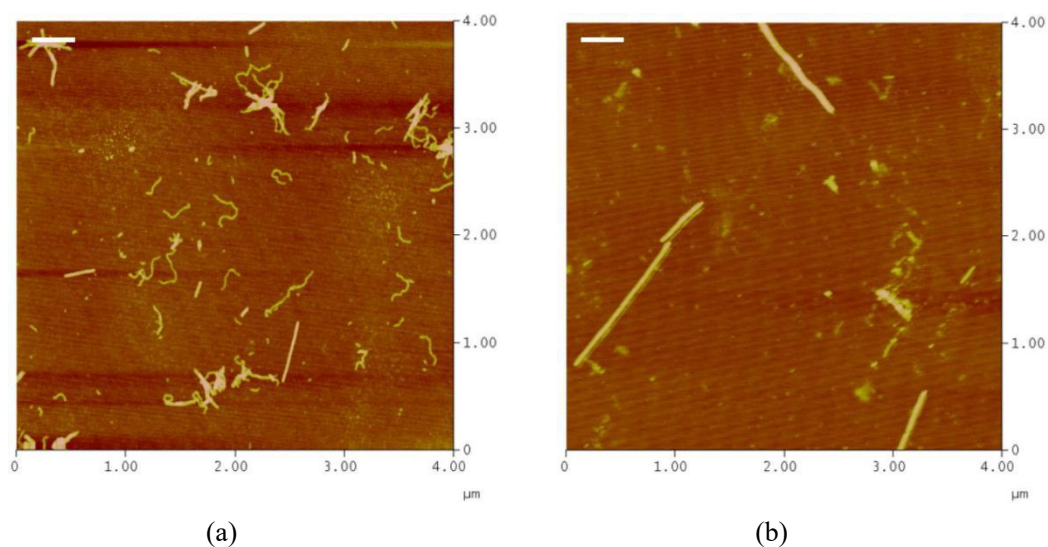


Figure V-6. SDS-PAGE profiles (12% separating gel) of OVTC, OGC and OLC after heating at pH 2 and 90°C for 24 h. Lanes from left to right are protein marker, heated OVTC, OGC and OLC.

As shown in Figure V-7a and Figure V-7b, in the case of OVTC fibrils, short fibrils (with contour length of 0–500 nm), medium-length fibrils (with contour length of 500–1000 nm) and long fibrils (with contour length above 1000 nm) coexisted. Both flexible and rigid fibrils were clearly observed. In terms of OGC fibrils, only short-length and medium-length fibrils with flexible nature were found. For OLC fibrils, short fibrils and medium-length fibrils existed simultaneously, and fibrils with flexible or rigid nature were observed. It was noticed that rigid nanofibrils disappeared after glycosylation of ovotransferrin, and long ovotransferrin fibrils (with contour length above 1000 nm) no longer existed after glycation. These phenomena may be explained by several speculations. First, building blocks of OGC fibrils are linked with more saccharides than those of OLC fibrils, and the steric hindrance

induced by covalent bound saccharides may impede linear aggregation. To diminish steric hindrance brought by saccharides, aggregation in a twisted coil way may be spontaneously adopted, leading to absence of rigid OGC fibrils. Second, building blocks of fibrils are linked by intermolecular β -sheets, and hydrophobic sequestering in the interior gap may be partly responsible for formation of β -sheets (14). The lower surface hydrophobicity may disrupt normal hydrophobic sequestering and prevent formation of more aligned β -sheets, leading to weaker assembly of building blocks and disappearance of long OGC fibrils and OLC fibrils. Figure V-8 shows contour length distribution of OVTC fibrils, OGC fibrils and OLC fibrils. The average contour length of OVTC fibrils, OGC fibrils and OLC fibrils was 326, 232 and 280 nm, respectively. It was apparent that glycation decreased average contour length of ovotransferrin fibrils. The nature of the bound saccharides affected morphology of ovotransferrin fibrils, and OGC fibrils were generally shorter than OLC fibrils.



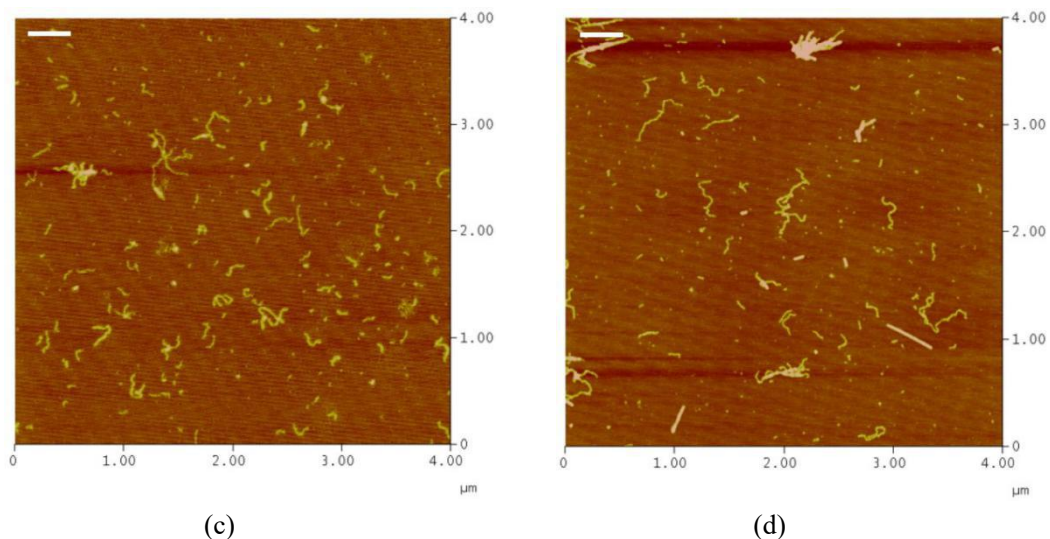
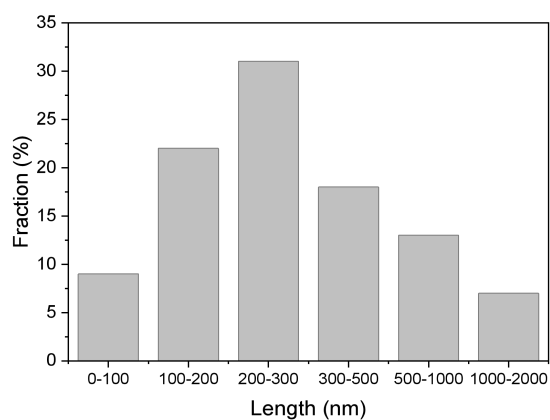
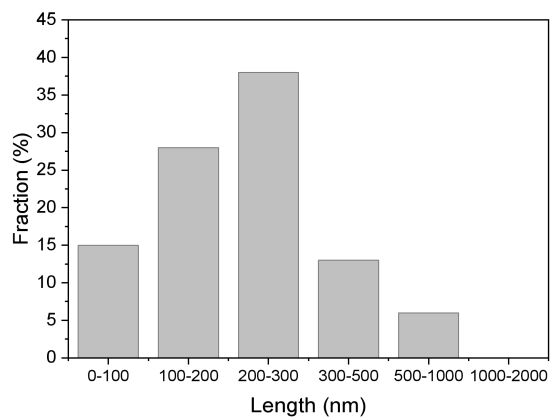


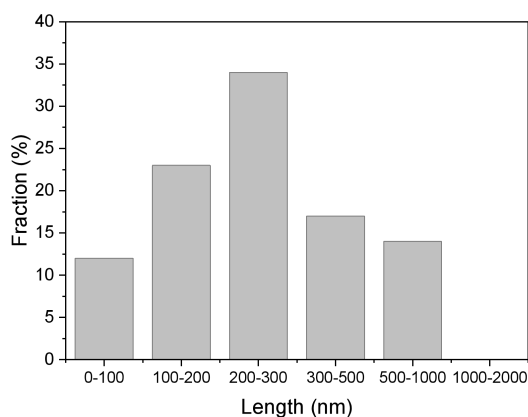
Figure V-7. AFM images of nanofibrils derived from OVTC, OGC and OLC: (a) OVTC fibrils with short or medium length, (b) long OVTC fibrils (c) OGC fibrils, (d) OLC fibrils. The scan size is $4\ \mu\text{m}\times 4\ \mu\text{m}$, and the z scale is 15 nm. The scale bar represents 400 nm.



(a)



(b)



(c)

Figure V-8. Contour length distribution of fibrils analyzed from AFM images: (a) OVTC fibrils, (b) OGC fibrils, (c) OLC fibrils.

3.3. Influence of covalent bound saccharides on Pickering emulsifier performance of nanofibrils

Figure V-9 shows Pickering emulsions stabilized by these fibrils at various fibril concentrations and oil fractions. Since all emulsions stabilized by fibrils could be dispersed well in water but not in oils, these Pickering emulsions were classified as oil-in-water emulsions. Table V-1 summarizes emulsified phase volume and stability index of these Pickering emulsions on the basis of height measurements after storage of 3 h and 15 days. As shown in Figure V-9 and Table V-1, when the fibril concentration was fixed, increasing oil fraction from 0.45 to 0.65 led to an increase in emulsified phase. While the oil fraction was fixed, increasing fibril concentration from 2 wt% to 4 wt% resulted in a rise of emulsified phase volume. It follows that increasing oil fraction and fibril concentration can elevate emulsified phase fraction of these Pickering emulsions. It was observed that emulsions stabilized by OVTC fibrils

had the least creaming among all emulsions, which could be ascribed to existence of long OVTC fibrils (with contour length above 1000 nm) and absence of long glycosylated fibrils. These long OVTC fibrils may crosslink with other OVTC fibrils at oil-water interfaces and form dense cross-linked network. These strong interparticle interactions and cross-linked network interface are beneficial to structural integrity of emulsion interfaces, which are responsible for enough steric barriers of Pickering emulsion interfaces and resisting structural breakdown (16). Based on aforementioned discussion, existence of long OVTC fibrils contributes to better Pickering emulsifier performance of OVTC fibrils. Considering that emulsified phase fractions of emulsions stabilized by OGC fibrils and OLC fibrils were lower than those of emulsions stabilized by OVTC fibrils in all investigated conditions, it might be concluded that covalent bound saccharides could weaken Pickering emulsifier performance of ovotransferrin fibrils.

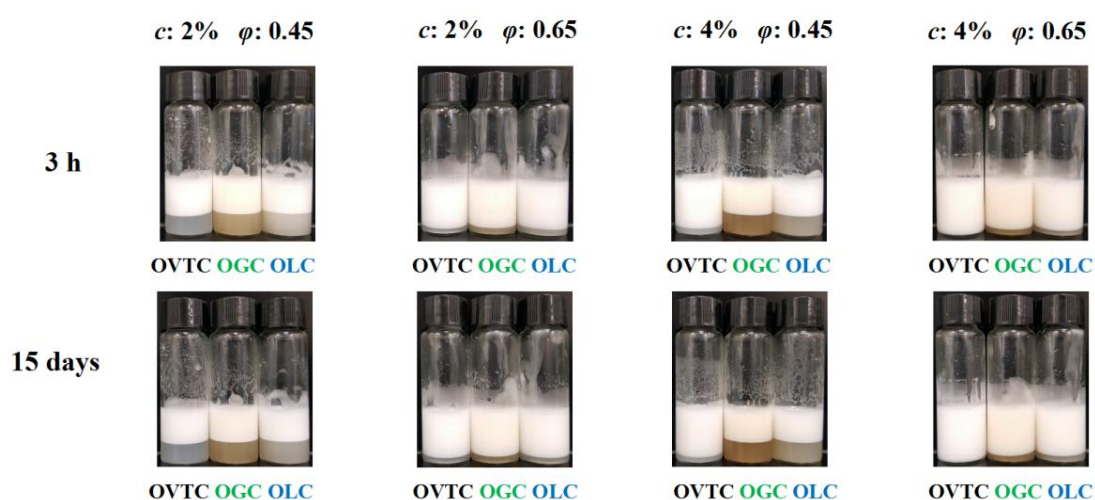


Figure V-9. Visual observation of Pickering emulsions stabilized by fibrils (OVTC fibrils, OGC fibrils and OLC fibrils) with different c (2–4 wt%) at various ϕ (0.45–0.65). Photographs were taken at 3 h and 15 days after preparation of fresh emulsions.

Table V-1. Emulsified phase volume fraction and stability index of Pickering emulsions stabilized by OVTC fibrils, OGC fibrils and OLC fibrils at different fibril concentrations and oil fractions

Pickering emulsion samples		Emulsified phase volume (%)		Stability index
		3 h	15 days	
OVTC fibril	2–0.45	65.2±0.1 ^c	65.2±0.1 ^c	100.0±0.1 ^c
OGC fibril	2–0.45	63.0±0.1 ^b	63.0±0.1 ^b	100.0±0.1 ^c
OLC fibril	2–0.45	62.1±0.1 ^a	62.1±0.2 ^a	100.0±0.1 ^c
OVTC fibril	2–0.65	91.9±0.2 ^j	91.9±0.2 ⁱ	100.0±0.1 ^c
OGC fibril	2–0.65	88.0±0.1 ^f	88.0±0.1 ^e	100.0±0.1 ^c
OLC fibril	2–0.65	88.5±0.1 ^g	88.5±0.1 ^f	100.0±0.1 ^c
OVTC fibril	4–0.45	91.2±0.2 ^h	91.2±0.2 ^{gh}	100.0±0.1 ^c
OGC fibril	4–0.45	65.9±0.2 ^e	65.7±0.2 ^d	99.7±0.1 ^{ab}
OLC fibril	4–0.45	65.5±0.1 ^d	65.3±0.2 ^{cd}	99.7±0.1 ^{ab}
OVTC fibril	4–0.65	97.8±0.1 ^k	97.3±0.1 ^j	99.5±0.1 ^a
OGC fibril	4–0.65	91.1±0.1 ^h	90.9±0.1 ^g	99.8±0.1 ^{bc}
OLC fibril	4–0.65	91.6±0.1 ⁱ	91.3±0.1 ^h	99.7±0.1 ^{ab}

Values are means±SD (n=3). Different superscript letters for the same column indicate significant differences ($p < 0.05$).

It was found that stability index of Pickering emulsions was above 99.4% in all cases, indicating excellent physical stability of all emulsions during 15-day storage. It was noteworthy that all Pickering emulsions stabilized by fibrils in this study were prepared in the presence of 150 mM NaCl, which could provide high ionic strength to induce electrostatic screening. Although Pickering emulsions are mainly stabilized through formation of steric interface barriers but not electrostatic repulsions in conventional emulsion cases, many Pickering emulsions stabilized by food-grade particles are still unstable at high salt concentrations (17). Previous studies reveal that Pickering emulsions stabilized by zein colloidal particles and thermal cross-linked

why protein nanoparticles are not stable at high ionic strength (18, 19), which can be explained by that these particles are dissociated or that these particles are detached from emulsion interfaces in the presence of high ionic strength. Since OVTC fibrils, OGC fibrils and OLC fibrils were synthesized at high ionic strength, the fibrils themselves should not dissociate at high ionic strength. Considering that Pickering emulsions stabilized by fibrils were stable during storage, these fibrils should attach to the oil-water interfaces firmly. Emulsions stabilized by fibrils with covalent bound saccharides may provide an approach to preparing stable food-grade Pickering emulsions at high ionic strength.

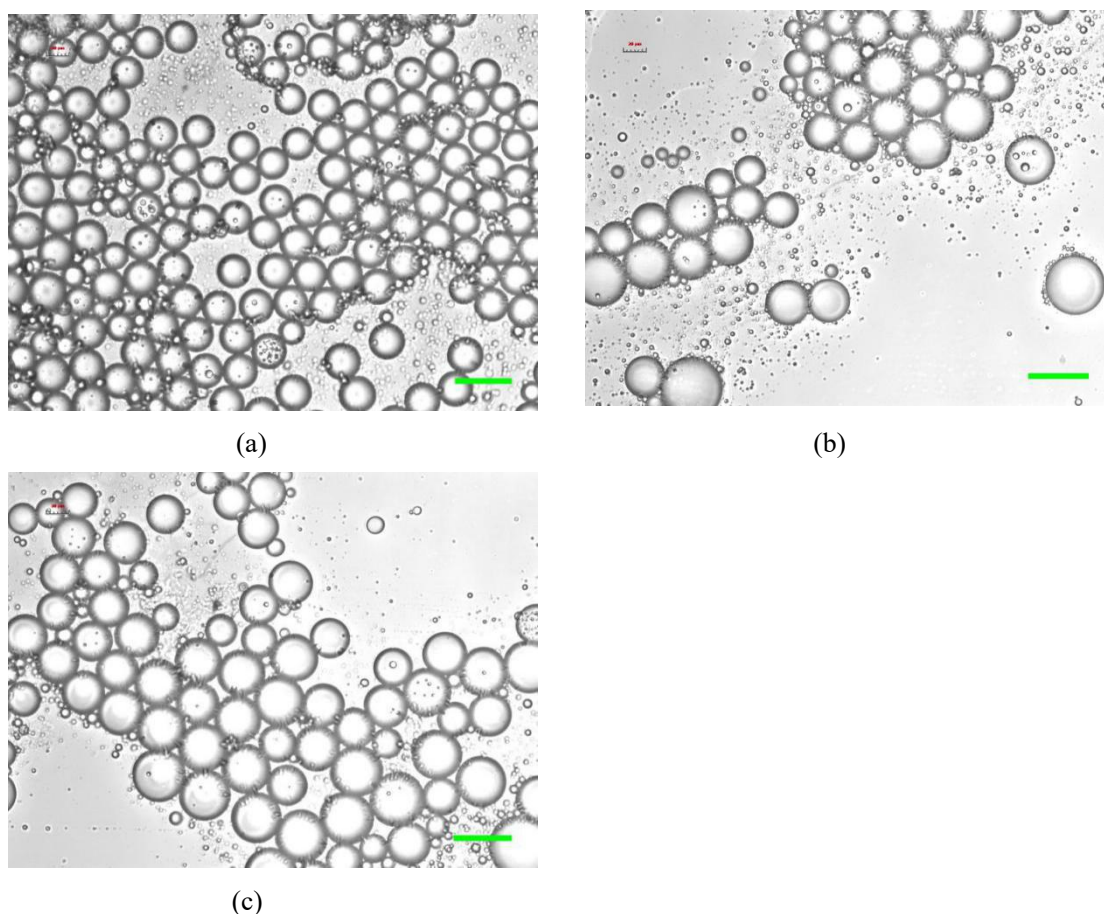


Figure V-10. Optical microscopic images of Pickering emulsions stabilized by fibrils (OVTC fibrils, OGC fibrils and OLC fibrils) at the fixed fibril concentration of 4 wt% and oil fraction of 0.65. The scale bars within the figures are 50 μm in length.

Considering that Pickering emulsions at the fixed fibril concentration of 4 wt% and oil fraction of 0.65 had the best emulsified volume fraction and high stability index, these emulsions were further studied in the rest of this research. Figure V-10 shows microstructures of the emulsion droplets stabilized by fibrils. The spherical emulsion droplets were evenly dispersed without evident flocculation or coalescence. As shown in Table V-2, average droplet size of Pickering emulsions stabilized by OVTC fibrils, OGC fibrils and OLC fibrils was 26.9, 34.0 and 32.9 μm , respectively. It was found that covalent bound saccharides on fibrils increased average emulsion droplet size, and droplet size of Pickering emulsions stabilized by OGC fibrils was the largest. Considering that glycation may weaken Pickering emulsifier performance of ovotransferrin fibrils and emulsifiers with poorer emulsibility can lead to larger droplet size, it's not difficult to understand why emulsions stabilized by OGC fibrils and OLC fibrils had larger droplet sizes.

Table V-2. Average emulsion droplet size of Pickering emulsions ($c = 4 \text{ wt}\%$, $\varphi = 0.65$) stabilized by OVTC fibrils, OGC fibrils and OLC fibrils

Emulsions stabilized by	Average emulsion droplet size (μm)
OVTC fibril	26.9 \pm 0.1 ^a
OGC fibril	34.0 \pm 0.2 ^c
OLC fibril	32.9 \pm 0.1 ^b

Values are means \pm SD (n=3). Different superscript letters indicate significant differences ($p < 0.05$).

4. Conclusion

Glycation could suppress fibrillation of ovotransferrin, and glycosylation exerted

stronger inhibitory impact on fibril formation than lactosylation. The major building blocks of OVTC fibrils, OGC fibrils and OLC fibrils were peptides, and building blocks of OGC fibrils and OLC fibrils had slightly larger molecular weight than those of OVTC fibrils. Glycation decreased average contour length of ovotransferrin fibrils, and average contour length followed the order: OVTC fibrils > OLC fibrils > OGC fibrils. Both rigid and flexible fibrils were observed in OVTC fibrils and OLC fibrils, and there was an absence of rigid fibrils in OGC fibrils. Covalent bound saccharides weakened Pickering emulsifier performance of ovotransferrin fibrils. At fixed fibril concentration of 4 wt% and oil fraction of 0.65, emulsion droplet size followed the order: OGC fibrils-stabilized emulsions > OLC fibrils-stabilized emulsions > OVTC fibrils-stabilized emulsions.

5. References

1. Li, Y., Zhong, F., Ji, W., Yokoyama, W., Shoemaker, C. F., Zhu, S., et al. (2013). Functional properties of Maillard reaction products of rice protein hydrolysates with mono-, oligo- and polysaccharides. *Food Hydrocolloids*, 30(1), 53–60.
2. Pirestani, S., Nasirpour, A., Keramat, J., Desobry, S., & Jasniewski, J. (2017). Effect of glycosylation with gum Arabic by Maillard reaction in a liquid system on the emulsifying properties of canola protein isolate. *Carbohydrate Polymers*, 157, 1620–1627.
3. Xia, S., Li, Y., Xia, Q., Zhang, X., & Huang, Q. (2015). Glycosylation of bovine serum albumin via Maillard reaction prevents epigallocatechin-3-gallate-induced protein aggregation. *Food Hydrocolloids*, 43, 228–235.
4. Laemmli, U. K. (1970). Cleavage of structural proteins during the assembly of head of bacteriophage T4. *Nature*, 227(5259), 680–685.
5. Church, F. C., Swaisgood, H. E., Porter, D. H., & Catignani, G. L. (1983). Spectrophotometric assay using o-phthaldialdehyde for determination of proteolysis in milk and isolated milk protein. *Journal of Dairy Science*, 66(6), 1219–1227.
6. Wei, Z., Yang, W., Fan, R., Yuan, F., & Gao, Y. (2015). Evaluation of structural and

functional properties of protein–EGCG complexes and their ability of stabilizing a model β -carotene emulsion. *Food Hydrocolloids*, 45, 337–350.

7. Alizadeh-Pasdar, N., & Li-Chan, E. C. Y. (2000). Comparison of protein surface hydrophobicity measured at various pH values using three different fluorescent probes. *Journal of Agricultural and Food Chemistry*, 48(2), 328–334.

8. Wei, Z., Zhu, P., & Huang, Q. (2019). Investigation of ovotransferrin conformation and its complexation with sugar beet pectin. *Food Hydrocolloids*, 87, 448–458.

9. Wei, Z., & Huang, Q. (2019). Edible Pickering emulsions stabilized by ovotransferrin–gum arabic particles. *Food Hydrocolloids*, 89, 590–601.

10. Zoppe, J. O., Venditti, R. A., & Rojas, O. J. (2012). Pickering emulsions stabilized by cellulose nanocrystals grafted with thermo-responsive polymer brushes. *Journal of Colloid and Interface Science*, 369(1), 202–209

11. Xiao, J., Wang, X. A., Gonzalez, A. J. P., & Huang, Q. (2016). Kafirin nanoparticles-stabilized Pickering emulsions: Microstructure and rheological behavior. *Food Hydrocolloids*, 54, 30–39.

12. de Oliveira, F. C., Coimbra, J. S. R., de Oliveira, E. B., Zuñiga, A. D. G., & Rojas, E. E. G. (2016). Food protein-polysaccharide conjugates obtained via the maillard reaction: A review. *Critical Reviews in Food Science and Nutrition*, 56(7), 1108–1125.

13. Nilsson, M. R. (2004). Techniques to study amyloid fibril formation in vitro. *Methods*, 34(1), 151–160.

14. Jones, O. G., & Mezzenga, R. (2012). Inhibiting, promoting, and preserving stability of functional protein fibrils. *Soft Matter*, 8(4), 876–895.

15. Meyer, E. E., Rosenberg, K. J., & Israelachvili, J. (2006). Recent progress in understanding hydrophobic interactions. *Proceedings of the National Academy of Sciences*, 103(43), 15739–15746.

16. Liu, F., & Tang, C. (2016). Soy glycinin as food-grade Pickering stabilizers: Part. I. Structural characteristics, emulsifying properties and adsorption/arrangement at interface. *Food Hydrocolloids*, 60, 606–619.

17. Berton-Carabin, C. C., & Schroën, K. (2015). Pickering emulsions for food applications: Background, trends, and challenges. *Annual Review of Food Science and Technology*, 6(1), 263–297.

18. de Folter, J. W. J., van Ruijven, M. W. M., & Velikov, K. P. (2012). Oil-in-water Pickering emulsions stabilized by colloidal particles from the water-insoluble protein zein. *Soft Matter*, 8(25), 6807–6815.

19. Wu, J., Shi, M., Li, W., Zhao, L., Wang, Z., Yan, X., et al. (2015). Pickering emulsions stabilized by whey protein nanoparticles prepared by thermal cross-linking. *Colloids and Surfaces B: Biointerfaces*, 127, 96–104.

CHAPTER VI. IMPACT OF POLYPHENOLS ON OVOTRANSFERRIN FIBRILS

1. Introduction

Interactions between proteins and polyphenols are inevitable in food systems, which can be classified into non-covalent and covalent interactions. Hydrogen bondings, van der Waals forces and hydrophobic interactions are the main non-covalent interactions, and Schiff Bases and Michael addition reactions following oxidation of polyphenols may result in covalent bonds (1–3). Non-covalent and covalent interactions between proteins and polyphenols may lead to formation of protein–polyphenol physical complexes and covalent complexes, respectively (3), and fibrillation of protein–polyphenol covalent complexes may differ from unmodified proteins and protein–polyphenol physical complexes. In addition, interactions between proteins and different amounts of polyphenols may lead to discrepancies in formation kinetic and physicochemical properties of fibrils, and there are few related studies yet.

(–)-Epigallocatechin-3-gallate (EGCG), a major catechin in green tea with molecular weight of 458.37, can function as antitumor agent or powerful antioxidant (4). In addition, EGCG shows beneficial effects in treating Parkinson or Alzheimer disease (4). Gallic acid, a versatile antioxidant with molecular weight 170.12 from plants and fungi, has a diverse range of industrial and therapeutic applications (5). Gallic acid (GA) displays multiple bioactivities such as neuroprotective effect and

anticancer activity (5, 6). EGCG and GA own dissimilar structural characteristics (4, 5), which may interact with proteins in distinctive ways. A systematic research on protein–EGCG fibrils and protein–GA fibrils may help to learn about influence of polyphenol structures on structural and functional properties of protein nanofibrils.

Thus, this chapter aimed to first modify OVT with different amounts of EGCG or GA in non-covalent or covalent ways, and then investigate how the fibrillation and fibril properties can be modulated by polyphenol structures, polyphenol content and distinct OVT–polyphenol interactions.

2. Materials and methods

2.1. Materials

Ovotransferrin (OVT, purity > 88%) was obtained from Neova Technologies Inc. (Abbotsford, Canada), and OVT had an iron binding activity >1000 µg Fe/g sample. The compound (–)-epigallocatechin-3-gallate (EGCG) with a purity of 95% was purchased from DSM Nutritional Products Ltd (Basel, Switzerland). Gallic acid (98%, purity) was obtained from Acros Organics (Geel, Belgium). PageRuler™ Plus prestained protein ladder (10 to 250 kDa) was obtained from Thermo Fisher Scientific, Inc. (Waltham, USA).

2.2. Preparation of OVT–polyphenol covalent complexes

OVT–polyphenol covalent complexes were prepared as follows. OVT (4 mg/mL) was dispersed in 10 mL of Milli-Q water, and pH of OVT solution was adjusted to 9 with 0.2 M NaOH. Sodium azide (0.02%, w/v) was added in order to impede microbial growth, and OVT solution was stirred overnight to ensure complete

dispersion and dissolution. Polyphenol (0.1, 0.2 or 0.4 mg/mL) dissolved in 10 mL of Milli-Q water was added to 10 mL of OVT solutions under continuous stirring, respectively. The polyphenols applied here were (-)-epigallocatechin-3-gallate (EGCG) and gallic acid (GA), respectively. The pH of solutions was adjusted to 9 upon addition of polyphenol. Thereafter, the mixtures were stirred continuously with free exposure to air at ambient temperature for 24 h. The samples were dialyzed against Milli-Q water at 4°C for 72 h to eliminate the free unbound polyphenol (molecular weight cutoff 3500 Da) and freeze-dried to obtain OVT–polyphenol covalent complexes. To make this paper more clear, abbreviations were used to denote different OVT–polyphenol covalent complexes. OEC-L, OEC-M and OEC-H were OVT–EGCG covalent complexes obtained by covalent modification of OVT (4 mg/mL) with different concentrations of EGCG (0.1, 0.2 or 0.4 mg/mL), respectively. OGC-L, OGC-M and OGC-H were OVT–GA covalent complexes obtained by covalent modification of OVT (4 mg/mL) with different concentrations of GA (0.1, 0.2 or 0.4 mg/mL), respectively. The protein content of OVT–polyphenol covalent complexes was measured using modified Lowry method (3, 7).

2.3. Characterization of OVT–polyphenol covalent complexes

2.3.1. Free amino groups

Free amino groups of OVT and OVT–polyphenol complexes were determined via an OPA method (8), and L-leucine standard curve was used to calculate the content of free amino groups.

2.3.2. Free sulfhydryl groups

The content of free sulfhydryl groups in OVT and OVT–polyphenol complexes were determined using Ellman's reagent as described previously (9).

2.3.3. Sodium dodecyl sulfate polyacrylamide gel electrophoresis (SDS-PAGE)

SDS-PAGE was performed as described in Chapter II.

2.4. Preparation of OVT–polyphenol physical complexes

The total phenolic content of OVT–polyphenol covalent complexes was determined according to the Folin–Ciocalteu method using EGCG and gallic acid as a standard (10), and the total phenol content was expressed as mg polyphenol (EGCG or GA) equivalents/g dry complex. If 1 g of OVT–polyphenol covalent complex consisted of M_1 g of OVT and M_2 g of polyphenol, then M_2 g of polyphenol (EGCG or GA) dissolved in Milli-Q water (pH 5) was added into aqueous dispersion (pH 5) containing M_1 g of OVT. The final OVT concentration was fixed as 2 mg/mL, and polyphenol concentration ranged between 0.05 and 0.2 mg/mL. The pH of the resultant mixture was adjusted to 5, and the solution was stirred at ambient temperature in the dark without exposure to air for 24 h. The final product was lyophilized to obtain OVT–polyphenol physical complexes without dialysis. OEP-L, OEP-M and OEP-H were OVT–EGCG physical complexes with the same phenolic content as OEC-L, OEC-M and OEC-H, respectively. OGP-L, OGP-M and OGP-H were OVT–GA physical complexes with the same phenolic content as OGC-L, OGC-M and OGC-H, respectively.

2.5. Preparation of fibrils

The optimal fibrillation parameters were obtained in our previous study (11).

OVT and OVT–polyphenol complexes were dispersed in pH-adjusted Milli-Q water (pH 2, 150 mM NaCl) at a protein concentration of 40 mg/mL. The samples were stirred mildly for 4 hours, and 1M HCl was used to maintain the pH. Sodium azide (0.02%, w/v) was added so as to impede microbial growth. The samples were filtered with 0.45 μm pore-sized syringe filters (Thermo Fisher Scientific, Waltham, USA) in order to remove impurities. The purified samples were placed into screw-capped vials flushed with nitrogen in the dark. The vials were heated in oil bath over a temperature-controlled hot plate stirrer (VWR International, Radnor, USA) at 90°C under magnetic stirring at 300 rpm. The heated samples were cooled in an ice-water bath and stored in a refrigerator at 4°C until further analysis. ThT fluorescence, SDS-PAGE and AFM were applied to analyze fibrillation process.

2.6. Characterization of fibrils

2.6.1. Thioflavin T (ThT) fluorescence

ThT fluorescence was measured as described in Chapter II.

2.6.2. Sodium Dodecyl Sulfate Polyacrylamide Gel Electrophoresis (SDS-PAGE)

SDS-PAGE was performed as described in Chapter II.

2.6.3. Atomic force microscopy (AFM)

AFM was measured as described in Chapter II.

2.6.4. Surface Hydrophobicity (H_0)

Surface hydrophobicity of samples was carried out as described in Chapter II.

3. Results and Discussion

3.1. Synthesis of OVT–polyphenol covalent complexes

Involvement of free amino groups and free sulfhydryl groups might occur during OVT modification. As indicated in Table VI-1, the free amino groups of OVT–polyphenol covalent complexes were significantly ($p < 0.05$) fewer than those of OVT, and the number of free amino groups in OVT–polyphenol covalent complexes declined with increasing amounts of polyphenols. Since SDS may destroy non-covalent protein interactions during measurements of free amino groups (12), it may be deduced that ϵ -amino groups of lysine indeed react with these polyphenols and a larger number of polyphenols may react irreversibly with more ϵ -amino groups in OVT.

Table VI-1. Free amino groups of OVT, OVT–EGCG covalent complexes and OVT–GA covalent complexes

Samples	Free amino groups (nmol/mg protein)
OVT	636.4±11.2 ^f
OEC-L	521.6±20.4 ^e
OEC-M	404.6±13.6 ^c
OEC-H	306.2±9.7 ^a
OGC-L	530.5±16.3 ^e
OGC-M	458.1±19.1 ^d
OGC-H	338.5±15.5 ^b

Different superscript letters in the same column indicate significant differences ($p < 0.05$).

Table VI-2 shows that the amount of free sulfhydryl groups of OVT–polyphenol covalent complexes was smaller when compared with that of OVT. Because conversion of sulfhydryl groups to disulphide bridges is prevented in the presence of

8 M urea (3, 12), it can be speculated that free sulfhydryl groups participate in cross-linking between OVT and polyphenols. It was also observed that GA showed stronger reactivity with free sulfhydryl groups than EGCG.

Table VI-2. Free sulfhydryl groups of OVT, OVT–EGCG covalent complexes and OVT–GA covalent complexes

Samples	Free sulfhydryl groups (nmol/mg protein)
OVT	6.08± 0.19 ^g
OEC-L	1.80±0.08 ^f
OEC-M	1.09±0.06 ^e
OEC-H	0.72±0.02 ^d
OGC-L	0.41±0.03 ^c
OGC-M	0.08±0.01 ^b
OGC-H	0.03±0.01 ^a

Different superscript letters in the same column indicate significant differences ($p < 0.05$).

Table VI-3. Total phenolic content of OVT–EGCG covalent complexes and OVT–GA covalent complexes

Samples	Total phenolic content (mg/g sample)
OEC-L	24.37±0.11 ^a
OEC-M	47.08±0.09 ^c
OEC-H	90.68±0.21 ^e
OGC-L	24.19±0.08 ^a
OGC-M	41.72±0.25 ^b
OGC-H	76.16±0.55 ^d

Different superscript letters in the same column indicate significant differences ($p < 0.05$).

Amount of bound polyphenols in OVT–polyphenol covalent complexes was quantified. As shown in Table VI-3, covalent modification of OVT with a higher concentration of the same kind of polyphenols led to complexes with more bound polyphenols. It was worth noting that OEC-M and OEC-H had higher total phenolic content than OGC-M and OGC-H, respectively, implying that more EGCG could bind to OVT than GA when covalent interactions occurred.

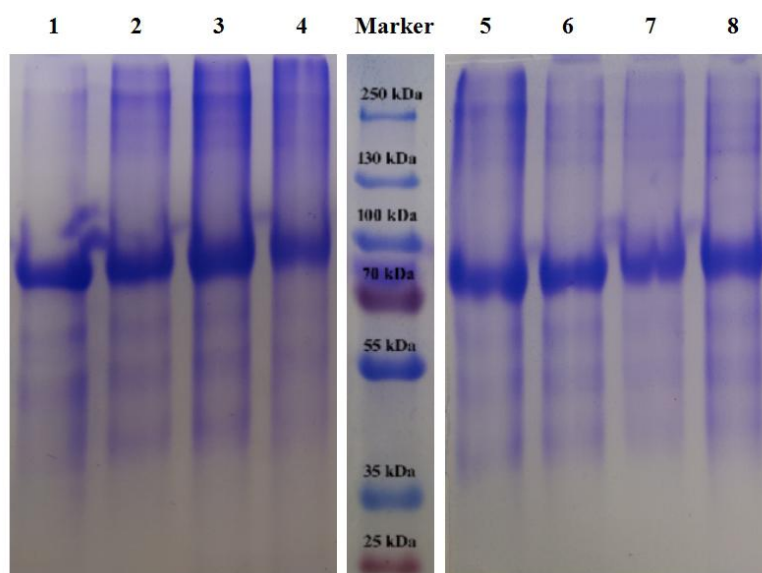


Figure VI-1. SDS-PAGE profiles (10% separating gel) of OVT and OVT–polyphenol covalent complexes. Lanes from left to right are OVT, OEC-L, OEC-M, OEC-H, protein marker, OVT, OGC-L, OGC-M, OGC-H.

SDS-PAGE was applied to further confirm the covalent binding of polyphenols to OVT. As depicted in Figure VI-1, the bands of OVT–polyphenol covalent complexes migrated up in comparison with the bands of OVT, suggesting increase of molecular weight upon conjugation. Since non-covalent interactions between proteins and polyphenols could be broken in the presence of SDS (12), the shift to higher

molecular weight could confirm the covalent coupling between OVT and polyphenols. In addition, it was observed that OVT–polyphenol covalent complexes with more bound polyphenols had larger molecular weight.

3.2. Preparation of OVT–polyphenol physical complexes

Table VI-4. Free amino groups of OVT, OVT–EGCG physical complexes and OVT–GA physical complexes

Samples	Free amino groups (nmol/mg protein)
OVT	636.4±11.2 ^a
OEP-L	635.8±8.6 ^a
OEP-M	637.1±15.8 ^a
OEP-H	634.0±13.0 ^a
OGP-L	634.9±10.3 ^a
OGP-M	636.8±15.9 ^a
OGP-H	635.0±17.7 ^a

Different superscript letters in the same column indicate significant differences ($p < 0.05$).

At acidic pHs polyphenols are structurally stable, and they may interact with proteins reversibly via non-covalent forces such as hydrogen bonding and hydrophobic bonding (3, 13). In order to rule out interference of polyphenol content on analyzing how the fibrillation and fibril properties can be affected by distinct OVT–polyphenol interactions during the rest of this research, the amount of polyphenols in OVT–polyphenol physical complexes was the same as that of corresponding OVT–polyphenol covalent complexes. As indicated in Table VI-4 and Table VI-5, the amount of free amino groups and free sulfhydryl groups remained unchanged upon physical complexation of OVT with polyphenols, suggesting that

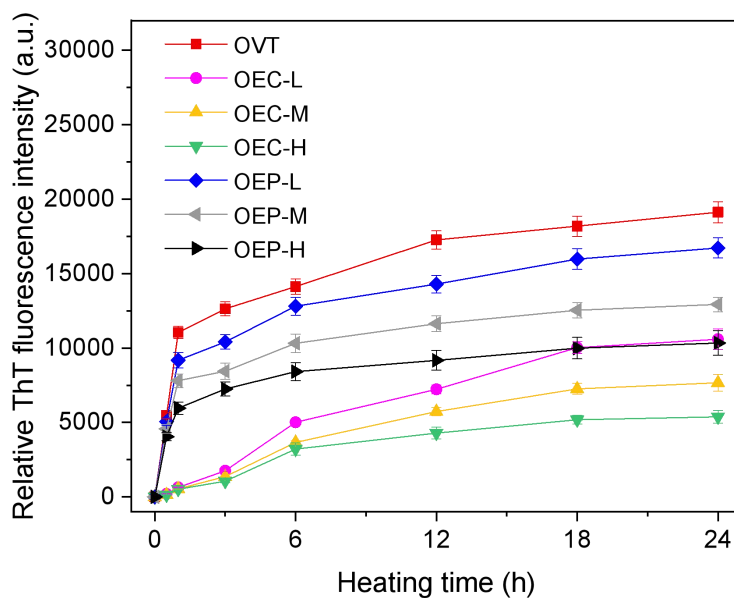
these active groups did not react with polyphenols at relatively low pHs.

Table VI-5. Free sulfhydryl groups of OVT, OVT–EGCG physical complexes and OVT–GA physical complexes

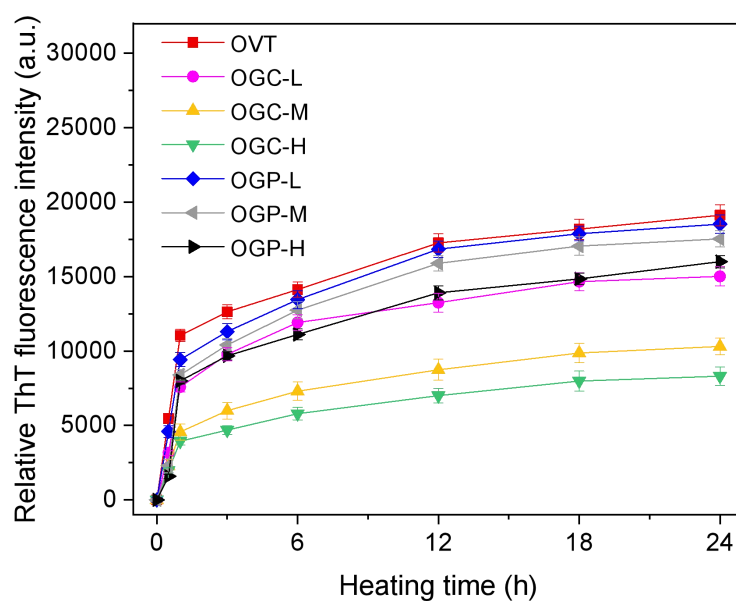
Samples	Free sulfhydryl groups ($\mu\text{M/g protein}$)
OVT	6.08 ± 0.19^a
OEP-L	6.10 ± 0.22^a
OEP-M	6.06 ± 0.13^a
OEP-H	6.07 ± 0.11^a
OGP-L	6.06 ± 0.10^a
OGP-M	6.08 ± 0.07^a
OGP-H	6.05 ± 0.24^a

Different superscript letters in the same column indicate significant differences ($p < 0.05$).

3.3. Influence of bound polyphenols on OVT fibrillation



(a)



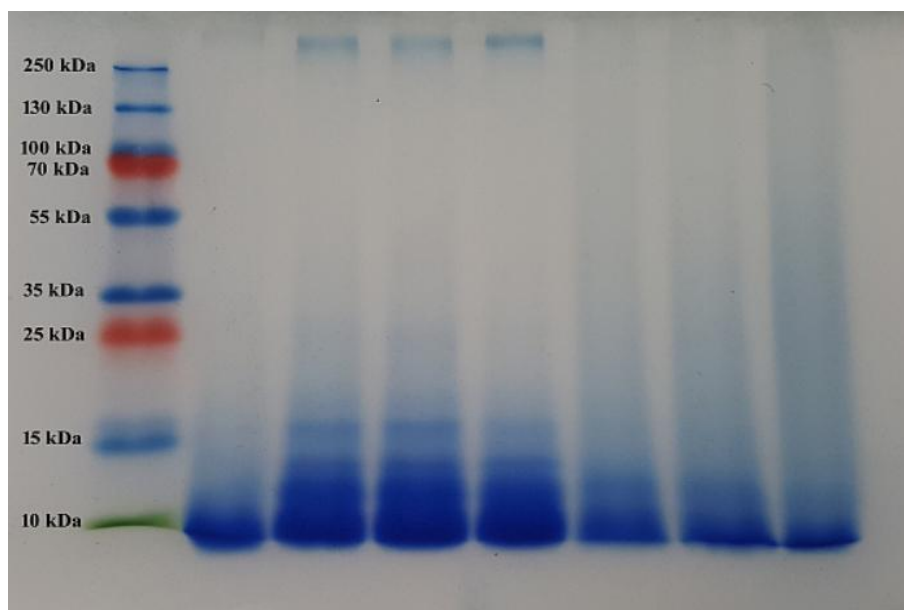
(b)

Figure VI-2. Thioflavin T (ThT) fluorescence of OVT and OVT–polyphenol complexes after heating at 90°C and pH 2.0.

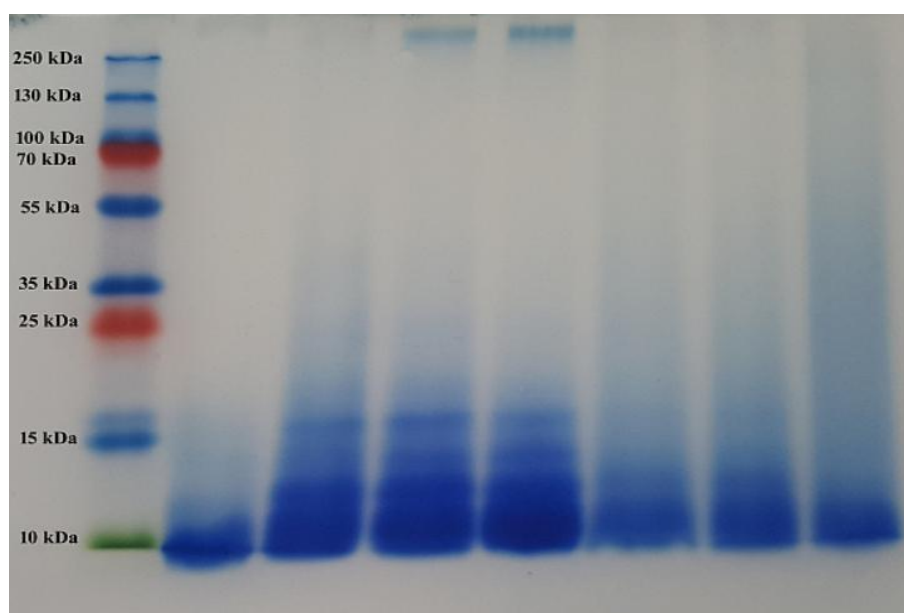
As depicted in Figure VI-2a, in the presence of bound EGCG, ThT intensities followed the order: OVT > OEP-L > OEP-M > OEC-L \approx OEP-H > OEC-M > OEC-H. In terms of influence of GA on kinetics of fibril formation, Figure VI-2b shows that ThT fluorescence followed the order: OVT > OGP-L > OGP-M > OGP-H > OGC-L > OGC-M > OGC-H. It was apparently observed that interactions with polyphenols had inhibitory effects on OVT nanofibrillation, and covalent interactions between OVT and polyphenols had stronger fibril-inhibitory activity than non-covalent interactions. The following explanations may account for these phenomena. First, since EGCG and GA are phenol molecules with very hydrophilic characteristic, OVT–polyphenol complexes are less hydrophobic when compared with unmodified OVT. Considering the fact that hydrophobic interactions are main driving forces for protein fibrillation

(14), the diminished hydrophobic interactions may have anti-formation and anti-extension effects on OVT nanofibrillation. No wonder covalent interactions with polyphenols repressed fibrillation more intensely than non-covalent interactions while taking into account significantly lower surface hydrophobicity of OVT–polyphenol covalent complexes. Second, the decrease of nanofibrils can be a result of disruptive effects of polyphenols on β -sheet structures. Given that ThT is a specific dye for β -sheet structures (15), the decline of ThT intensities may be interpreted as loss of β -sheet structures. Polyphenols may have structural similarities to some fibril inhibitors (16), and the polyphenols may have non-covalent interactions with β -sheet structures, preventing self-assembly of more building blocks into amyloid fibrils.

SDS-PAGE was conducted to explore building blocks of fibrils in the absence and presence of bound polyphenols. As shown in Figure VI-3, for hydrolysis of OVT, SDS-PAGE bands with molecular weight around 10 kDa were observed, suggesting that the building blocks were peptides with molecular weight around 10 kDa. It was observed that hydrolyzed OVT–polyphenol physical complexes had molecular weight range of around 10–15 kDa, and partial hydrolysates of OVT–polyphenol covalent complexes had molecular weights above 15 kDa. It was apparent that peptides derived from OVT–polyphenol complexes were generally larger than those originated from OVT. It may be postulated that peptides with smaller molecular weight are more beneficial to OVT nanofibrillation, which can account for differences among ThT intensities of OVT, OVT–polyphenol covalent complexes and physical complexes.



(a)

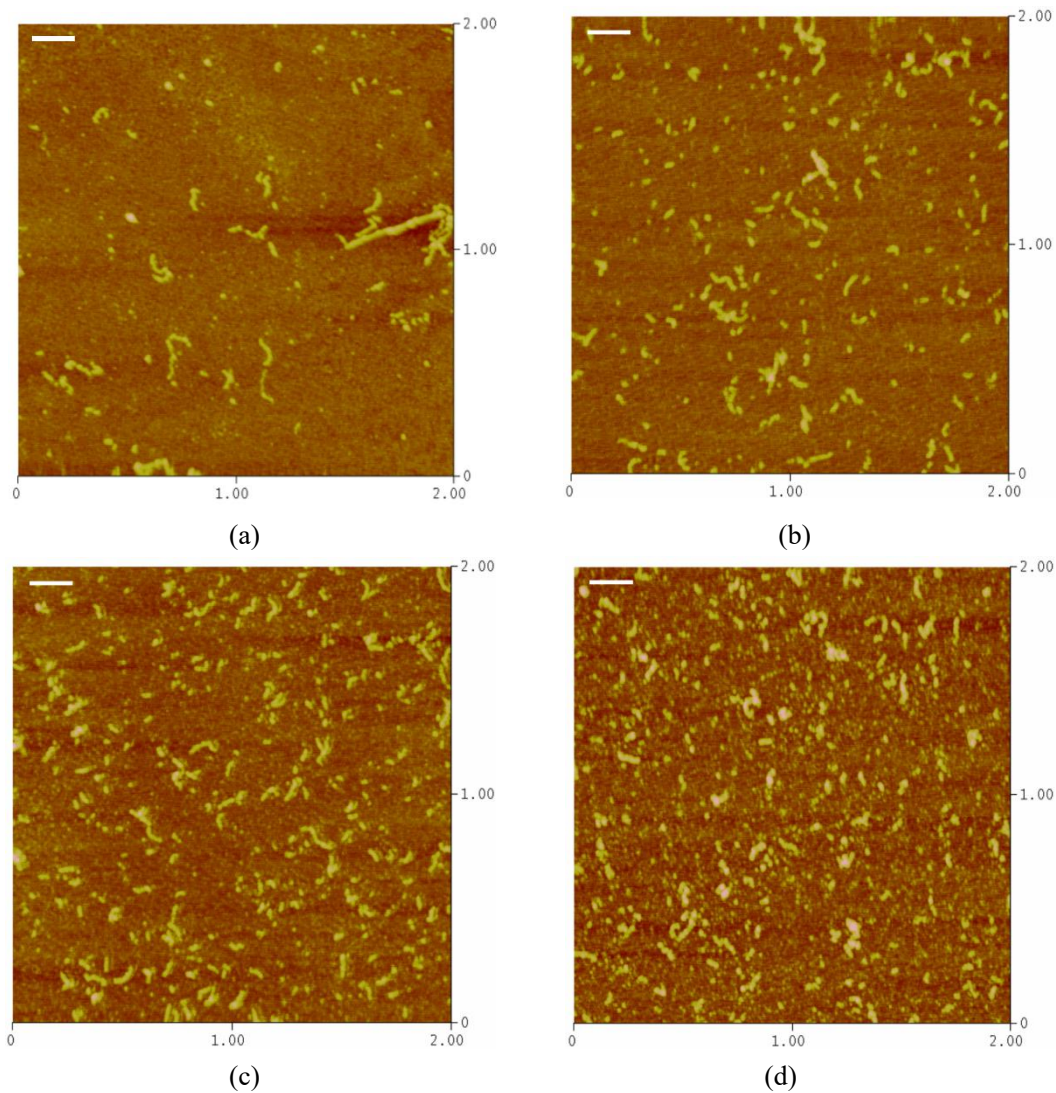


(b)

Figure VI-3. SDS-PAGE profiles (12% separating gel) of OVT and OVT–polyphenol complexes after heating at pH 2.0 and 90°C for 24 h. For Figure a, lanes from left to right are marker, heated OVT, OEC-L, OEC-M, OEC-H, OEP-L, OEP-M and OEP-H. For Figure b, lanes from left to right are marker, heated OVT, OGC-L, OGC-M, OGC-H, OGP-L, OGP-M and OGP-H.

It was worth noting that SDS-PAGE bands with molecular weight over 250 kDa were observed after heat treatment of OVT–polyphenol covalent complexes, and this

may be explained by that polyphenol quinones can act as molecule cross-linkers and some peptide fragments are coupled together to larger biomacromolecules (17). The occurrence of SDS-PAGE bands above 250 kDa implies that the polyphenol-crosslinked peptide aggregates may be building blocks of nanofibrils derived from OVT–polyphenol covalent complexes.



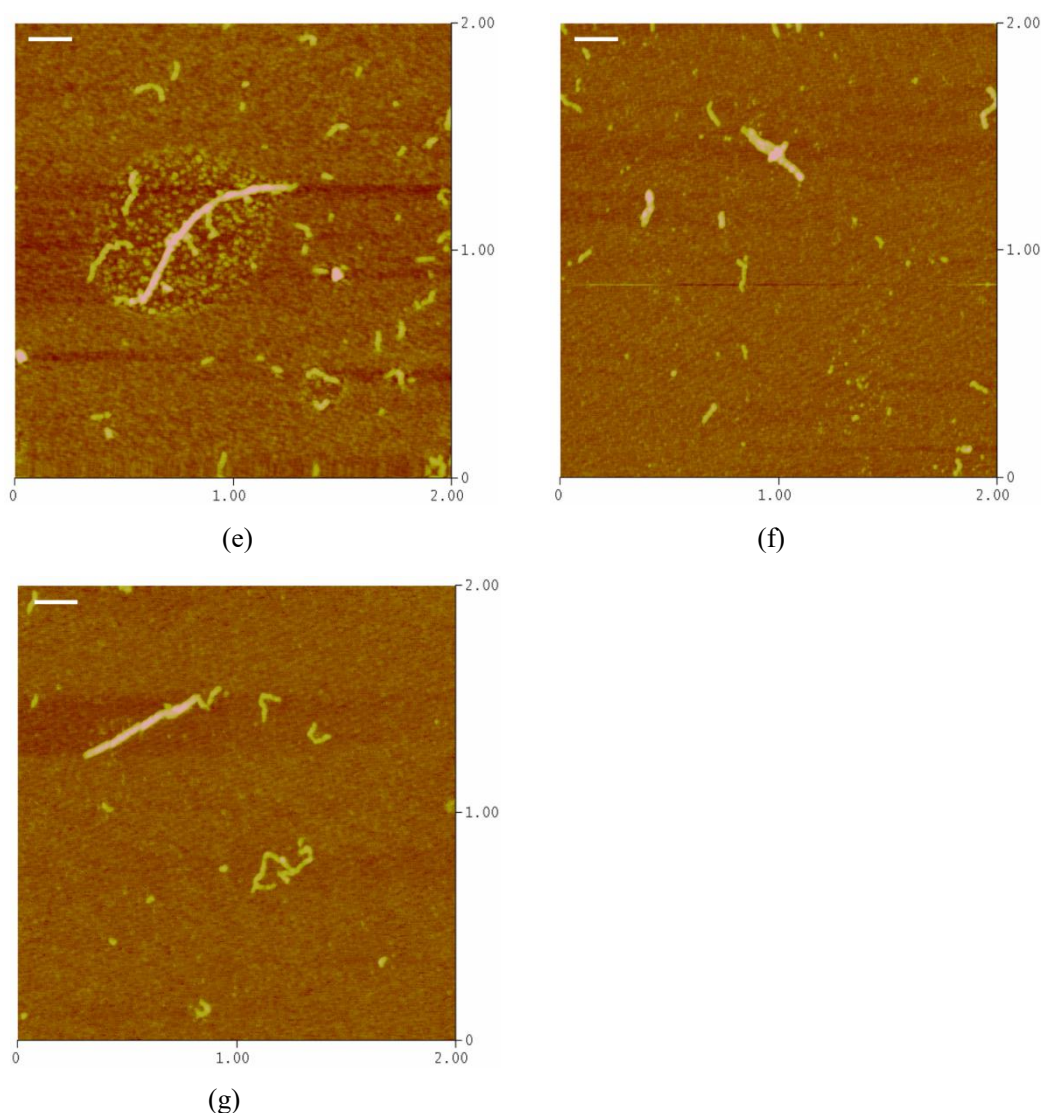
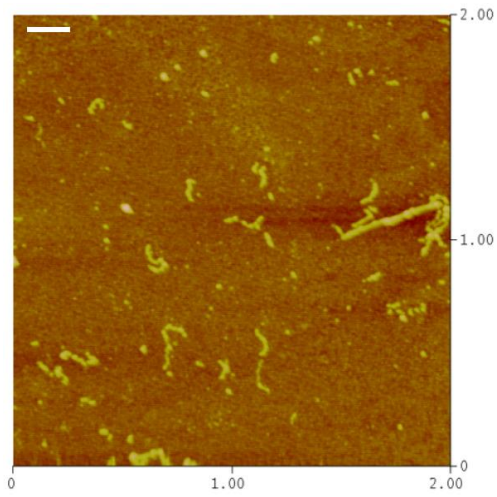


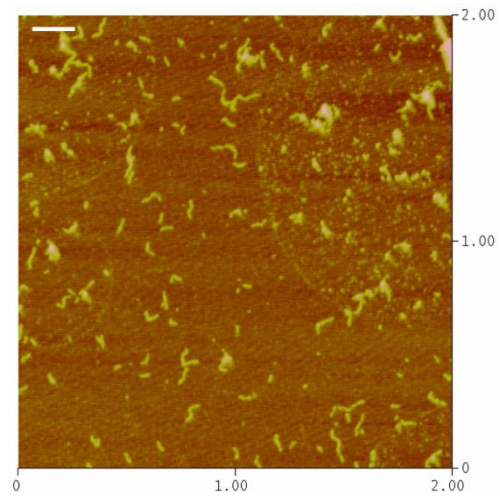
Figure VI-4. AFM images of nanofibrils derived from OVT and OVT-EGCG complexes after heating at pH 2.0 and 90°C for 24 h: (a) OVT, (b) OEC-L, (c) OEC-M, (d) OEC-H, (e) OEP-L, (f) OEP-M, (g) OEP-H. The scan size is 2 μm \times 2 μm , and the z scale is 20 nm. The scale bar represents 200 nm.

AFM was utilized to provide qualitative information regarding OVT nanofibrillation and investigate whether presence of polyphenols induced changes in morphology of OVT nanofibrils. Figure VI-4 depicts AFM images of OVT nanofibrils prepared in the absence and presence of covalent or non-covalent bound EGCG. In

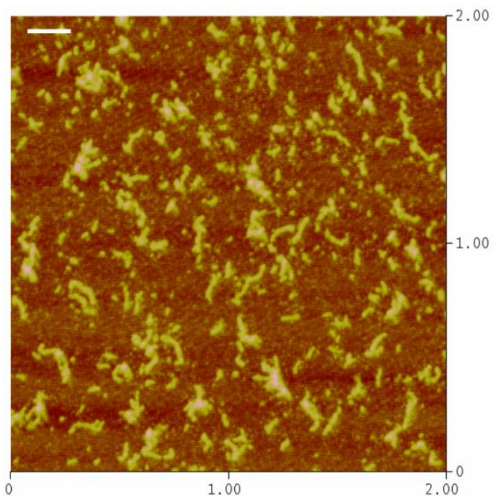
the case of OVT nanofibrils, apart from long and rigid fibrils, short and curly fibrils were also observed. The fibrils derived from OVT–EGCG covalent complexes were short with maximum contour length below 200 nm, and the average contour length of fibrils derived from OEC-L, OEC-M and OEC-H was 92, 67 and 58 nm, respectively. It was summarized that the more the covalent bound EGCG was, the shorter the OVT fibrils were. As shown in Figure VI-4, long and rigid fibrils were still observed in the presence of non-covalent bound EGCG, implying that non-covalent interactions with EGCG did not alter morphology of OVT nanofibrils obviously. In terms of impact of bound GA on OVT fibrillation, Figure VI-5 shows that fibrils derived from OVT–GA covalent complexes were shorter when compared with those originated from unmodified OVT, and the average contour length of fibrils derived from OGC-L, OGC-M and OGC-H was 127, 100 and 92 nm, respectively. It was found that fibrils prepared from OVT–GA covalent complexes were longer than those from corresponding OVT–EGCG covalent complexes, suggesting that covalent bound EGCG have stronger anti-elongation effects than covalent bound GA. No significant changes in morphology of OVT fibrils were induced upon non-covalent complexations with GA. It was noteworthy that although complexations with polyphenols could disrupt conversion of OVT into amyloid fibrils, very few amorphous aggregates were viewed in these AFM pictures, suggesting that transformation of amyloid fibrils into amorphous aggregates is not a major mechanism of anti-fibrillation of the bound polyphenols.



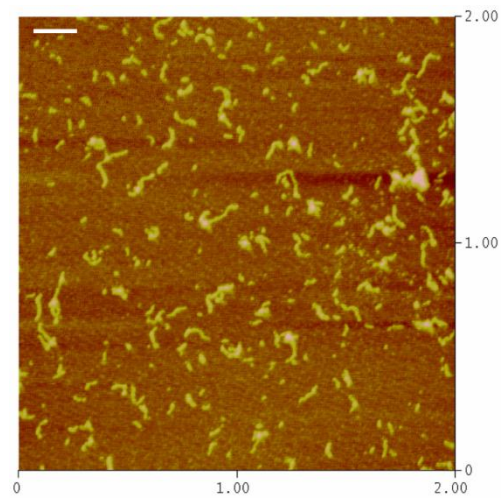
(a)



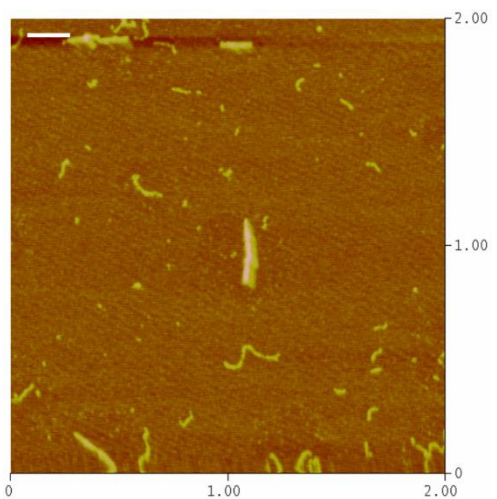
(b)



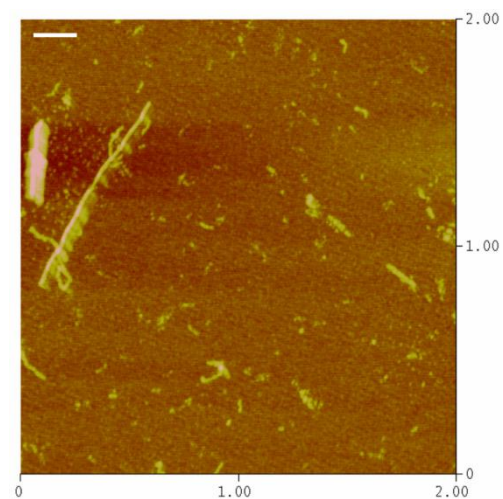
(c)



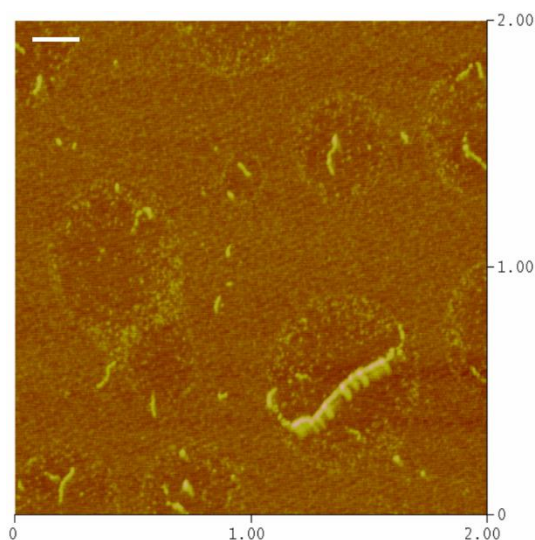
(d)



(e)



(f)



(g)

Figure VI-5. AFM images of nanofibrils derived from OVT and OVT–GA complexes after heating at pH 2.0 and 90°C for 24 h: (a) OVT, (b) OGC-L, (c) OGC-M, (d) OGC-H, (e) OGP-L, (f) OGP-M, (g) OGP-H. The scan size is 2 μm \times 2 μm , and the z scale is 20 nm. The scale bar represents 200 nm.

To sum up, covalent complexations of OVT with polyphenols could shorten nanofibrils and higher levels of covalent modification led to shorter nanofibrils, while non-covalent interactions between OVT and polyphenols exerted little influence on morphology of OVT nanofibrils.

3.4. Surface hydrophobicity

Study of surface hydrophobicity can provide valuable information about how covalent or non-covalent bound polyphenols modulate surface structure of OVT nanofibrils. Surface hydrophobicity of unheated proteins was also investigated to provide background for understanding how nanofibrillation impact location and amount of hydrophobic or hydrophilic patches. As shown in Table VI-6, fibrils derived from OVT, OVT–EGCG covalent complexes, OVT–EGCG physical complexes and OVT–GA physical complexes possessed significantly lower surface

hydrophobicity than corresponding unheated proteins, which could be accounted for by following explanation. Hydrophobic interactions are major driving forces of protein nanofibrillation, and the hydrophobic patches on β -sheets could align to ordered structures during self-assembly of building blocks into nanofibrils (18). Involvement of hydrophobic patches in construction of ordered structures may lead to a lack of hydrophobic patches on fibril surfaces, resulting in lower surface hydrophobicity upon fibril formation. It was noteworthy that not all proteins underwent decreases in surface hydrophobicity upon fibrillation, and the exception was OVT-GA covalent complexes. For the special case, surface hydrophobicity of OVT-GA covalent complexes increased during the process of fibril formation. It may be assumed that covalent bound GA can participate in building internal structures among building blocks of nanofibrils, leading to a decrease of hydrophilic GA molecules on the surface. In this way surface hydrophobicity undergoes an increase. Table VI-6 also shows that bound polyphenols made surfaces of fibrils more hydrophilic, and fibrils with covalent bound polyphenols had lower surface hydrophobicity than those with corresponding non-covalent bound polyphenols. The phenomenon may be explained by that covalent complexations of OVT with polyphenols can introduce more hydrophilic groups to fibril surfaces than corresponding non-covalent complexations.

Table VI-6. Surface hydrophobicity of OVT, OVT–polyphenol complexes and fibrils derived from OVT and OVT–polyphenol complexes.

Samples	Surface hydrophobicity	Samples	Surface hydrophobicity
OVT	1519.6±31.7 ⁱ	OVT fibril	1021.4±19.2 ^k
OEC-L	748.5±21.3 ^e	OEC-L fibril	306.6±16.4 ^e
OEC-M	654.6±19.7 ^d	OEC-M fibril	195.5±12.8 ^c
OEC-H	501.7±13.6 ^c	OEC-H fibril	98.9±9.6 ^a
OEP-L	1217.3±46.1 ^h	OEP-L fibril	491.6±23.4 ^g
OEP-M	866.6±34.0 ^f	OEP-M fibril	392.2±27.3 ^f
OEP-H	629.9±27.7 ^d	OEP-H fibril	269.6±23.2 ^d
OGC-L	231.7±18.4 ^b	OGC-L fibril	373.4±24.9 ^f
OGC-M	119.8±12.1 ^a	OGC-M fibril	243.9±17.5 ^d
OGC-H	87.9±9.7 ^a	OGC-H fibril	158.9±10.3 ^b
OGP-L	1211.7±43.2 ^h	OGP-L fibril	831.0±9.7 ^j
OGP-M	929.1±36.7 ^g	OGP-M fibril	717.4±28.4 ⁱ
OGP-H	740.0±27.5 ^e	OGP-H fibril	628.9±19.6 ^h

Values are means ± SD (n=3). Different superscript letters in the same column indicate significant differences ($p < 0.05$).

4. Conclusion

In summary, the bound polyphenols (EGCG and GA) could inhibit OVT nanofibrillation, and higher level of complexation of OVT with more polyphenols showed stronger fibril-inhibitory activity. Covalent bound polyphenols exerted stronger inhibitory influence on OVT nanofibrillation than corresponding non-covalent bound polyphenols. Building blocks of OVT fibrils with bound polyphenols were generally larger than those of OVT fibrils. In terms of fibril morphology, covalent bound polyphenols significantly shortened OVT nanofibrils,

while non-covalent bound polyphenols exerted little influence on morphology of OVT nanofibrils. When it came to surface characteristics, covalent bound polyphenols could lower surface hydrophobicity of OVT fibrils better than corresponding non-covalent bound polyphenols.

5. References

1. Ognjenović, J., Stojadinović, M., Milčić, M., Apostolović, D., Vesić, J., Stambolić, I., et al. (2014). Interactions of epigallo-catechin 3-gallate and ovalbumin, the major allergen of egg white. *Food Chemistry*, 164, 36–43.
2. Rawel, H. M., & Rohn, S. (2010). Nature of hydroxycinnamate-protein interactions. *Phytochemistry Reviews*, 9(1), 93–109.
3. Wei, Z., Yang, W., Fan, R., Yuan, F., & Gao, Y. (2015). Evaluation of structural and functional properties of protein–EGCG complexes and their ability of stabilizing a model β -carotene emulsion. *Food Hydrocolloids*, 45, 337–350.
4. Singh, B. N., Shankar, S., & Srivastava, R. K. (2011). Green tea catechin, epigallocatechin-3-gallate (EGCG): Mechanisms, perspectives and clinical applications. *Biochemical Pharmacology*, 82(12), 1807–1821.
5. Badhani, B., Sharma, N., & Kakkar, R. (2015). Gallic acid: a versatile antioxidant with promising therapeutic and industrial applications. *RSC Advances*, 5(35), 27540–27557.
6. Lu, Z., Nie, G., Belton, P. S., Tang, H., & Zhao, B. (2006). Structure–activity relationship analysis of antioxidant ability and neuroprotective effect of gallic acid derivatives. *Neurochemistry International*, 48(4), 263–274.
7. Winters, A. L., & Minchin, F. R. (2005). Modification of the Lowry assay to measure proteins and phenols in covalently bound complexes. *Analytical Biochemistry*, 346(1), 43–48.
8. Church, F. C., Swaisgood, H. E., Porter, D. H., & Catignani, G. L. (1983). Spectrophotometric Assay Using o-Phthaldialdehyde for Determination of Proteolysis in Milk and Isolated Milk Proteins. *Journal of Dairy Science*, 66(6), 1219–1227.
9. Beveridge, T., Toma, S. J., & Nakai, S. (1974). Determination of SH- and SS-groups in some food proteins using Ellman's reagent. *Journal of Food Science*, 39(1), 49–51.
10. Singleton, V. L., Orthofer, R., & Lamuela-Raventós, R. M. (1999). Analysis of

total phenols and other oxidation substrates and antioxidants by means of folin-ciocalteu reagent. *Methods in Enzymology*, 299, 152–178.

11. Wei, Z., & Huang, Q. (2019). Assembly of iron-bound ovotransferrin amyloid fibrils. *Food Hydrocolloids*, 89, 579–589.

12. Kroll, J., Rawel, H. M., & Rohn, S. (2003). Reactions of plant phenolics with food proteins and enzymes under special consideration of covalent bonds. *Food Science and Technology Research*, 9(3), 205–218.

13. Ozdal, T., Capanoglu, E., & Altay, F. (2013). A review on protein–phenolic interactions and associated changes. *Food Research International*, 51(2), 954–970.

14. Cejas, M. A., Kinney, W. A., Chen, C., Vinter, J. G., Almond, H. R., Balss, K. M., et al. (2008). Thrombogenic collagen-mimetic peptides: Self-assembly of triple helix-based fibrils driven by hydrophobic interactions. *Proceedings of the National Academy of Sciences*, 105(25), 8513–8518.

15. Nilsson, M. R. (2004). Techniques to study amyloid fibril formation in vitro. *Methods*, 34(1), 151–160.

16. Porat, Y., Abramowitz, A., & Gazit, E. (2006). Inhibition of amyloid fibril formation by polyphenols: structural similarity and aromatic interactions as a common inhibition mechanism. *Chemical Biology & Drug Design*, 67(1), 27–37.

17. Chen, R., Wang, J. B., Zhang, X. Q., Ren, J., & Zeng, C. M. (2011). Green tea polyphenol epigallocatechin-3-gallate (EGCG) induced intermolecular cross-linking of membrane proteins. *Archives of Biochemistry and Biophysics*, 507(2), 343–349.

18. Raman, B., Chatani, E., Kihara, M., Ban, T., Sakai, M., Hasegawa, K., et al. (2005). Critical Balance of Electrostatic and Hydrophobic Interactions Is Required for β 2-Microglobulin Amyloid Fibril Growth and Stability. *Biochemistry*, 44(4), 1288–1299.

CHAPTER VII. FOOD-GRADE PICKERING EMULSIONS STABILIZED BY OVOTRANSFERRIN FIBRILS

The work in this chapter has been published in Food Hydrocolloids.

1. Introduction

Pickering emulsions refer to emulsions stabilized by solid colloidal particles instead of conventional emulsifiers (low-molecular-weight surfactants or amphiphilic macromolecules), and Pickering emulsions recently attract increasing attention due to their outstanding stability against coalescence and irreversible interface adsorption (1, 2). To date understanding towards Pickering emulsions has been mostly based on Pickering emulsions stabilized by inorganic and synthetic particles, and the biocompatibility and biodegradability concerns seriously limit application of these Pickering emulsions (2, 3). The developing trend is to utilize biopolymer-based particles as Pickering emulsifiers in place of inorganic and synthetic particles (1, 4, 5). Polymer assembly using food-grade ingredients may be a bottom-up tool to fabricate food-grade biopolymer particles. To meet basic prerequisites for Pickering stabilizers, the food-grade colloidal particles with proper wettability and particle size should remain intact and insoluble in both dispersed and continuous phases over a long period of time (2). Successful fabrication of more food-grade Pickering emulsifiers may expand application of Pickering emulsions in fields of foods and pharmaceuticals.

Peptides and proteins may self-assemble into protein fibrils with ordered

supramolecular structures (6–8). Protein fibrils are linear aggregates with a few nanometers in diameter, and the major driving force of fibrillation and stabilization mechanism of fibrils is generally believed to be hydrophobic interactions (9–11). The major building blocks of many protein fibrils are released peptides during hydrolysis (12, 13). Protein fibrils are intriguing biomaterials with peculiar mechanical properties due to high aspect ratio (fibril length versus thickness), but comparatively little is known about application of protein fibrils in food systems (6). Previous studies point out that amyloid-like food protein fibrils have no direct toxicity to *in vitro* human cells, suggesting that food protein fibrils can be exploited as edible biomaterials without safety concerns (8, 14).

During the past few years, formation and rearrangement of protein fibrils at interfaces have attracted a lot of scholarly attention (15, 16), and protein fibrils have been utilized as layers of many food polymeric structures (17). Since protein fibrils are intrinsically insoluble particles with intermediate wettability, protein fibrils may potentially be applied in food-grade Pickering emulsions.

The available literature about application of fibrils derived from food proteins focus on β -lactoglobulin fibrils (18). However, application of β -lactoglobulin fibrils in food systems is faced with several problems. First, β -lactoglobulin fibrils are relatively long and stiff, and the length of β -lactoglobulin fibrils can exceed 10 μm (6). It is hard to construct small-sized food delivery systems with β -lactoglobulin fibrils. Second, a previous study reveals that ferric ions can inhibit formation of β -lactoglobulin fibrils (19). Therefore, it is difficult to fortify ferric ion in food

products which contain β -lactoglobulin fibrils, and the infeasibility of fortifying iron in food products may lead to iron deficiency (20). Since morphology and functional properties of fibrils are closely related to molecular structure of peptides or proteins (21), fibrils derived from different proteins may possess distinct morphology and functional properties. Thus, it is essential to explore food application of fibrils from other food proteins.

Ovotransferrin (OVT) is an iron-binding glycoprotein associated with numerous bioactivities such as antifungal, antiviral and antibacterial activity (22). Meanwhile, since OVT accounts for 12% of egg white proteins and high-purity OVT can be separated from egg white, OVT is deemed to be a renewable biomaterial with sufficient supply (23–25). Our previous study demonstrates that OVT fibrils possess no *in vitro* cytotoxicity (8), implying great application potential in food industry. When it comes to food application of OVT fibrils, OVT fibrils have several advantages. First, OVT fibrils are relatively short and flexible (8), which is beneficial to construction of various food delivery systems. Second, OVT fibrils are iron-bound fibrils (8), and application of OVT fibrils in food products is a natural iron supplementation strategy.

It is meaningful to explore application of OVT fibrils such as feasibility of OVT fibrils as Pickering emulsifiers. Because electrostatic interactions contributed relatively little in stabilizing fibrils, fibrils may possibly be stable and intact at different ionic strengths over a wide range of pH. OVT fibrils may stabilize Pickering emulsions better at high ionic strengths and diverse pHs in comparison with some

food-grade colloidal particles such as protein–polysaccharide electrostatic complexes. In addition, Pickering emulsions with desirable thermal stability have promising use for high-temperature applications, and it is intriguing to understand thermal stability of OVT fibril-stabilized Pickering emulsions. A systematic research to explore feasibility of fabricating Pickering emulsions with OVT fibrils may help to open up new possibilities for stable food-grade Pickering emulsions with a long shelf life.

Therefore, the main objectives of this chapter were to prepare and verify OVT fibrils as effective Pickering stabilizers, to characterize the morphology of Pickering emulsions stabilized by OVT fibrils, and to investigate the impact of pH as well as ionic strength on structure and rheological properties of OVT fibril-stabilized Pickering emulsions. Finally, thermal stability of OVT fibril-stabilized Pickering emulsions was studied. This study may provide a new strategy to fabricate food-grade Pickering emulsions with excellent stability.

2. Materials and Methods

2.1. Materials

Ovotransferrin (OVT) with a purity greater than 88% was purchased from Neova Technologies Inc (Abbotsford, Canada). Pre-stained protein marker and methanol were purchased from Thermo Fisher Scientific, Inc. (Waltham, USA). Sodium chloride was purchased from Sigma-Aldrich (St. Louis, USA). Medium chain triacylglycerol oil (MCT, Neobee 1053) was kindly provided by Stepan Company (Northfield, USA). Milli-Q water (Millipore Corporation, Burlington, USA) was used to prepare solutions.

2.2. Preparation and characterization of OVT fibrils

2.2.1. Preparation of OVT fibrils

The optimal fibrillation condition was obtained in preliminary experiments. OVT was dispersed in pH-preset Milli-Q water (pH 2, 100 mM NaCl) at a protein concentration of 50 mg/mL, followed by stirring to ensure dissolution. After filtration with 0.45 μm pore-sized syringe filters, OVT solution was placed into screw-capped vials. OVT solution was heated at 90 $^{\circ}\text{C}$ and a stirring speed of 350 rpm in the sealed vials. After heating for 26 h, OVT fibril dispersions were obtained. The acquired OVT fibrils were dialyzed (molecular weight cutoff 1000 Da) against several changes of pH-preset Milli-Q water (pH 2) at 4 $^{\circ}\text{C}$ for 18 h to remove NaCl in fibril dispersions. The concentration of OVT fibril dispersion decreased due to increasing volume of sample during dialysis, and final concentration of OVT fibril dispersion was carefully adjusted to 35 mg/mL with addition of pH-preset Milli-Q water (pH 2). OVT fibril dispersions were stored at 4 $^{\circ}\text{C}$ and used within 12 h.

2.2.2. Atomic force microscopy (AFM)

Morphology of OVT fibrils was investigated at 20 $^{\circ}\text{C}$ using NanoScope IIIA Multimode AFM (Veeco Instruments Inc., Santa Barbara, USA), and tapping mode AFM images were collected. In order to facilitate imaging of single fibrils, fibril dispersions were diluted prior to imaging and the dilution did not affect fibril appearance (26). Diluted fibril dispersions were spread onto surface of freshly cleaved mica and dried using nitrogen stream. The AFM data were analyzed employing NanoScope Analysis Software and FiberApp (27), and contour length distribution of

fibrils was obtained after analysis of at least seven AFM images.

2.3. Preparation of Pickering emulsions stabilized by OVT fibrils

OVT fibril dispersions with lower fibril concentration (0.5–2.5 wt%) were obtained by diluting fibril dispersions (3.5 wt%) with pH-preset Milli-Q water (pH 2). Sodium azide (0.02%, w/v) was added to suppress microbial growth. OVT fibril dispersions (0.5–3.5 wt%) were mixed with MCT to obtain mixtures (total volume = 8 mL) with different oil fractions φ (0.5–0.7). An Ultra-Turrax (IKA-Werke GMBH & CO., Germany) was utilized to homogenize the mixtures at 9000 rpm for 2 min. The Pickering emulsions were named as A–B (A: fibril concentration c ; B: oil fraction φ) and stored at 20 °C. The type of Pickering emulsion was determined by examining the dispersibility of Pickering emulsions in water or MCT. Oil-in-water (water-in-oil) emulsions dispersed rapidly in water (MCT) but stayed immiscible in MCT (water) (4). OVT fibril-stabilized Pickering emulsions at different fibril concentrations and oil fractions were characterized as described in 2.5.

2.4. Confirmation of Pickering emulsion droplets stabilized by OVT fibrils

2.4.1. Raman imaging of Pickering emulsion droplets

In order to observe morphology of OVT fibrils at emulsion interfaces, Raman images of Pickering emulsion droplets were captured at 20 °C using DXRTM2xi Raman Imaging Microscope (Thermo Scientific, Waltham, USA). Pickering emulsions stabilized by OVT fibrils ($c = 3.5$ wt%, $\varphi = 0.6$) were diluted to facilitate picture imaging.

2.4.2. Confocal laser scanning microscopy

Confocal laser scanning microscopy (CLSM) (LSM 800, Zeiss, Oberkochen, Germany) was further employed to confirm adsorption of OVT fibrils at emulsion interfaces. OVT fibrils and oil in OVT fibril-stabilized Pickering emulsion ($c = 3.5$ wt%, $\phi = 0.7$) were stained with thioflavin T (ThT, excitation at 355 nm) and Nile red (excitation at 488 nm), respectively. CLSM was performed at 20 °C after preparing Pickering emulsion droplets.

2.4.3. Fluorescence microscopy images of Pickering emulsion droplets

To further confirm adsorption of OVT fibrils onto oil–water interfaces, fluorescence microscopy of OVT fibril-stabilized Pickering emulsion ($c = 3.5$ wt%, $\phi = 0.6$) was conducted using a Nikon Eclipse TE2000-U polarized microscope (Nikon Corporation, Tokyo, Japan). OVT fibrils were stained with rhodamine B (0.02 wt%) before Pickering emulsification, and excess rhodamine B was removed via dialysis (molecular weight cutoff 3500 Da) against pH-preset Milli-Q water (pH 2). The microstructures under fluorescence field were captured at 20 °C after Pickering emulsification.

2.5. Characterization of OVT fibril-stabilized Pickering emulsions

2.5.1. Measurement of emulsified phase volume fraction and stability index

The prepared Pickering emulsions might consist of cream phase (emulsified phase) and aqueous serum phase (29). The height of cream phase (H_c) and total emulsion height (H_t) after specific storage (3 h and 20 days) at 20 °C were recorded. The emulsified phase volume fraction (EPVF) was calculated as previously described (5, 30):

$$EPVF = (H_c/H_t) \times 100 \quad (1)$$

The stability index was calculated as previously described (5, 30, 31):

$$\text{stability index} = \frac{\text{EPVF after 20 - day storage}}{\text{EPVF after 3 - h storage}} \times 100 \quad (2)$$

2.5.2. Microstructure observation

Microstructures of Pickering emulsions stabilized by OVT fibrils were visualized at 20 °C using a Nikon Eclipse TE2000-U polarized microscope (Nikon Corporation, Tokyo, Japan). To facilitate microstructure observation, OVT fibril-stabilized Pickering emulsion samples were diluted 100 times with Milli-Q water at corresponding pHs and ionic strengths. The average diameter of Pickering emulsion was estimated using Image J software, and 400 emulsion droplets chosen randomly in different captured images were measured to estimate emulsion droplet size (5, 32).

2.5.3. Rheological measurements

A Discovery HR-2 rheometer (TA Instruments, New Castle, USA) with a parallel plate geometry (diameter 25 mm, gap 1 mm) was employed to characterize rheological behavior of Pickering emulsions stabilized by OVT fibrils. Rheology data were collected at 20 °C after Pickering emulsions were deposited on the rheometer plate for a 5-min thermal equilibrium (5). Steady-state flow measurements were performed to obtain apparent viscosity of Pickering emulsions as function of shear rate (0.1–50 s⁻¹). Dynamic frequency sweep test was conducted at a fixed strain amplitude of 1% (within the linear viscoelastic region), and frequency-dependent curves (within frequency range of 0.1–10 rad/s) of storage modulus (G') and loss modulus (G'') of emulsions were measured.

2.6. Pickering emulsions stabilized by OVT fibrils at different ionic strengths and pHs

2.6.1. Preparation of Pickering emulsions at different ionic strengths and pHs

Pickering emulsification capabilities of OVT fibrils at different ionic strengths and pHs were investigated. For this purpose, sodium chloride was added to OVT fibril dispersions (3.5 wt%, pH 2) to an ionic strength of 100 mM, 300 mM, 500 mM or 1000 mM. In terms of pH effects, OVT fibril dispersions (3.5 wt%, 0 mM ionic strength) were adjusted to pH values of 3, 4, 5, 6 or 7 by adding NaOH solutions with concentration gradients (0.05, 0.1, 0.25, 0.5 and 1 M) carefully to minimize the effect of dilution. The OVT fibril dispersions (3.5 wt%) at different ionic strengths or pHs were mixed with MCT to obtain mixtures at oil fraction of 0.7, followed by homogenization procedures as described above. Afterwards, OVT fibril-stabilized Pickering emulsions at different ionic strengths and pHs were stored at 20 °C. OVT fibril-stabilized Pickering emulsions at different ionic strengths and pHs were characterized as described in 2.5.

2.6.2. Zeta potential measurements

OVT fibril dispersion was first diluted to a concentration of 2 mg/mL, and zeta potential of OVT fibril dispersion over the pH range of 2 to 7 was determined at 20 °C using Zetasizer Nano-ZS90 instrument (Malvern Instruments, Worcestershire, UK). Influence of ionic strength on zeta potential was also studied. Sodium chloride was added into OVT fibril dispersions at pH 2 to reach an ionic strength of 100 mM, 300 mM, 500 mM or 1000 mM, followed by electrophoretic mobility measurements in fibril dispersions. Smoluchowski model was employed for zeta potential analysis.

2.7. Thermal stability of Pickering emulsions

Pickering emulsion stabilized by OVT fibrils ($c = 3.5$ wt%, $\varphi = 0.7$) at pH 2 and 0 mM ionic strength was stored at 50 °C in darkness for 10 days. Visual observation and optical microscopy were utilized to evaluate influence of thermal treatment on emulsion stability.

2.8. Statistical analysis

Each experiment was carried out in triplicate. All statistical analysis was performed employing OriginPro 2018.

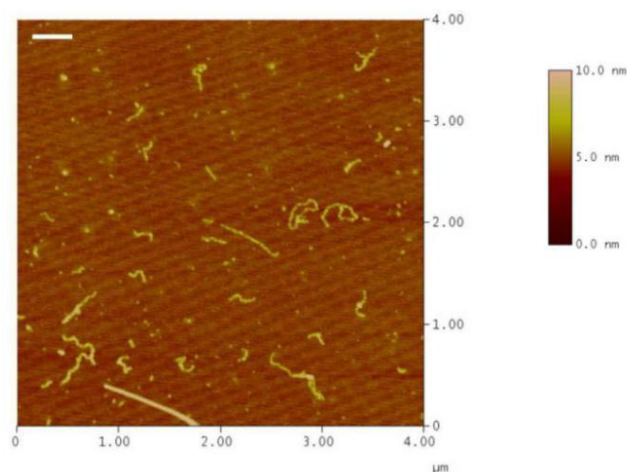
3. Results and Discussion

3.1. Preparation of OVT fibrils as Pickering emulsifiers

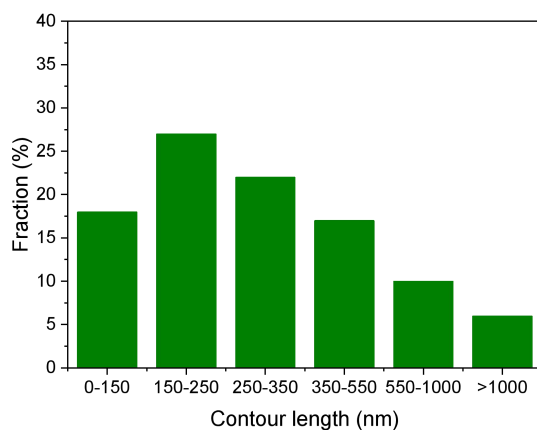
Taking into account that critical aggregation concentration of proteins during fibrillation decreased significantly with increasing ionic strength and moderate ionic strength facilitated fibril formation during the growth phase of fibrillation (33, 34), OVT fibrils were prepared at moderate ionic strength (100 mM) in this research. Afterwards, NaCl in OVT fibril dispersions was ultimately eliminated via dialysis. The amount of OVT fibrils did not decrease after dialysis, as evidenced by thioflavin T spectroscopic assay (data not shown) (35).

The morphology of OVT fibrils was investigated using AFM. As shown in Figure VII-1a, both straight and worm-like fibrils were observed. Figure VII-1b showed contour length distribution of OVT fibrils, and OVT fibrils with a contour length range of 150–550 nm occupied 66 percent of total fibrils. Statistical analysis revealed that the average contour length of OVT fibrils was 337 nm. Since qualified

emulsifiers should have substantially smaller particle size than targeted emulsion droplet size and targeted emulsion droplet size in this research was above $15\ \mu\text{m}$ (2), OVT fibrils with an average size of 337 nm met the requirement of eligible Pickering emulsifiers.



(a)



(b)

Figure VII-1. (a) AFM image of OVT nanofibrils. The scan size is $4\ \mu\text{m} \times 4\ \mu\text{m}$, and the z scale is 10 nm. The scale bar in the upper left corner represents 400 nm. (b) Contour length distribution of OVT fibrils analyzed from AFM images.

3.2. Confirmation of OVT fibril-stabilized Pickering emulsion droplets

Since Raman imaging microscopy could help to view fibrils adsorbed at emulsion interfaces, Pickering stabilization mechanism of OVT fibrils was confirmed with the aid of Raman imaging microscopy. OVT fibril-stabilized emulsion ($c = 3.5$ wt%, $\varphi = 0.6$) was chosen to confirm the adsorption of OVT fibrils at emulsion interfaces. Figure VII-2 showed Raman microscopy image of Pickering emulsion droplet stabilized by OVT fibrils. It was observed that a significant amount of OVT fibrils were found to surround the interface of emulsion droplets, indicating that the emulsion droplets were indeed stabilized by OVT fibrils and followed Pickering stabilization mechanism. It was noteworthy that OVT fibrillar structures at the emulsion droplet interface were thicker and longer than those shown in Figure VII-1. Since previous study showed that protein fibrils at interfaces could rearrange after adsorption onto interfaces (15), thicker and longer OVT fibrillar structures were possibly due to rearrangement of OVT fibrils into fibril bundles.

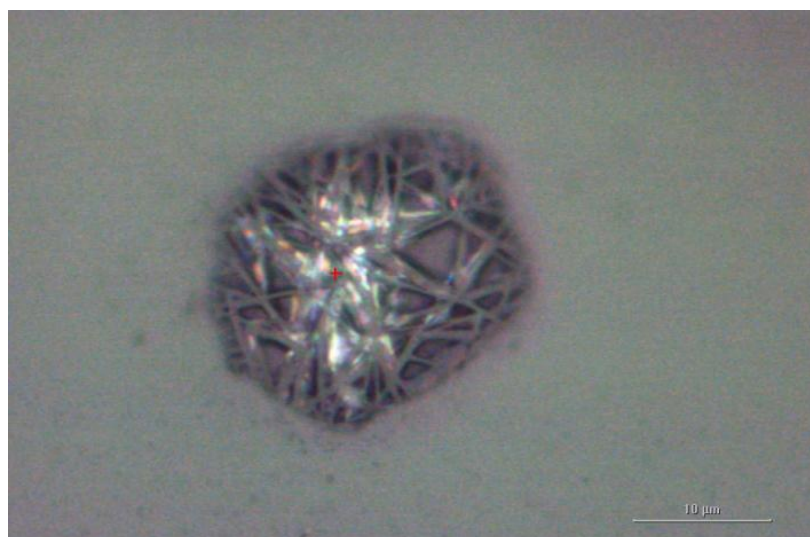
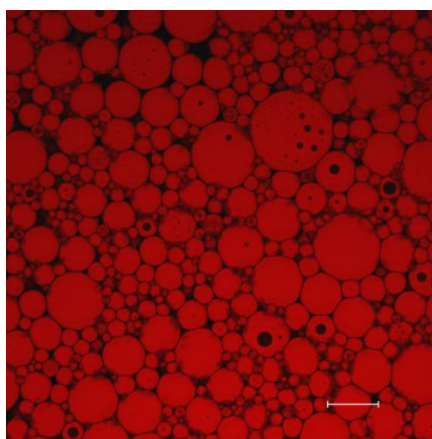
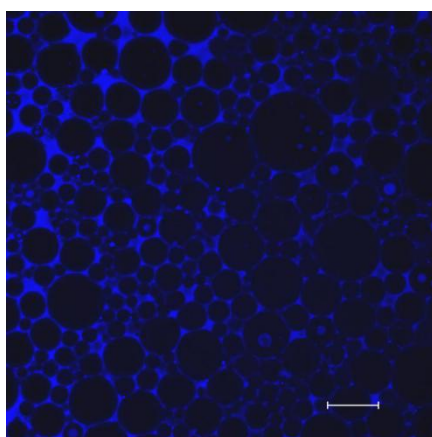


Figure VII-2. Raman microscopy image of Pickering emulsion droplet stabilized by OVT fibrils ($c = 3.5$ wt%, $\varphi = 0.6$). The scale bar in the lower right corresponds to 10 μm .

CLSM was also utilized to confirm the adsorption of OVT fibrils at oil–water interfaces, and Figure VII-3 showed that CLSM image of OVT fibril-stabilized Pickering emulsion droplets. Since thioflavin T (ThT) was a dye that could bind to protein fibrils specifically but not to native proteins or peptides (35), ThT was utilized to stain OVT fibrils during CLSM measurement. As depicted in Figure VII-3, ThT-labeled glowing layers, which corresponded to OVT fibrils only, were located at oil-water interfaces. This phenomenon clearly indicated that these emulsion droplets were indeed stabilized by OVT fibrils via Pickering stabilization mechanism.



(a)



(b)

Figure VII-3. CLSM image of Pickering emulsion ($\phi=0.7$) stabilized by OVT fibrils ($c = 3.5$ wt%): (a) excitation at 488 nm, (b) excitation at 355 nm. Oil dyed with Nile

red was shown in red, and OVT fibrils stained with thioflavin T (ThT) were shown in blue. The scale bar within the figure is 50 μm in length.

Besides, fluorescence microscopy was conducted to confirm formation of OVT fibril-stabilized Pickering emulsion droplets. As presented in Figure VII-4, the green fluorescence glowing layer around emulsion droplets corresponded to OVT fibrils on the interface, suggesting that OVT fibrils were adsorbed at the emulsion interfaces. The result was in consistence with fluorescence microscopy result of a previous study, which showed that β -lactoglobulin fibrils could effectively adsorb at Pickering emulsion droplets (36). Based on result of high-resolution optical microscopy, CLSM and fluorescence microscopy, it could be concluded that OVT fibril-stabilized emulsions were indeed Pickering emulsions.

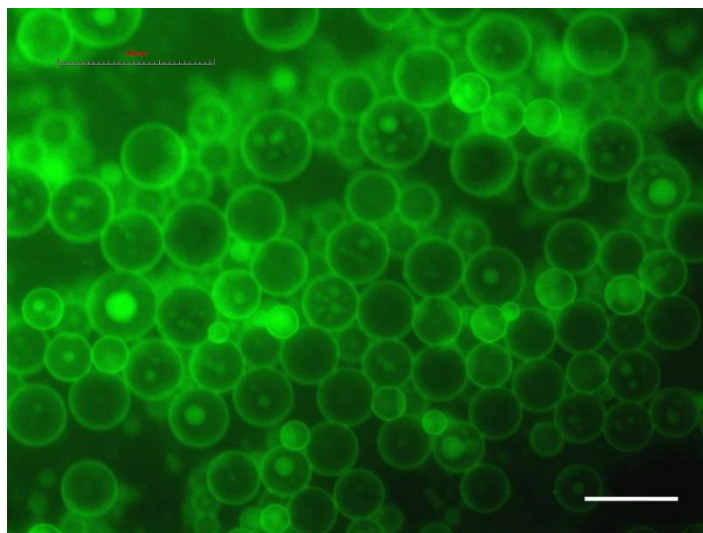


Figure VII-4. Fluorescence microscopy images of Pickering emulsions stabilized by OVT fibrils at the fixed concentration of 3.5 wt% and oil fraction of 0.6. The white scale bar in the lower right is 60 μm in length.

3.3. Characterization of OVT fibril-stabilized Pickering emulsions at different fibril concentrations and oil fractions

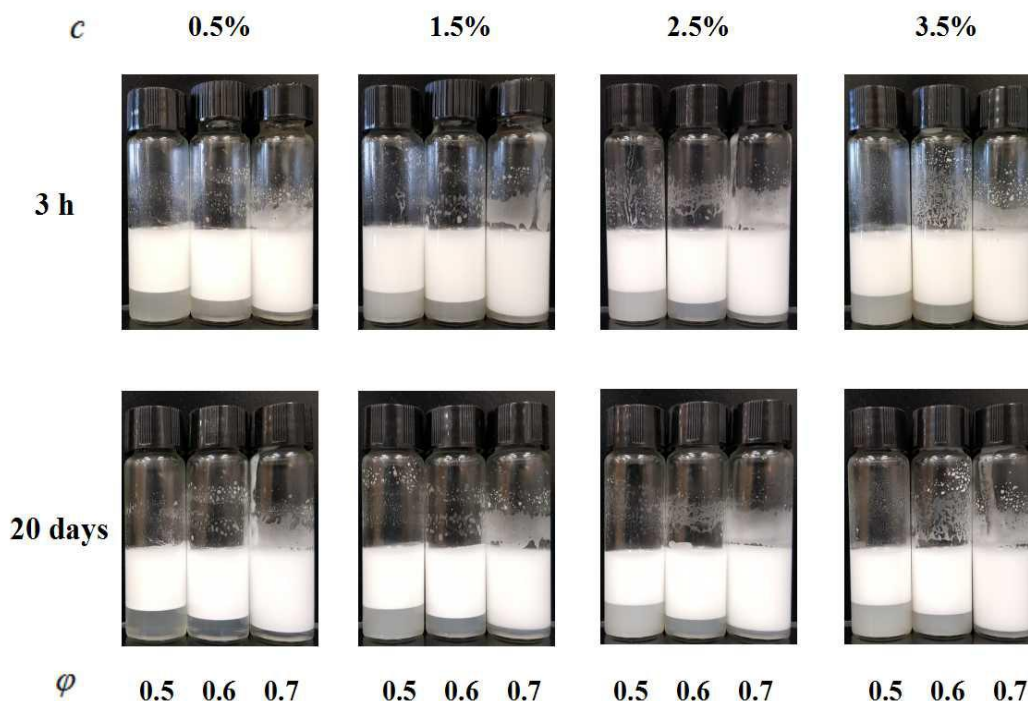


Figure VII-5. Visual observation of Pickering emulsions stabilized by OVT fibrils with different c (0.5–3.5 wt%) at various φ (0.5–0.7). The photographs were taken at 3 h and 20 days after preparation of fresh emulsions, and the storage was carried out at 20 °C.

As shown in Figure VII-5, a series of Pickering emulsions with various OVT fibril concentrations and oil phase fractions were prepared. Since these Pickering emulsions dispersed readily in water but not in MCT, OVT fibril-stabilized Pickering emulsions could be identified as oil-in-water emulsions, which verified speculation that OVT fibrils were preferentially wetted by water over oil. Given that freshly prepared Pickering emulsions could undergo a fast creaming process within first 2 h and collecting stable data was difficult (5, 32), visual appearance of Pickering emulsions was evaluated after 3-h storage. Figure VII-5 demonstrates that the

minimum concentration of OVT fibrils required to make long-term stable emulsions was 0.5 wt %, and fresh OVT fibril-stabilized Pickering emulsion ($c = 3.5$ wt%, $\varphi = 0.7$) consisted of predominant cream phase and negligible serum phase.

Table VII-1 summarizes emulsified phase volume and stability index of these emulsions after storage of 3 h and 20 days. It was reasonable to conclude that increasing fibril concentration from 0.5 wt% to 3.5 wt% could lead to a progressive increase in emulsified phase volume of Pickering emulsions at identical oil fractions, and higher oil fraction resulted in gradually higher emulsified phase volume when OVT fibril concentration was fixed. It was noteworthy that stability index of Pickering emulsions was above 96.8% in all cases, suggesting that OVT fibril-stabilized Pickering emulsions remained stable after 20-day storage. The outstanding physical stability of OVT fibril-stabilized Pickering emulsions should be mainly due to Pickering stabilization mechanism. Since energy required for detachment of particles (Pickering emulsifiers) from interfaces is generally large (2), particle adsorption at interfaces may be regarded as irreversible. The strong interfacial adsorption of OVT fibrils contributes to superior physical stability of OVT fibril-stabilized Pickering emulsions. Another explanation for excellent stability of OVT fibril-stabilized Pickering emulsions is high viscosity and gel-like behavior. Generally speaking, higher viscosity may result in better physical stability of emulsions, and gel-like structures of emulsions may trap continuous phase between the droplets in the network, which leads to limited phase separation (37).

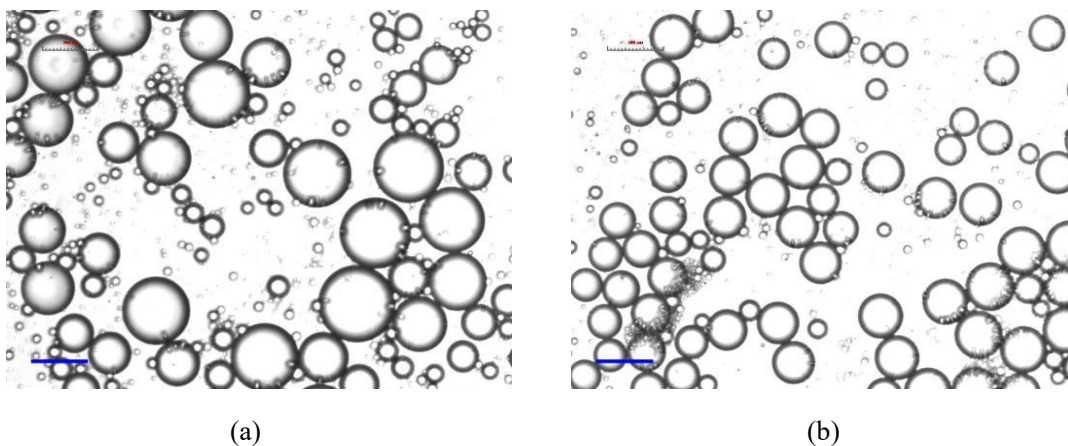
Table VII-1. Emulsified phase volume fraction and stability index of Pickering emulsions stabilized by OVT fibrils at different fibril concentrations and oil fractions

Samples	Emulsified phase volume (%)		Stability index
	3 h	20 days	
0.5–0.5	66.6±0.2 ^a	66.6±0.2 ^a	100.0±0.2 ^d
0.5–0.6	77.7±0.1 ^d	77.7±0.1 ^d	100.0±0.2 ^d
0.5–0.7	88.5±0.2 ^g	88.5±0.2 ^f	100.0±0.1 ^d
1.5–0.5	68.5±0.1 ^b	67.8±0.1 ^b	99.0±0.2 ^c
1.5–0.6	78.9±0.1 ^e	78.9±0.1 ^e	100.0±0.2 ^d
1.5–0.7	88.9±0.1 ^h	88.9±0.1 ^g	100.0±0.2 ^d
2.5–0.5	68.5±0.1 ^b	67.9±0.1 ^{bc}	99.1±0.3 ^c
2.5–0.6	79.0±0.1 ^e	78.9±0.1 ^e	100.0±0.2 ^d
2.5–0.7	91.1±0.1 ⁱ	91.1±0.1 ^h	100.0±0.2 ^d
3.5–0.5	70.4±0.1 ^c	68.2±0.2 ^c	96.9±0.4 ^a
3.5–0.6	79.6±0.1 ^f	78.9±0.2 ^e	99.1±0.3 ^c
3.5–0.7	95.2±0.1 ^j	93.7±0.1 ⁱ	98.4±0.2 ^b

Values are means±SD (n=3). Different superscript letters for the same column indicate significant differences ($p < 0.05$).

Figure VII-6 and Figure VII-7 show microstructures of fresh OVT fibril-stabilized emulsions at various fibril concentrations and oil fractions, and Figure VII-8 summarizes their average droplet sizes. No droplet coalescence was detected in all cases, indicating that steric barriers provided by OVT fibril networks could restrain instability mechanisms of emulsions. As depicted in Figure VII-8a, when oil fraction was fixed, the average emulsion droplet size decreased from 87.3 μm to 20.1 μm as OVT fibril concentration was increased from 0.5 wt% to 3.5 wt%. As oil fraction is fixed, it is easy to deduce that total interfacial area of emulsion droplets may be smaller when average emulsion droplet size is larger. We should also be aware that droplet coalescence and emulsion destabilization may occur when insufficient

particles cover emulsion interfaces (38), and emulsion droplets with smaller interfacial area may facilitate enough surface coverage of Pickering emulsifiers. Based on these understandings, it is supposed that at lower OVT fibril concentrations OVT fibril-stabilized emulsions tend to have larger emulsion droplets. Figure VII-8b showed that average droplet size of emulsions increased from 20.1 μm to 39.5 μm when oil fraction increased from 0.5 to 0.7, which could be explained as follows. As oil fraction is elevated, total interfacial area of emulsion droplets increases, and OVT fibrils are not ample to fully stabilize extra oil droplets, which results in loss of original equilibrium. To achieve new equilibrium with ample interfacial coverage of OVT fibrils, larger emulsion droplets with smaller interfacial area are fabricated at higher oil fraction. Figure VII-8c and Figure VII-8d show average droplet size of OVT-fibril stabilized Pickering emulsions at different fibril concentrations and oil fractions after 20-day storage at 20 °C. It was found that average droplet size of these Pickering emulsions remained almost the same after 20-day storage, indicating that OVT-fibril stabilized Pickering emulsion droplets were stable.



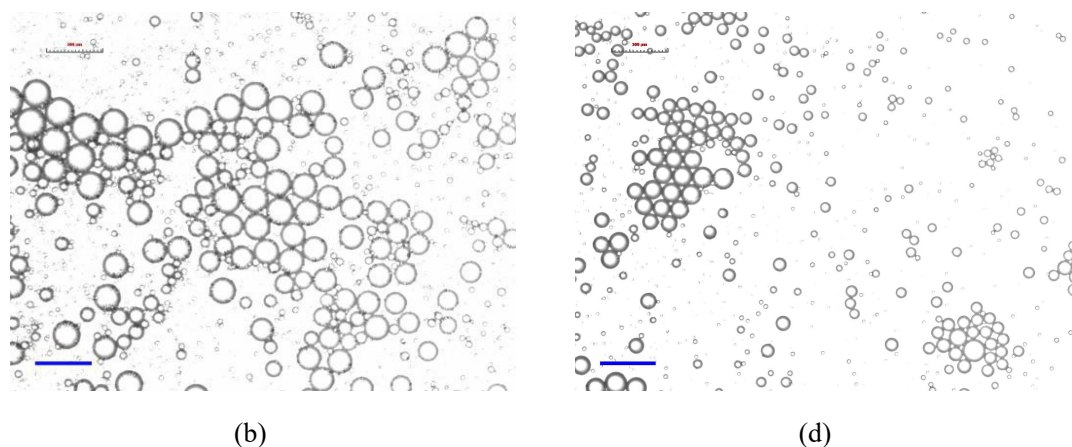


Figure VII-6. Optical microscopic images of emulsions stabilized by OVT fibrils with different c (0.5–3.5 wt%) at the fixed oil fraction of 0.5: (a) $c = 0.5$ wt%, (b) $c = 1.5$ wt%, (c) $c = 2.5$ wt%, (d) $c = 3.5$ wt%. The scale bars within the figures are 100 μm in length.

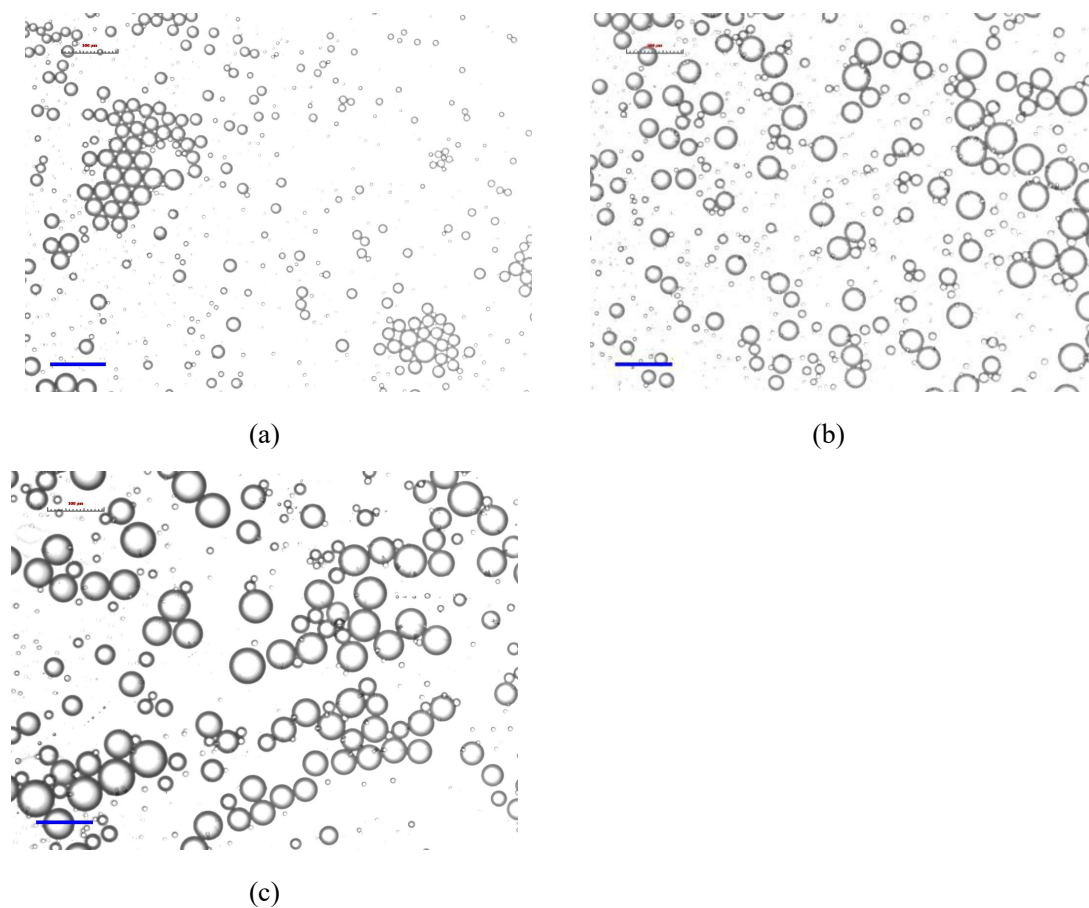


Figure VII-7. Optical microscopic images of emulsions stabilized by OVT fibrils ($c = 3.5$ wt%) at different oil fractions (ϕ): (a) $\phi = 0.5$, (b) $\phi = 0.6$, (c) $\phi = 0.7$. The scale bars within the figures are 100 μm in length.

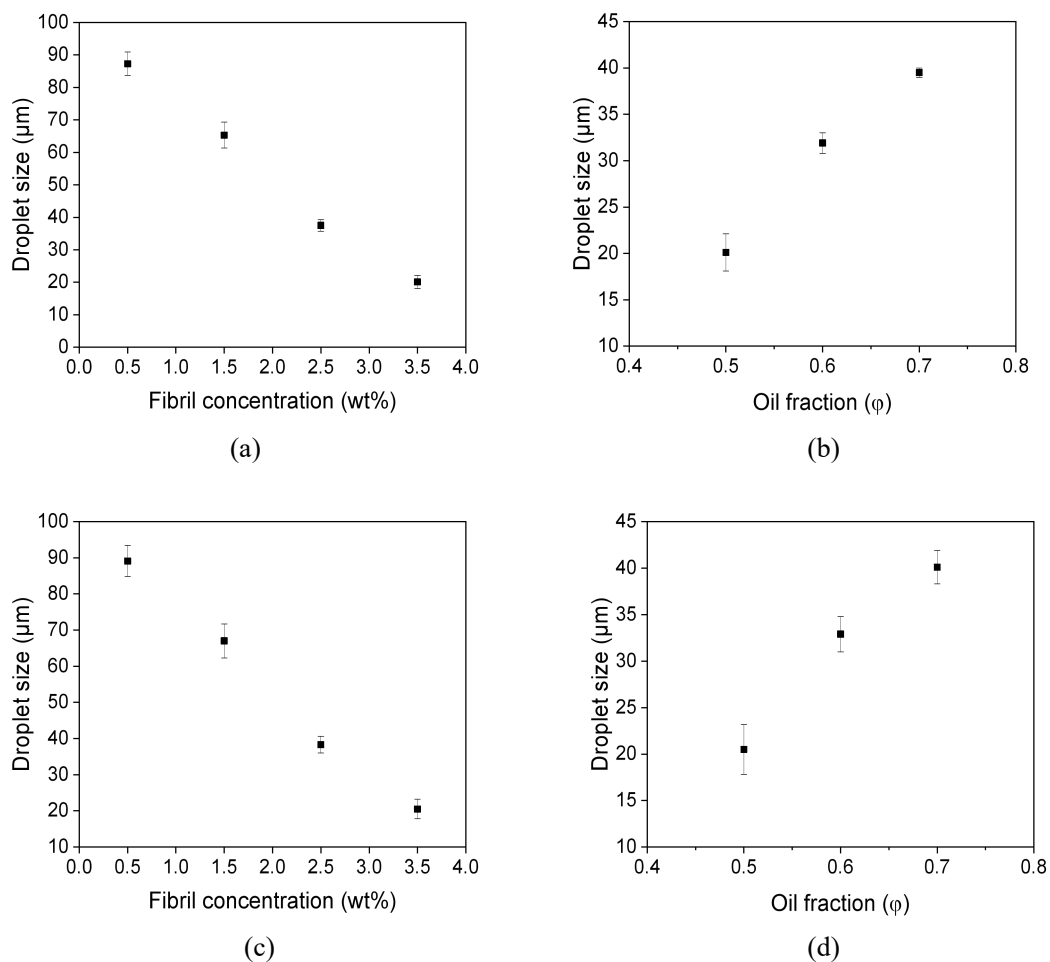
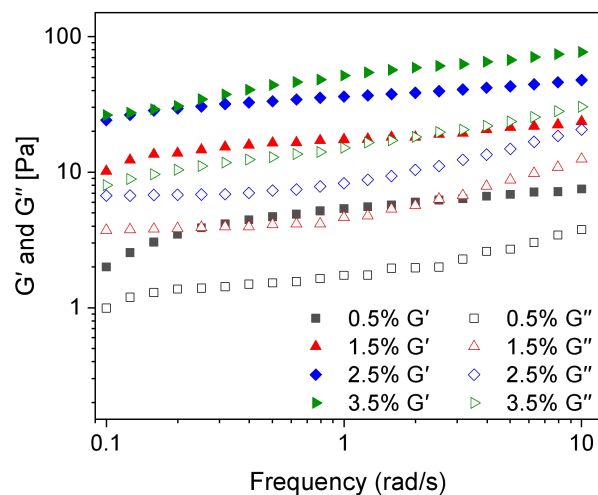


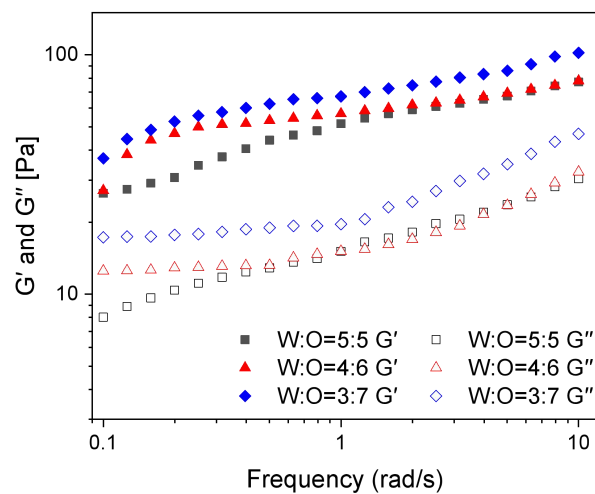
Figure VII-8. (a) Average droplet size of freshly prepared Pickering emulsions stabilized by OVT fibrils with different c (0.5–3.5 wt%) at the fixed oil fraction of 0.5. (b) Average droplet size of freshly prepared Pickering emulsions stabilized by OVT fibrils ($c = 3.5$ wt%) at different oil fractions. (c) Average droplet size of Pickering emulsions stabilized by OVT fibrils with different c (0.5–3.5 wt%) at the fixed oil fraction of 0.5 after 20-day storage at 20 °C. (d) Average droplet size of Pickering emulsions stabilized by OVT fibrils ($c = 3.5$ wt%) at different oil fractions after 20-day storage at 20 °C.

Rheological measurements were performed to provide a better understanding about stability and microstructure of OVT fibril-stabilized emulsions. Figure VII-9 and Figure VII-10 show storage modulus (G'), loss modulus (G'') as well as apparent viscosity of OVT fibril-stabilized emulsions at various fibril concentrations and oil fractions. G' was always larger than corresponding G'' in all cases, suggesting that

gel-like behavior dominated OVT fibril-stabilized Pickering emulsions.

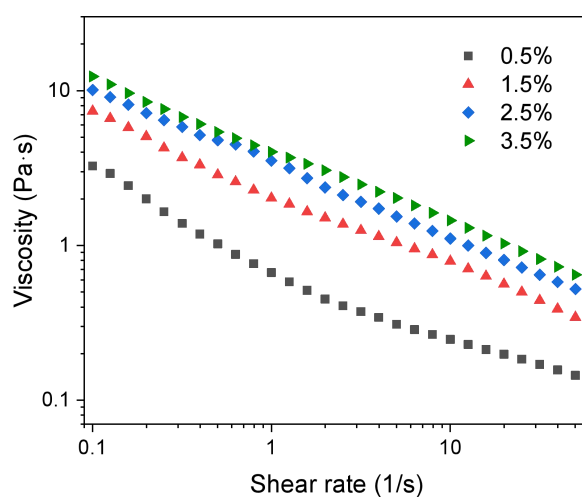


(a)

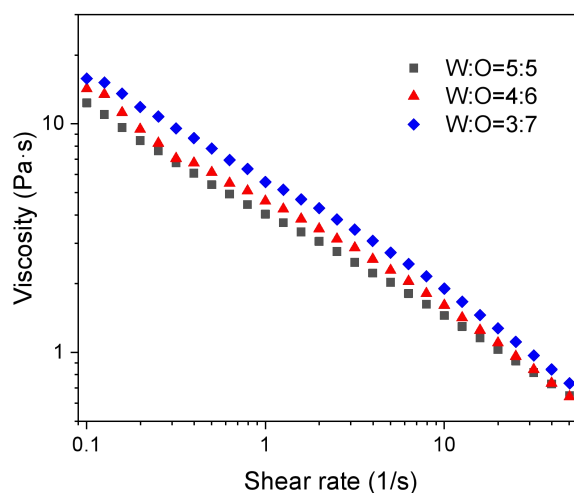


(b)

Figure VII-9. (a) Storage modulus (G') and loss modulus (G'') of Pickering emulsions stabilized by OVT fibrils with different c (0.5–3.5 wt%) at the fixed oil fraction of 0.5. (b) Storage modulus (G') and loss modulus (G'') of Pickering emulsions stabilized by OVT fibrils ($c = 3.5$ wt%) at different oil fractions.



(a)



(b)

Figure VII-10. (a) Apparent viscosity of Pickering emulsions stabilized by OVT fibrils with different c (0.5–3.5 wt%) at the fixed oil fraction of 0.5. (b) Apparent viscosity of Pickering emulsions stabilized by OVT fibrils ($c = 3.5$ wt%) at different oil fractions.

As depicted in Figure VII-9a and Figure VII-10a, G' , G'' and viscosity of the Pickering emulsions increased with rising fibril concentrations at fixed oil concentration, which could be explained by following arguments. First, multiple studies confirm that emulsion droplet size may affect bulk properties of emulsion, and

smaller emulsion droplet size may result in higher viscosity and gel strength of emulsions (39, 40). Second, the existence of more fibrils may result in more crosslinked networks in the continuous phase, which contributed to higher storage modulus and viscosity. As depicted in Figure VII-9b and Figure VII-10b, increasing oil fraction led to higher viscosity and gel strengthening at constant fibril concentration of Pickering emulsions, and the increase in viscosity and storage modulus could be ascribed to variation in packing of emulsion droplets. As shown in Figure VII-7, increasing oil fraction resulted in a denser packing of Pickering emulsion droplets. The tighter emulsion network could lead to stronger resistance against deformation and confined mobility of emulsion droplets, leading to higher viscosity and modulus.

3.4. Characterization of OVT fibril-stabilized Pickering emulsions at different ionic strengths

Although controlled destabilization of stimuli-responsive emulsions may be sometimes essential and temporary stability is acceptable when exposed to external triggers including ionic strength and pH (41), long-term emulsion stability is desirable in most application cases. The major challenge now is to fabricate long-term stable Pickering emulsions stabilized by food-grade particles in the presence of external stimuli. Accordingly, it was expected that OVT fibril-stabilized emulsions could withstand environmental ionic stress. Considering that Pickering emulsion at OVT fibril concentration of 3.5 wt% and oil fraction of 0.7 had the best emulsified volume fraction among all emulsions at various fibril concentrations and oil fractions, which

indicated great potential for food-related applications, OVT fibril-stabilized emulsions ($c = 3.5 \text{ wt\%}$, $\phi = 0.7$) were further investigated in the rest of this study. Figure VII-11 showed visual appearance of OVT fibril-stabilized emulsions prepared at different ionic strengths, and emulsion creaming was diminished with rising ionic strength. With regards to emulsions at ionic strength of 300, 500 and 1000 mM, OVT fibril-stabilized emulsions had emulsified phase alone and no serum phase.

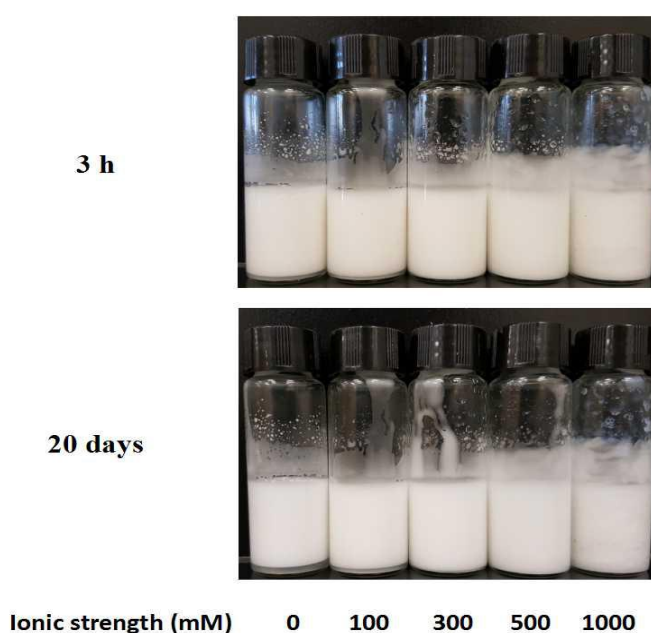


Figure VII-11. Visual observation of Pickering emulsions stabilized by OVT fibrils ($c = 3.5 \text{ wt\%}$, $\phi = 0.7$) at different ionic strengths. All photographs were taken at 3 h and 20 days after preparation of fresh emulsions, and the storage was carried out at $20 \text{ }^\circ\text{C}$.

The stability index was used to characterize emulsion stability. Table VII-2 showed that stability index of all emulsions after 20-day storage was above 98.3%, and stability index of emulsions at ionic strength above 100 mM was as high as 100%, indicating superior storage stability of OVT fibril-stabilized emulsions over a wide range of ionic strength.

Table VII-2. Emulsified phase volume fraction and stability index of Pickering emulsions stabilized by OVT fibrils at different ionic strengths

Samples	Emulsified phase volume (%)		Stability index
	3 h	20 days	
0	95.2±0.1 ^a	93.7±0.1 ^a	98.4±0.2 ^a
100 mM	97.4±0.1 ^b	97.0±0.1 ^b	99.6±0.1 ^b
300 mM	99.6±0.0 ^c	99.6±0.0 ^c	100.0±0.0 ^c
500 mM	100.0±0.0 ^d	100.0±0.0 ^d	100.0±0.0 ^c
1000 mM	100.0±0.0 ^d	100.0±0.0 ^d	100.0±0.0 ^c

Values are means±SD (n=3). Different superscript letters for the same column indicate significant differences ($p < 0.05$).

Electrophoresis mobility of OVT fibril dispersion as function of ionic strength was investigated to provide background for impact of ionic strength on OVT fibril-stabilized emulsions. As shown in Figure VII-12, electrophoresis mobility decreased significantly when ionic strength increased to 1000 mM, which was ascribed to electrostatic screening effect of salts (42). In view of the fact that increasing ionic strengths could significantly screen the charges of OVT fibrils, the creaming disappearance and outstanding stability of Pickering emulsions at high ionic strengths may be a result of following factors. First, adsorption and anchoring of OVT fibrils at emulsion interfaces should not be taken for granted, and actually various factors such as charge repulsions that dominate the particle–oil interactions may impede sufficient coverage of particles (43). Specifically speaking, when some OVT fibrils adsorb at emulsion interfaces, the oil-water interfaces turn positively charged, and electrical repulsions between unadsorbed OVT fibrils and positively charged

emulsion interfaces may prevent further fibril adsorption and Pickering emulsification (43). When enough salts exist in the system, the charge repulsion effect weakens and sufficient OVT fibrils accumulate at the interface. The enough surface coverage contributes to higher emulsified phase volume and stability index. Second, excellent stability of OVT fibril-stabilized emulsions can be reasonably expected due to structural stability and integrity of OVT fibrils at higher ionic strengths. In our preliminary experiments OVT fibrils were found to be salt-tolerant (data not shown), since OVT fibrils were mainly stabilized by hydrogen bonds instead of electrostatic interactions once formed (10, 11).

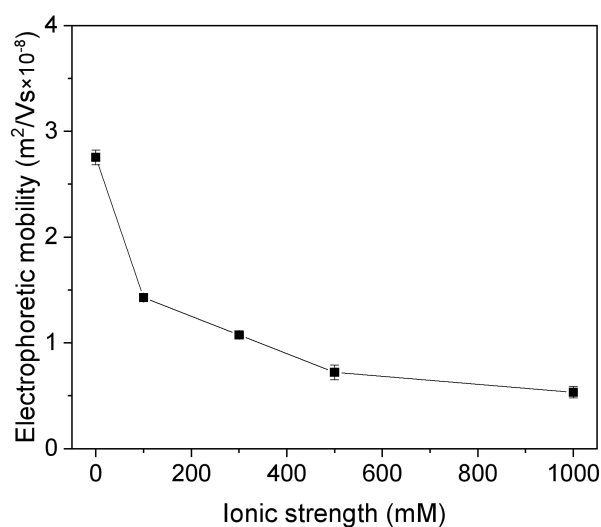
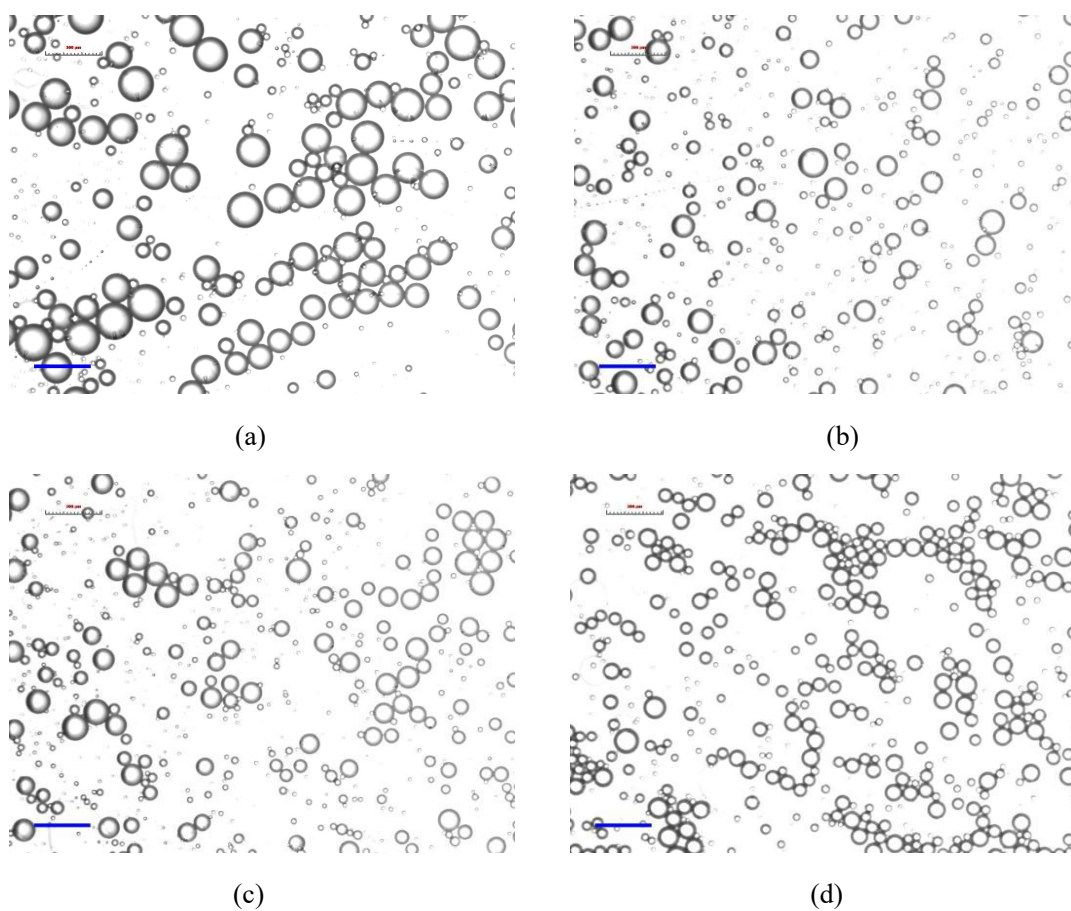
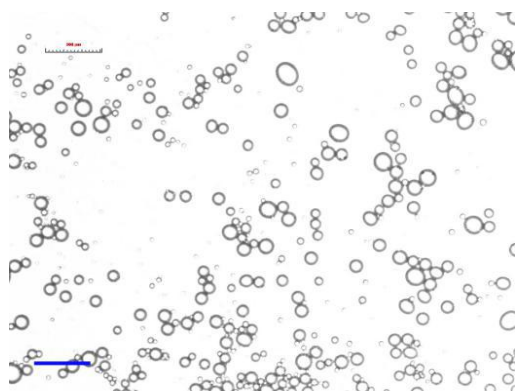


Figure VII-12. Influence of ionic strength (0–1000 mM) on electrophoresis mobility of OVT fibril dispersion at pH 2.

Although visual appearance of emulsions at various ionic strengths looked the same in Figure VII-11, Figure VII-13 presents that microstructures of these emulsions were quite different. As depicted in Figure VII-14, when ionic strength increased from

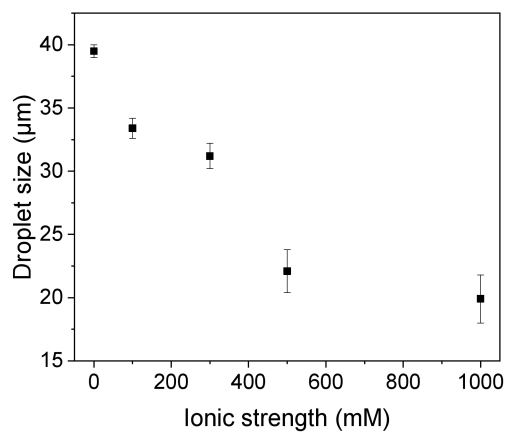
0 mM to 1000 mM, the average droplet size decreased from approximately 39.5 μm to 19.9 μm . The emulsion droplets remained stable and no fractures were observed, suggesting OVT fibril barriers at emulsion interfaces could resist the osmotic pressure gradients. As depicted in Figure VII-14, average droplet size of Pickering emulsions at various ionic strengths remained almost the same after 20-day storage at 20 $^{\circ}\text{C}$, which confirmed that OVT fibril-stabilized emulsion droplets were stable against high ionic strengths.



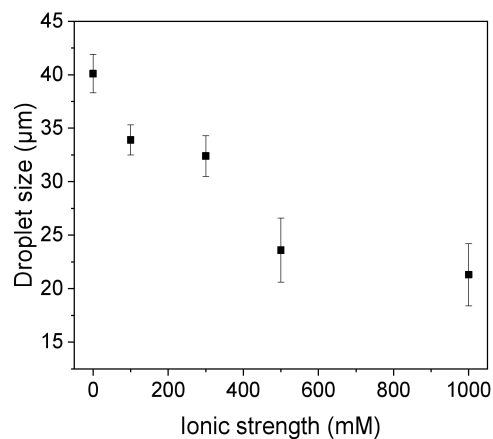


(e)

Figure VII-13. Optical microscopic images of freshly prepared emulsions stabilized by OVT fibrils ($c = 3.5$ wt%, $\phi = 0.7$) at different ionic strengths: (a) 0 mM, (b) 100 mM, (c) 300 mM, (d) 500 mM, (e) 1000 mM. The scale bars within the figures are $100\ \mu\text{m}$ in length.



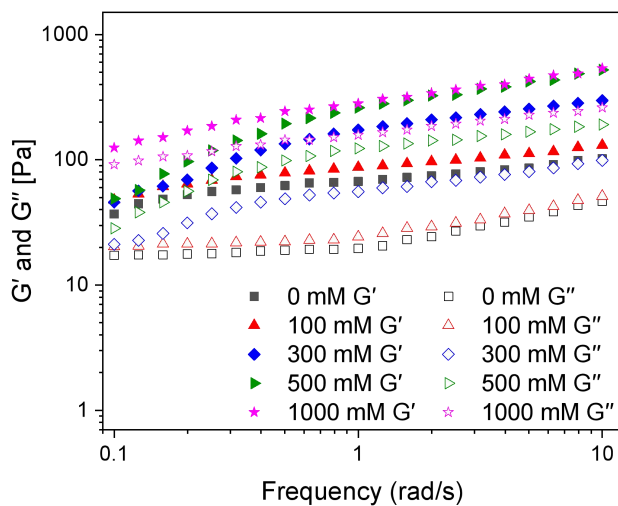
(a)



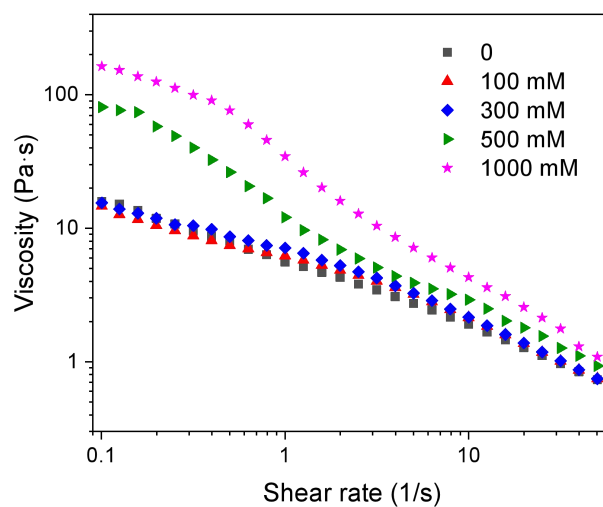
(b)

Figure VII-14. (a) Average droplet size of freshly prepared Pickering emulsions

stabilized by OVT fibrils ($c = 3.5$ wt%, $\varphi = 0.7$) at different ionic strengths. (b) Average droplet size of Pickering emulsions stabilized by OVT fibrils ($c = 3.5$ wt%, $\varphi = 0.7$) at different ionic strengths after 20-day storage at 20 °C.



(a)



(b)

Figure VII-15. (a) Storage modulus (G') and loss modulus (G'') of Pickering emulsions stabilized by OVT fibrils ($c = 3.5$ wt%, $\varphi = 0.7$) at different ionic strengths.

As shown in Figure VII-15, the emulsion stiffness was dependent on ionic strengths, and storage modulus and viscosity of Pickering emulsions increased with

rising ionic strength. The gel strengthening effect of Pickering emulsions may be due to bridging behavior of fibrils at high ionic strengths. As electrostatic charges were gradually screened, the increasing number of fibril bridges result in highly crosslinked emulsion networks and an increase in storage modulus of Pickering emulsions (3).

3.5. Characterization of OVT fibril-stabilized Pickering emulsions at different pHs

Tuning emulsion pH based on actual requirements is essential, and it is necessary to study emulsibility of OVT fibrils at different pHs. Zeta potential of OVT fibril dispersion as function of pH was studied to provide background for impact of pH on OVT fibril-stabilized emulsions. As shown in Figure VII-16, when pH increased from 2 to 7, OVT fibrils carried fewer positive charges, and zeta potential of OVT fibrils was as low as approximately 0.8 mV at pH 7, indicating that isoelectric point of OVT fibrils was around pH 7. Figure VII-17 showed visual appearance of OVT fibril-stabilized emulsions prepared at various pHs. Only very limited creaming was observed in emulsions at pH 2 and 3, and homogeneous emulsions without serum phase were prepared at pH 4–7.

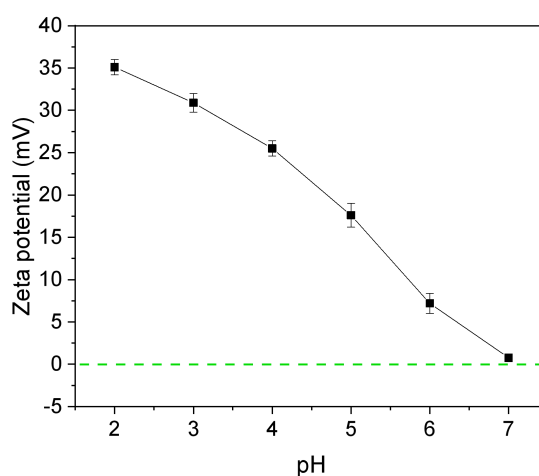


Figure VII-16. Zeta potential of OVT fibril dispersion as function of pHs.

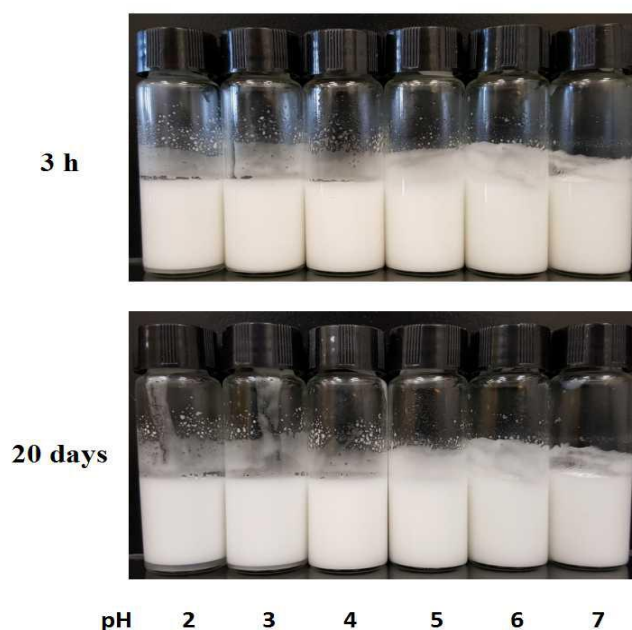


Figure VII-17. Visual observation of Pickering emulsions stabilized by OVT fibrils ($c = 3.5$ wt%, $\phi = 0.7$) at different pHs. All photographs were taken at 3 h and 20 days after preparation of fresh emulsions, and the storage was carried out at 20 °C.

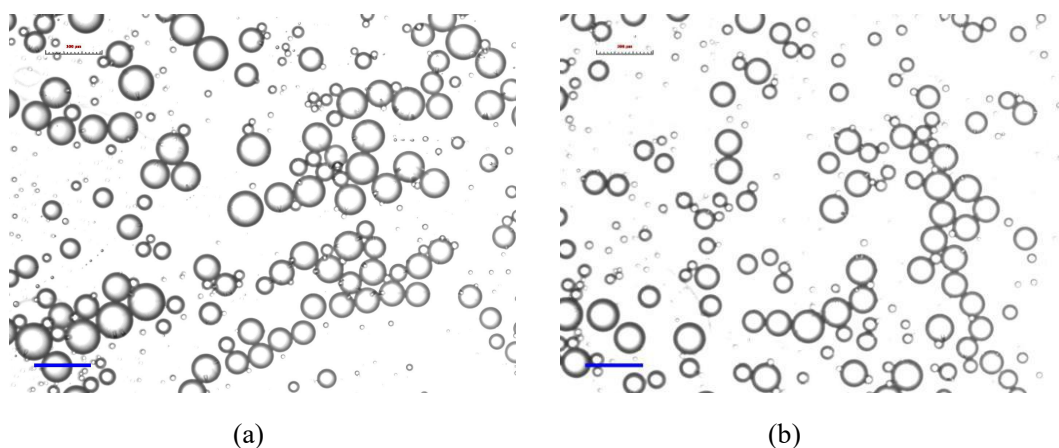
As shown in Table VII-3, emulsions at various pHs were extremely stable. Considering that many Pickering emulsions may be pH-sensitive and demulsify at certain pH range (44, 45), OVT fibrils had excellent Pickering emulsibility at different pHs, which may be explained by theory mentioned earlier. As pH increases, electrostatic repulsions between fibrils and emulsion interfaces anchored with some fibrils may decrease, contributing to ample surface coverage of fibrils at emulsion interfaces and better Pickering emulsification (43). In addition, our preliminary experiments indicated that OVT fibrils themselves were stable at different pHs (data not shown), and the intact structures at oil-water interface could ensure irreversible adsorption of OVT fibrils.

Table VII-3. Emulsified phase volume fraction and stability index of Pickering emulsions stabilized by OVT fibrils at different pHs

Samples	Emulsified phase volume (%)		Stability index
	3 h	20 days	
pH 2	95.2±0.1 ^a	93.7±0.1 ^a	98.4±0.2 ^a
pH 3	98.1±0.1 ^b	97.0±0.2 ^b	98.9±0.3 ^b
pH 4	100.0±0.0 ^c	100.0±0.0 ^c	100.0±0.0 ^c
pH 5	100.0±0.0 ^c	100.0±0.0 ^c	100.0±0.0 ^c
pH 6	100.0±0.0 ^c	100.0±0.0 ^c	100.0±0.0 ^c
pH 7	100.0±0.0 ^c	100.0±0.0 ^c	100.0±0.0 ^c

Values are means±SD (n=3). Different superscript letters for the same column indicate significant differences ($p < 0.05$).

As depicted in Figure VII-18 and Figure VII-19, the average emulsion droplet size decreased from 39.5 μm to 29.1 μm as pH increased from 2 to 7. As shown in Figure VII-19b, average droplet size of Pickering emulsions at various pHs was almost unchanged after 20-day storage at 20 °C, confirming that OVT fibril-stabilized emulsion droplets were stable against various pHs.



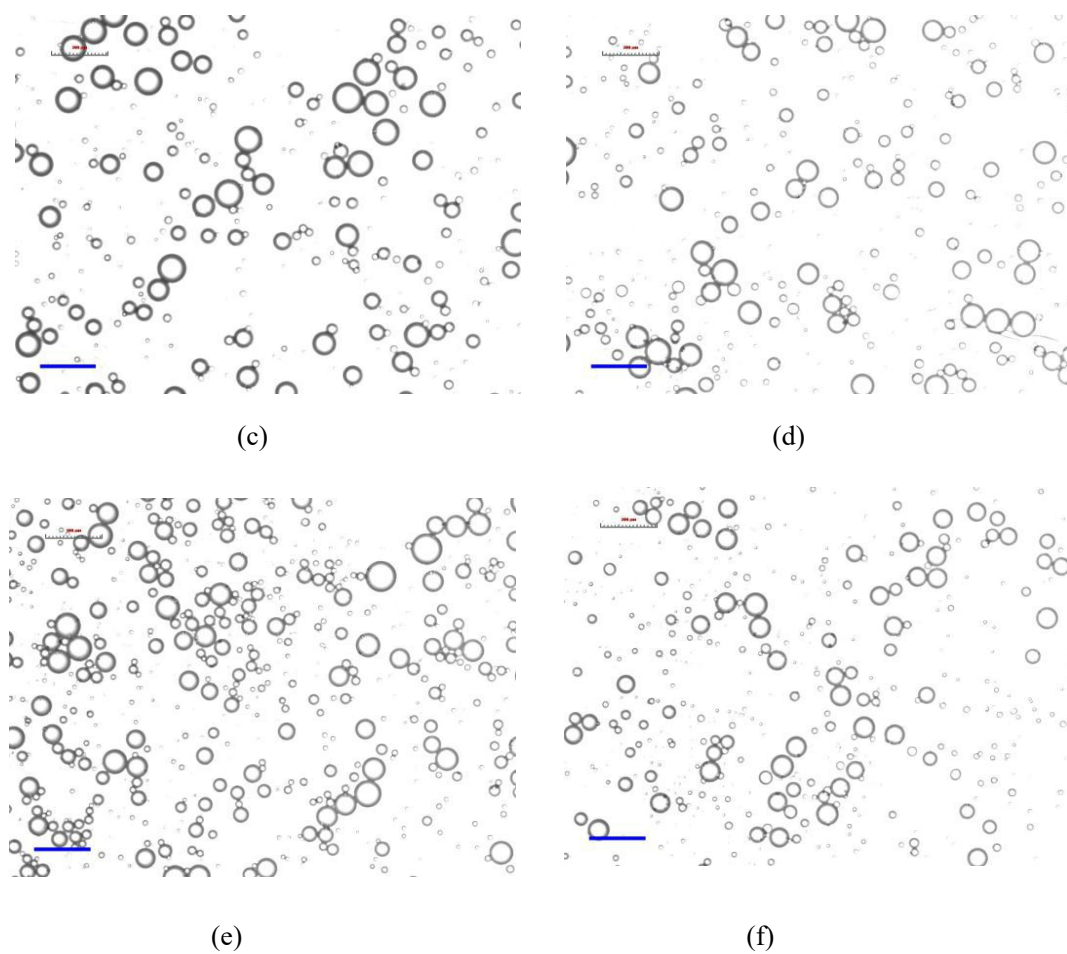
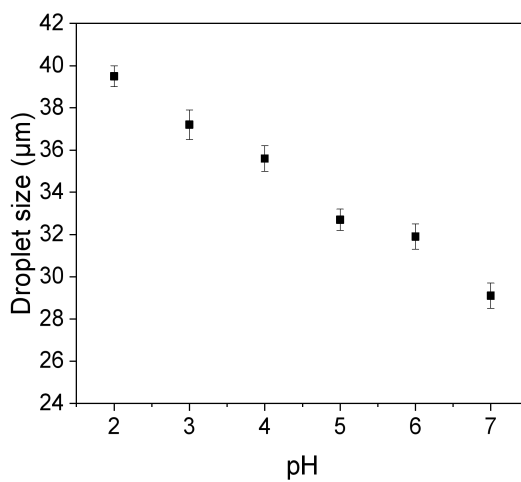


Figure VII-18. Optical microscopic images of emulsions stabilized by OVT fibrils ($c = 3.5$ wt%, $\varphi = 0.7$) at different pHs: (a) pH 2, (b) pH 3, (c) pH 4, (d) pH 5, (e) pH 6, (f) pH 7. The scale bars within the figures are 100 μm in length.



(a)

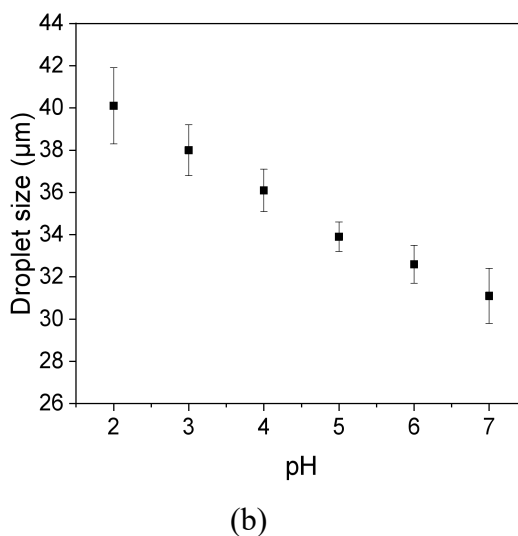
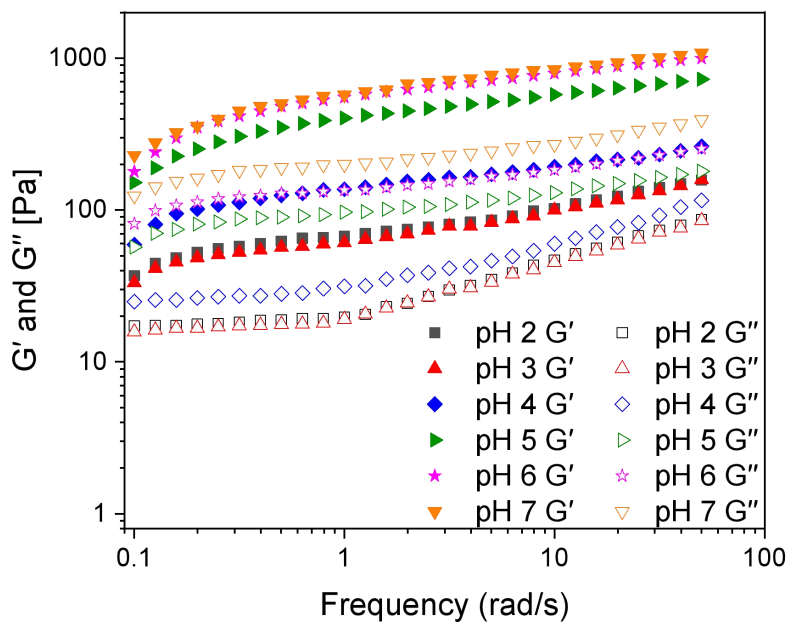
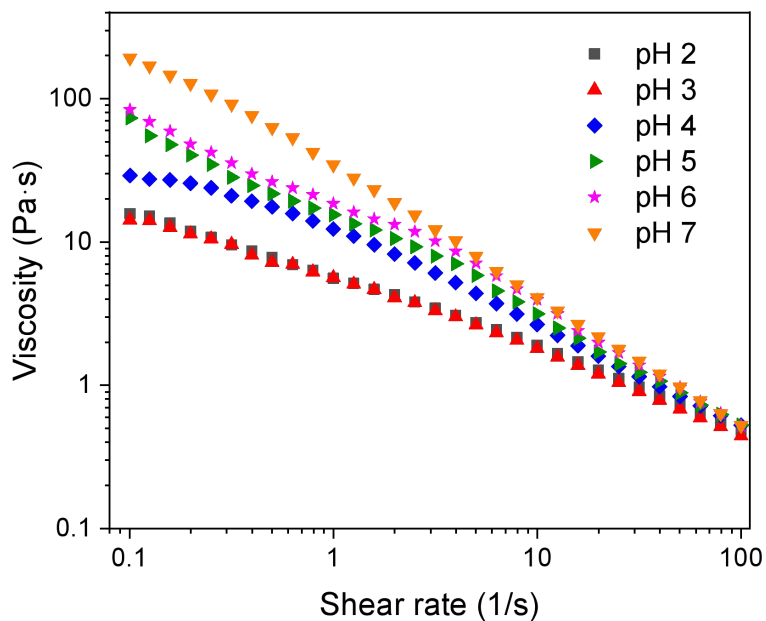


Figure VII-19. (a) Average droplet size of freshly prepared Pickering emulsions stabilized by OVT fibrils ($c = 3.5$ wt%, $\phi = 0.7$) at different pHs. (b) Average droplet size of Pickering emulsions stabilized by OVT fibrils ($c = 3.5$ wt%, $\phi = 0.7$) at different pHs after 20-day storage at 20 °C.

Figure VII-20 shows rheological properties of emulsions at different pHs, and storage modulus and viscosity progressively increased as pH increased, Gel strengthening and thickening of emulsions may be ascribed to two factors. First, since smaller emulsion droplet size leads to higher viscosity and gel strength of emulsions (39, 40), small emulsion droplets at high pHs are in favor of gel-like behavior. Second, as discussed earlier, increasing pH leads to enhanced surface coverage of fibrils. More OVT fibrils may allow for stronger interparticle interactions and participate in constructing tight emulsion networks, resulting in gel strengthening and thickening of OVT fibril-stabilized emulsions at high pHs.



(a)



(b)

Figure VII-20. (a) Storage modulus (G') and loss modulus (G'') of Pickering emulsions stabilized by OVT fibrils ($c = 3.5$ wt%, $\phi = 0.7$) at different pHs. (b) Apparent viscosity of Pickering emulsions stabilized by OVT fibrils ($c = 3.5$ wt%, $\phi = 0.7$) at different pHs.

3.6. Thermal stability of OVT fibril-stabilized Pickering emulsions

Although Pickering emulsions have outstanding stability against Ostwald ripening, macroscopic phase separation and droplet coalescence, Pickering emulsions cannot be unconditionally stable in all circumstances (46, 47). Actually multiple factors may deteriorate overall emulsion stability especially for emulsions stabilized by food-grade particles (47). Previous studies reveal that some Pickering emulsions may be unstable at high temperatures due to heat susceptibility of Pickering emulsifiers (48), and long-term stability of Pickering emulsions should take temperature stimuli into account. Therefore, Pickering emulsion stabilized by OVT fibrils ($c = 3.5$ wt%, $\phi = 0.7$) at 0 mM ionic strength and pH 2 was selected as a model to evaluate thermal stability of OVT fibril-stabilized Pickering emulsions. Figure VII-21 showed visual appearance of OVT fibril-stabilized Pickering emulsion before and after storage at 50 °C. It was observed that visual appearance of OVT fibril-stabilized Pickering emulsion barely changed after 10-day storage, and stability index of emulsions 10 days later was $98.3\% \pm 0.1\%$, indicating excellent storage stability at relatively high temperature. Figure VII-22 depicts microstructure of OVT fibril-stabilized Pickering emulsion after 10-day storage at 50 °C, and no obvious droplet coalescence and Ostwald ripening were observed. Based on estimation using Image J software the average droplet size of emulsion after thermal treatment was 39.9 ± 0.4 μm . Considering that the average droplet size of emulsion before thermal treatment was 39.5 ± 0.5 μm , it could be concluded that microstructure of OVT fibril-stabilized Pickering emulsion remained almost unchanged at 50 °C. In summary,

stability of OVT fibril-stabilized Pickering emulsions was temperature-independent, which could be explained by the fact that OVT fibrils themselves were generated at 90 °C and high temperature could not damage structures of OVT fibrils.



Figure VII-21. Visual observation of Pickering emulsions stabilized by OVT fibrils at fibril concentration of 3.5 wt% and oil fraction of 0.7 before and after storage at 50 °C for 10 days.

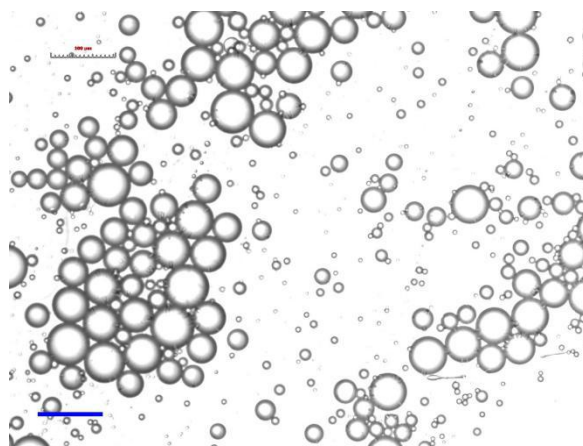


Figure VII-22. Optical microscopic images of emulsions stabilized by OVT fibrils at fibril concentration of 3.5 wt% and oil fraction of 0.7 after storage at 50 °C for 10 days. The scale bar within the figure is 100 μm in length.

4. Conclusion

In summary, Pickering emulsion droplets stabilized by OVT fibrils were successfully prepared. It was found that OVT fibrils could stabilize Pickering emulsions with high emulsified phase volume and stability index at different fibril concentrations and oil fractions. OVT fibrils could be employed to fabricate stable Pickering emulsions at various ionic strengths (0–1000 mM) and pHs (2–7). Increasing ionic strengths and pHs of emulsions was conducive to higher emulsified phase volume fraction and formation of smaller emulsion droplets. Increasing either ionic strength or pH of emulsions could lead to an increase of gel strength and viscosity. Visual appearance and microstructure of OVT fibril-stabilized Pickering emulsions were stable during 10-day storage at 50 °C. The knowledge obtained in this work may provide a promising strategy to produce stable food-grade emulsion systems over a wide range of ionic strength, pH and temperature.

5. References

1. Dickinson, E. (2017). Biopolymer-based particles as stabilizing agents for emulsions and foams. *Food Hydrocolloids*, 68, 219–231.
2. Xiao, J., Li, Y., & Huang, Q. (2016). Recent advances on food-grade particles stabilized Pickering emulsions: fabrication, characterization and research trends. *Trends in Food Science & Technology*, 55, 48–60.
3. Griffith, C., & Daigle, H. (2018). Manipulation of Pickering emulsion rheology using hydrophilically modified silica nanoparticles in brine. *Journal of Colloid and Interface Science*, 509, 132–139.
4. de Folter, J. W. J., van Ruijven, M. W. M., & Velikov, K. P. (2012). Oil-in-water Pickering emulsions stabilized by colloidal particles from the water-insoluble protein zein. *Soft Matter*, 8, 6807–6815.
5. Wei, Z., & Huang, Q. (2019). Edible Pickering emulsions stabilized by

- ovotransferrin–gum arabic particles. *Food Hydrocolloids*, 89, 590–601.
6. Loveday, S. M., Anema, S. G., & Singh, H. (2017). β -Lactoglobulin nanofibrils: The long and the short of it. *International Dairy Journal*, 67, 35–45.
 7. Straub, J. E., & Thirumalai, D. (2011). Toward a molecular theory of early and late events in monomer to amyloid fibril formation. *Annual Review of Physical Chemistry*, 62, 437–463.
 8. Wei, Z., & Huang, Q. (2019). Assembly of iron-bound ovotransferrin amyloid fibrils. *Food Hydrocolloids*, 89, 579–589.
 9. Adamcik, J., Jung, J. M., Flakowski, J., De Los Rios, P., Dietler, G., & Mezzenga, R. (2010). Understanding amyloid aggregation by statistical analysis of atomic force microscopy images. *Nature Nanotechnology*, 5(6), 423–428.
 10. Cejas, M. A., Kinney, W. A., Chen, C., Vinter, J. G., Almond, H. R., Balss, K. M., et al. (2008). Thrombogenic collagen-mimetic peptides: Self-assembly of triple helix-based fibrils driven by hydrophobic interactions. *Proceedings of the National Academy of Sciences*, 105(25), 8513–8518.
 11. Meijer, J. T., Roeters, M., Viola, V., Löwik, D. W., Vriend, G., & van Hest, J. C. (2007). Stabilization of peptide fibrils by hydrophobic interaction. *Langmuir*, 23, 2058–2063.
 12. Akkermans, C., Venema, P., van der Goot, A. J., Gruppen, H., Bakx, E. J., Boom, R. M., et al. (2008). Peptides are building blocks of heat-induced fibrillar protein aggregates of β -lactoglobulin formed at pH 2. *Biomacromolecules*, 9(5), 1474–1479.
 13. Tang, C., & Wang, C. (2010). Formation and characterization of amyloid-like fibrils from soy β -conglycinin and glycinin. *Journal of Agricultural and Food Chemistry*, 58(20), 11058–11066.
 14. Lassé, M., Ulluwishewa, D., Healy, J., Thompson, D., Miller, A., Roy, N., et al. (2016). Evaluation of protease resistance and toxicity of amyloid-like food fibrils from whey, soy, kidney bean, and egg white. *Food Chemistry*, 192, 491–498.
 15. Jordens, S., Riley, E. E., Usov, I., Isa, L., Olmsted, P. D., & Mezzenga, R. (2014). Adsorption at liquid interfaces induces amyloid fibril bending and ring formation. *ACS Nano*, 8(11), 11071–11079.
 16. Shen, L., Adachi, T., Vanden Bout, D., & Zhu, X. Y. (2012). A mobile precursor determines amyloid β peptide fibril formation at interface. *Journal of the American Chemical Society*, 134(34), 14172–14178.
 17. Humblet-Hua, N. K., van der Linden, E., & Sagis, L. M. C. (2012). Microcapsules with protein fibril reinforced shells: Effect of fibril properties on mechanical strength of the shell. *Journal of Agricultural and Food Chemistry*, 60(37), 9502–9511.
 18. Serfert, Y., Lamprecht, C., Tan, C. P., Keppler, J. K., Appel, E., Rossier-Miranda, F. J., et al. (2014). Characterization and use of β -lactoglobulin fibrils for microencapsulation of lipophilic ingredients and oxidative stability thereof. *Journal of Food Engineering*, 143, 53–61.
 19. Guzzi, R., Rizzuti, B., Labate, C., Zappone, B., & De Santo, M. P. (2015). Ferric ions inhibit the amyloid fibrillation of β -lactoglobulin at high temperature. *Biomacromolecules*, 16(6), 1794–1801.

20. Theil, E. C. (2004). Iron, ferritin, and nutrition. *Annual Review of Nutrition*, 24, 327–343.
21. vandenAkker, C. C., Engel, M. F., Velikov, K. P., Bonn, M., & Koenderink, G. H. (2011). Morphology and persistence length of amyloid fibrils are correlated to peptide molecular structure. *Journal of the American Chemical Society*, 133, 18030–18033.
22. Giansanti, F., Leboffe, L., Pitari, G., Ippoliti, R., & Antonini, G. (2012). Physiological roles of ovotransferrin. *Biochimica et Biophysica Acta (BBA)–General Subjects*, 1820, 218–225.
23. Abeyrathne, E. D. N. S., Lee, H. Y., & Ahn, D. U. (2014). Separation of ovotransferrin and ovomucoid from chicken egg white. *Poultry Science*, 93, 1010–1017.
24. Brand, J., Dachmann, E., Pichler, M., Lotz, S., & Kulozik, U. (2016). A novel approach for lysozyme and ovotransferrin fractionation from egg white by radial flow membrane adsorption chromatography: Impact of product and process variables. *Separation and Purification Technology*, 161, 44–52.
25. Wei, Z., Zhu, P., & Huang, Q. (2019). Investigation of ovotransferrin conformation and its complexation with sugar beet pectin. *Food Hydrocolloids*, 87, 448–458.
26. Oboroceanu, D., Wang, L., Brodkorb, A., Magner, E., & Auty, M. A. E. (2010). Characterization of β -lactoglobulin fibrillar assembly using atomic force microscopy, polyacrylamide gel electrophoresis, and in situ Fourier transform infrared spectroscopy. *Journal of Agricultural and Food Chemistry*, 58, 3667–3673.
27. Usov, I., & Mezzenga, R. (2015). FiberApp: An open-source software for tracking and analyzing polymers, filaments, biomacromolecules, and fibrous objects. *Macromolecules*, 48, 1269–1280.
28. Laemmli, U. K. (1970). Cleavage of structural proteins during the assembly of the head of bacteriophage T4. *Nature*, 227, 680–685.
29. Kargar, M., Fayazmanesh, K., Alavi, M., Spyropoulos, F., & Norton, I. T. (2012). Investigation into the potential ability of Pickering emulsions (food-grade particles) to enhance the oxidative stability of oil-in-water emulsions. *Journal of Colloid and Interface Science*, 366, 209–215.
30. Wei, Z., & Huang, Q. (2019). Developing organogel-based pickering emulsions with improved freeze-thaw stability and hesperidin bioaccessibility. *Food Hydrocolloids*, 93, 68–77.
31. Zoppe, J. O., Venditti, R. A., & Rojas, O. J. (2012). Pickering emulsions stabilized by cellulose nanocrystals grafted with thermo-responsive polymer brushes. *Journal of Colloid and Interface Science*, 369, 202–209.
32. Xiao, J., Wang, X., Gonzalez, A. J. P., & Huang, Q. (2016). Kafirin nanoparticles-stabilized Pickering emulsions: Microstructure and rheological behavior. *Food Hydrocolloids*, 54, 30–39.
33. Arnaudov, L. N., & de Vries, R. (2006). Strong impact of ionic strength on the kinetics of fibrillar aggregation of bovine β -lactoglobulin. *Biomacromolecules*, 7, 3490–3498.
34. Loveday, S. M., Wang, X. L., Rao, M. A., Anema, S. G., Creamer, L. K., & Singh,

- H. (2010). Tuning the properties of β -lactoglobulin nanofibrils with pH, NaCl and CaCl₂. *International Dairy Journal*, 20, 571–579.
35. Nilsson, M. R. (2004). Techniques to study amyloid fibril formation in vitro. *Methods*, 34, 151–160.
36. Gao, Z., Zhao, J., Huang, Y., Yao, X., Zhang, K., Fang, Y., et al. (2017). Edible Pickering emulsion stabilized by protein fibrils. Part 1: Effects of pH and fibrils concentration. *LWT - Food Science and Technology*, 76, 1–8.
37. Tadros, T. (2004). Application of rheology for assessment and prediction of the long-term physical stability of emulsions. *Advances in Colloid and Interface Science*, 108–109, 227–258.
38. Liu, F., & Tang, C. H. (2016). Soy glycinin as food-grade Pickering stabilizers: Part. II. Improvement of emulsification and interfacial adsorption by electrostatic screening. *Food Hydrocolloids*, 60, 620–630.
39. Derkach, S. R. (2009). Rheology of emulsions. *Advances in Colloid and Interface Science*, 151, 1–23.
40. Pal, R. (1996). Effect of droplet size on the rheology of emulsions. *AIChE Journal*, 42, 3181–3190.
41. Tang, J., Quinlan, P. J., & Tam, K. C. (2015). Stimuli-responsive Pickering emulsions: recent advances and potential applications. *Soft Matter*, 11, 3512–3529.
42. Sharp, K. A., & Honig, B. (1990). Electrostatic interactions in macromolecules: theory and applications. *Annual Review of Biophysics and Biophysical Chemistry*, 19, 301–332.
43. Wang, H., Singh, V., & Behrens, S. H. (2012). Image charge effects on the formation of Pickering emulsions. *The Journal of Physical Chemistry Letters*, 3, 2986–2990.
44. Dyab, A. K. F. (2012). Destabilisation of Pickering emulsions using pH. *Colloids and Surfaces A: Physicochemical and Engineering Aspects*, 402, 2–12.
45. Luo, Z., Murray, B. S., Ross, A. L., Povey, M. J. W., Morgan, M. R. A., & Day, A. J. (2012). Effects of pH on the ability of flavonoids to act as Pickering emulsion stabilizers. *Colloids and Surfaces B: Biointerfaces*, 92, 84–90.
46. Saigal, T., Dong, H., Matyjaszewski, K., & Tilton, R. D. (2010). Pickering emulsions stabilized by nanoparticles with thermally responsive grafted polymer brushes. *Langmuir*, 26, 15200–15209.
47. Tavernier, I., Wijaya, W., Van der Meeren, P., Dewettinck, K., & Patel, A. R. (2016). Food-grade particles for emulsion stabilization. *Trends in Food Science & Technology*, 50, 159–174.
48. Binks, B. P., & Rocher, A. (2009). Effects of temperature on water-in-oil emulsions stabilised solely by wax microparticles. *Journal of Colloid and Interface Science*, 335, 94–104.

CHAPTER VIII. OVOTRANSFERRIN FIBRIL-STABILIZED PICKERING EMULSIONS AS DELIVERY VEHICLES FOR CURCUMIN

1. Introduction

Curcumin, a naturally occurring polyphenol, possesses biological activities such as anti-cancer, anti-inflammatory and neuroprotective efficacy (1, 2). As a lipophilic nutraceutical component, curcumin is susceptible to chemical degradation in the presence of light, heat and so on (2). Thus, curcumin emulsion can be employed as a model to evaluate protective effects of Pickering emulsions on lipophilic compounds against harsh environments. Meanwhile, curcumin has poor absorption and low bioaccessibility (1), endowing curcumin a good candidate for bioaccessibility research. Based on these understandings, curcumin can be chosen as a nutraceutical model to study protective effect and digestion of OVT fibril-stabilized Pickering emulsions.

The chapter aimed to study protective effects and nutraceutical bioaccessibility of OVT fibril-stabilized Pickering emulsions, and curcumin was chosen as a model nutraceutical here. Protective effects of OVT fibril-stabilized Pickering emulsions at different ionic strengths and pHs on curcumin were investigated. Curcumin bioaccessibility of OVT fibril-stabilized Pickering emulsions was studied in TIM-1 digestion model, and the digestion result in TIM-1 dynamic digestion model was compared with that in pH-stat static digestion model.

2. Materials and Methods

2.1. Materials

Ovotransferrin (OVT, purity > 88%) was purchased from Neova Technologies Inc. (Abbotsford, British Columbia, Canada), and OVT had an iron binding capacity of 1099 $\mu\text{g Fe/g}$ based on analysis report provided by the manufacturer. Medium chain triglyceride (MCT, Neobee 1053) consisting of 55% caprylic triglyceride and 44% capric triglyceride was kindly provided by Stepan Company (Northfield, Illinois, USA). Curcumin (85% purity with 11% of demethoxycurcumin and 4% of bisdemethoxy curcumin as impurities) was a gift from Sabinsa Corporation (East Windsor, New Jersey, USA). Pepsin, pancreatin and lipase were purchased from Sigma-Aldrich (St. Louis, Missouri, USA). Methanol was purchased from Thermo Fisher Scientific, Inc. (Waltham, Massachusetts, USA).

2.2. Formation of OVT fibrils

Preparation of OVT fibrils was performed as described in the chapter VII.

2.3. Preparation of curcumin-loaded Pickering emulsions stabilized by OVT fibrils

Curcumin was first dissolved in MCT oil under sonication and heating to a final concentration of 3 mg/mL. Preparation of curcumin-loaded Pickering emulsions stabilized by OVT fibrils was conducted based on the chapter VII. OVT fibril dispersion (3.5 wt%, pH 2, 0 mM ionic strength) was mixed with curcumin-loaded MCT oil to obtain mixture with an oil fraction of 0.7, and sodium azide (0.02%, w/v) was added to prevent microbial growth in emulsions. Afterwards, the mixture was homogenized at 9000 rpm for 2 min employing an Ultra-Turrax (IKA-Werke GMBH & CO., Germany) to obtain OVT fibril-stabilized emulsion. To better understand

protective effect and nutraceutical delivery performance of OVT fibril-stabilized emulsions, curcumin-loaded MCT oil with a curcumin concentration of 3 mg/mL was applied as control in the rest of this study.

Curcumin-loaded Pickering emulsions stabilized by OVT fibrils at different ionic strengths and pHs were prepared to facilitate investigating curcumin protection of OVT fibril-stabilized emulsions with different structures. In terms of fabricating OVT fibril-stabilized curcumin emulsions at various ionic strengths, sodium chloride was added to OVT fibril dispersions (3.5 wt%, pH 2) to reach an ionic strength of 300 mM, 500 mM or 1000 mM. The OVT fibril dispersions (3.5 wt%, pH 2) at different ionic strengths were mixed with MCT oil to obtain mixtures with an oil fraction of 0.7, followed by homogenization procedures as described above. Regarding preparation of OVT fibril-stabilized curcumin emulsions at different pHs, pH of OVT fibril dispersions was first adjusted to pH 4 or 6 with addition of NaOH solution carefully. Subsequently, OVT fibril dispersions (3.5 wt%, 0 mM ionic strength) at different pHs (pH 2, 4 or 6) were mixed with MCT oil to obtain mixtures with an oil fraction of 0.7, followed by homogenization procedures as described above.

2.4. Stability of encapsulated curcumin in emulsions against ultraviolet (UV) light exposure

The OVT fibril-stabilized Pickering emulsions at different ionic strengths and pHs were exposed to UV radiation (6 W, 365 nm) via a UV radiation equipment in a lightproof cabinet, and curcumin dissolved in MCT oil was applied as control (3). At designated time points a 100 μ L aliquot was sampled from each Pickering emulsion.

To recover curcumin from emulsions, 1.2 mL of methanol was thoroughly mixed with the 100 μ L aliquot, followed by centrifugation at 12000 rpm for 10 min to fully separate the supernatant layer. The curcumin recovery procedures were repeated three times. After proper dilution the absorbance of methanolic extract was recorded at 425 nm using a UV-vis spectrophotometer, and a prepared calibration curve of absorbance versus curcumin concentration was used to determine curcumin concentration. The residual curcumin level was used for chemical stability analysis and calculated as $(C/C_0) \times 100\%$, where C was the concentration of curcumin at any designated time point during UV radiation, C_0 was the initial concentration of curcumin.

2.5. Digestion of OVT fibril-stabilized curcumin emulsion in TIM-1 digestion model

2.5.1. In vitro digestion of OVT fibril-stabilized curcumin emulsion in TIM-1 dynamic digestive system

To study the bioaccessibility of curcumin in OVT fibril-stabilized emulsion and MCT oil, these curcumin-loaded samples were fed into the stomach compartment for TIM-1 digestion run. Specifically, during sample feeding 50 g of OVT fibril-stabilized curcumin emulsion (at pH 6 and 0 mM ionic strength) was mixed with 50 g of deionized water for rinse purpose, 95 g of gastric electrolyte solution as well as 5 g of gastric start residue. The mixture was then introduced in the gastric compartment through a funnel. Since 50 g of OVT fibril-stabilized curcumin emulsion (oil fraction = 0.7) contained 35 g of curcumin-loaded oil, 35 g of curcumin-loaded MCT oil was fed as control into TIM-1 digestion model to compare curcumin bioaccessibility in OVT fibril-stabilized emulsion and MCT oil. The TIM-1 digestion run lasted for 6 h

(4, 5). To measure the amount of bioaccessible curcumin, jejunal and ileal filtrates which passed through hollow fiber membranes (Spectrum Milikros modules M80S-300-01P) were collected at 30, 60, 90, 120, 180, 240, 300 and 360 min. Meanwhile, the volume of jejunal and ileal filtrates during a specific period of time was recorded. The collected jejunal and ileal filtrates were stored in an ice bath until HPLC quantification of curcumin, and HPLC analysis of curcumin was conducted as described in section 2.5.2. The amount of bioaccessible curcumin during each specific period of time was calculated based on filtrate volume and curcumin concentration in filtrates. Subsequently, cumulative amount of bioaccessible curcumin after feeding samples in TIM-1 digestion model was determined. Curcumin bioaccessibility in TIM-1 digestion model was expressed as bioaccessible fraction of curcumin in total curcumin input.

2.5.2. High-performance liquid chromatography (HPLC) analysis of curcumin

An UltiMate 3000 HPLC system (Dionex, Sunnyvale, USA) equipped with a C18 Nova-Pak (Waters, Milford, USA) column (150×3.9 mm i.d.) was employed to measure curcumin concentration in jejunal and ileal filtrates. The elution was conducted at a flow rate of 1.0 mL/min with gradient solvent systems. The mobile phase solvents consisted of (A) acetonitrile and (B) water containing 0.2% acetic acid. The elution conditions were programmed as follows: 0–2 min, 35% A and 65% B; 2–17 min, linear gradient from 35% to 55% A; 17–22 min, held at 55% A; 22–23 min, A went from 55% to 35% linearly. The detection wavelength was set as 425 nm, and the amount of curcumin was obtained by referring to a standard curve of curcumin.

2.6. Digestion of OVT fibril-stabilized curcumin emulsion in pH-stat digestion model

2.6.1. In vitro digestion of OVT fibril-stabilized emulsion in static digestive system

In vitro digestion of OVT fibril-stabilized curcumin emulsion at pH 6 and 0 mM ionic strength was also investigated in pH-stat digestion model (6). Simulated gastric fluid without pepsin was freshly prepared by dissolving 1 g of sodium chloride into 0.5 L of pH-adjusted Milli-Q water (pH 1.2) (7). Curcumin-loaded samples (MCT oil and OVT fibril-stabilized emulsion at pH 6) containing 3 g of oil were mixed with 24 mL of simulated gastric fluid, followed by incubation in a water bath (37.0 ± 0.2 °C) under magnetic stirring (3). To start gastric digestion, 3 mL of simulated gastric fluid (with freshly dissolved pepsin) was added to reach a final pepsin concentration of 1.6 mg/mL in the mixture. The simulated gastric digestion took 2 h, and the digesta of simulated gastric phase were adjusted to pH 7.0 to inactivate pepsin and end gastric digestion (3).

For the simulated small intestinal phase, simulated intestinal fluid was freshly prepared by dissolving 10 mM CaCl_2 and 10 mg/mL bile salt into pH-adjusted Milli-Q water (pH 7.0), followed by addition of pancreatin to make a lipase concentration of 3.2 mg/mL in simulated intestinal fluid. To initiate intestinal digestion, the gastric digesta were mixed with an equal volume of simulated intestinal fluid, and simulated intestinal digestion lasted for 2 h (3, 8). During the intestinal digestion the mixture was incubated in a water bath (37.0 ± 0.2 °C) under continuous stirring. NaOH (0.25 M) was added to maintain pH at 7.0 during 2-h lipolysis, and the volume of added NaOH solution as function of time was recorded and used to

calculate concentration of generated free fatty acids (6). After gastrointestinal digestion in pH-stat digestion model, the digesta were centrifuged at 10000 g (Beckman Coulter Avanti J-E centrifuge, Fullerton, USA) for 30 min, and the clear micelle phase was collected for quantification of bioaccessible curcumin.

The release of free fatty acids (FFA) was employed to characterize lipolysis in samples. It was assumed that 1 mol of triglycerides released 2 mol of FFA and consumed 2 mol of NaOH (8, 9), and the percentage of FFA released was calculated as follows:

$$\% \text{ FFA} = 100 \times \frac{M_{\text{lipid}} \times V_{\text{NaOH}} \times m_{\text{NaOH}}}{w_{\text{lipid}} \times 2} \quad (1)$$

where M_{lipid} is the molecular mass of the triacylglycerol oil (in g/mol), V_{NaOH} is the volume of NaOH solution used to neutralize the released FFA (in mL), m_{NaOH} is the molarity of NaOH solution (in mol/mL), and w_{lipid} is the total mass of initially present triacylglycerol oil (in g) (6).

The amount of curcumin in the micelle phase was quantified using HPLC analysis as described in 2.6.2. Curcumin bioaccessibility in pH-stat digestion model was determined according to the following equation:

$$\% \text{ bioaccessibility} = \frac{\text{curcumin content in the micelle phase}}{\text{total curcumin content in the formulations}} \times 100\% \quad (2)$$

2.6.2. Analysis of curcumin content

An UltiMate 3000 HPLC system (Dionex, Sunnyvale, USA) equipped with a C18 Nova-Pak (Waters, Milford, USA) column (150×3.9 mm i.d.) was employed to measure curcumin concentration in the micelle phase. Curcumin content was determined using the procedures described in section 2.5.2.

2.7. Statistical analysis

All experiments were conducted in triplicate, and statistical analysis was performed employing OriginPro 2019 software (OriginLab Corporation, Northampton, USA). Statistical differences were tested using one-way analysis of variance (ANOVA) with Fisher LSD test, and the differences were considered significant if $P < 0.05$.

3. Results and Discussion

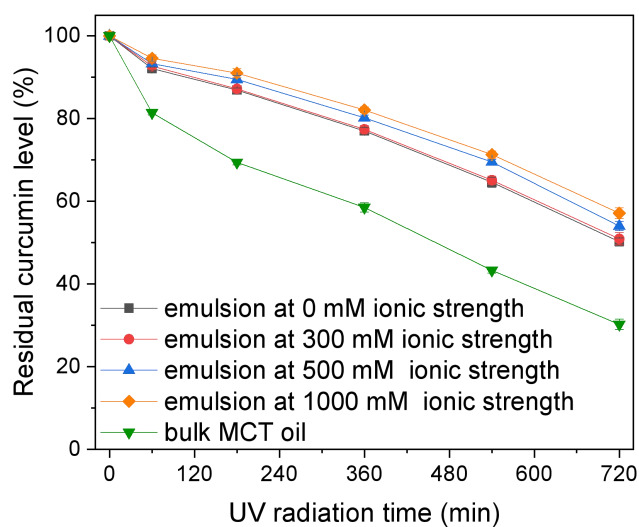
3.1. Protective effects of OVT fibril-stabilized Pickering emulsions at different ionic strengths on curcumin

In our previous chapter, it was found that OVT fibril-stabilized Pickering emulsions were stable under different ionic strength conditions, so protective impact of food-grade Pickering emulsions at different ionic strengths on nutraceuticals was tested in OVT fibril-stabilized emulsions. Figure VIII-1a shows visual appearance of OVT fibril-stabilized curcumin emulsions, and it was observed that emulsified phase volume fraction of OVT fibril-stabilized Pickering emulsions at all ionic strengths was above 95%, which was in consistence with our previous chapter. Since curcumin was vulnerable to degradation as a result of UV light (2, 3), the retention of curcumin during UV radiation was determined to reflect protective impact of OVT fibril-stabilized emulsions. As shown in Figure VIII-1b, the retention of curcumin in all samples decreased after UV light treatment, and only 30.2% of curcumin remained in curcumin-loaded MCT oil after 720 min. There was a smaller loss of curcumin in OVT fibril-stabilized emulsions against UV light, suggesting that OVT fibril layer around the oil droplets could contribute to slowdown of physicochemical degradation

and high retention of curcumin.



(a)



(b)

Figure VIII-1. (a) Visual appearance of curcumin-loaded Pickering emulsions stabilized by OVT fibrils at different ionic strengths. The emulsions from left to right are stabilized at ionic strength of 0, 300 mM, 500 mM and 1000 mM, respectively. (b) Residual curcumin level in bulk MCT oil and Pickering emulsions stabilized by OVT fibrils at different ionic strengths after UV radiation.

Table VIII-1. Reaction rate constants (k) of curcumin degradation against UV light exposure in bulk MCT oil and OVT fibril-stabilized Pickering emulsions at different ionic strengths

Sample	k (s^{-1})	R^2
MCT oil	$(2.73 \pm 0.04) \times 10^{-5d}$	0.981
Emulsion at 0 mM ionic strength	$(1.48 \pm 0.02) \times 10^{-5c}$	0.970
Emulsion at 300 mM ionic strength	$(1.45 \pm 0.03) \times 10^{-5c}$	0.972
Emulsion at 500 mM ionic strength	$(1.30 \pm 0.02) \times 10^{-5b}$	0.945
Emulsion at 1000 mM ionic strength	$(1.18 \pm 0.03) \times 10^{-5a}$	0.946

Values are means \pm SD ($n=3$). Different superscript letters for the same column indicate significant differences ($p < 0.05$).

The degradation rate constant of curcumin in all samples was calculated using the first-order kinetic model:

$$\ln C / C_0 = -kt \quad (3)$$

where C_0 was the initial concentration of curcumin, C was concentration of curcumin after UV radiation, t was UV treatment time and k was degradation rate constant (10).

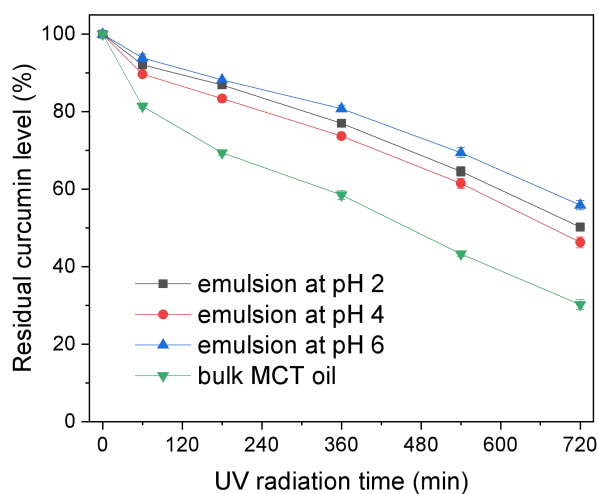
Degradation rate constants of curcumin in MCT oil and OVT fibril-stabilized Pickering emulsions at all ionic strengths were shown in Table VIII-1. Curcumin degradation rate constant followed the order: emulsion at 1000 mM ionic strength < emulsion at 500 mM ionic strength < emulsion at 300 mM ionic strength < emulsion at 0 mM ionic strength < bulk MCT oil, indicating that a rise of ionic strength in OVT fibril-stabilized Pickering emulsions could lead to better curcumin protection. This phenomenon can be explained as follows. As demonstrated in our previous chapter, addition of salts into emulsion systems can weaken charge repulsion effect among

OVT fibrils and ensure sufficient OVT fibrils at oil-water interface, which leads to thicker and denser OVT fibril layer around oil droplets. The thickly and densely packed OVT fibril layers may provide better protection for curcumin than thinly and loosely packed layers. Accordingly, it may be concluded that OVT fibril-stabilized Pickering emulsions at 1000 mM ionic strengths exhibited the best chemical stability among emulsions at all investigated ionic strengths.

3.2. Protective effects of OVT fibril-stabilized Pickering emulsions at different pHs on curcumin



(a)



(b)

Figure VIII-2. (a) Visual appearance of curcumin-loaded Pickering emulsions

stabilized by OVT fibrils at different pHs. The emulsions from left to right are stabilized at pH 2, 4 and 6, respectively. (b) Residual curcumin level in bulk MCT oil and Pickering emulsions stabilized by OVT fibrils at different pHs after UV radiation.

Since OVT fibril-stabilized Pickering emulsions have much better pH-stability than Pickering emulsions stabilized by zein particles and whey protein particles (11, 12), impact of food-grade Pickering emulsions at different pHs on nutraceuticals was explored in OVT fibril-stabilized emulsion model. As depicted in Figure VIII-2a, homogeneous curcumin emulsions stabilized by OVT fibrils were stable at pH 2, 4 and 6, which was in consistence with our previous study. Because curcumin was prone to degradation against UV light (2), chemical stability of OVT fibril-stabilized curcumin emulsions at various pHs was studied against UV light exposure. As depicted in Figure VIII-2b, curcumin in OVT fibril-stabilized Pickering emulsions at various pHs degraded slower than that in bulk MCT oil, suggesting that interfacial layers composed of OVT fibrils could provide protective barriers against UV radiation. Degradation rate constants of curcumin in samples were determined using aforementioned first-order kinetic model and summarized in Table VIII-2. As demonstrated in Figure VIII-2b and Table VIII-2, residual curcumin level of OVT fibril-stabilized Pickering emulsions after UV treatment followed the order: emulsion at pH 6 > emulsion at pH 2 > emulsion at pH 4, indicating that Pickering emulsion at pH 6 provided the best protection for curcumin. Several explanations may account for the phenomenon. First, emulsion droplet size may affect the volume-to-surface area ratio of emulsion droplets. When total volume of emulsion droplets is fixed, decreasing emulsion droplet size may increase total surface area of emulsion droplets

(13). Generally speaking, curcumin in emulsions with larger interfacial area may degrade faster. As discussed in our previous study, OVT fibril-stabilized emulsion at pH 4 has smaller droplet than that at pH 2, and that is why emulsion at pH 4 provides worse protection. Second, decreasing electrostatic repulsions at increasing pH may lead to highly crosslinked and bridging fibrils at interfacial layers (14), and the denser interfacial fibril layers at pH 6 may be beneficial to curcumin protection (15). It should be noted that although OVT fibril-stabilized emulsion at pH 6 has the smallest droplet size and the largest interfacial area among these emulsions at different pHs, the beneficial effect on curcumin protection from denser interfacial fibril layers can outweigh adverse effect from larger interfacial area. Based on these understandings, OVT fibril-stabilized emulsion at pH 6 provided the best interfacial barrier for curcumin protection and exhibited excellent potential as suitable delivery vehicles for curcumin.

Table VIII-2. Reaction rate constants (k) of curcumin degradation against UV light exposure in bulk MCT oil and OVT fibril-stabilized Pickering emulsions at different pHs

Sample	k (s ⁻¹)	R ²
MCT oil	(2.73 ± 0.04) × 10 ^{-5d}	0.981
Emulsion at pH 2	(1.48 ± 0.02) × 10 ^{-5b}	0.970
Emulsion at pH 4	(1.67 ± 0.03) × 10 ^{-5c}	0.965
Emulsion at pH 6	(1.24 ± 0.02) × 10 ^{-5a}	0.966

Values are means ± SD (n=3). Different superscript letters for the same column indicate significant differences ($p < 0.05$).

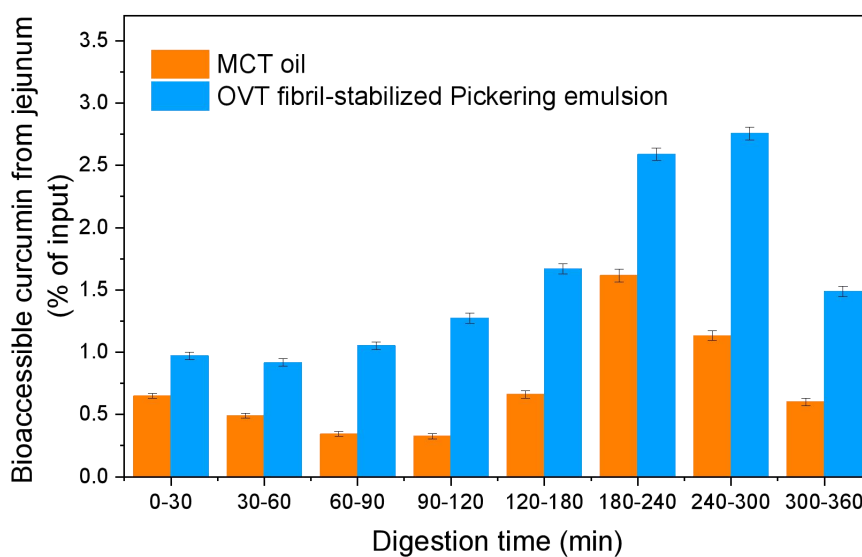
As shown in Table VIII-1 and Table VIII-2, degradation rate constant of

curcumin in Pickering emulsion at 1000 mM ionic strength was 4.8% lower than that in emulsion at pH 6, indicating that Pickering emulsion at 1000 mM ionic strength provides slightly better protection and exhibits potential to function as curcumin-loaded delivery vehicles. However, after overall consideration about potential health hazard of a high-salt diet, OVT fibril-stabilized curcumin emulsion at pH 6 and 0 mM ionic strength was further studied in the rest of this research.

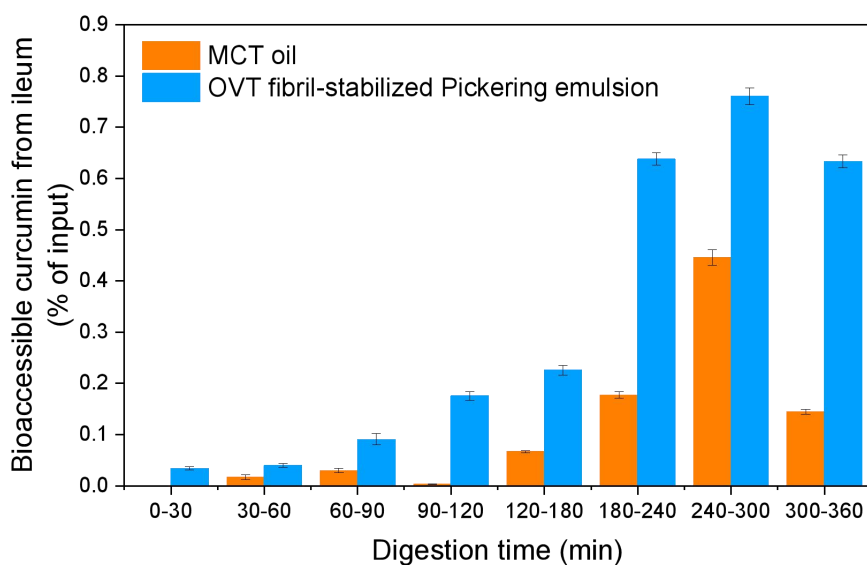
3.3. Digestion of OVT fibril-stabilized Pickering emulsions in TIM-1 dynamic digestive system

TIM-1 digestion model may simulate *in vivo* dynamic physiological processes realistically by taking many factors such as controlled physiological transit times, peristalsis movement, sequential secretion of enzymes in physiological amounts as well as elimination of digestion products into consideration (5, 16). It is generally believed that TIM-1 digestion model may have a better correlation with *in vivo* animal model in predicting nutraceutical bioavailability when compared with other *in vitro* digestion models (4, 16). *In vitro* gastrointestinal digestion of OVT fibril-stabilized Pickering emulsion was investigated using TIM-1 dynamic digestion model, and digestion of MCT oil was examined as control to better understand potential value of OVT fibril-stabilized Pickering emulsions as nutraceutical delivery systems. Curcumin bioaccessibility in TIM-1 dynamic digestion model was expressed as fraction of absorbed curcumin into jejunal and ileal compartments in original curcumin input (16). Figure VIII-3a shows curcumin bioaccessibility within a specified period of time from jejunum section, and it was observed that the rate of

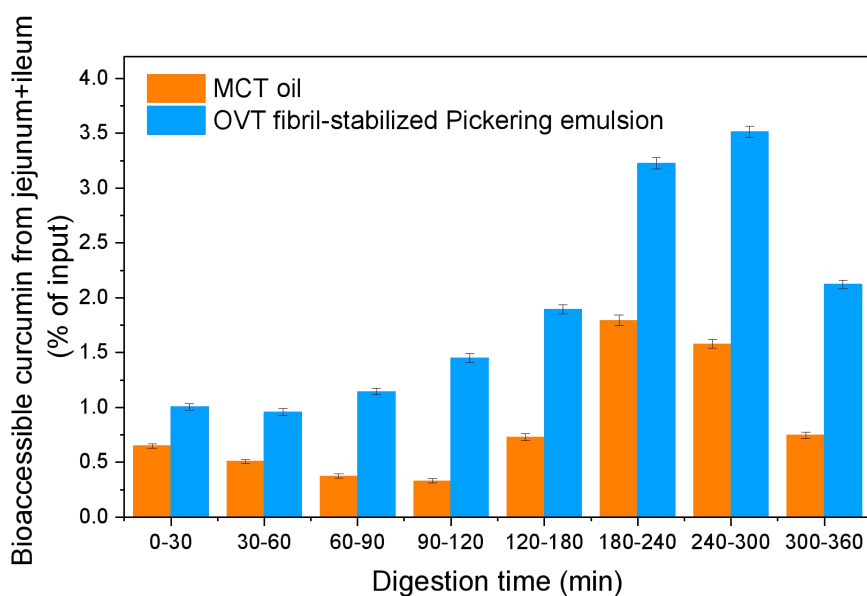
curcumin becoming bioaccessible from jejunum section was higher in OVT fibril-stabilized Pickering emulsion than that in MCT oil. As depicted in Figure VIII-3b, a very small amount of curcumin (around 0.074% of total curcumin input) in OVT fibril-stabilized Pickering emulsion was absorbed into ileum compartment during the first 1 h of TIM-1 digestion, and the rate of curcumin becoming bioaccessible from ileum section was the highest within 240–300 min after feeding OVT fibril-stabilized Pickering emulsion or MCT oil. Figure VIII-3c shows total curcumin bioaccessibility within a specified period of time from both jejunum and ileum sections, and it was found that curcumin bioaccessibility of OVT fibril-stabilized Pickering emulsion during each time period was higher than that of MCT oil.



(a)



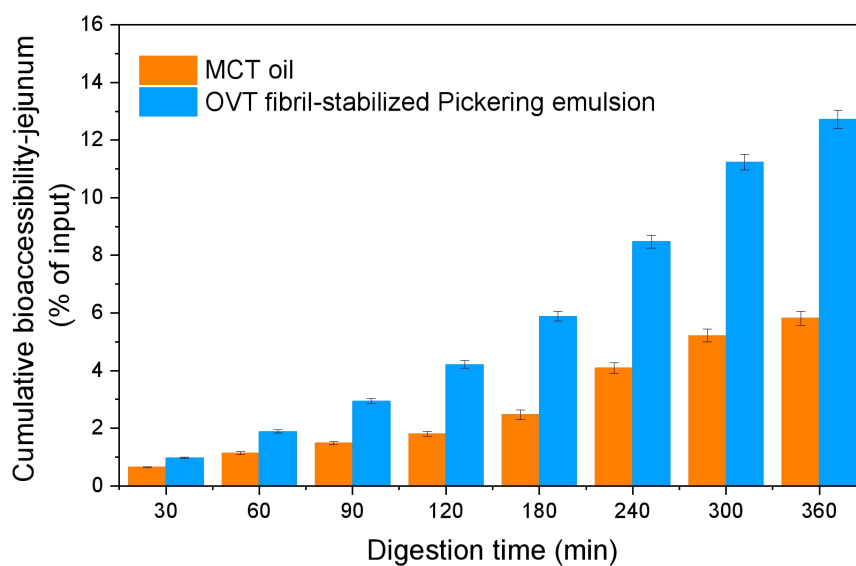
(b)



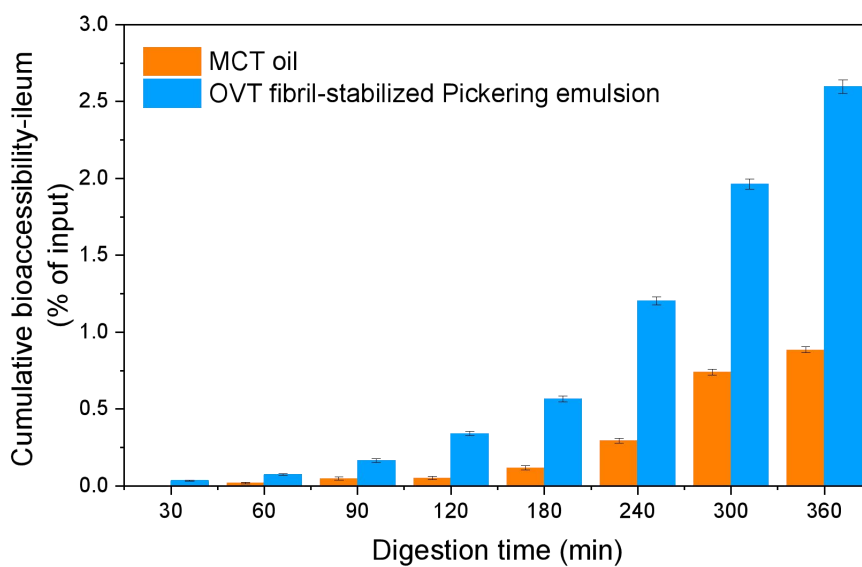
(c)

Figure VIII-3. Bioaccessible curcumin (% of input) within a specified period of time after feeding MCT oil and OVT fibril-stabilized Pickering emulsion in TIM-1 model. The samples were analyzed every 30 min during the first 2 h, and they were analyzed every 60 min during the following 4 hours. (a) Bioaccessible curcumin from jejunum section of the TIM-1 system. (b) Bioaccessible curcumin from ileum section of the TIM-1 system. (c) Total bioaccessible curcumin from both jejunum and ileum sections of the TIM-1 system.

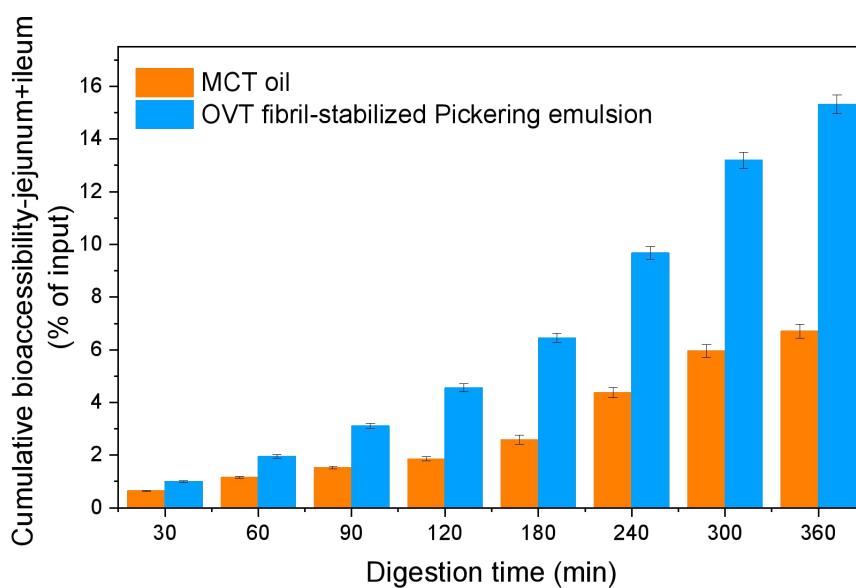
As shown in Figure VIII-4a, cumulative curcumin bioaccessibility from jejunum section of MCT oil and OVT fibril-stabilized Pickering emulsion increased progressively as digestion continued, and after 360 min cumulative curcumin bioaccessibility from jejunum section was 5.8% and 12.7% for MCT oil and OVT fibril-stabilized Pickering emulsion, respectively. Figure VIII-4b demonstrates that negligible amount of curcumin (less than of 0.017% of total curcumin input) in MCT oil was adsorbed into ileum compartment during the first 1 h of digestion, and after 360 min cumulative curcumin bioaccessibility from ileum section was 0.9% and 2.6% for MCT oil and OVT fibril-stabilized Pickering emulsion, respectively. Upon analysis of cumulative curcumin bioaccessibility from either jejunum section or ileum section, it was found that most of bioaccessible curcumin was recovered in jejunum compartment instead of ileum section, indicating that jejunum section in the small intestine was the main site of curcumin absorption.



(a)



(b)



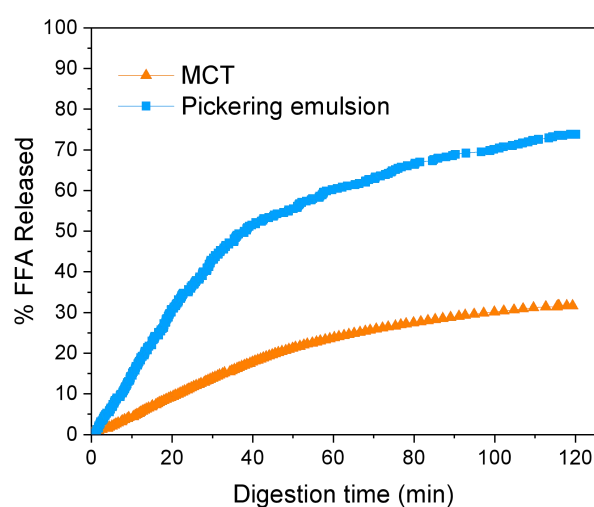
(c)

Figure VIII-4. Cumulative curcumin bioaccessibility after feeding MCT oil and OVT fibril-stabilized Pickering emulsion in TIM-1 model: (a) from jejunum section of the TIM-1 system; (b) from ileum section of the TIM-1 system. (c) from both jejunum and ileum sections of the TIM-1 system.

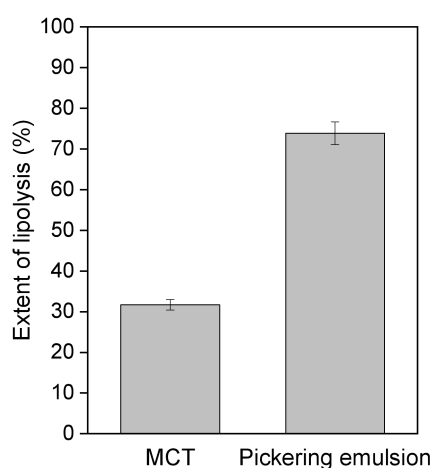
As depicted in Figure VIII-4c, after 360 min of TIM-1 digestion, cumulative

curcumin bioaccessibility from both jejunum and ileum sections was 6.7% and 15.3% for MCT oil and OVT fibril-stabilized Pickering emulsion, respectively. The higher cumulative curcumin bioaccessibility of OVT fibril-stabilized Pickering emulsion was due to faster dissolution rate of hydrophobic nutraceuticals.

3.4. Digestion of OVT fibril-stabilized Pickering emulsions in pH-stat static digestive system



(a)



(b)

Figure VIII-5. (a) Release profile of free fatty acids (FFA) in MCT oil and OVT fibril-stabilized Pickering emulsion in pH-stat digestion model. (b) The extent of

lipolysis of MCT oil and OVT fibril-stabilized Pickering emulsion in pH-stat digestion model.

Due to easy operation pH-stat static digestion model has been the most popular *in vitro* digestion model so far, and pH-stat gastrointestinal digestion model generally includes treatments with simulated gastric fluid and simulated intestinal fluid (3). *In vitro* digestion of OVT fibril-stabilized Pickering emulsion was further investigated using pH-stat static digestion model. Figure VIII-5a shows release profile of free fatty acids (FFA) in MCT oil and OVT fibril-stabilized Pickering emulsion in pH-stat digestion model. It was found that lipolysis rate of OVT fibril-stabilized Pickering emulsion was faster than that of MCT oil, which could be explained as follows. First, since lipid digestion is an interfacial phenomenon, the rate of lipid digestion is closely associated with interfacial surface area around oil droplets. Larger interfacial surface area may facilitate sufficient contact of lipase with oil, which subsequently leads to faster lipolysis kinetics (17). Because OVT fibril-stabilized Pickering emulsion has much larger interfacial area with digestive juice than bulk MCT oil, faster lipolysis occurs in OVT fibril-stabilized Pickering emulsion. Second, direct oil-lipase contact is another factor affecting lipid digestion. In terms of bulk MCT oil, direct oil-lipase contact is immediately available when oil is mixed with digestive juice. For OVT fibril-stabilized Pickering emulsion, interfacial fibril layers locate between oil and lipase at the very start of digestion, which goes against rapid lipid digestion. However, proteases in digestive juice may breakdown interfacial fibril layers immediately (18), which makes direct and sufficient contact of oil with lipase possible shortly.

Eliminating constraint of interfacial fibril barrier facilitates lipolysis of OVT fibril-stabilized Pickering emulsion. The extent of lipolysis is shown in Figure VIII-5b, and the extent of lipolysis was increased from 31.7% to 73.9% upon Pickering emulsification with OVT fibrils.

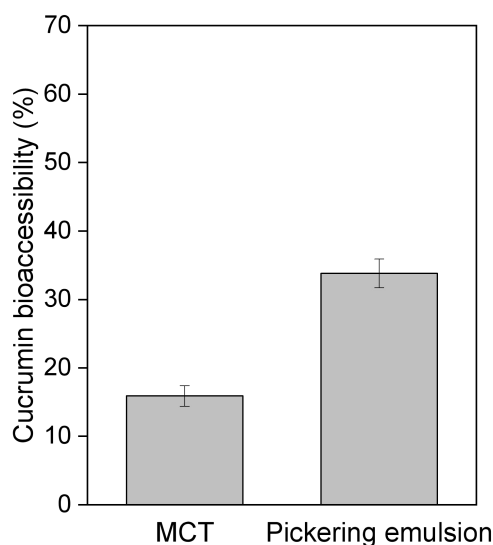


Figure VIII-6. The bioaccessibility of curcumin in MCT oil and OVT fibril-stabilized Pickering emulsion in pH-stat digestion model.

Curcumin bioaccessibility of OVT fibril-stabilized Pickering emulsion and MCT oil in pH-stat static digestion model was shown in Figure VIII-6. It was found that curcumin bioaccessibility was 15.8% and 33.8% for MCT oil and OVT fibril-stabilized Pickering emulsion respectively, suggesting that curcumin bioaccessibility increased by 114% after Pickering emulsification with OVT fibrils. As demonstrated in our previous study, hydrophobic curcumin should be solubilized in the micelle cores before becoming bioaccessible (9). Because more micelles were produced in OVT fibril-stabilized Pickering emulsion due to a larger amount of

released free fatty acids, the bioaccessibility of lipophilic curcumin was enhanced significantly.

It was essential to compare the bioaccessibility result between TIM-1 dynamic digestion model and pH-stat static digestion model. In TIM-1 digestion model, curcumin bioaccessibility increased by around 129% while incorporated into Pickering emulsion droplets. In pH-stat digestion model, after formulated into OVT fibril-stabilized droplets curcumin bioaccessibility increased by around 114%. Interestingly, curcumin bioaccessibility increased by $121\% \pm 8\%$ in both TIM-1 and pH-stat digestion models, suggesting that both TIM-1 and pH-stat digestion models could give almost consistent measurements of improved percentage in curcumin bioaccessibility. In addition, it was found that curcumin bioaccessibility of OVT fibril-stabilized emulsion in TIM-1 dynamic digestion model and pH-stat digestion model was 15.3% and 33.8% respectively, indicating that pH-stat digestion model overestimated curcumin bioaccessibility when compared with TIM-1 digestion model.

4. Conclusion

The chapter showed that interfacial OVT fibril layer around the oil droplets in OVT fibril-stabilized Pickering emulsion led to slowdown of physicochemical degradation and high retention of curcumin. OVT fibril-stabilized Pickering emulsions at different ionic strengths and pHs could provide distinct curcumin protection due to differences in interfacial OVT fibril layers. OVT fibril-stabilized Pickering emulsion at an ionic strength of 1000 mM provided the best curcumin protection. OVT fibril-stabilized Pickering emulsion at pH 6 provided better curcumin

protection than those at pH 2 and 4. In TIM-1 dynamic gastrointestinal digestion model, curcumin bioaccessibility in OVT fibril-stabilized emulsion increased by 129% when compared with that in bulk oil. In pH-stat static gastrointestinal digestion model, OVT fibril-stabilized Pickering emulsions had higher extent of lipolysis than bulk oil, and curcumin bioaccessibility increased by 114% after formulated into OVT fibril-stabilized Pickering emulsion droplets. Interestingly, both TIM-1 dynamic and pH-stat static digestion models could give almost consistent measurements of improved percentage in curcumin bioaccessibility. Curcumin bioaccessibility of OVT fibril-stabilized emulsion in TIM-1 dynamic digestion model and pH-stat static digestion model was 15.3% and 33.8% respectively, indicating that pH-stat static digestion model overestimated curcumin bioaccessibility when compared with TIM-1 dynamic digestion model.

5. References

1. Esatbeyoglu, T., Huebbe, P., Ernst, I. M. A., Chin, D., Wagner, A. E., & Rimbach, G. (2012). Curcumin—From molecule to biological function. *Angewandte Chemie International Edition*, 51(22), 5308–5332.
2. Salem, M., Rohani, S., & Gillies, E. R. (2014). Curcumin, a promising anti-cancer therapeutic: a review of its chemical properties, bioactivity and approaches to cancer cell delivery. *RSC Advances*, 4(21), 10815–10829.
3. Xiao, J., Li, C., & Huang, Q. (2015). Kafirin nanoparticle-stabilized Pickering emulsions as oral delivery vehicles: Physicochemical stability and in vitro digestion profile. *Journal of Agricultural and Food Chemistry*, 63(47), 10263–10270.
4. Ting, Y., Zhao, Q., Xia, C., & Huang, Q. (2015). Using in vitro and in vivo models to evaluate the oral bioavailability of nutraceuticals. *Journal of Agricultural and Food Chemistry*, 63(5), 1332–1338.

5. Van Loo-Bouwman, C. A., Naber, T. H. J., Minekus, M., Van Breemen, R. B., Hulshof, P. J. M., & Schaafsma, G. (2014). Food matrix effects on bioaccessibility of β -carotene can be measured in an in vitro gastrointestinal model. *Journal of Agricultural and Food Chemistry*, 62(4), 950–955.
6. Li, Y., & McClements, D. J. (2010). New mathematical model for interpreting pH-stat digestion profiles: Impact of lipid droplet characteristics on in vitro digestibility. *Journal of Agricultural and Food Chemistry*, 58(13), 8085–8092.
7. Sarkar, A., Goh, K. K. T., Singh, R. P., & Singh, H. (2009). Behaviour of an oil-in-water emulsion stabilized by β -lactoglobulin in an in vitro gastric model. *Food Hydrocolloids*, 23(6), 1563–1569.
8. Minekus, M., Alminger, M., Alvito, P., Ballance, S., Bohn, T., Bourlieu, C., et al. (2014). A standardised static *in vitro* digestion method suitable for food—an international consensus. *Food & Function*, 5(6), 1113–1124.
9. Yu, H., & Huang, Q. (2012). Improving the oral bioavailability of curcumin using novel organogel-based nanoemulsions. *Journal of Agricultural and Food Chemistry*, 60(21), 5373–5379.
10. Martynenko, A., & Chen, Y. (2016). Degradation kinetics of total anthocyanins and formation of polymeric color in blueberry hydrothermodynamic (HTD) processing. *Journal of Food Engineering*, 171, 44–51.
11. de Folter, J. W. J., van Ruijven, M. W. M., & Velikov, K. P. (2012). Oil-in-water Pickering emulsions stabilized by colloidal particles from the water-insoluble protein zein. *Soft Matter*, 8(25), 6807–6815.
12. Wu, J., Shi, M., Li, W., Zhao, L., Wang, Z., Yan, X., et al. (2015). Pickering emulsions stabilized by whey protein nanoparticles prepared by thermal cross-linking. *Colloids and Surfaces B: Biointerfaces*, 127, 96–104.
13. Wei, Z., & Huang, Q. (2019). Edible Pickering emulsions stabilized by ovotransferrin–gum arabic particles. *Food Hydrocolloids*, 89, 590–601.
14. Wang, H., Singh, V., & Behrens, S. H. (2012). Image charge effects on the formation of Pickering emulsions. *The Journal of Physical Chemistry Letters*, 3, 2986–2990.
15. Chevalier, Y., & Bolzinger, M. A. (2013). Emulsions stabilized with solid nanoparticles: Pickering emulsions. *Colloids and Surfaces A: Physicochemical and Engineering Aspects*, 439, 23–34.
16. Ting, Y., Jiang, Y., Lan, Y., Xia, C., Lin, Z., Rogers, M. A., et al. (2015). Viscoelastic emulsion improved the bioaccessibility and oral bioavailability of crystalline compound: A mechanistic study using in vitro and in vivo models. *Molecular Pharmaceutics*, 12(7), 2229–2236.
17. Salvia-Trujillo, L., Qian, C., Martín-Belloso, O., & McClements, D. J. (2013). Influence of particle size on lipid digestion and β -carotene bioaccessibility in emulsions and nanoemulsions. *Food Chemistry*, 141(2), 1472–1480.
18. Bateman, L., Ye, A., & Singh, H. (2010). In vitro digestion of β -lactoglobulin fibrils formed by heat treatment at low pH. *Journal of Agricultural and Food Chemistry*, 58(17), 9800–9808.

CHAPTER IX. DEVELOPMENT OF ORGANOGEL-BASED PICKERING EMULSIONS STABILIZED BY OVOTRANSFERRIN FIBRILS

The work in this chapter has been submitted to Food Hydrocolloids in the title of “Developing organogel-based Pickering emulsions with improved freeze-thaw stability and hesperidin bioaccessibility”.

1. Introduction

Unlike hydrogels in which water is the dispersion medium (1), organogels are a class of gels composed of organic liquids entrapped within three-dimensional cross-linked and thermo-reversible networks (2, 3). Food-grade organogels have found a variety of applications in food industry due to their unique properties such as plasticity, texture, sensory properties, physical stability and so on (3–5). Since animal fats have relatively limited supply and high levels of saturated fats, hydrogenation of vegetable oils has been applied to improve the plasticity of oils for decades, which may result in production of harmful trans fats (3, 4). Developing organogels with desirable plasticity for food applications may function as a promising strategy to replace saturated and trans fats. Another application of organogels is to prolong release of entrapped nutraceuticals, and that's because organogel network offers a physical barrier and delays nutraceutical release (5). Furthermore, organogels have great potential to load more nutraceuticals, since a large quantity of non-dissolved nutraceuticals can be trapped within the gel compartments. In consideration of

application versatility, research about food-grade organogels has recently gained wide scholarly attention (6–10).

Organogel-based delivery systems, which may enhance product stability and improve the dispersibility of nutraceuticals encapsulated in organogels, are relatively novel in food science and technology (4, 8, 10). Organogel-based oil-in-water emulsions, which were first developed for food application by Yu and Huang (8), are a major class of organogel-based delivery systems. However, most of the previous researches about organogel-based emulsions are nanoemulsions stabilized by small-molecular weight surfactants (7, 8, 10). The surfactants applied may have detrimental effects on gut microbiota (11), which seriously limits application of organogel-based nanoemulsions stabilized by surfactants in food industry. To the best of our knowledge, no research related to organogel-based Pickering emulsions stabilized by particles has been reported. It is of great interest to understand the performance of organogel-based Pickering emulsions in delivering nutraceuticals and tolerating environmental stresses during food storage. Considering that protein fibrils are excellent Pickering emulsifiers (12), protein fibrils have potential to stabilize organogel-based Pickering emulsions well. Ovotransferrin (OVT), which occupies 12% of egg white proteins, is a monomeric glycoprotein with 686 amino acids (13). Since OVT fibrils have no cytotoxicity and ovotransferrin (OVT) has abundant resource as well as high nutrition value (13–15), OVT fibrils are highly desirable to be used as potential Pickering stabilizers for organogel-based Pickering emulsions.

Freezing is a common treatment to extend shelf life of food products by

inhibiting the growth of microorganisms, and thawing process is often required before serving. Thus, it is expected that food products should have outstanding freeze-thaw stability (16). However, many food products especially food emulsions may become extremely unstable during freezing-thawing treatment, and improving freeze-thaw stability of food emulsions are associated with various challenges (17). So far, freeze-thaw stability of organogel-based emulsions has seldom been investigated. A previous study demonstrates that semi-solid organogels can withstand several cycles of freezing-thawing process (18), suggesting that organogel-based Pickering emulsions may possibly own excellent freeze-thaw stability. Since some food-grade Pickering emulsions cannot withstand freeze-thaw cycles (19), organogel-based emulsion technique may provide new insight into improving freeze-thaw stability of Pickering emulsions.

Hesperidin is a naturally occurring bioflavonoid with health benefits such as anti-inflammatory effects, and hydrophobic hesperidin has poor water-solubility, which seriously limits its oral bioavailability (20). Thus, improving the bioaccessibility of hesperidin is a critical step to enhance its oral bioavailability and bioefficacy. Food emulsions are common delivery systems to enhance the oral bioavailability of nutraceuticals (8, 21). However, conventional emulsions stabilized by small-molecular weight surfactants often have poor freeze-thaw stability (22). Therefore, due to advantages such as increased extent of lipolysis biopolymer-stabilized Pickering emulsions have been developed to address these two challenges (i.e., bioaccessibility and freeze-thaw stability) (23).

This chapter started with preparation of edible organogels using food-grade organogelators. Afterwards, organogel-based Pickering emulsions stabilized by OVT fibrils were prepared and characterized with tools such as microscopy and rheology. Freeze-thaw stability of organogel-based Pickering emulsions was investigated and compared with that of conventional Pickering emulsions (without organogels). Finally, *in vitro* lipolysis and hesperidin bioaccessibility in organogel-based Pickering emulsions were examined. The chapter may provide a new route to improve freeze-thaw stability of Pickering emulsions and nutraceutical bioaccessibility.

2. Materials and Methods

2.1. Materials

Ovotransferrin (OVT, purity above 88%) was bought from Neova Technologies Inc. (Abbotsford, Canada). Monostearin (glycerol monostearate) was purchased from TCI America (Portland, USA). Sugar ester with a monoester content of 20% (S-370F, esterified with stearic acid) was provided by Mitsubishi-Chemical Foods Corporation (Tokyo, Japan). Soybean oil was purchased from a local market, and hesperidin (HPLC purity 98%) was obtained from Kingherbs Limited (Yongzhou, China). All other chemicals were bought from Sigma-Aldrich (St. Louis, USA), unless otherwise stated. Milli-Q water (Millipore Corporation, Burlington, USA) was applied throughout the experiment.

2.2. Metastable solubility of hesperidin in soybean oil

Different amounts of hesperidin powders (0.5–20 mg/mL) were added into soybean oil. The oil was heated at ~120 °C under stirring for 10 min, followed by

cooling down to ambient temperature. After storage at ambient temperature for 120 h, the presence of non-dissolved (crystalline) hesperidin was checked in hesperidin-loaded soybean oil. Hesperidin-loaded soybean oil was centrifuged at 10,000g for 5 min, and there was non-dissolved hesperidin if precipitation existed in centrifuged soybean oil. For soybean oils without crystalline hesperidin, the maximum amount of dissolved hesperidin was defined as metastable solubility of hesperidin in soybean oil.

2.3. Preparation of hesperidin-loaded organogels

Hesperidin-loaded oil was prepared by dispersing and dissolving hesperidin (10 mg/mL) in soybean oil under heating. Afterwards, desired weight percentage (1–20% (w/v) based on oil) of gelator (monostearin or sugar ester) was added into hesperidin-loaded soybean oil, and the mixture of oil and gelator was heated at 90 °C and a stirring speed of 400 rpm for 10 min in vials, followed by cooling (undisturbed) to room temperature. Prior to characterization of these gel samples, they were aged for 7 days at room temperature (6). Successful preparation of organogels was checked using test tube inverting method (24). The vials were first inverted, and samples without flow over 30 min at room temperature were considered as organogels.

2.4. Gel-sol melting temperatures of organogels

Typical tube inversion method was employed to measure gel-sol melting temperature of organogels (6). Organogels were first structured by different amounts of monostearin or sugar ester in vials, and these vials were inverted and immersed in water-bath (25 °C). Subsequently, the temperature of the water bath was slowly

increased (0.5 °C/min) while observing the flow of organogel samples. Gel-sol melting temperature was determined by flow or no-flow criterion after holding inverted samples at different temperature points for 1 min (24). The temperature at which the organogels melted and flowed was recorded as gel-sol melting temperature (6).

2.5. Fibril Formation

Optimum condition for OVT fibrillation was acquired in preliminary experiments. OVT (60 mg/mL) was dispersed in pH-preset Milli-Q water (pH 2, 100 mM NaCl), followed by stirring until dissolved. Sodium azide (0.02%, w/v) was added to depress microbial growth (25). OVT solution was filtered with 0.22 µm pore-sized syringe filters and transferred into screw-capped vials. OVT solution was heated at 95 °C and a stirring speed of 500 rpm for 26 h in the sealed vials. Afterwards, uniform OVT fibril dispersion was acquired. The obtained OVT fibrils were dialyzed (molecular weight cutoff 1000 Da) against pH-preset Milli-Q water (pH 2, 4 °C) to remove NaCl. OVT fibril dispersion was carefully diluted to a final concentration of 40 mg/mL with addition of pH-preset Milli-Q water (pH 2). OVT fibril dispersion was stored in the refrigerator (4 °C) and used within 24 h.

2.6. Atomic force microscopy (AFM)

Morphology of OVT fibrils was observed using tapping-mode atomic force microscopy (Veeco NanoScope IIIA Multimode, Santa Barbara, USA). Prior to AFM analysis, OVT fibrils were diluted to facilitate imaging of single fibrils, and the fibril morphology was not affected by dilution (26). The fresh mica surface was prepared by

cleaving mica of uniform thickness, and OVT fibrils were spread onto the surface, followed by drying with a nitrogen stream. Data analysis was performed using NanoScope Analysis Software and FiberApp (27).

2.7. Preparation of organogel-based Pickering emulsion

Hesperidin-loaded organogels structured by 3% (w/v) monostearin were applied in the rest of this study. OVT fibril dispersions (40 mg/mL) were mixed with hesperidin-loaded organogels to obtain mixtures with different oil fractions φ (0.5–0.85) at room temperature. In order to inhibit microbial growth, sodium azide (0.02%, w/v) was added. An Ultra-Turrax T25 (IKA-Werke GMBH & CO., Germany) was applied to homogenize the mixtures at 12000 rpm for 3 min. Upon emulsion formation, the emulsion type was identified by measuring the dispersibility of organogel-based Pickering emulsions stabilized by OVT fibrils. Oil-in-water (water-in-oil) emulsions stayed immiscible in soybean oil (water), but dispersed rapidly in water (soybean oil) (28).

The emulsified phase volume fraction of Pickering emulsions was determined as:

$$\text{Emulsified phase volume fraction} = (H_e/H_t) \times 100 \quad (1)$$

Here H_e and H_t were the height of emulsified phase and total emulsion height, respectively (29). Long-term stability of emulsions was studied during 2-week storage at room temperature (29), and stability index was calculated as:

$$\text{stability index} = \frac{\text{emulsified phase volume fraction after 2-week storage}}{\text{emulsified phase volume fraction of freshly prepared emulsions}} \times 100 \quad (2)$$

The rest of this study focused on organogel-based Pickering emulsion with oil fraction

$\varphi = 0.7$.

2.8. Microstructure of organogel-based Pickering emulsion

Microstructures of organogel-based Pickering emulsion ($\phi = 0.7$) stabilized by OVT fibrils were observed employing optical microscope (Nikon Eclipse TE 2000-U, Nikon Corporation, Tokyo, Japan). To facilitate microstructure observation, the Pickering emulsion was diluted 100 times with pH-preset Milli-Q water (pH 2) based on preliminary experiments. The droplet sizes of organogel-based Pickering emulsion were estimated using Image J software (30), and 500 emulsion droplets selected randomly in different captured images were measured to estimate emulsion droplet size.

Fluorescence microscopy technique was applied to verify adsorption of OVT fibrils at emulsion interfaces. Nile red and rhodamine B were used to stain oil phase and OVT fibrils, respectively. The organogel-based Pickering emulsion labeled with individual fluorescence dye (Nile red or rhodamine B) was subject to optical microscopy observation under fluorescence field.

2.9. Rheological Measurements

Rheological properties of organogels and organogel-based Pickering emulsions stabilized by OVT fibrils were investigated using a Discovery HR-2 rheometer (TA Instruments, New Castle, USA) with a parallel plate geometry (diameter 25 mm, gap 1 mm). Around 0.3 mL of the sample was carefully deposited over the plateau of the rheometer using measuring spoons prior to measurement (31). Apparent viscosities of emulsions as function of shear rate (0.1–10 1/s) were measured by performing steady-state flow measurements at $25 \pm 0.1^\circ\text{C}$. Linear viscoelastic regions (LVE) of

samples were acquired using dynamic strain sweep test. Dynamic frequency sweep tests were conducted at a fixed strain amplitude of 0.2% (within the LVE), and storage modulus (G') as well as loss modulus (G'') of samples were recorded as function of sweep frequency (0.1–20 rad/s).

2.10. Freeze-thaw treatment of Pickering emulsions

Freeze-thaw stability of organogel-based Pickering emulsions stabilized by OVT fibrils and conventional Pickering emulsions stabilized by OVT fibrils was compared. For this purpose, conventional Pickering emulsions stabilized by OVT fibrils were prepared according to the following procedures. Hesperidin-loaded oil was prepared by dissolving hesperidin (4 mg/mL) in soybean oil under heating. OVT fibril dispersions (40 mg/mL) were mixed with hesperidin-loaded soybean oil to obtain mixtures with oil fractions of 0.7, followed by homogenization procedures as described in preparation of organogel-based Pickering emulsion. Considering that ionic strength could improve freeze-thaw stability of Pickering emulsions (19), impact of ionic strength on freeze-thaw stability of OVT fibril-stabilized Pickering emulsions was also studied. Sodium chloride was added to OVT fibril dispersions to reach different ionic strengths (100, 300 and 500 mM) before emulsification, and Pickering emulsions stabilized by OVT fibrils at different ionic strengths were fabricated via the aforementioned homogenization method.

In terms of one freeze-thaw cycle, Pickering emulsion samples were incubated in a refrigerator ($-20\text{ }^{\circ}\text{C}$) for 24 h. Subsequently, the emulsion samples were thawed in an oven ($30\text{ }^{\circ}\text{C}$) for 2 h (32). Visual appearance of all emulsion samples was

examined to evaluate freeze-thaw stability. For organogel-based Pickering emulsions stabilized by OVT fibrils, after completion of one freeze-thaw cycle, they were further treated for another two freeze-thaw cycles.

2.11. Lipolysis and bioaccessibility of hesperidin in organogel-based Pickering emulsions

Simulated gastric fluid without pepsin was prepared by dissolving 1 g of sodium chloride into 500 mL of pH-adjusted water (pH 1.2) (23). The samples (organogel and organogel-based Pickering emulsion stabilized by OVT fibrils) containing 2 g of oil were mixed with 16 mL of simulated gastric fluid, which were subsequently incubated under continuous agitation in a water bath (37.0 ± 0.1 °C). To start simulated gastric digestion, pepsin dissolved in 2 mL of simulated gastric fluid was added to make a final pepsin concentration of 1.6 mg/mL. After a period of digestion (120 min), pH of digesta was elevated to 7.5 to inactivate pepsin and end gastric digestion (23).

Simulated intestinal fluid was obtained by dissolving pancreatin, bile salt and CaCl_2 in pH-adjusted water (pH 7.5). The gastric digesta were mixed with an equal volume of simulated intestinal fluid to initiate intestinal digestion, and final concentrations of bile salt, CaCl_2 and lipase were 5 mg/mL, 5 mM and 1.6 mg/mL respectively (33). The mixture was incubated under stirring in a water bath (37.0 ± 0.1 °C) for 120 min. Since digestion of triacylglycerols could release free fatty acids (FFA) and lead to pH decrease during intestinal digestion, 0.25 M NaOH was added manually to maintain pH at 7.5. The volume of added NaOH solution was recorded over time during simulated intestinal digestion. The digesta were centrifuged

at 10000 g for 40 min after simulated gastrointestinal digestion, and the clear micelle phase was carefully collected for analysis of hesperidin bioaccessibility.

Release of free fatty acids (FFA) could be employed to analyze lipolysis of samples. It was assumed that digestion of 1 mol of triglycerides consumed 2 mol of FFA (8, 23), and the fraction of FFA released was determined as follows:

$$\% \text{ FFA} = 100 \times \frac{M_{\text{soyoil}} \times V_{\text{NaOH}} \times m_{\text{NaOH}}}{w_{\text{soyoil}} \times 2} \quad (3)$$

where M_{soyoil} was the molecular mass of the soybean oil (in g/mol), V_{NaOH} was the volume of NaOH solution used to neutralize the released FFA (in L), m_{NaOH} was the molarity of NaOH solution (in mol/L), and w_{soyoil} was the total mass of initially present soybean oil (in g) (34). The average molecular mass of soybean oil was taken as 920 g/mol (35). Since digestion of 1 mol of monostearin could consume 1 mol of NaOH (8), impact of monostearin was considered while calculating the fraction of FFA.

The amount of hesperidin in the clear micelle phase was determined using HPLC (high-performance liquid chromatography), and hesperidin bioaccessibility was calculated as follows:

$$\% \text{ bioaccessibility} = \frac{\text{hesperidin content in the micelle phase}}{\text{total hesperidin content in the formulations}} \times 100\% \quad (4)$$

2.12. High-performance liquid chromatography (HPLC) quantification of hesperidin

An UltiMate 3000 HPLC system (Dionex, Sunnyvale, USA) with a Synergi hydro RP (Phenomenex, Macclesfield, UK) column (250×4.6 mm i.d.) was used to quantify hesperidin. The HPLC mobile phase consisted of (A) water containing 0.1%

phosphoric acid and (B) acetonitrile. Elution condition was set as follows: 0–10 min, A went from 60% to 45% linearly; 10–15 min, linear gradient from 45% to 30% A; 15–17 min, A went from 30% to 0% linearly; 17–24 min, linear gradient from 0% to 60% A. Quantification of hesperidin based on a standard curve of hesperidin was carried out at wavelength 286 nm.

2.13. Statistical analysis

All experiments were conducted in triplicate. All statistical analysis was performed using OriginPro 2018.

3. Results and Discussion

3.1. Formation and characterization of food-grade organogel

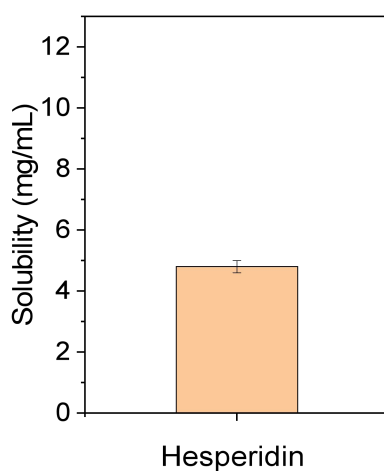


Figure IX-1. Metastable solubility of hesperidin in soybean oil.

Since soybean oil has the highest production among all vegetable oils and most consumers have the habit of purchasing soybean oil (36), soybean oil-based organogels were developed in this study. While designing organogel-based system for hesperidin delivery, the first step was to know solubility of hesperidin in soybean oil.

Solubility of many hydrophobic nutraceuticals such as curcumin and hesperidin is often very low in vegetable oils at room temperature. To enhance loading amount of nutraceuticals in oils, these nutraceuticals can be dissolved in heated oils and remain soluble without any precipitation at room temperature (9). Since a previous study demonstrates that thermal treatment for a short period of time causes no degradation of hesperidin (37), hesperidin solubility can be ameliorated via dissolution in heated oils. Figure IX-1 shows that metastable solubility of hesperidin in soybean oil was 4.8 ± 0.2 mg/mL. Considering that plenty of non-dissolved hesperidin might be trapped within organogel network, loading amount of hesperidin in soybean oil-based organogels was set as 10 mg/mL, which was about twice as much as metastable solubility of hesperidin in soybean oil.

Two food-grade organogelators (monostearin and sugar ester) were chosen to fabricate soybean oil-based organogels. As shown in Table IX-1, organogels could be prepared using 3–20 % (w/v) monostearin, and the minimum concentration of sugar ester required to form organogels was 15 % (w/v), indicating that monostearin was more effective in structuring soybean oil. The difference in the minimum gelling concentration was ascribed to distinct organizations. Monostearin is an organogelator with self-assembly mechanism, and organogels are generated through self-organization of monostearin within oil phases. Sugar ester is an organogelator with crystal particle mechanism, and sugar esters may form crystals throughout the nucleation to produce organogels (5). Since low concentrations of structuring agents helped to reduce product cost, 3 % (w/v) monostearin was chosen to structure soybean

oil-based organogels in the rest of this study. As shown in Figure IX-2, organogels structured by 3 % (w/v) monostearin had little light transmittance and withstood inversion without any gravitational flow for 30 min, implying firm organogel network.

Table IX-1. Gel-sol melting temperature of soybean oil-based organogels structured by different amounts of monostearin or sugar ester

Organogel structured by	Gel formation	T_m (°C)
1% (w/v) monostearin	No	—
3% (w/v) monostearin	Yes	44.0±0.5 ^a
5% (w/v) monostearin	Yes	49.0±0.5 ^c
10% (w/v) monostearin	Yes	54.0±0.5 ^d
15% (w/v) monostearin	Yes	59.5±0.5 ^e
20% (w/v) monostearin	Yes	65.5±0.5 ^f
1% (w/v) sugar ester	No	—
3% (w/v) sugar ester	No	—
5% (w/v) sugar ester	No	—
10% (w/v) sugar ester	No	—
15% (w/v) sugar ester	Yes	46.0±0.5 ^b
20% (w/v) sugar ester	Yes	48.5±0.5 ^c

Values are means±SD (n=3). Different superscript letters in the table indicate significant differences ($p < 0.05$).

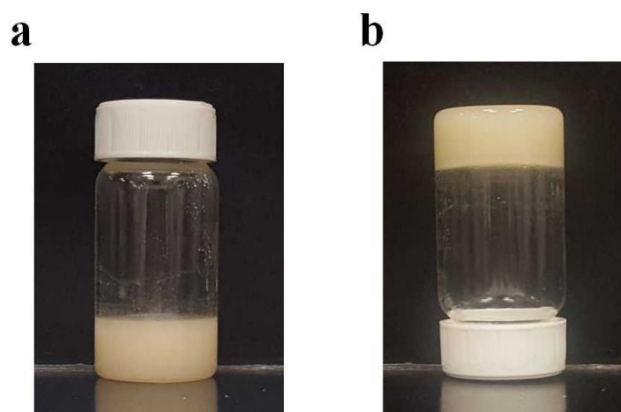


Figure IX-2. (a) Photograph of hesperidin-loaded organogel structured by 3% (w/v)

monostearin. (b) Photograph of inverted hesperidin-loaded organogel after inverting the vial for 30 min.

Since organogels are thermoreversible and can transform into the sol phase at higher temperature (5, 6), gel-sol melting temperature of organogels was investigated and shown in Table IX-1. Melting temperatures of soybean oil-based organogels ranged from 44.0 °C to 65.5 °C, indicating melting behavior of these resultant organogels was different. It was found that there was a rise in melting temperature of organogels when organogelator concentration increased, which could be ascribed to an increase in intermolecular hydrogen bonding (2). It was noteworthy that organogels structured by 3 % (w/v) monostearin had the lowest gel-sol melting temperature (44.0±0.5 °C) among all investigated gels. It was apparent that organogel in sol state facilitated adsorption of fibrils at emulsion interfaces. During the homogenization, high speed shearing and shear friction heat could transform gel-state soybean oil structured by 3 % (w/v) monostearin into sol-state at relatively low temperatures, which facilitated OVT fibril adsorption. After emulsion formation, organogel might turn into gel state again at room temperature. Based on these understandings, organogels structured by 3 % (w/v) monostearin had great potential to be integrated into organogel-based delivery systems at relatively low temperatures.

3.2. Preparation and characterization of organogel-based Pickering emulsions stabilized by OVT fibrils

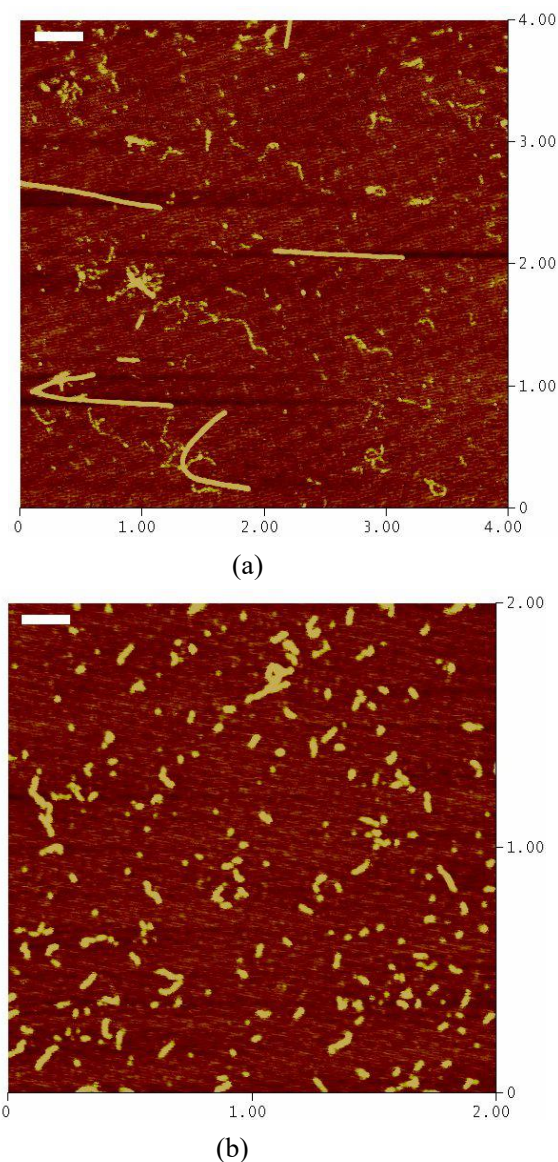


Figure IX-3. (a) AFM image of long OVT fibrils. The scan size is 4 μm \times 4 μm , and the scale bar in the upper left corner represents 400 nm. (b) AFM image of short OVT fibrils. The scan size is 2 μm \times 2 μm , and the scale bar represents 200 nm. In both images z scale is 5 nm.

Protein fibrils, which are anisotropic protein particles with high aspect ratio, are insoluble and dominated by β -sheet structures (38, 39). Recent studies demonstrate that protein fibrils can stabilize Pickering emulsions well (12, 40), so OVT fibrils were prepared to stabilize organogel-based Pickering emulsions here. Since agitation and high ionic strength is beneficial to fibril formation (41), OVT fibrils were

prepared with constant stirring (500 rpm) and 100 mM NaCl. The mechanism of OVT fibrillation was a balance of hydrophobic short-range attraction, cooperative hydrogen bonds and weak electrostatic long-range repulsion (14). Figure IX-3 shows AFM morphology of resultant OVT fibrils. Apart from long OVT fibrils (with contour length of 200–2000 nm), short OVT fibrils (with contour length below 200 nm) coexisted. The mixture of long and short OVT fibrils was used without separation in following emulsion research.

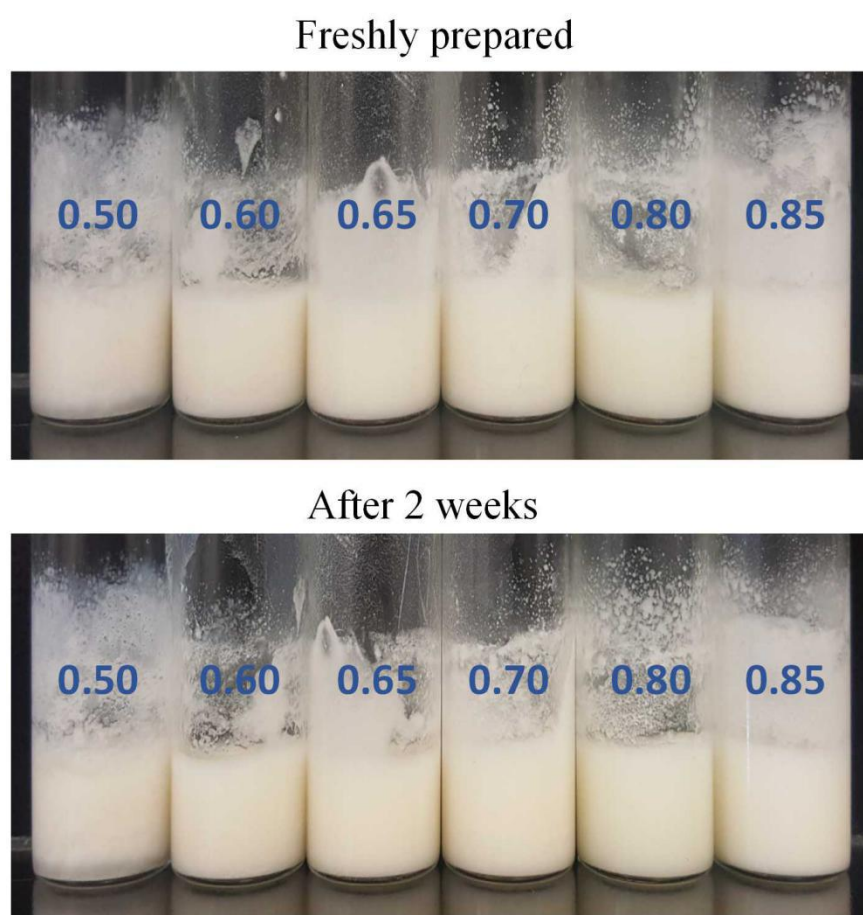


Figure IX-4. Visual observation of organogel-based Pickering emulsions stabilized by OVT fibrils at various ϕ (0.50–0.85) before and after storage at room temperature. The oil fraction ϕ is labeled in each vial.

Figure IX-4 shows freshly prepared organogel-based Pickering emulsions stabilized by OVT fibrils at various oil fractions. Because all of investigated

emulsions could disperse readily in water but not in soybean oil, organogel-based Pickering emulsions stabilized by OVT fibrils were identified as oil-in-water emulsions. Table IX-2 indicates that stability index of all organogel-based Pickering emulsions was above 98.3%, implying that these Pickering emulsions were quite stable during 2-week storage. As shown in Table IX-2, all emulsions had an emulsified volume fraction above 85.5%, and organogel-based Pickering emulsions with oil fractions of 0.6–0.85 had emulsified phase alone and no serum phase. It was worthwhile to note that OVT fibrils could stabilize organogel-based Pickering emulsions excellently at such high internal phase volume ratio, since emulsions with oil fractions of 0.8–0.85 could be classified as high internal phase Pickering emulsions and there were only a few examples of food-grade high internal phase Pickering emulsions (42–46). Although emulsions with higher internal phase ratio may load more hydrophobic nutraceuticals at the same emulsion volume, fluidity needs to be taken into account while developing organogel-based delivery systems. In our experiments it was found that organogel-based Pickering emulsions with oil fractions of 0.8–0.85 had very limited flowability due to high viscosity, which could hinder application of organogel-based Pickering emulsions. Since lower serum phase existed in emulsion with oil fraction of 0.5, the inhomogeneous appearance impeded its food application. In addition, as we decided to compare freeze-thaw stability of organogel-based Pickering emulsions and conventional Pickering emulsions afterwards, we should prepare these two emulsions at the same oil ratio. Since conventional Pickering emulsions stabilized by OVT fibrils had homogeneous

appearance with good stability only at oil fraction around 70% in our preliminary experiments, organogel-based Pickering emulsion with 70% oil should be selected to facilitate comparison in freeze-thaw stability. After an overall consideration mentioned above, organogel-based Pickering emulsion with an oil fraction of 0.7 was studied during the rest of this study.

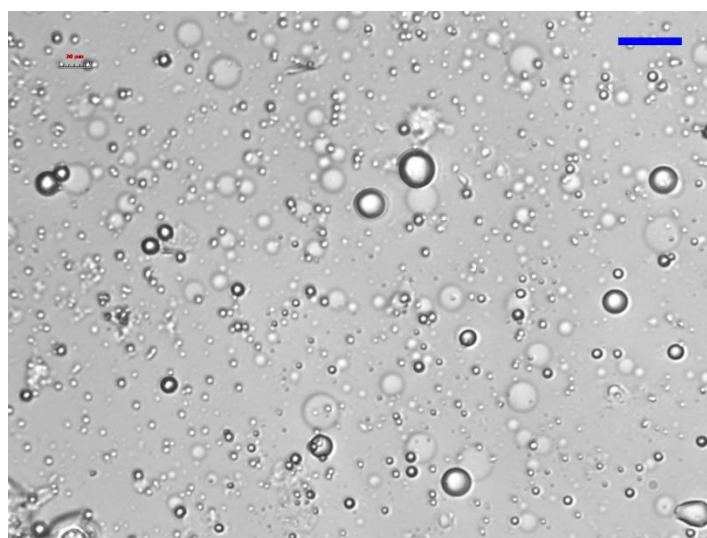
Table IX-2. Emulsified phase volume fraction and stability index of organogel-based Pickering emulsions stabilized by OVT fibrils at different oil fractions

Emulsions with oil fraction of	Emulsified phase volume (%)		Stability index
	Fresh	After 2 weeks	
0.50	85.7±0.2 ^a	84.3±0.3 ^a	98.4±0.2 ^a
0.60	100.0±0.1 ^b	100.0±0.1 ^b	100.0±0.1 ^b
0.65	100.0±0.1 ^b	100.0±0.1 ^b	100.0±0.1 ^b
0.70	100.0±0.1 ^b	100.0±0.1 ^b	100.0±0.1 ^b
0.80	100.0±0.1 ^b	100.0±0.1 ^b	100.0±0.1 ^b
0.85	100.0±0.1 ^b	100.0±0.1 ^b	100.0±0.1 ^b

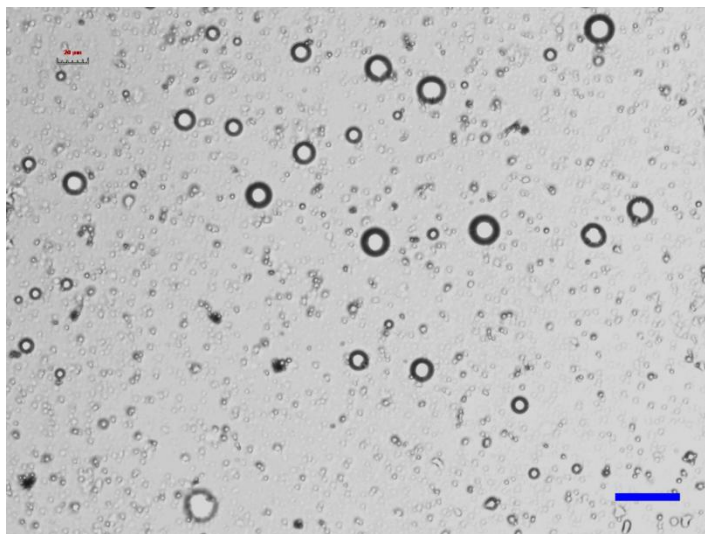
Values are means±SD (n=3). Different superscript letters for the same column indicate significant differences ($p < 0.05$).

Figure IX-5a shows microstructure of organogel-based Pickering emulsion with an oil fraction of 0.7. With the aid of Image J software (30), it was found that most of emulsion droplets were spherical-like ones with an average droplet diameter of $14.5 \pm 1.3 \mu\text{m}$. Formation of spherical-like organogel-based Pickering emulsion droplets may be owing to vulnerability of organogels structured by 3 % (w/v) monostearin to melting. Unlike gel-state soybean oil, sol-state soybean oil is conducive to forming spherical-like emulsion droplets. While cooling back to room

temperature, sol-state soybean oil in these emulsion droplets forms organogel again. Meanwhile, it was observed that a few non-spherical emulsion droplets existed in Figure IX-5a, which could possibly be explained by following speculation. Although high speed shearing (strong agitation similar to sonication) and shear friction heat can transform most of gel-state soybean oil into sol-state one, a few organogels may still maintain weak gel network and exist as small-sized micro-organogels (47). The existence of micro-organogels will be explored by additional experiments in our future study about micro-organogels. The shapes of some emulsion droplets may depend on the shape of fragmented micro-organogels, leading to occurrence of some non-spherical Pickering emulsion droplets. Previous studies demonstrate that stable non-spherical emulsion droplets can be detected for some Pickering emulsion samples (48, 49), and non-spherical Pickering emulsion droplets may facilitate better emulsion stability (49).



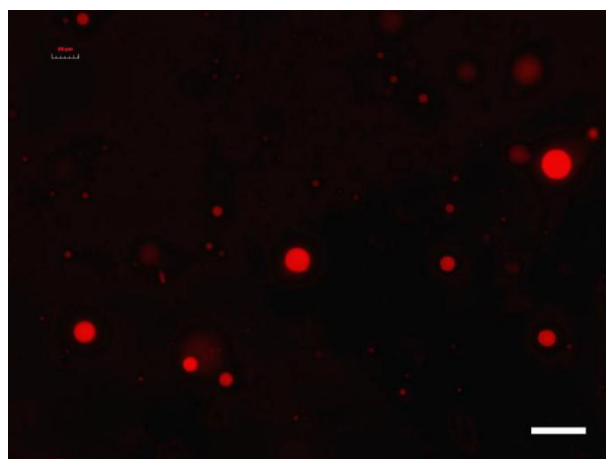
(a)



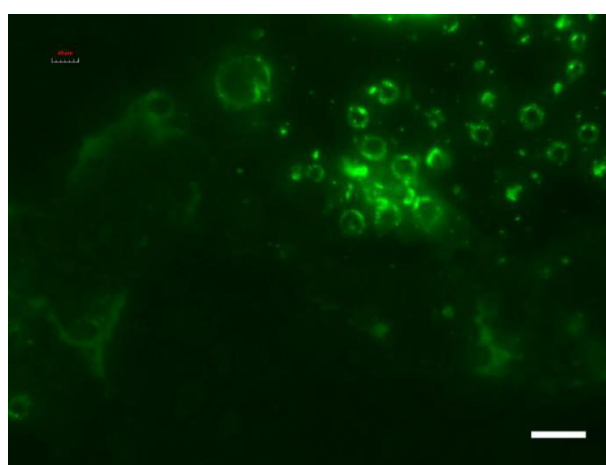
(b)

Figure IX-5. (a) Optical microscopic image of freshly prepared organogel-based Pickering emulsion (oil fraction $\phi = 0.7$, ionic strength = 0) stabilized by OVT fibrils. The blue scale bar represents 40 μm . (b) Optical microscopic image of organogel-based Pickering emulsion (oil fraction $\phi = 0.7$, ionic strength = 0) stabilized by OVT fibrils after three freeze-thaw cycles. The blue scale bar represents 40 μm .

Figure IX-6 shows fluorescence pictures of organogel-based Pickering emulsion labeled with individual fluorescence dyes. Red spherical-like regions in Figure IX-6a corresponded to dyed oil phase of emulsion droplets, and green fluorescence glowing layers in Figure IX-6b corresponded to dyed OVT fibrils at the oil-water interface. The fluorescence images indicated that organogel-based emulsion was indeed stabilized by OVT fibrils at the emulsion interface.



(a)



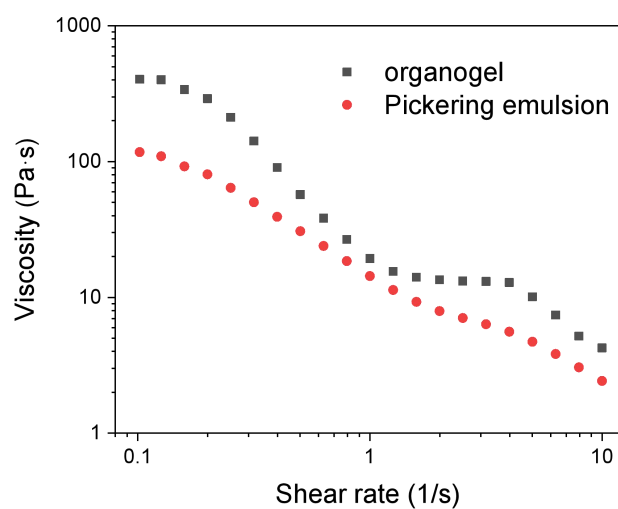
(b)

Figure IX-6. (a) Fluorescence image of organogel-based Pickering emulsion (stained with Nile red only). Nile Red was used to stain the oil phase (=red color). (b) Fluorescence image of organogel-based Pickering emulsion (stained with rhodamine B only). Rhodamine B was used to stain OVT fibrils (=green color). The white scale bar in all images represents 40 μm .

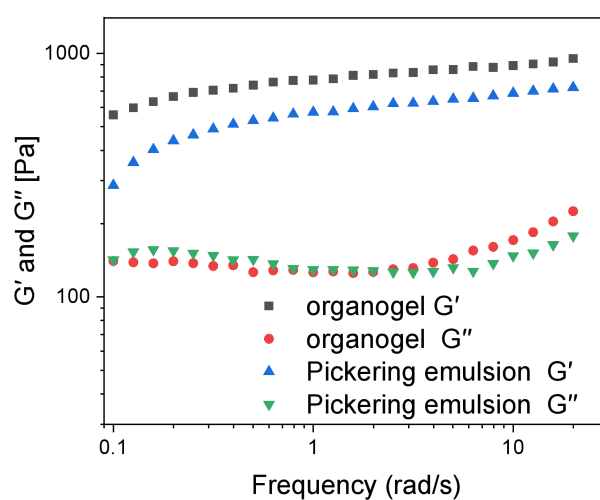
Rheology is closely linked with application of food products and vital to storage stability (50). Herein, rheological properties of organogel-based Pickering emulsions stabilized by OVT fibrils were investigated. As depicted in Figure IX-7a, organogel-based Pickering emulsion had high viscosity ($117.5 \pm 8.9 \text{ Pa}\cdot\text{s}$ at shear rate of 0.1 1/s), which facilitated long-term physical stability of emulsions (50). This was confirmed by stability data shown in Figure IX-4 and Table IX-2. When compared

with soybean oil-based organogel, organogel-based Pickering emulsion had lower viscosity. The lower viscosity of organogel-based Pickering emulsion than organogel was also confirmed by test tube inversion test. Inversion of organogel-based Pickering emulsion resulted in sample flow, and no flow existed in the organogel as shown in Figure IX-2b. Since organogel-based Pickering emulsion was an oil-in-water emulsion, organogel-based Pickering emulsion could have relatively loosely mechanical network with weaker molecular interactions, and the decrease in resistance to flow resulted in lower viscosity than the organogel. Because organogels may be too viscous for some particular applications (concentrated beverages, etc), decreasing viscosity via organogel-based Pickering emulsion technology may broaden use of organogel-based systems. Figure IX-7a also shows that both organogel and organogel-based Pickering emulsion displayed shear-thinning behavior. The prominent shear-thinning behavior of organogels is ascribed to breakdown of gel structures at high shearing rates, which is also reported in a shellac oleogel study (51). For organogel-based Pickering emulsion, the emulsion droplets may rearrange in the flow direction, and an ordered distribution of emulsion droplets can result in a decrease in resistance to flow, leading to shear-thinning nature of emulsion. Figure IX-7b shows storage and loss modulus data. Since storage modulus G' and loss modulus G'' represented elastic and viscous part of emulsion systems (52), the transcend of G' over G'' indicated gel-like structures of soybean oil-based organogel and organogel-based Pickering emulsion stabilized by OVT fibrils. It was observed that organogel-based Pickering emulsion had lower storage modulus than organogel,

implying lower gel strength. Generally, loss modulus G'' represented the deformation energy dissipated via internal friction during flowing (52). It was observed that G'' of organogel and organogel-based Pickering emulsion was almost the same at frequency range of 0.1–5 rad/s, indicating that there was not significant difference in lost deformation energy of two samples.



(a)



(b)

Figure IX-7. (a) Apparent viscosity of organogel and organogel-based Pickering emulsion (oil fraction $\phi = 0.7$, ionic strength = 0) stabilized by OVT fibrils. (b) Storage modulus (G') and loss modulus (G'') of organogel and organogel-based

Pickering emulsion (oil fraction $\phi = 0.7$, ionic strength = 0) stabilized by OVT fibrils.

3.3. Freeze-thaw stability of organogel-based Pickering emulsions stabilized by OVT fibrils

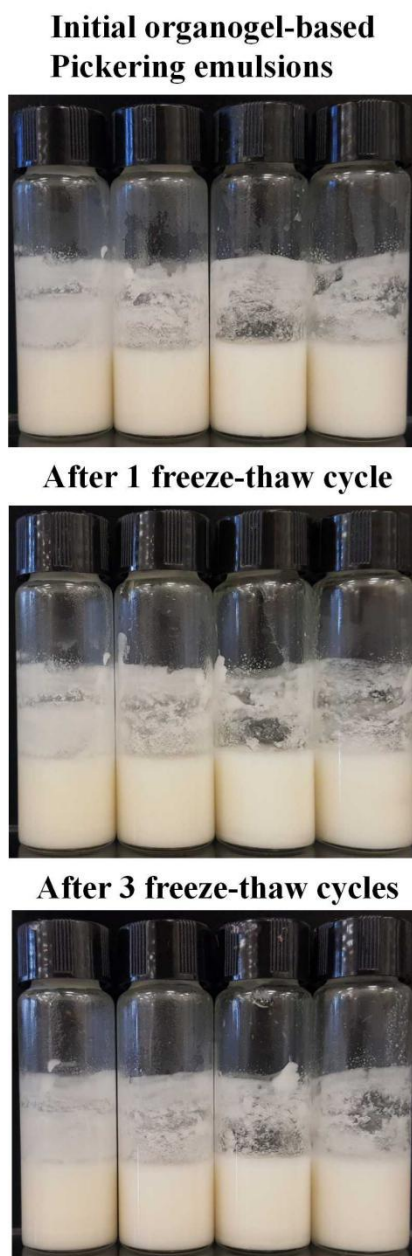


Figure IX-8. Visual observation of initial and freeze-thawed organogel-based Pickering emulsions (oil fraction $\phi = 0.7$) stabilized by OVT fibrils. Organogel-based Pickering emulsions (from left to right) were prepared at an ionic strength of 0, 100, 300 and 500 mM, respectively.

As depicted in Figure IX-8, organogel-based Pickering emulsions stabilized by OVT fibrils at different ionic strengths could withstand 3 freeze-thaw cycles, and Figure IX-9 shows that organogel-based Pickering emulsions were quite stable against either freezing or thawing treatment. Figure IX-5b shows microstructures of organogel-based Pickering emulsion droplets after freeze-thaw cycles, which was similar to those of freshly prepared emulsion droplets in Figure IX-5a. Stable microstructures confirmed outstanding freeze-thaw stability of organogel-based Pickering emulsions.



(a)



(b)

Figure IX-9. (a) Visual observation of organogel-based Pickering emulsions stabilized by OVT fibrils after freezing for 24 h but without thawing (b) Visual observation of organogel-based Pickering emulsions stabilized by OVT fibrils after freezing for 24 h and thawing for 0.5 h. Organogel-based Pickering emulsions (from left to right) were prepared at an ionic strength of 0, 100, 300 and 500 mM,

respectively.



Figure IX-10. Visual observation of initial and freeze-thawed conventional Pickering emulsions stabilized by OVT fibrils (oil fraction $\phi = 0.7$). Conventional Pickering emulsions (from left to right) were prepared at an ionic strength of 0, 100, 300 and 500 mM, respectively.

To better understand influence of organogel incorporation into Pickering emulsions on freeze-thaw stability, freeze-thaw stability of conventional Pickering emulsions (without organogels) stabilized by OVT fibrils was also studied. Figure IX-10 and Table IX-3 show that freshly prepared conventional Pickering emulsions were homogeneous and contained almost only emulsified phase. As shown in Figure IX-10, conventional Pickering emulsions were highly unstable after 1 freeze-thaw cycle and two phases (OVT fibril phase and oil phase) were almost fully separated,

indicating poor freeze-thaw stability.

Table IX-3. Emulsified phase volume fraction of freshly prepared conventional Pickering emulsions stabilized by OVT fibrils

Emulsions prepared at ionic strength of	Upper phase	oil phase	Lower phase	serum	Emulsified volume (%)	phase
0	None		None		100.0±0.1	
100 mM	None		None		100.0±0.1	
300 mM	None		None		100.0±0.1	
500 mM	None		None		100.0±0.1	



(a)



(b)

Figure IX-11. (a) Visual observation of conventional Pickering emulsions stabilized by OVT fibrils after freezing for 24 h but without thawing (b) Visual observation of conventional Pickering emulsions stabilized by OVT fibrils after freezing for 24 h and thawing for 0.5 h. Conventional Pickering emulsions (from left to right) were prepared at an ionic strength of 0, 100, 300 and 500 mM, respectively.

Table IX-4. Emulsified phase volume fraction of conventional Pickering emulsions stabilized by OVT fibrils after freezing for 24 h but without thawing

Emulsions prepared at ionic strength of	Upper phase	oil	Lower phase	serum	Emulsified volume (%)	phase
0	None		Exist		95.5±0.3 ^a	
100 mM	None		Exist		96.7±0.3 ^b	
300 mM	None		Exist		97.5±0.3 ^c	
500 mM	Exist		None		97.8±0.2 ^c	

Values are means±SD (n=3). Different superscript letters for the same column indicate significant differences ($p < 0.05$).

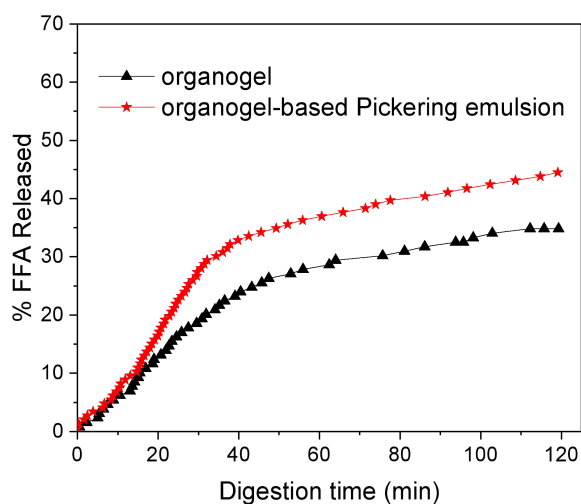
To determine whether freezing or thawing process caused collapse of conventional Pickering emulsions stabilized by OVT fibrils, stability of conventional Pickering emulsions after freezing but without thawing was studied. As shown in Figure IX-11 and Table IX-4, after freezing emulsified phase volume in all conventional Pickering emulsions slightly decreased and light oiling-off was observed in conventional Pickering emulsion at an ionic strength of 500 mM, suggesting that freezing might deteriorate the emulsion stability. Considering that emulsified phase volume fraction of conventional Pickering emulsions after freezing but without thawing was higher than 95% and large-scale emulsion breakdown occurred just after thawing for 0.5 h, it could be inferred that thawing process could destroy stability of conventional Pickering emulsions stabilized by OVT fibrils. Although emulsion products could be considered as stable if there were no visible changes in its overall appearance (17), there was still a possibility that serious emulsion breakdown occurred during freeze process but could only be observed after thawing.

Although concentrated conventional Pickering emulsions had gel-like structures and existence of high ionic strength could strengthen interfacial particle films due to weakened image charge repulsion as well as inhibit ice crystal formation (19, 32, 53), which might significantly improve freeze-thaw stability, conventional Pickering emulsions stabilized by OVT fibrils still could not withstand freeze-thaw treatments. The excellent freeze-thaw stability of organogel-based Pickering emulsions stabilized by OVT fibrils can be explained by following reasons. First, one instability mechanism of freeze-thawed emulsions is that formed ice crystals can penetrate into oil droplets and subsequently disrupt interfacial emulsifier layers, which leads to severe coalescence upon thawing (17). Because organogel in emulsion droplets exist in semi-solid state (3), it is hard for ice crystals to penetrate into organogel phase and cause damage to interfacial layers, which contributes to better thawing stability. Second, for conventional Pickering emulsion, a large amount of ice crystals are generated during freezing, forcing fat droplets to gather in concentrated nonfrozen aqueous phase, which promotes droplet coalescence and oiling-off during thawing (17). Since coalescence of emulsion droplets composed of crystalline fat can be strongly inhibited (17), organogel-based Pickering emulsion may have very limited coalescence and eventual freeze-thaw stability. Generally, partial coalescence of emulsion droplets only occurs when partially crystalline fat droplets are clumped together (17). Considering that fats in organogel-based Pickering emulsion droplet exist in the gel state both at room temperature and freezing temperature, it may be inferred that partial coalescence does not exist in organogel-based Pickering emulsion

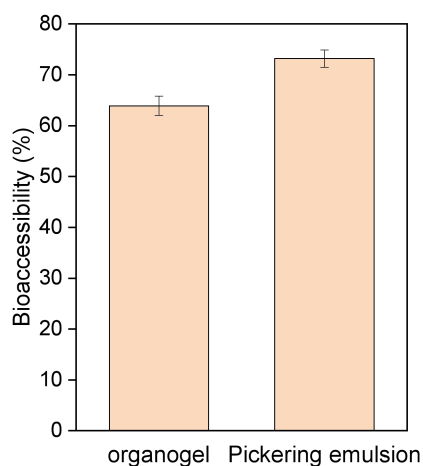
system.

3.4. Lipolysis and bioaccessibility of hesperidin in organogel-based Pickering emulsion

Lipid digestibility during *in vitro* digestion could be determined by analysis of lipolysis (7). Figure IX-12a shows that fraction of FFA released in organogel-based Pickering emulsion (44.5%) was higher than that in soybean oil-based organogel (34.8%), indicating a greater extent of lipolysis. A more complete lipid digestion in organogel-based Pickering emulsion may be accounted for by several factors. First, organogel-based Pickering emulsion can be dispersed easily in simulated intestinal juice, but organogel has low flowability in water-based digestive juice. Chunks of organogel may be suspended, which goes against ample contact between oil phase and lipase. Second, since organogel-based Pickering emulsion has a small droplet size ($\sim 14.5 \mu\text{m}$), organogel-based Pickering emulsion has a much larger interfacial area than bulk organogel, which facilitates an increase in the lipase-oil interface and faster lipolysis. Third, for organogel-based Pickering emulsion, although interfacial fibril films are located between organogel and lipase during digestion, protease such as pepsin and trypsin may breakdown structures of OVT fibrils and dissociate interfacial emulsifier film (54), which makes sufficient oil-lipase contact and rapid lipolysis possible.



(a)



(b)

Figure IX-12. (a) Release profile of free fatty acids (FFA) in organogel and organogel-based Pickering emulsion (oil fraction $\phi = 0.7$, ionic strength = 0) stabilized by OVT fibrils. (b) The bioaccessibility of hesperidin in organogel and organogel-based Pickering emulsion (oil fraction $\phi = 0.7$, ionic strength = 0) stabilized by OVT fibrils after *in vitro* digestion.

Gastrointestinal fate of delivered hesperidin was investigated in terms of *in vitro* bioaccessibility. As shown in Figure IX-12b, hesperidin bioaccessibility was increased from 63.9% to 73.2% after incorporation of hesperidin-loaded organogel into Pickering emulsion, which was possibly owing to a larger number of released FFAs

(8). When compared with soybean oil-based organogel, more micelles composed of released FFAs were generated during digestion of organogel-based Pickering emulsion. Because hydrophobic hesperidin should become bioaccessible after solubilization in the micelle cores, more bioaccessible hesperidin can be delivered employing organogel-based Pickering emulsion stabilized by OVT fibrils.

4. Conclusion

In conclusion, food-grade organogel-based Pickering emulsions with a higher loading of hesperidin were developed. Organogel-based Pickering emulsions stabilized by OVT fibrils had excellent storage stability, and OVT fibrils could stabilize organogel-based Pickering emulsions well at a very high internal phase volume ratio (0.80–0.85). Organogel-based Pickering emulsions stabilized by OVT fibrils at different ionic strengths could withstand up to 3 freeze-thaw cycles. Freeze-thaw stability of organogel-based Pickering emulsions stabilized by OVT fibrils was better than that of conventional Pickering emulsions (without organogel) stabilized by OVT fibrils. In comparison with soybean oil-based organogel, organogel-based Pickering emulsion could improve both extent of lipolysis and hesperidin bioaccessibility. The obtained results in this chapter may facilitate designing of Pickering emulsions with high nutraceutical loading, outstanding freeze-thaw stability and improved nutraceutical bioaccessibility.

5. References

1. Ahmed, E. M. (2015). Hydrogel: Preparation, characterization, and applications: A review. *Journal of Advanced Research*, 6(2), 105–121.

2. Baran, N., Singh, V. K., Pal, K., Anis, A., Pradhan, D. K., & Pramanik, K. (2014). Development and characterization of soy lecithin and palm oil-based organogels. *Polymer-Plastics Technology and Engineering*, 53(9), 865–879.
3. Chaves, K. F., Barrera-Arellano, D., & Ribeiro, A. P. B. (2018). Potential application of lipid organogels for food industry. *Food Research International*, 105, 863–872.
4. Patel, A. R., & Dewettinck, K. (2016). Edible oil structuring: an overview and recent updates. *Food & Function*, 7, 20–29.
5. Siraj, N., Shabbir, M. A., Ahmad, T., Sajjad, A., Khan, M. R., Khan, M. I., et al. (2015). Organogelators as a saturated fat replacer for structuring edible oils. *International Journal of Food Properties*, 18(9), 1973–1989.
6. Jadhav, S. R., Hwang, H., Huang, Q., & John, G. (2013). Medium-chain sugar amphiphiles: A new family of healthy vegetable oil structuring agents. *Journal of Agricultural and Food Chemistry*, 61(49), 12005–12011.
7. Lu, M., Cao, Y., Ho, C. T., & Huang, Q. (2016). Development of organogel-derived capsaicin nanoemulsion with improved bioaccessibility and reduced gastric mucosa irritation. *Journal of Agricultural and Food Chemistry*, 64(23), 4735–4741.
8. Yu, H., & Huang, Q. (2012). Improving the oral bioavailability of curcumin using novel organogel-based nanoemulsions. *Journal of Agricultural and Food Chemistry*, 60(21), 5373–5379.
9. Yu, H., Shi, K., Liu, D., & Huang, Q. (2012). Development of a food-grade organogel with high bioaccessibility and loading of curcuminoids. *Food Chemistry*, 131(1), 48–54.
10. Zahi, M. R., Wan, P., Liang, H., & Yuan, Q. (2014). Formation and stability of d-limonene organogel-based nanoemulsion prepared by a high-pressure homogenizer. *Journal of Agricultural and Food Chemistry*, 62(52), 12563–12569.
11. Chassaing, B., Koren, O., Goodrich, J. K., Poole, A. C., Srinivasan, S., Ley, R. E., et al. (2015). Dietary emulsifiers impact the mouse gut microbiota promoting colitis and metabolic syndrome. *Nature*, 519, 92–96.
12. Gao, Z., Zhao, J., Huang, Y., Yao, X., Zhang, K., Fang, Y., et al. (2017). Edible Pickering emulsion stabilized by protein fibrils. Part 1: Effects of pH and fibrils concentration. *LWT - Food Science and Technology*, 76, 1–8.
13. Abeyrathne, E., Lee, H. Y., & Ahn, D. U. (2013). Egg white proteins and their potential use in food processing or as nutraceutical and pharmaceutical agents—a review. *Poultry Science*, 92(12), 3292–3299.
14. Wei, Z., & Huang, Q. (2019). Assembly of iron-bound ovotransferrin amyloid fibrils. *Food Hydrocolloids*, 89, 579–589.
15. Wei, Z., Zhu, P., & Huang, Q. (2019). Investigation of ovotransferrin conformation and its complexation with sugar beet pectin. *Food Hydrocolloids*, 87, 448–458.
16. Wei, Z., & Gao, Y. (2016). Physicochemical properties of β -carotene bilayer emulsions coated by milk proteins and chitosan–EGCG conjugates. *Food Hydrocolloids*, 52, 590–599.

17. Degner, B. M., Chung, C., Schlegel, V., Hutkins, R., & McClements, D. J. (2014). Factors influencing the freeze-thaw stability of emulsion-based foods. *Comprehensive Reviews in Food Science and Food Safety*, 13(2), 98–113.
18. Shah, D. K., Sagiri, S. S., Behera, B., Pal, K., & Pramanik, K. (2013). Development of olive oil based organogels using sorbitan monopalmitate and sorbitan monostearate: A comparative study. *Journal of Applied Polymer Science*, 129(2), 793–805.
19. Zhu, X. F., Zheng, J., Liu, F., Qiu, C. Y., Lin, W. F., & Tang, C. H. (2018). Freeze-thaw stability of Pickering emulsions stabilized by soy protein nanoparticles. Influence of ionic strength before or after emulsification. *Food Hydrocolloids*, 74, 37–45.
20. Garg, A., Garg, S., Zaneveld, L. J. D., & Singla, A. K. (2001). Chemistry and pharmacology of the citrus bioflavonoid hesperidin. *Phytotherapy Research*, 15(8), 655–669.
21. Ting, Y., Jiang, Y., Lan, Y., Xia, C., Lin, Z., Rogers, M. A., et al. (2015). Viscoelastic emulsion improved the bioaccessibility and oral bioavailability of crystalline compound: A mechanistic study using *in vitro* and *in vivo* models. *Molecular Pharmaceutics*, 12(7), 2229–2236.
22. Donsi, F., Wang, Y., & Huang, Q. (2011). Freeze-thaw stability of lecithin and modified starch-based nanoemulsions. *Food Hydrocolloids*, 25(5), 1327–1336.
23. Xiao, J., Li, C., & Huang, Q. (2015). Kafirin nanoparticle-stabilized Pickering emulsions as oral delivery vehicles: Physicochemical stability and *in vitro* digestion profile. *Journal of Agricultural and Food Chemistry*, 63(47), 10263–10270.
24. Chung, Y., Simmons, L., Gutowska, A., & Jeong, B. (2002). Sol–gel transition temperature of PLGA-g-PEG aqueous solutions. *Biomacromolecules*, 3(3), 511–516.
25. Wei, Z., Yang, W., Fan, R., Yuan, F., & Gao, Y. (2015). Evaluation of structural and functional properties of protein–EGCG complexes and their ability of stabilizing a model β -carotene emulsion. *Food Hydrocolloids*, 45, 337–350.
26. Oboroceanu, D., Wang, L., Brodkorb, A., Magner, E., & Auty, M. A. E. (2010). Characterization of β -lactoglobulin fibrillar assembly using atomic force microscopy, polyacrylamide gel electrophoresis, and *in situ* fourier transform infrared spectroscopy. *Journal of Agricultural and Food Chemistry*, 58(6), 3667–3673.
27. Usov, I., & Mezzenga, R. (2015). FiberApp: An open-source software for tracking and analyzing polymers, filaments, biomacromolecules, and fibrous objects. *Macromolecules*, 48(5), 1269–1280.
28. de Folter, J. W. J., van Ruijven, M. W. M., & Velikov, K. P. (2012). Oil-in-water Pickering emulsions stabilized by colloidal particles from the water-insoluble protein zein. *Soft Matter*, 8(25), 6807–6815.
29. Wei, Z., & Huang, Q. (2019). Edible Pickering emulsions stabilized by ovotransferrin–gum arabic particles. *Food Hydrocolloids*, 89, 590–601.
30. Xiao, J., Wang, X., Gonzalez, A. J. P., & Huang, Q. (2016). Kafirin nanoparticles-stabilized Pickering emulsions: Microstructure and rheological behavior. *Food Hydrocolloids*, 54, 30–39.
31. Wei, Z., & Gao, Y. (2016). Physicochemical properties of β -carotene emulsions

- stabilized by chitosan–chlorogenic acid complexes. *LWT-Food Science and Technology*, 71, 295–301.
32. Zhu, X. F., Zhang, N., Lin, W. F., & Tang, C. H. (2017). Freeze-thaw stability of pickering emulsions stabilized by soy and whey protein particles. *Food Hydrocolloids*, 69, 173–184.
33. Li, Y., Hu, M., & McClements, D. J. (2011). Factors affecting lipase digestibility of emulsified lipids using an in vitro digestion model: Proposal for a standardised pH-stat method. *Food Chemistry*, 126(2), 498–505.
34. Li, Y., & McClements, D. J. (2010). New mathematical model for interpreting pH-stat digestion profiles: impact of lipid droplet characteristics on in vitro digestibility. *Journal of Agricultural and Food Chemistry*, 58(13), 8085–8092.
35. Patzek, T. W. (2009). A first law thermodynamic analysis of biodiesel production from soybean. *Bulletin of Science, Technology & Society*, 29(3), 194–204.
36. Carneiro, J. d. D. S., Minim, V. P. R., Deliza, R., Silva, C. H. O., Carneiro, J. C. S., & Leão, F. P. (2005). Labelling effects on consumer intention to purchase for soybean oil. *Food Quality and Preference*, 16(3), 275–282.
37. Dhuique-Mayer, C., Tbatou, M., Carail, M., Caris-Veyrat, C., Dornier, M., & Amiot, M. J. (2007). Thermal degradation of antioxidant micronutrients in citrus juice: kinetics and newly formed compounds. *Journal of Agricultural and Food Chemistry*, 55(10), 4209–4216.
38. Rambaran, R. N., & Serpell, L. C. (2008). Amyloid fibrils: abnormal protein assembly. *Prion*, 2(3), 112–117.
39. Schleegeer, M., vandenAkker, C. C., Deckert-Gaudig, T., Deckert, K., Velikov, K. P., Koenderink, G., et al. (2013). Amyloids: From molecular structure to mechanical properties. *Polymer*, 54(10), 2473–2488.
40. Peng, J., Simon, J. R., Venema, P., & Van Der Linden, E. (2016). Protein fibrils induce emulsion stabilization. *Langmuir*, 32(9), 2164–2174.
41. Sicorello, A., Torrassa, S., Soldi, G., Gianni, S., Travaglini-Allocatelli, C., Taddei, N., et al. (2009). Agitation and high ionic strength induce amyloidogenesis of a folded PDZ domain in native conditions. *Biophysical Journal*, 96(6), 2289–2298.
42. Cameron N. R. (2005). High internal phase emulsion templating as a route to well-defined porous polymers. *Polymers*, 46(5), 1439–1449.
43. Patel, A. R., Rodriguez, Y., Lesaffer, A., & Dewettinck, K. (2014). High internal phase emulsion gels (HIPE-gels) prepared using food-grade components. *RSC Advances*, 4(35), 18136–18140.
44. Xu, Y. T., Tang, C. H., Liu, T. X., & Liu, R. (2018). Ovalbumin as an outstanding Pickering nanostabilizer for high internal phase emulsions. *Journal of Agricultural and Food Chemistry*, 66(33), 8795–8804.
45. Xu, Y. T., Liu, T. X., & Tang, C. H. (2019). Novel pickering high internal phase emulsion gels stabilized solely by soy β -conglycinin. *Food Hydrocolloids*, 88, 21–30.
46. Yang, T., Zheng, J., Zheng, B. S., Liu, F., Wang, S., & Tang, C. H. (2018). High internal phase emulsions stabilized by starch nanocrystals. *Food Hydrocolloids*, 82, 230–238.
47. Du, X., Li, Z., Xia, J., Zhang, F., & Wang, Z. (2019). Facile

sonochemistry-assisted assembly of the water-loving drug-loaded micro-organogel with thermo- and redox-sensitive behavior. *Colloids and Surfaces A: Physicochemical and Engineering Aspects*, 561, 47–56.

48. Bon, S. A. F., Mookhoek, S. D., Colver, P. J., Fischer, H. R., & van der Zwaag, S. (2007). Route to stable non-spherical emulsion droplets. *European Polymer Journal*, 43(11), 4839–4842.

49. Wu, L., Liao, Z., Liu, M., Yin, X., Li, X., Wang, M., et al. (2016). Fabrication of non-spherical Pickering emulsion droplets by cyclodextrins mediated molecular self-assembly. *Colloids and Surfaces A: Physicochemical and Engineering Aspects*, 490, 163–172.

50. Tadros, T. (2004). Application of rheology for assessment and prediction of the long-term physical stability of emulsions. *Advances in Colloid and Interface Science*, 108–109, 227–258.

51. Patel, A. R., Schatteman, D., De Vos, W. H., Lesaffer, A., & Dewettinck, K. (2013). Preparation and rheological characterization of shellac oleogels and oleogel-based emulsions. *Journal of Colloid and Interface Science*, 411, 114–121.

52. Pal, R. (2011). Rheology of simple and multiple emulsions. *Current Opinion in Colloid & Interface Science*, 16(1), 41–60.

53. Wang, H., Singh, V., & Behrens, S. H. (2012). Image charge effects on the formation of Pickering emulsions. *The Journal of Physical Chemistry Letters*, 3, 2986–2990.

54. Bateman, L., Ye, A., & Singh, H. (2010). In vitro digestion of β -lactoglobulin fibrils formed by heat treatment at low pH. *Journal of Agricultural and Food Chemistry*, 58(17), 9800–9808.

SUMMARY AND FUTURE WORK

In this thesis, OVT fibrils were assembled, characterized and subsequently applied in food emulsion systems. First of all, the optimal environmental condition for OVT fibrillation was obtained, and OVT fibrils consisted of both long and short fibrils. Both intact monomers and peptides were the building blocks of OVT fibrils. Internal structures of OVT amyloid fibrils could be stacked β -sheet. OVT amyloid fibrils had no *in vitro* cytotoxicity, suggesting great application potential. In terms of fibril stability, OVT fibrils were stable over a wide pH range, and OVT fibrils possessed excellent stability against environmental stresses such as frozen storage–lyophilization–rehydration. The excellent stability indicated that OVT fibrils could be applied in design of nutraceutical delivery systems.

OVT fibrillation could be affected by many other food ingredients in complex food systems. When it came to polyols, the presence of glycerol or sorbitol could reduce the rate of OVT fibrillation, and slowdown of OVT fibrillation was strongly dependent on concentration of glycerol or sorbitol. Regarding impact of Maillard reaction, glycation could suppress fibrillation of ovotransferrin, and glycosylation exerted stronger inhibitory impact on fibril formation than lactosylation. Glycation decreased average contour length of ovotransferrin fibrils, When it came to influence of polyphenols, the bound polyphenols (EGCG and GA) could inhibit OVT nanofibrillation, and higher level of complexation of OVT with more polyphenols showed stronger fibril-inhibitory activity. Covalent bound polyphenols exerted

stronger inhibitory influence on OVT nanofibrillation than corresponding non-covalent bound polyphenols.

Afterwards, application of OVT fibrils was explored in emulsion systems. OVT fibrils were verified as effective Pickering emulsifiers, and OVT fibrils could stabilize Pickering emulsions with high emulsified phase volume and stability index at different fibril concentrations and oil fractions. OVT fibrils could be employed to fabricate stable Pickering emulsions at various ionic strengths (0–1000 mM) and pHs (2–7). OVT fibril-stabilized Pickering emulsions could provide curcumin protection. As demonstrated in TIM-1 and pH-stat digestion models, OVT fibril-stabilized Pickering emulsions could increase curcumin bioaccessibility. To improve freeze-thaw stability of Pickering emulsion systems, organogel-based Pickering emulsions stabilized by OVT fibrils were developed. Organogel-based Pickering emulsions stabilized by OVT fibrils had excellent storage stability, and freeze-thaw stability of organogel-based Pickering emulsions stabilized by OVT fibrils was better than that of conventional Pickering emulsions (without organogel) stabilized by OVT fibrils. In comparison with soybean oil-based organogel, organogel-based Pickering emulsion could improve both extent of lipolysis and hesperidin bioaccessibility. The acquired knowledge in this thesis may facilitate assembly, characterization and application of food protein fibrils.

Future work will be conducted in the following directions:

1. The underlying mechanisms of OVT fibrillation will be further explored to obtain deeper understandings.

2. Surface coverage of OVT fibrils at the oil-water interface in OVT fibril-stabilized Pickering emulsions will be studied.
3. Digestion of organogel-based Pickering emulsions will be studied in TIM-1 digestion model.